NASA CR-182202
UTRC R88-957367-31

SUPERSONIC THROUGH-FLOW FAN ASSESSMENT

by C. E. Kepler and G. A. Champagne

United Technologies Research Center

prepared for

NATIONAL AERONAUTICS AND SPACE ADMINISTRATION

NASA Lewis Research Center
Contract NAS3-24843

1. Report No.	2. Government Accession No.	3. Recipient's Catalog No.
NASA CR-182202		

4. Title and Subtitle	5. Report Date
Supersonic Through-Flow Fan Assessment	November 1988
	6. Performing Organization Code

7. Author(s)	8. Performing Organization Report No.
C. E. Kepler, G. A. Champagne	UTRC R88-957367-31
	10. Work Unit No.

9. Performing Organization Name and Address	11. Contract or Grant No.
United Technologies Research Center East Hartford, CT	NAS3-24843
	13. Type of Report and Period Covered Contractural Report 1/86 - 11/88

12. Sponsoring Agency Name and Address	14. Sponsoring Agency Code
NASA Lewis Research Center Cleveland, Ohio	

15. Supplementary Notes

NASA Project Manager - L. C. Franciscus

16. Abstract

A study was conducted to assess the performance potential of a supersonic through-flow fan engine for supersonic cruise aircraft. It included a mean-line analysis of fans designed to operate with in-flow velocities ranging from subsonic to high supersonic speeds. The fan performance generated was used to estimate the performance of supersonic fan engines designed for four applications: a Mach 2.3 supersonic transport, a Mach 2.5 fighter, a Mach 3.5 cruise missile, and a Mach 5.0 cruise vehicle. For each application an engine was conceptualized, fan performance and engine performance were calculated, weight estimates were made, the engine was insatlled in a hypothetical vehicle, and a mission analysis was conducted.

17. Key Words (Suggested by Author(s))	18. Distribution Statement
Supersonic Fan, Supersonic Inflow Fan, Through-Flow Fan, Transonic Fan, Supersonic Engine, Supersonic Aircraft	General Release

19. Security Classif. (of this report)	20. Security Classif. (of this page)	21. No. of Pages	22. Price*
Unclassified	Unclassified	165	

*For sale by the National Technical Information Service, Springfield, Virginia 22161

TABLE OF CONTENTS

LIST OF TABLES

LIST OF FIGURES

LIST OF FIGURES (Cont'd)

LIST OF FIGURES (Cont'd)

LIST OF FIGURES (Cont'd)

LIST OF SYMBOLS

A	Flow area
Ac	Inlet capture area
b	Gap between blades
c	Chord
c_p	Specific heat at constant pressure
C_f	Skin friction coefficient
C_T	Thrust coefficient, F_N/q_oA_c
F_N	Net thrust
h	Enthalpy
k	Blade shape parameter (see Eq. 11)
h_T	Total enthalpy
I	Thrust specific impulse, sec
ℓ	Length along chord line
M	Mach number, also Mn
M_o	Free–stream Mach number
M_1	Fan inlet Mach number
M_R	Rotor Mach number
N_c	Corrected rotor speed, $N/\sqrt{\theta}$
P	Static pressure
P_T	Total pressure
P_{T_R}	Fan total pressure ratio
P_R	Inlet pressure recovery
q	Dynamic pressure, $1/2\rho v^2$
R	Gas constant
S	Entropy
T	Static temperature

LIST OF SYMBOLS (Cont'd)

T_T	Total temperature
TSFC	Thrust specific fuel consumption, hr^{-1}
V_c	Corrected Velocity, $V/\sqrt{\theta}$
$\dot{W}$	Weight flow rate, lb/sec
Wc	Corrected weight flow, $\dot{w}\sqrt{\theta}/\delta$
W_R	Inlet relative weight flow
x	Axial length
y	Length, normal to x
α	Mean flow angle
β	Mean camber angle
γ	Ratio of specific heats
δ	Flow deflection through shock and P_T/P_{REF}
ϵ	Flow inclination relative to camber angle
ζ	Normalized length, ℓ/c
η_b	Burner efficiency
η_c	Fan efficiency
θ	Blade surface flow angle and T_T/T_{REF}
λ	Loss coefficient
μ	Mach angle
ν	Prandtl–Meyer expansion angle
ρ	Density
ϕ	Fuel stoichiometry

subscripts:

0	–	Free stream
1	–	Fan face or blade entrance
2	–	Fan exit or blade exit
3	–	Supersonic diffuser throat

LIST OF SYMBOLS (Cont'd)

4	–	Combustor entrance
5	–	Primary nozzle throat
6	–	Primary nozzle exit
By	–	Bypass nozzle
R	–	Rotor

superscripts

(prime)'	–	Relative conditions

1.0 SUMMARY

A study was conducted to evaluate the potential benefits of supersonic through-flow fan engines for supersonic cruise aircraft. A fan that can operate with supersonic inlet Mach numbers would eliminate most of the losses incurred in diffusing the flow to subsonic velocities at the fan face; furthermore, the size and weight of the inlet to the supersonic fan would be substantially lower than that of a conventional mixed-compression inlet. Therefore, an engine employing such a fan has the potential to be light weight, provide high thrust, and operate efficiently at supersonic flight speeds.

The supersonic-through-flow fans used in these studies were designed and the performance evaluated using a two-dimensional, mean-line analysis described herein. This analysis was extended to include the strong shock solution for transonic operation when operating with subsonic inflow velocities. In order to start up and provide a continuum of operation between subsonic and supersonic flight speeds, the fans were assumed to have variable-pitch rotor and stator blades which could be adjusted during flight to provide the optimum blade angle-of-attack. These studies led to a particular fan design called a "variable-pitch, split-blade" configuration, in which the front parts of the rotors and stators can be rotated but the rear parts are fixed. Such blading varies the amount of turning done on the flow; it acts much like a variable camber blade, or like a wing with a flap. This type of blade can be used from subsonic to supersonic and higher-speed windmilling conditions.

The merits of a supersonic fan engine were evaluated for four applications having significant supersonic cruise requirements. They were a Mach 2.3 supersonic transport, a Mach 2.5 fighter, a Mach 3.5 cruise missile, and a Mach 5.0 cruise vehicle. For each application an engine was conceptualized; fan performance and engine performance were calculated; weight estimates were made; the engine was installed in a hypothetical vehicle; and a mission analysis was conducted. The engine performance and weight, and the mission performance were then compared with that of a conventional fan engine.

Mach 2.3 supersonic transport: A supersonic fan with a total pressure ratio (at cruise) of 3.5 was used in a two-spool engine having a cruise bypass ratio of 1.0. This propulsion system (inlet & engine & nacelle) was 30% lighter and had a 9% lower averaged cruise TSFC than the conventional turbofan. This resulted in a 14% range advantage for a fixed take-off gross-weight vehicle.

Mach 2.5 fighter: The same supersonic fan was used in this application, it was run at a higher speed to provide a total pressure ratio of 4.0 at the supersonic cruise condition. The STFF propulsion system (inlet & engine) was 7% heavier because a larger airflow was required to meet the subsonic maneuverability requirements, since the supersonic fan engine could not burn the bypass flow. The supersonic cruise TSFC was 4% lower than the conventional turbofan. This engine resulted in a 2% lighter take-off gross-weight aircraft.

Mach 3.5 cruise missile: A total pressure ratio 1.6 supersonic fan was designed for this application; it was used in a two-spool engine having a bypass ratio of 0.33 at cruise. This propulsion systems (inlet & engine) was 5% lighter, and had the same cruise TSFC as a conventional turbojet. This engine resulted in a 1% cruise range advantage.

Mach 5.0 Cruise Vehicle: A hydrogen fueled, air-turbo-rocket (ATR) engine was used for this application. The supersonic fan used in this engine was the variable-pitch, split-blade fan which had a total pressure ratio of about 3.5 at low supersonic speeds, dropping off at higher speeds to less than one when windmilling at the Mach 5 cruise condition. The comparative engine was an over/under conventional ATR/ramjet (RJ) propulsion system. When sized for the same thrust at Mach 3, the STFF-ATR engine was 28% lighter. At subsonic flight speeds this engine provided approximately twice the thrust and

a 25% lower TSFC. At the Mach 5 cruise condition, the TSFC was 8% lower. When the STFF–ATR engine was resized to provide the same take–off thrust loading, the aircraft take–off gross weight was 62% less than the reference vehicle using the over/under conventional ATR/RJ.

Conclusions

A variable–pitch split–blade fan has the potential capability of extending the speed range of the supersonic fan into the transonic speed range where it operates like a conventional fan, generating a substantial pressure rise with subsonic outflow velocities. This fan can also operate above its supersonic design point and be feathered for windmilling at high Mach numbers where the engine is operated like a ramjet.

A variable–pitch supersonic through–flow–fan engine can provide a significant range advantage for an aircraft having a substantial supersonic cruise requirement, like a supersonic transport. Conversely, it is not as attractive for a fighter which has a significant subsonic cruise and maneuverability requirement.

A supersonic through–flow–fan engine did not show a performance advantage for a missile which was boosted to its Mach 3.5 cruise conditions.

A variable–pitch, split–blade fan air–turbo–rocket engine will provide substantial performance advantages to a Mach 5 cruise vehicle when compared with an over/under conventional ATR/RJ. The variable–pitch fan allowed this engine to operate as a ramjet at the Mach 5 cruise condition, using the same flow path (inlet, combustor, nozzle) used at lower flight speeds.

Recommendations

A technology base should be developed for the variable–pitch, split–blade supersonic through–flow fan. This would include: detailed CFD calculations of the fan performance especially at the transonic operating condition, mechanical design studies of fan attachment and rotation mechanisms, cascade tests of split–blade configurations at simulated fan conditions, and (subsequent) rotor tests of small–scale fan configurations.

Conduct more detailed design studies of the variable–pitch, supersonic–through–flow, turbo–fan engine for the supersonic cruise application. Establish the mechanical arrangement and structural integrity of the engine, and conduct a weight analysis to provide better means for estimating STFF inlets, fans, supersonic diffuser, and bypass nozzle weights.

Conduct more detailed design studies of the variable–pitch supersonic through flow ATR engine for the high–speed cruise vehicle. Establish the mechanical arrangement and structural integrity of the engine, and refine the weight estimates of the engine components.

2.0 INTRODUCTION

Renewed interest in high-speed flight has revived interest in the supersonic fan as a possible component for advanced high-speed propulsion systems for sustained supersonic cruise or as accelerators for hypersonic vehicles. Cycle studies have indicated that substantial improvements can be obtained by using a fan that is capable of accepting supersonic axial flow during supersonic flight. Ferri (1) was the first (1956) to point out the potential advantages of eliminating the subsonic portion of the supersonic inlet and providing a fan capable of accepting supersonic axial inflow. In the 60's both GASL and UTRC (2) studied turbojet engine concepts employing supersonic compressors. The UTRC concept employed a two-stage, counter-rotating compressor which provided a total pressure ratio of 20 at transonic flight conditions. The UTRC study also included supersonic cascade tests of supersonic compressor blades and supersonic diffuser tests of simulated fan exit flow. The cascade tests indicated that high efficiencies would be obtained with supersonic through-flow stages, and that supersonic stages can be operated over a wide range of incidence angles. In that same time period, Boxer (3) proposed a high bypass ratio turbofan engine/ramjet combination which utilized a variable-pitch fan capable of operating with both subsonic and supersonic inflow velocities. At flight speeds below about 1.5 the fan would operate with subsonic inflow, and at higher speeds the fan would operate with supersonic inflow and the fan pitch would be adjusted to maximize fan performance. At flight Mach number greater than 3.5 the engine would operate as a subsonic ramjet with the fan, being held stationary by a brake, providing additional compression beyond that provided by the inlet. In the 70's, NASA sponsored studies by Pratt and Whitney and General Electric to identify propulsion systems that would be suitable for long-range supersonic cruise aircraft (Ref. 4-10). These studies considered a variety of conventional and variable cycle concepts. An alternative concept, the supersonic through-flow fan was studied by Trucco (11) of Advanced Technology Laboratories, Inc. under a NASA contract. Additional studies at NASA Lewis by Franciscus (12) compared the performance of several supersonic through-flow fan engines to a reference turbofan engine for a Mach 2.32 suspersonic transport (SST) application and concluded that use of a supersonic through-flow fan engine could reduce specific fuel consumption and lead to a significant improvement in range. More recently, Taveres (13) and Franciscus (14) published additional studies concluding that supersonic fans would provide improved performance for SST's operating in the Mach 3 speed range.

With the current renewed interest in SST aircraft, and in light of the study conclusions by Franciscus, Trucco, and Tavares, a more in depth look at the supersonic fan engine should be made by an engine manufacturer to evaluate its potential for the SST application and other applications having substantial supersonic cruise requirements.

The present study is an assessment of advanced engines employing supersonic through-flow fans. Four applications were considered: a Mach 2.3 supersonic transport, a Mach 2.5 fighter, a Mach 3.5 cruise missile, and a Mach 5.0 cruise vehicle. For each application a supersonic fan engine was conceptualized, performance calculated, and evaluated on the bases of performing the mission requirements. The supersonic fan engines are compared with conventional engines for performing the same mission. The objective of this study was to identify those applications and engine configurations which may benefit from using supersonic through-flow fans.

3.0 FAN ANALYSIS

The supersonic fans conceptualized for the engine study were designed to operate with supersonic inflow and supersonic exit flow, i.e., a supersonic through-flow fan (STFF); however, it soon became evident during this study that it would be highly desirable to provide variable pitch, and operate with subsonic inflow (transonic operation) over the low speed portion of the flight path, similar to the type of operation suggested by Boxer (3) in 1967. This fan evolved, during the study, into the variable-pitch, split-blade fan described herein. The first section describes the blade design and performance prediction procedures for the supersonic through-flow fan; the second section describes the subsonic inflow mode of operation; the third section discusses the problems of operating over the subsonic to supersonic speed range; and the fourth section discusses the performance characteristics of the variable-pitch split- blade fan. The specific fan blade designs and performance calculated and used in the engine applications are presented in the sections describing the STFF engine performance.

3.1 Supersonic Through-Flow Fan

A supersonic through-flow fan is like a shrouded propeller which can operate with supersonic flow coming into the blades. The flow remains supersonic as it passes through the blade row, and it emerges with a greater supersonic velocity. The velocity diagram shown in Figure 1 is used to explain how it operates. The first velocity triangle shows the conditions flowing into the fan: the axial velocity (V_1) is 2000 ft/sec, the rotor velocity (V_R) is 1500 ft/sec, and the velocity relative to the moving blades (V_1') is 2500 ft/sec. If the relative flow is turned 30° while passing through the blade row with no change in the static pressure and no dissipative losses, the relative exit flow velocity (V_2') would be 2500 ft/sec and the velocity diagram would be that shown on the right. After vectorially adding the rotational velocity to the exiting relative velocity, the resulting absolute velocity (V_2) would be 2700 ft/sec. Thus, the flow is accelerated to a higher velocity and gains kinetic energy as it passes through the blade row. For this example, the increase in energy (total temperature) is approximately 40%, and the total pressure of the exiting flow is increased to approximately three times the incoming total pressure.

It can be shown that the work done on the air which passes through the blade row is equal to the product of the tangential velocity imparted to the air by the rotor (ΔV_T) times the rotational velocity of the blades (V_R) .

$$\text{i.e.,}\quad \text{Work} = \Delta V_T V_R \qquad \text{(Eq. 1)}$$

The change in kinetic energy of the air is equal to this work because there was assumed to be no other change in the thermodynamic state of the gas exiting the blade row. This basic relationship describing the work done on the air, is the same as that which has always been used for conventional compressors.

A computer program was developed at UTRC (with corporate funding) to design and predict the performance of the STFF fan. The procedures used to design the blades, the flow modeling, and approach used to calculate the mean-line blade performance are described herein.

Fan design. – The supersonic through-flow fan design procedure is comprised of three different subroutines which are used to specify the blade geometries: (1) a routine which calculates the amount of flow turning required to generate a specified design total pressure ratio, (2) a blade shape routine which calculates the coefficients which specify the blade shape, and (3) a wave geometry routine which calculates the chord length for a specified number of shock reflections.

Flow turning: The first routine calculates the amount of flow turning required by the rotor to generate the design total pressure ratio for a given set of fan inlet flow conditions. The input and output parameters are shown below:

Input

inlet conditions M_1, α_1

rotor conditions M_R, P_2/P_1

desired performance P_{T_2}/P_{T_1}, η_c

Output

exit conditions M_2, T_2/T_1, A_2/A_1

flow turning α_2

where:

M_1	– inlet Mach number
M_2	– exit Mach number
α_1	– inlet flow direction
α_2	– exit flow direction
M_R	– rotor Mach number
P_2/P_1	– static pressure ratio across rotor
P_{T_2}/P_{T_1}	– desired total pressure ratio
T_2/T_1	– static temperature across rotor
A_2/A_1	– flow area ratio across rotor
η_c	– assumed fan efficiency

Note, that as well as specifying the inlet conditions (M_1, α_1) and rotor speed (M_R), the static pressure ratio across the blade row is an independent parameter and must be specified. The compressor efficiency must be assumed (at least initially) in order to evaluate the work done on the air:

$$\text{WORK} = h_{T_1}\left((P_{T_2}/P_{T_1})^{\frac{\gamma-1}{\gamma}} - 1 \right)/\eta_c \qquad \text{Eq. 2}$$

when h_{T_1}, total enthalpy of the incoming air.

The flow losses (entropy gain) across blade row are:

$$\frac{\Delta S}{R} = \frac{\gamma}{\gamma - 1} \ln\left(1 + \frac{WORK}{h_{T_1}}\right) - \ln(P_{T_2}/P_{T_1}) \qquad \text{Eq. 3}$$

The static temperature across the blade row can be calculated from the flow losses and the specified static pressure ratio

$$T_2/T_1 = \left((P_2/p_1)e^{(\frac{\Delta S}{R})}\right)^{\frac{\gamma-1}{\gamma}} \qquad \text{Eq. 4}$$

Then the exit velocity (V_2) can be calculated using the energy equation

$$\frac{1}{2}V_2^2 = h_{T_1} + WORK - c_p T_2 \qquad \text{Eq. 5}$$

The exit flow direction (α_2) can then be calculated from the compressor work relationship (Eq. 1); when $\alpha_1 = 0$ then $\Delta V_T = V_2 \sin \alpha_2$ and

$$\sin \alpha_2 = \frac{WORK}{V_2 V_R} \qquad \text{Eq. 6}$$

The angle, α_2, evaluated from Eq. 6 is the absolute angle leaving the blade row. Note, for the vector diagram shown in Figure 1, V_R is negative; therefore α_2 is negative or downward, as shown in the figure. The flow direction relative to the moving blades can be calculated by vectorially subtracting the rotational velocity to the absolute velocity. Then the relative inlet and exit flow angles are:

$$\tan \alpha_1' = \frac{-V_R}{V_1} \qquad (\text{for } \alpha_1 = 0) \qquad \text{Eq. 7}$$

and

$$\tan \alpha_2' = \frac{V_2 \sin \alpha_2 - V_R}{V_2 \cos \alpha_2} \qquad \text{Eq. 8}$$

There relative angles show the amount of turning required by the blade row. An example showing the flow turning through the rotor, $\Delta\alpha'$, required to provide a specified total pressure ratio, P_{T_R}, across

the fan is shown in Figure 2. This figure shows the flow turning is directly proportional to the total pressure ratio (compression work) and inversly proportional to the rotor Mach number (velocity) as shown by Eq. 6. For the conditions used in this example ($M_1 = 2.0$ and $\eta_c = .85$, and a rotor Mach number of 1.5) a total pressure ratio of 2.5 can be achieved with about 27 deg of turning.

The desired flow turing through the stator is usually equal (in magnitude) and opposite to the absolute turning through the rotor, since fans are usually designed with zero exit swirl.

$$\Delta\alpha_{STATOR} = -\Delta\alpha_{ROTOR} \qquad \text{Eq. 9}$$

Blade shape: The total turning (or camber) of the rotor and stator blades is approximately equal to the flow turning required. The nomenclature used in specifying the blade geometry is shown in Figure 3. The relative inlet and outlet flow angles are α_1' and α_2' as defined previously. The mean camber angle at the leading and trailing edges of the blade are β_1 and β_2. The mean chord angle is, β_c. The difference between the α's and the β's are the ϵ's; where ϵ_1, is the angle–of–attack of the blade and ϵ_2 is the flow mismatch angle at the trailing edge. ● is an arbituary input, but ϵ_2 is a result; however, an initial guess may be used and improved upon later after running the performance program.

The blade surface angles are defined by two quadratic equation describing the front and rear portions of each (upper and lower) surface.

$$\theta \text{ front } = \theta_1 + A\zeta + B\zeta^2 \quad 0 < \zeta < \zeta_T$$

$$\theta \text{ rear } = \theta_2 + C(1-\zeta) + D(1-\zeta)^2 \quad \zeta_T < \zeta < 1 \qquad \text{Eq. 10}$$

where ζ is a normalized blade coordinate

ζ_T is the transition point

θ_1 leading edge angle including thickness

θ_2 trailing edge angle including thickness

For a circular are profile B & D would be zero, and $A = \theta_2 - \theta_1$.

Introducing K

$$A = K(\theta_2 - \theta_1) \qquad \text{Eq. 11}$$

When K=1, the profile shape is a circular arc. When K = 0, the curvature $d\theta/d\zeta = 0$ near the leading edge is zero and the curvature near the middle is increased. With K being an arbitrary input, the valves of B, C, and D are solved which satisfy the following at $\zeta = \zeta_T$

$$\int \theta d\zeta \text{ front} = \int \theta d\zeta \text{ rear}$$

$$\theta \text{ front} = \theta \text{ rear} \qquad \text{Eq. 12}$$

$$d\theta/d\zeta \text{ front} = d\theta/d\zeta \text{ rear}$$

Wave geometry: The chord length or conversely gap/chord ratio, b/c, is chosen for a specified wave geometry. For the example shown in Figure 3 the dashed lines crossing the flow represent the wave pattern for an up–down wave system which intersects the trailing edge. This is the wave patterns used in the design of all the fans presented herein. Alternative wave patterns that could be employed are: a single down wave, and a down–up wave pattern. The procedure for calculating the gap/chord ratio is iterative, a guess is made, the wave pattern calculated and then the value of b/c is adjusted to let the wave intersect the trailing edge.

Fan performance. – The key features of the supersonic through–flow fan performance procedure are identified in Figure 4. The program calculates the overall performance across a rotor–stator configuration given the blade geometry and spacing. It generates a rudimentary wave structure, checks for limits of the flow incidence angle, boundary layer separation, and flow choking. If these conditions are met, the program calculates the shock and friction losses through the blade row and the mean direction of the exiting flow. This information is used to calculate the work done, the average total temperature, and average total pressure of the fan discharge flow.

Wave structure: A rudimentary wave structure is calculated for the flow passage between the blades. As currently formulated, a simple characteristics system for the up–wave family and down–wave families are calculated separately and then the solutions are added. For example, consider the down–wave family eminating from the compression surface (see Fig. 4). The initial strength of this shock can be calculated knowing the flow deflection angle, $\delta_1 = \alpha_1 - \theta_1$, at the leading edge of the compression surface. This wave is propigated across the channel and reflects as an up wave. The strength of this wave increases as it crosses the channel due to compression waves eminating from the curved compression surface. An emperical relationship is built into the deck to account for the strengthening of waves eminating from a compression surface, i.e. $\delta > \delta_1$. The local flow condition upstream of this first reflected wave are calculated using the method of characteristics for isentropic flow up to that point; i.e., the losses through the other shock family are neglected when calculating the flow properties upstream of this reflection. The properties across this wave are calculated using oblique shock relationships for the deflection angle, δ. The initial conditions across the reflected wave are also calculated using oblique shock relationships for the same δ. The reflected wave is then propigated across the duct, and if it were to reflect again (second reflection not shown in Figure 4), the properties upstream of this reflection point would be calculated using the method of characteristics which include the losses through the initial down shock, but neglecting the losses through the wave family eminating from the lower blade. A similar calculation is made for the up–wave family which neglects the losses through the down–wave family.

Although this wave calculation procedure is rather simplistic, it does capture the primary features of the shock wave pattern as shown by the results presented in Figure 5 for fan configuration STFF–3. This figure compares the shock deflection angles at 5 locations which are calculated by the method used in the STFF program and by a detailed method of characteristics solution. Point A, B, & C compare the δ value calculated for the up–wave family; the initial values at "A" are the same; the values at "B" were reduced by the expansions from the convex top surface, and the values at "C" were increased by compression from the concave lower surface. At both locations, the procedure used in the STFF program over corrected the change; however the maximum error was less than 1/2 deg. A similar result is shown for the down wave family at points "D" and "E". The average exit flow angles at "F", calculated by two methods

differed by one degree, after a total flow turning of about 25 deg. On the basis of results such as these, it is felt that the present wave procedure is adequate for estimating the shock losses and average flow turning through the blade row.

Limiting Conditions: While calculating the wave pattern discussed above, there are several conditions which would terminate the calculation. For initial relative Mach numbers above 1.6 (which includes most cases of interest for supersonic through-flow operation) the flow deflection angle cannot exceed that allowed by the oblique shock relationships. In addition, if a reflected wave is too strong it could separate the boundary layer and unstart the passage. A reflected shock strength limit of $\delta \leq 15$ deg was imposed to comply with this boundary layer separation limitation.

The passage area normal to the flow is calculated through the blade row. If the flow (including shock losses) would choke at the minimum area station, the calculation would be terminated.

Exit Flow Conditions: The mean flow angle used in calculating the work done by the rotor is the arithmetic average of the up-and down-wave calculation procedures discussed earlier

$$\alpha_2' = \frac{1}{2}(\alpha'_{2_{up}} + \alpha'_{2_{dn}}) \qquad \text{Eq. 13}$$

however, the shock losses calculated by the two procedures are added

$$\left(\frac{\Delta S}{R}\right)_{SH} = \Sigma\left(\frac{\Delta S}{R}\right)_{up} + \Sigma\left(\frac{\Delta S}{R}\right)_{dn} \qquad \text{Eq. 14}$$

where the symbol, Σ , implies the summation of the losses across all the shocks within the blade passage.

The boundary layer losses are calculated from

$$\left(\frac{\Delta S}{R}\right)_{BL} = C_{f_1}\frac{\gamma}{2}M_1'^2(S/A)_1 + C_{f_2}\frac{\gamma}{2}M_2'^2(S/A)_2 \qquad \text{Eq. 15}$$

where C_{f_1} and C_{f_2} are the average skin fraction coefficients based on the upstream and downstream Mach numbers M_1' and M_2' , and $(S/A)_1$, and $(S/A)_2$ are the surface to flow area ratios for the upstream and downstream portions of the blades. The total losses through the blade row are

$$\left(\frac{\Delta S}{R}\right)_{TOT} = \left(\frac{\Delta S}{R}\right)_{SH} + \left(\frac{\Delta S}{R}\right)_{BL} \qquad \text{Eq. 16}$$

and the relative total pressure ratio is

$$P'_{T_R} = e^{-\left(\frac{\Delta S}{R}\right)_{TOT}} \qquad \text{Eq. 17}$$

The relative flow area A_2'/A_1' across the blade row is

$$\frac{A_2'}{A_1'} = \frac{A_2}{A_1} \frac{\cos a_2'}{\cos a_1'} \qquad \text{Eq. 18}$$

where A_2/A_1 is the absolute flow area ratio across the blade row which is specified from the design deck. The relative exit Mach number, M_2 is calculated using the continuity equation, the relative area ratio, and the relative total pressure ratio.

$$M_1'\left(1+\frac{\gamma-1}{2}M_1'^2\right)^{-\frac{(\gamma+1)}{2(\gamma-1)}} \Big/ \left(\frac{A_2'}{A_1'}\, P'_{T_R}\right) = M_2'\left(1+\frac{\gamma-1}{2}M_2'^2\right)^{-\frac{(\gamma+1)}{2(\gamma-1)}} \qquad \text{Eq. 19}$$

All the terms are known, but M_2'; the Mach number term on the right hand side is solved to determine the relative exit Mach number. The static temperature ratio is

$$\frac{T_2}{T_1} = \frac{1+\frac{\gamma-1}{2}M_1'^2}{1+\frac{\gamma-1}{2}M_2'^2} \qquad \text{Eq. 20}$$

and the static pressure ratio is

$$\frac{P_2}{P_1} = \left(\frac{T_2}{T_1}\right)^{\frac{\gamma}{\gamma-1}} P'_{T_R} \qquad \text{Eq. 21}$$

Fan performance: The work done by the rotor is calculated using a form derived from Eq. 1

$$\frac{\text{WORK}}{h_{T_1}} = \frac{-(\gamma-1)M_R\left(M_1' \sin a_1' - M_2'\sqrt{T_2/T_1}\sin a_2'\right)}{\left(1+\frac{\gamma-1}{2}M_1^2\right)} \qquad \text{Eq. 22}$$

The ideal total pressure is

$$\frac{P_{T_{id}}}{P_{T_1}} = \left(1 + \frac{\text{WORK}}{h_{T_1}}\right)^{\frac{\gamma}{\gamma-1}} \qquad \text{Eq. 23}$$

The actual total pressure is

$$\frac{P_{T_2}}{P_{T_1}} = \frac{P_{T_{id}}}{P_{T_1}} \times P'_{T_R} \qquad \text{Eq. 24}$$

The ideal work done

$$\frac{\text{IDEAL WORK}}{h_{T_1}} = \left(\left(\frac{P_{T_2}}{P_{T_1}}\right)^{\frac{\gamma-1}{\gamma}} - 1\right) \qquad \text{Eq. 25}$$

The stage efficiency is

$$\eta_c = \frac{\text{IDEAL WORK}}{\text{WORK}} \qquad \text{Eq. 26}$$

There is no work done by the stator, but there are losses which can be calculated as described above for the rotor. The overall total pressure ratio is:

$$\frac{P_{T_2}}{P_{T_1}} = \left(\frac{P_{T_2}}{P_{T_1}}\right)_{\text{ROTOR}} * \left(\frac{P_{T_2}}{P_{T_1}}\right)_{\text{STATOR}} \qquad \text{Eq. 27}$$

and the overall efficiency is still defined by Eq. 25, but the ideal work is based on the overall total pressure ratio.

An example of the supersonic through-flow performance calculated by this procedure is presented in Figure 6. This figure shows the total pressure ratio for a fixed-geometry fan configuration STFF-3 over a range of supersonic inlet and rotor Mach numbers. The design point is for inlet Mach number of 2.0, a rotor Mach number of 1.5, and a total pressure ratio of 2.5. Operation at higher wheel speeds provides greater compression, and lower wheel speeds less compression. When operating at the design rotor Mach number of 1.5, the minimum inlet Mach number is 1.5; thus, the relative flow angle, α_1, at this condition is 45 deg. The mean chord angle β_1 is 36.9 deg. Thus, the blade angle-of-attack; ϵ_1, is 8.1 deg. Since the leading edge half angle its 4 deg, the strength of the down-shock is 12.1 deg. This shock is increased to approximately 14 deg where it reflects from the expansion surface. This reflected shock strength just

passed the boundary layer separation criteria which was $\delta < 15$ deg. Operation at a lower inflow Mach number, at a higher incidence angle, would not pass this limiting criteria. The range of calculated points show the operating range as limited by the boundary layer separation criteria, except at the upper end of the higher rotor speeds, since no calculations were made above Mach 2.2.

The fan efficiency for this configuration is shown in Figure 7. The maximum efficiency at each rotor speed is near the inlet Mach number where the relative flow angle is near the design incidence angle of 36.9 deg. The fan exit Mach number is shown in Figure 8. Note that there is a significant increase in the flow Mach number across the blade row; the increase is greater at higher rotor Mach numbers.

3.2 Transonic Fan

Early on in the study of supersonic fans it became evident that it would be highly desirable to operate the supersonic fan with subsonic inflow conditions during start up or when flying at subsonic velocities. When operating at with subsonic inflow conditions, it is theoretically possible to accelerate the flow to supersonic velocities and generate significant total pressure ratios; however, the high velocity exit flow would have to be diffused to subsonic velocities to be utilized effectively in a turbo–fan engine. The additional losses associated with this deceleration would degrade the cycle efficiency. It was concluded that it would be highly desirable to operate in a mode similar to that suggested by Boxer (3); that is, utilize a variable pitch fan which could operate with subsonic inlet flow up to some low supersonic Mach number (about Mach 1.5) and than transit to supersonic inflow conditions. Here, the author differs from Boxer, who proposed that the flow would be decelerated inside the fan stage to subsonic velocities. Efficient deceleration of this flow does not appear feasible; however, efficient acceleration of the flow is possible. That is, the fan should transit to supersonic through–flow operation as discussed in the previous section. In order to evaluate the subsonic inflow or transonic mode of operation, the UTRC supersonic through–flow computer program was extended (with corporate funding) into this operating range. The procedures used to model this flow are discussed in the next section.

Flow Modeling. – The word "transonic" is used herein to the refer to those initial condition where the absolute inflow is subsonic, but the relative inflow (after vectorially subtracting the rotor speed) is supersonic. These are the conditions under which conventional fans operate. A state–of–the–art fan may operate with subsonic inflow velocity, of $M_1 = .6$ and a tip speeds of $M_R = 1.5$. At such condition, the relative Mach number, $M'_1 = 1.6$. The relative supersonic flow is decelerated through the blade row to a subsonic exit velocity; this is accompanied by a substantial increase in the static pressure. The transonic fan analysis described herein is a relatively simple procedure, intended to characterize the essential features of this flow without getting into detailed CFD calculations.

The flow model assumed for this analysis is shown in Figure 9. The supersonic relative flow, M_1', into the blade row is decelerated through a strong shock to a subsonic velocity, this flow is further diffused and turned to the exit condition. The analysis takes into account the following features listed on the right of the figure which are discussed below.

Incoming flow adjustment: Because the incoming flow is subsonic, it can be influenced by the presence of the fan. The program calculates a critical inflow velocity which is related to the rotor speed. Because the incoming flow is subsonic and the relative flow is supersonic, the rotor will generate a characteristic wave from the leading edge of the rotor which will propigate forward into the oncoming flow. If the surface angle near the leading edge of the expansion surface is misalligned with the flow, a shock or expansion wave will be generated, and this up–wave will propigate upstream. A series of shock waves eminating from the rotor blades would decelerate the incoming flow, increasing the relative flow angle, α'_1, which decreases the strength of the forward propigating shock, this process would continue until the incoming relative flow is alligned with the initial expansion surface of the blade. Conversely, a series of expansion waver eminating from the rotor blades would accelerate the incoming flow, decreasing the relative flow angle until the relative flow as also alligned with the initial expansion surface of the blade.

The equilibrium or critical incoming Mach number which satisfies this flow angularity criterion is

$$\text{CRIT } M_1 = \frac{-M_R}{\tan\theta} \qquad \text{Eq. 28}$$

when θ in the average surface angle near the leading edge of the expansion surface (for an absolute flow direction $\alpha_1 = 0$).

When operating with subsonic exit flow, it is assumed that high back pressure conditions could force the strong shock to become detached, sending weak waves into the incoming flow, decelerating it to a lower equilibrium velocity. In order to accommodate this condition a minimum or stall velocity is calculated which assumes a maximum flow misallignment of 0.2 radians

$$\text{STALL } M_1 = \frac{-M_R}{\tan\ (\theta + .2)} \qquad \text{Eq. 29}$$

Solutions in the transonic flow regime with subsonic outflow are permitted between the stall and critical inlet Mach numbers.

Strong shock: A single strong oblique shock is assumed to be stabilized in the flow passage by back pressure conditions imposed upon the rotor. This shock is probably not planar, and the conditions along this shock would not be uniform. The flow losses across this wave may vary from those for a normal shock to those for sonic downstream flow; the latter having slightly less losses. Presuming that the downstream conditions may be adjusted to minimize the shock losses and the occurrance of boundary layer separations, the conditions picked for this strong shock wave were those at the maximum deflection angle. At this condition, the downstream Mach number is slightly less than 1 and the static pressure rise across the wave is somewhat less than that for a normal shock. For example, at $M_1' = 1.6$ the static pressure rise through a normal shock would be, $\Delta P/P = 1.82$, compared to a value $\Delta P/P = 1.32$ at the maximum deflection condition. Although the boundary layer may be in trouble with the lower pressure rise, it would probably separate with the higher value. A maximum static pressure rise $\Delta P/P = 1.4$ was set as a limit for boundary layer separation. This limiting value of the static pressure rise limits the relative inflow Mach number M_1' to approximately 1.65.

Boundary layer losses: Two kinds of boundary layer losses are included in this procedure: the skin friction losses, per se, which are calculated in the same manner used for the all-supersonic flow (see Eq. 15). In addition, there is assumed thickening of the boundary layer near the shock intersection as shown in Figure 9. This thickening acts like a blockage reducing the effective minimum area when checking for choking conditions, and it is considered to be a cause of additional subsonic diffusion losses discussed in the next section.

Subsonic diffusion losses: The flow downstream of the strong shock is near sonic velocity. Typically, the flow area downstream of the shock increases, the flow is diffused to a lower velocity, and the

pressure increases. This subsonic diffusion is treated like a subsonic diffuser having a loss coefficient which is the sum of three effects. The first is the effect of incidence angle

$$\lambda_1 = c_1(\alpha_1' - \theta_1) \qquad \text{Eq. 30}$$

This loss coefficient is assumed to be proportional to the difference between the relative flow angle and the initial expansion surface. Increasing angle of attack increases the loss coefficient; incidentally, it does not become negative when $\alpha_1' < \theta_1$, then $\lambda_1 = 0$.

The second, is the effect of turning or blade camber

$$\lambda_2 = c_2|\beta_2 - \beta_1|(b/c)\cos\beta_c \qquad \text{Eq. 31}$$

This loss coefficient is assumed to be proportional to the absolute magnitude of the total turning, $|\beta_2 - \beta_1|$ times the height–to–length ratio of the passage, $(b/c)\cos\beta_c$.

The third is the effect of the boundary layer distortion caused by the static pressure increase across the shock.

$$\lambda_3 = c_3\left(\frac{\Delta P}{q}\right)^2_{SHOCK} \qquad \text{Eq. 32}$$

This loss coefficient is proportional to the square of the pressure coefficient across the shock, $\Delta P/q$.

These loss coefficients are used in the following manner to estimate the subsonic diffusion losses.

$$\left(\frac{\Delta S}{R}\right)_{SUB} = (\lambda_1 + \lambda_2 + \lambda_3)\left(\frac{\gamma}{\gamma - 1}\right) \ln\left(\frac{T_2}{T_R}\right) \qquad \text{Eq. 33}$$

where T_2 is the average static temperature of the flow at the exit of the blade passage after diffusion and T_R is the average static temperature after the oblique shock. It should be noted that the actual losses depend on this temperature ratio which is related to both the shock and exit Mach numbers. For a passage having little diffusion the exit velocity is high, T_2 is slightly greater than T_R, and the losses are small; however, for a passage having a large increase in area, the exit velocity is low, T_2 is increased and the losses are increased. This equation is used in an iterative manner with the procedure used to calculate the exit Mach number (Eq. 19). This above expression (Eq. 33) is also used for an all subsonic condition in which there is no shock; then T_R is set equal to the static temperature of the incoming subsonic flow.

Flow turning: For this subsonic outflow condition the mean flow angle is assumed to be equal to the local surface angle at the training edge of the compression surface.

Limiting conditions: Various limits were identified during the previous discussion. They are summarized here

- Stall M_1 and critical M_1
- max $\Delta P/P$ across strong shock
- **Choking at minimum effective area.**

Exit flow conditions: The exit flow conditions are calculated using the manner (using Eq. 17–21) discussed previously for the all supersonic fan; with minor additions to the equations for calculating the flow losses to include subsonic diffusion losses

$$\left(\frac{\Delta S}{R}\right)_{TOT} = \left(\frac{\Delta S}{R}\right)_{SH} + \left(\frac{\Delta S}{R}\right)_{BL} + \left(\frac{\Delta S}{R}\right)_{SUB} \qquad \text{Eq. 34}$$

Fan performance: The fan performance is calculated in the same manner, (using Eq. 22–26) discussed previously for the all supersonic fan. This calculation procedure was developed to be an extension of the supersonic–through–flow procedure into the transonic operating regime of conventional fans. The performance of conventional compressors is usually presented in terms of the corrected airflow, Wc, and the corrected wheel speed Nc or corrected rotor velocity Vc. These corrected parameters are related to the Mach number parameters used in the program calculation procedure by the following relationships.

$$\frac{Wc}{A} = \frac{W\sqrt{\theta}}{A\delta} = 85.37M_1\left(1+\frac{\gamma-1}{2}M_1^2\right)^{-\frac{1}{2}\left(\frac{\gamma+1}{\gamma-1}\right)} \qquad \text{Eq. 35}$$

and

$$V_c = \frac{V}{\sqrt{\theta}} = 1117\left|\frac{M_R}{\sqrt{1+\frac{\gamma-1}{2}M_1^2}}\right| \qquad \text{Eq. 36}$$

where $\theta = T_T/T_{REF}$, $T_{REF} = 519R$

$\delta = P_T/P_{REF}$, $P_{REF} = 14.7psi$

To be consistent with the nomenclature used by the compressor community, some conversion subroutines were added to the deck to enable there variables to be specified independently.

Transonic performance comparison. – The transonic analysis described above was developed to provide a relatively simple way for estimating fan performance in the complex transonic flow regime without resorting to a complicated CFD analysis. It was hoped that this procedure would capture the

essential features of the flow and predict the correct level of fan performance. This procedure was checked out by using it to predict the performance of an experimental fan whose performance was known, and the results are compared herein. The fan designated TS27 was tested at P&W under the energy efficient engine program (Ref. 15) which was sponsored by NASA. The actual fan had a hub/tip ratio of .34, and was designed to provide a total pressure ratio of 1.72 at the design rotor speed N_D having a corrected tip velocity, V_c = 1463 ft/sec, and a fan corrected weight flow per unit area, Wc/A = 42 lbs/sec/ft^2. The measured performance of this fan is presented in Figure 10.

The present transonic calculation procedure was developed to estimate the mean line performance of a fan having a high hub–to–tip ratio. The ST27 fan is certainly not that; therefore, it was decided to model the outer portion of the fan and assumed that the mean–span performance calculated for a section was representative of the overall fan performance.

The mean blade shape used for this example is shown in Figure 11. It is the blade shape given at the 85% span location of the TS27 fan. It had very little overall camber, near zero turning over the slender front portion and a few degrees of down turning over the rear portion. In addition to specifying the blade shape it was also necessary to specify the amount of contraction of the flow passage. A local area ratio of .75 was assumed for this calculation. The total pressure ratio which was calculated for the specified geometry is presented in Figure 12. The performance is in general agreement with the measured performance shown in Figure 10; the critical weight flow and knee of the total pressure ratio curves are in good agreement; but the throttled performance (lower Wc/A) has a higher slope than the measured data. Although not shown, the fan efficiencies are also in general agreement, ranging from about 85% to 92% at the knee of the curve at the design speed. The amount of agreement shown here was as much as should be expected for such a limited representation of the actual hardware. These results indicate that the simple procedures used model the essential features of the flow.

3.3 Subsonic–to–Supersonic Fan

Calculations were made to evaluate the performance capabilities of a fan (designed for supersonic through–flow) over the entire speed range from subsonic to the supersonic operating conditions. The fan geometry used for these calculations was configurations STFF–4 shown in Figure 13. It had a pressure ratio of 2.4 at an inlet Mach number of 2.0 and a rotor Mach number of 1.5. The rotor geometry for this fan was fixed but the stators were assumed to have variable pitch capability in order to provide the fan with a means for accommodating the wide range of flow conditions. The fan performance calculated for this fixed rotor configuration is shown in Figure 14. The supersonic performance is similar to that presented previously. The subsonic performance which survived the various limiting criteria is mainly that for the all subsonic case, i.e. where the relative inlet Mach number was also less than 1; there were only two points in the transonic operating range which survived. There were so few solutions in this (high subsonic inflow) region because of the low pitch of the rotor blades (see Fig. 13). For most of the cases in this region the relative angle of attack was too high, the required deflection angle exceeded the limiting criteria, and the cases were terminated. For the remaining cases, which were calculated through the rotor, the stator choked, terminating the calculation and for the two cases which survived (at a rotor Mach number of 0.9 and inlet Mach numbers of 0.9 and 0.95) the flow conditions were just within the limiting wave deflection conditions which were built into the program. Slightly more stringent conditions would have eliminated these two points as well, leaving this map with a void of operating conditions over the inlet Mach number range from 0.6 to 1.0.

Conventional compressors operate in this transonic regime, and as shown previously, the program described herein will predict performance in the transonic regime for blades having a higher pitch (see Fig. 12) which allow a higher rotor speed. Thus, the performance of configuration STFF 4 was calculated assuming a variable–pitch rotor and stator configuration, to investigate the performance potential when the blades could be aligned with the flow over inflow velocities ranging from subsonic to supersonic speeds. For the transonic operating conditions, the rotor and stators were varied to have an incidence angle, ϵ_1 , of 4 deg. The results are shown in Figure 15. With the variable pitch rotor blading, solutions to the transonic flow condition were obtained for inflow Mach numbers ranging from 0.4 to 0.9. Furthermore the amount of compression available with this strong shock mode of operation is quite high. Total pressure ratios between 3 and 4 appear feasible during operation at supersonic rotor velocities comparable to those used in state–of–the–art compressors.

The supersonic through–flow performance of this configuration is also very interesting; the total pressure ratio is relatively flat with inlet Mach number. This is because the amount of flow turning generated by the blades is relatively independent of the inlet velocity—it is primarily a function of the camber of the rotor blade. Thus the work done (Eq. 1) is mainly a function of the rotor speed. Note the change in the level of performance between subsonic and supersonic operations. Greater total pressures are generated when operating in the subsonic outflow mode. This is because more work is done when the exit flow velocity is subsonic. The low end of the supersonic inflow speed range could be increased by increasing the incidence angle of the rotor blades; but within the range of initial strength permitted, these points could not be raised as high as the transonic points with subsonic outflow.

There is nothing of particular note about the efficiencies of these data; they are mainly in the mid 80's; however the flow discharge angle leaving the stator is very large for the transonic cases as shown in Figure 16. An extremely large amount of swirl is left in this subsonic exit flow; some additional blading would be required to eliminate this problem. As shown, the swirl for the supersonic through–flow cases is small.

This mode of operation allowing the fan to have variable–pitch rotor and stator, enabling it to operate over the speed range from subsonic to supersonic inflow velocities, was selected for the fans

designed from the Mach 2.32 supersonic transport and Mach 2.5 fighter. The performance of the variable pitch fan configuration STFF-8 used for these applications is presented in the section which discusses the supersonic transport applications.

3.4 Variable–Pitch, Split–Blade Fan

The variable–pitch rotor and stator configuration described above had two major difficulties which were not solved in time to impact the fan performance generated for supersonic transport and supersonic fighter studies. The first is the mechanical problems of rotating the large chord blades, and the second is large amounts of swirl left in the subsonic exit flow of the transonic cases.

The mechanical problems include: (1) the geometric constraints imposed when rotating a large chord blade in a converging annular passage, (2) the blade stresses which would result when large chord blades extend considerably beyond the circular root structure, (3) the means for attaching the blade, and (4) providing a mechanism for rotating the variable–pitched rotor blade. A mechanical investigation of these problems would be a substantial study all on its own and is not the subject of this aerodynamic evaluation. However these problems were realized and various means for alleviating them were considered. A configuration which appears to solve, or at least reduce the mechanical and aerodynamic problems associated with a variable–pitch fan, is a split–blade fan in which the rotor and stator bladers are each composed of two blades which provide the same overall chord and camber as a single blade. Such a variable–pitch spit–blade configuration, VPRS–1, is shown in Figure 17. It was derived from the single blade configuration, STFF–4, discussed previously. The front portions of each of these blade sets is rotatable and the rear portion is fixed. For the rotor, the variable portion is only 40% of the original blade length, this would greatly reduce the attachment problem, the blade stress problem, and the geometric constraints. It also reduces the swirl problem because the exit flow is turned nearly axial by the fixed aft stator blade.

A schematic diagram showing the rotor blade geometries for various operating conditions is shown in Figure 18. The middle set of rotor blades shows the configuration at the supersonic design condition with the front and aft blades are aligned (as shown previously in Fig. 17) to provide the flow geometry needed at this supersonic inflow condition. The front blade is rotatable, and can be aligned with the incoming (relative) flow direction as shown in the upper (transonic) and lower (high–speed) blade sets.

At the high–speed, condition, the front and aft blades are nearly parallel and the flow passes through with little flow turning or velocity change. Little or no work is done at this high–speed (windmilling) condition.

At the low–speed, transonic condition, the front blade is rotated considerably to be aligned with the flow when the incoming flow is subsonic ($M_1 = 0.8$) and the relative flow is supersonic ($M_1' = 1.6$). At this condition, the front blades act like a "conventional" high speed fan; a strong shock (shown by dashed line) forms in the blade row, the flow is decelerated to subsonic velocity, and a substantial static pressure rise is realized. The aft blades are at a considerable angle to the front blades; they now act like a slotted wing flap to do additional turning on the subsonic flow. At this condition there is substantial flow turning and substantial static pressure rise. A large amount of work is done on the flow and there is a substantial increase in the total pressure of the incoming air flow. A variable–pitch, split–stator (also shown in Fig. 17) is required to accommodate the large range of flow angles leaving the rotor. This stator blading acts in a similar manner; the blades would be oriented to do little turning at the high speed condition and a large amount of turning at the low speed condition.

Theoretical calculations were made to evaluate the performance potential of this configuration. The results, shown in Figure 19, present the total pressure ratio generated for both the transonic (subsonic inflow) and supersonic through–flow operating regimes. Note that the speed lines (for a given rotor Mach number, M_R, are not continuous between the subsonic and supersonic inflow operating conditions; however, it is possible to jump from one to the other by changing fan exit flow conditions. As shown in this

figure this variable–pitch split–blade fan configuration has the potential for producing extremely large pressure ratios at subsonic and low supersonic speeds, dropping off at higher supersonic speeds to the windmilling condition at incoming flow Mach numbers above these shown in this figure. This is the type of a total pressure ratio variation that is desired for an advanced engines; high at low speeds, and gradually reducing at the high speeds where total pressure generated by the high speed flight is sufficient to provide good engine performance.

The variable–pitch, split–rotor/split–stator acts like a variable–camber blade, enabling it to accept a wide range of inflow velocities. It also offers the unique capability at subsonic speeds to combining the capabilities of a conventional fan plus an "aft" flap for additional flow turning. It also offers structural advantages; the short front movable blade would be lighter and easier to move than a single blade having a chord equal to the sum of the two blades.

This type of blading was assumed for the fans used in the air–turbo–rocket engine study for the Mach 5 cruise vehicle discussed in the next section. The fan performance used in this study is presented subsequently in the sections which discusses the Mach 5 cruise vehicle applications.

4.0 STFF APPLICATIONS

Four potential applications for the supersonic through-flow fan were selected for analyses. They included a supersonic transport, an advanced tactical fighter, a supersonic inter-continental cruise missile; and a hypersonic cruise vehicle. Each application has a significant supersonic flight requirement where the supersonic through-flow fan should be attractive. Previous analysis of these applications had determined appropriate conventional propulsion systems, vehicle aerodynamics, and system weights which can achieve the specified mission. Alternative engines with supersonic through-flow fans were formulated in this study. Appropriate inlet and nacelle characteristics were then selected for each alternative engine in order to establish installed engine performance and weight. Improvement in mission performance or vehicle weight was determined for each application.

4.1 Supersonic Transport

The supersonic transport selected for analysis in this study was the Langley - LTV arrow wing vehicle described in NASA CR-132374 (Ref. 16). Its nominal performance characteristics include Mach 2.7 cruise, 4000 nm range, and 292 passenger payload. The vehicle design was developed under the NASA Supersonic Cruise Airplane Research (SCAR) program and was used for various advanced propulsion system studies. During Phase III of the NASA sponsored Advanced Supersonic Propulsion Study (Ref. 8), Pratt & Whitney concluded that the Variable Stream Control Engine (VSCE) was the most promising concept for advanced commercial supersonic aircraft. That engine concept, referred to as the VSCE-502B, was updated to reflect year 2000 technology and used to establish a conventional fan engine baseline. Various unconventional engine concepts were also considered in the Advanced Supersonic Propulsion Study; among them, the supersonic fan engine. Analysis at that time indicated no advantage for the supersonic fan engine; however, only approximate component performance levels were available. In the current study, the supersonic fan engine performance estimates were revised using the fan analysis described herein and year 2000 technology.

Conventional engine. - The conventional engine evaluated for the supersonic transport is a two-spool turbofan with the bypass (duct) stream augmented. A schematic diagram of the conventional engine and the supersonic-fan engine is shown in Figure 20. This engine incorporates a two-stage fan, a five-stage high pressure compressor, a one-stage high-pressure turbine, and a two-stage low-pressure turbine. This engine configuration and cycle characteristics (fan pressure ratio, bypass ratio, overall compression ratio, and combustion temperature) were optimized in earlier supersonic transport studies (Ref. 8). The inlet for the conventional fan engine is a Mach 2.32 mixed compression design with external compression below Mach 1.6. Installed engine performance includes inlet additive drag, five percent boundary layer bleed, and nacelle friction drag. Because of the highly integrated installation, no attempt was made to estimate cowl pressure or nozzle boat-tail drags. Table 1 summarizes the cycle and performance characteristics at the sea level static and Mach 2.32 supersonic cruise conditions.

TABLE 1. - SST CONVENTIONAL ENGINE CHARACTERISTICS

Altitude, Ft.	0	57,000
Mach Number	0	2.32
Fan Inlet Corrected Airflow, lb/sec	858	639
Fan Pressure Ratio	3.3	2.5
Bypass Ratio	1.3	1.5
Overall Compression Ratio	20	12
Combustor Temperature, R	2700	3260
Inlet Ram Recovery	1.0	0.93
Fan Efficiency, %	89	89
High Turbine Efficiency, %	92	93
Low Turbine Efficiency, %	93	92
Net Thrust (Dry Power), lbs	46,700	14,390
Specific Fuel Consumption, lb/hr-lb	0.578	1.191
Inlet Capture Area, ft_2	28.3	28.3
Inlet/Nacelle Drag, lbs	0	1910
Installed Net Thrust, lbs	46,700	12,470
Installed TSFC, lb/hr-lb	.578	1.373

Supersonic through-flow fan engine. - The supersonic through-flow fan (STFF) engine shown in Figure 20 is also a two-spool turbofan engine. A single stage supersonic fan replaces the two-stage subsonic fan of the conventional engine; a fixed-geometry supersonic diffuser is located downstream of the fan to provide subsonic flow into the high-pressure compressor; and the core stream is afterburned to provide thrust augmentation. The following sections present the fan performance characteristics of the STFF engine.

Fan performance: The supersonic through-flow fan for the STFF-SST engine was designed to provide a pressure ratio of 3.5 at the 57,000 ft, Mach 2.32 cruise condition. At this flight condition the local Mach number at the fan face is approximately Mach 2.0 and the local sound speed is approximately 1000 ft/sec. A mean rotor velocity of 1500 ft/sec was selected for this design point. For this mean velocity and a rotor having a hub-to-tip ratio 0.5, the tip velocity would be approximately 1900 ft/sec. This tip velocity, although high, was considered feasible for year 2000 technology.

The supersonic fan chosen for this application (STFF-8) was designed for a fan-face Mach number of 2.0 and a mean rotor Mach number of 1.5; the design total pressure ratio was 3.5 with a static pressure ratio of 1.0. The blade chord was calculated for a two-shock wave cancellation on the expansion surface (see section 3). This resulted in the blade shapes shown in Figure 21. The leading and trailing mean camber angles at the design condition are shown in the figure. The total turning of the rotor was 33.5 deg and the stator 28.4 deg. The gap/chord of the rotor was .337 and the stator .276. The flow-passage area ratio of the rotor was .826 and the stator .885. The blades were assumed to be rotatable so that the blades could be aligned with the flow at off-design conditions. With such high solidity in a contracting passage, rotation of the entire blade may not be feasible, as discussed in the previous section, and a split-

blade configuration in which only part of the blade rotates may be more practical. At the time this study was done, the split-blade configuration could not be analyzed. Therefore, the performance of a variable-pitch single blade configuration was calculated to be representative of what might be obtained with variable-pitch, split blading. The subsonic inflow performance of this configuration in presented in Figures 22 and 23 using conventional fan notation; i.e. total pressure ratio and fan efficiency are plotted as a function of the corrected weight flow per unit area, Wc/A, and a corrected mean wheel speed, Vc. This fan map looks different from that for a conventional fan because the variable-pitch blading allows the blade to be aligned with the flow, thereby avoiding compressor stall over a wide range of weight flows. The supersonic performance of this configuration is presented in Figures 24 & 25 as a function of the inflow Mach number, M_1, and the mean rotor Mach number, M_R. Also shown in this figure are the values of the corrected flow per unit area for these supersonic inflow conditions. Note that the Wc/A scale is decreasing, covering the same range of values used for the subsonic inflow conditions. Because this might give rise to an ambiguity, all the supersonic through-flow performance is plotted on a function of the fan inlet Mach number.

Engine-characteristics: The STFF engine (see Fig. 20) includes a fixed-geometry inlet, a single-stage supersonic through-flow fan, an aft fixed-geometry supersonic diffuser to decelerate the core flow into a conventional five-stage high-pressure compressor, a one-stage high-pressure turbine, a two-stage low pressure turbine, a core afterburner, and a variable convergent-divergent (C-D) nozzle. The performance of these components and the integration of these components into a conceptual STFF engine are described herein.

The inlet for the STFF engine is a 16-deg half-angle cone. The inlet total pressure recovery and airflow characteristics are shown in Figure 26. This figure shows the flow characteristics for both the subsonic and supersonic modes of operation. The inlet and fan were assumed to operate in the supersonic mode from the design condition ($M_0 = 2.32$) down to a Mach number of 1.3, and accept the supersonic flow generated by the inlet. At lower flight speeds the fan was operated in the subsonic mode; at low supersonic speeds ($M_o = 1.0 - 1.3$), the fan limited the flow and forced a normal shock upstream of the fan face; the shock decelerated the flow to subsonic velocities at the fan face. Over this narrow range of velocities the local Mach number on the conical forebody is near one, and the total pressure losses across this normal shock are insignificant.

The STFF fan inlet corrected airflow is shown in Figure 27. During supersonic operation the corrected flow is set by the inlet; as shown during subsonic operation, the flow was scheduled to achieve a fan inlet specific flow of 42 lb/sec/ft^2 at a flight $M_o = 0.9$. Figure 28 shows how the fan inlet and exit flow Mach numbers vary with flight Mach number. Note that during supersonic operation the fan face Mach number varies from 1.2 to 2.0; the fan accelerates the flow; and the exit Mach number varies from 2.2 to 2.8. During subsonic inflow operation, the fan face Mach number varies from 0.6 to 0.9 while the exit Mach number is approximately a constant 0.4 Mach number. The fan pressure ratio schedule is shown in Figure 29. The fan is operated at a pressure ratio of 3.57 at the Mach 2.32 condition, it drops off only slightly down to 3.5 at the transition Mach number of 1.3 and remains constant through the transonic speed range, and drops off at lower subsonic flight speeds. The conventional fan maintains a neary constant total pressure ratio of 3.3 up to a flight Mach number of 1.42, and then drops off to a value of 2.5 at the supersonic cruise condition. Figure 30 shows the fan operating lines for both engines. For the conventional fan engine, the fan pressure ratio is reduced as corrected airflow is lowered to maintain adequate stall margin. For the supersonic through-flow fan, flow and pressure ratio have a similar operating line at subsonic flight conditions. During supersonic flight, however, the fan can operate at a fan pressure ratio greater than 3.5 to provide the increased thrust.

The fixed-geometry supersonic diffuser aft of the fan acts like a second inlet to provide subsonic flow to the high-pressure compressor. This diffuser is designed at the Mach 2.32 flight condition (fan exit

Mn = 2.8) to capture 55% of the total fan exit flow. Of this flow, ten percent is then bled off to control the shock–boundary–layer interaction. The total pressure recovery and flow characteristics of this diffuser are shown in Figure 31. As shown in this figure, the fraction of fan flow delivered to the high pressure compressor varies from 50% at the Mach 2.32 design point down to 40% at the transition Mach number. The core engine was designed to accept the flow delivered by this diffuser at these two flight conditions. In between, an additional amount of bleed is required to match the flow requirements of the high compressor. Figure 32 shows the diffuser bleed flow requirements during supersonic operation of the STFF engine.

High pressure compressor operating lines for the conventional and supersonic–fan engines are illustrated in Figure 33. The STFF engine's high compressor operates at it's maximum airflow and pressure ratio at the Mach 1.3 flight condition, which corresponds to the maximum fan inlet corrected airflow (as shown in Fig. 27).

The overall compression ratios (OPR) for the STFF and conventional fan engines are shown in Figure 34. The amount of compression was restrained to keep the maximum high compressor discharge temperature below the 1860 R goal for engines with a technology availability date of 2000. For the conventional engine, the fan and high compressor operating points are held fixed below Mach 1.42. Above Mach 1.42, as fan airflow is reduced, fan pressure ratio is reduced to maintain a constant corrected flow into the bypass duct while the high compressor pressure ratio and corrected flow is reduced. This causes the overall compression ratio to drop from 20 to 12 at the Mach 2.32 cruise condition. Because the high compressor corrected flow is reduced at higher Mach number while the bypass duct flow is held constant, the bypass ratio increases from 1.3 (at low speed operation) to 1.5 at the cruise condition, as shown in Figure 35. For the STFF engine, the bypass ratio (based on the flow to the inlet of the high compressor after the diffuser bleed is removed) is lowered as flight Mach number is increased. Between Mach 0.0 and 1.3 the BPR is reduced slightly because of the increased corrected airflow to the high compressor (Fig. 33). Between Mach 1.3 and 2.32, the fan pressure ratio is held nearly constant, while the fan inlet corrected flow is reduced. This causes the fan exit corrected airflow to be reduced faster than the high compressor inlet flow as illustrated in Figure 36. This reduces the bypass ratio.

The variation of the combustor exit temperature (CET) with flight speed for both the conventional and STFF engine is shown in Figure 37. The maximum combustor temperature (at cruise) for the STFF engine is 3155 versus 3260 for the conventional engine. This lower temperature plus the lower bypass ratio results in a lower thrust specific fuel consumption for the STFF engine.

As shown previously in Figure 29, the pressure ratio across the STFF fan is kept at a high value (3.5) over the entire range of supersonic flight speeds. To maintain a fixed pressure ratio, the fan work must be proportional to the total temperature associated with the flight speed. In order to provide increased power to the fan, the core stream exhaust nozzle area is opened, as shown in Figure 38, to increase the low turbine expansion ratio and work output. As flight Mach number is raised from 1.3 to 2.32 the exhaust nozzle area is increased from 1060 in. to 1490 in. Correspondingly, the low turbine expansion ratio is raised from 3.09 to 4.34. The conventional engine is operated with a fixed core nozzle area of 840 in. up to Mach 2.1 to achieve the desired inlet flow schedule. The nozzle is then opened to 920 in. at Mach 2.32. The low turbine expansion ratio varies from 3.03 at Mach numbers below 2.1 to 3.24 at Mach 2.32.

Table 2 summarizes the STFF engine cycle characteristics and component and engine performance at the sea level static and supersonic cruise conditions. The supersonic fan allows the engine to be matched to a higher fan pressure ratio as flight Mach number is increased, while the supersonic diffuser behind the fan increases flow to the compressor as Mach number is increased, thereby reducing the

bypass ratio. These characteristics increase the intermediate (dry) power specific thrust at the supersonic cruise condition.

TABLE 2. – SST SUPERSONIC FAN ENGINE CHARACTERISTICS

Altitude	0	57,000
Mach Number	0	2.32
Fan Inlet Corrected Airflow, lb/sec	960	670
Fan Pressure Ratio	3.09	3.57
Bypass Ratio	**1.54**	1.035
Overall Compression Ratio	15.9	11.5
Combustor Exit Temperature, R	2900	3155
Main Inlet Ram Recovery	1.0	0.989
Supersonic Diffuser Recovery	.92	.86
Boundary Layer Bleed,% Core Flow	10	10
Fan Efficiency, %	79	86
High Compressor Efficiency, %	85	89
High Turbine Efficiency, %	92	93
Low Turbine Efficiency, %	92	93
Low Turbine Expansion Ratio	3.3	4.2
Core Stream Nozzle Area, in^2	1162	1493
Net Thrust Intermediate Power, lbs	49,700	17,430
Specific Fuel Consumption, lb/hr–lb	0.640	1.191
Inlet Capture Area, ft^2	29.93	29.93
Inlet/Nacelle Drag, lbs	0	654
Installed Intermediate Net Thrust, lbs	49,700	16776
Installed TSFC, lb/hr–lb	0.640	1.237

Vehicle Mission Analysis. – The conventional and supersonic fan engines were installed on the Langley – LTV arrow wing supersonic transport and evaluated on a typical supersonic cruise mission. The mission profile (shown in Fig. 39) includes a 15 min ground idle, acceleration to climb speed, climb/accelerate to a subsonic cruise speed of Mach 0.9 at 27,500 ft, cruise for 300 nm, climb/accelerate to a supersonic cruise speed of Mach 2.32 at 57,000 ft, and cruise on remaining fuel, less reserves. No range or fuel flow estimates were made for the descent portion of the mission. Fuel reserves included an in route contingency of five percent of mission fuel, 260 nm diversion at best nm/lb of fuel, and a 30 min hold at 15,000 ft at min TSFC. Vehicle takeoff gross weight was held constant at 762,000 pounds by varying the fuel load to compensate for changes in inlet, nacelle, and engine weight.

Engine size was adjusted to meet all mission requirements and achieve maximum range. The takeoff field length requirement was held at 10,500 ft which required a 0.28 takeoff thrust to weight ratio. One of the unique features of the VSCE engine is its ability to achieve reduced sideline jet noise by augmenting the bypass stream and establishing an inverse velocity profile. It has been reported that up to 8 dB of noise attenuation can be achieved if the outer stream velocity of two co–annular jets is sufficiently greater than that of the inner stream (Ref. 6). Since the supersonic fan stream can't be augmented to achieve an inverse velocity profiles, noise requirements must be achieved through reduced thrust per pound of air-

flow. This results in a 960 lb/sec minimum flow size for the supersonic fan engine, while the VSCE requires a flow size of only 780 lb/sec to meet takeoff field length and sideline noise requirements.

Figure 40 shows the variation of aircraft range with engine size for the supersonic transport mission. A range of 6140 nm is reached with the 960 lb/sec STFF engine which is the minimum size which meets the FAR 36 noise requirements. The conventional engine produces a maximum range of 5400 nm, at a flow size of 858 lb/sec which exceeds the FAR 36 noise requirements. The increased range of the STFF engine results from reduced weight and lower TSFC due to operation without augmentation during cruise as shown in Figure 41. The STFF engine is seen to be penalized by the FAR 36 noise requirement in that mission range is still increasing with reduction in engine size below the required 960 lb/sec.

Summary of results. – Table 3 summarizes the supersonic transport aircraft and engine characteristics for the conventional and supersonic fan engines. The STFF engine powered aircraft has a 14% greater range because it carries five percent more fuel (lighter engine, inlet, and nacelle) and has a nine percent better specific range, which is a result of its six percent higher inlet pressure recovery and an inlet and nacelle drag that is 34% of that of the conventional engine system. The improved inlet recovery and lower inlet nacelle drag, combined with improved engine cycle characteristics result in reduction in specific fuel consumption of 11 and 4 percent at the beginning and end of the supersonic cruise.

TABLE 3. – SUPERSONIC TRANSPORT SYSTEM SUMMARY

Engine	Conv	STFF	Δ%
Range, nm	5,400	6,140	+14
Airflow Size (SLS), lb/sec	858	960	+12
Aircraft Takeoff Gross Weight, lbs.	762,000	762,000	–
Empty Weight, lbs.	259,000	259,900	–
Payload, lbs.	61,000	61,000	–
Fuel, lbs.	381,600	400,000	+5
Inlets/Nacelles (4), lbs.	21,800	8,800	−60
Engines (4), lbs.	37,700	32,300	−14
Specific Range n. mi./lb. fuel	.01415	.01535	+9
Inlet Pressure Recovery (M_0 = 2.32)	0.93	0.989	+6
Inlet & Nacelle Drag (M_0 = 2.32), lbs.	1913	654	−66
Begin Cruise Thrust (M_0 = 2.32), lbs.	16120	16030	
Begin Cruise TSFC lb/hr/lb.	1.40	1.24	−11
End Cruise Thrust (M_0 = 2.32), lbs.	11910	11880	
End Cruise TSFC, lb/hf/lb.	1.38	1.32	−4

4.2 Mach 2.5 Fighter

The Mach 2.5 fighter is a projected early year 2000 twin engine air superiority aircraft. The aircraft model is based on a MCAIR high-altitude cruise aircraft having a low wing loading. It has an 69 deg swept, aspect ratio 2.0 wing, and a low cross-sectional, area-ruled fuselage. These characteristics would be typical of an air superiority fighter, having exceptional transonic and supersonic maneuverability and overall mission performance capable of countering the expected threat.

Conventional engine. - The conventional engine cycle characteristics for this advanced fighter were optimized in a P&W study conducted in 1983 (Ref. 7). A schematic diagram of this engine and the supersonic fan engine is illustrated in Figure 42. The conventional engine incorporates an advanced 3-stage fan, a 3-stage high compressor, and single-stage high and low pressure turbines. This engine is sized to meet the 6.5G load factor at 30,000 ft, 0.9 Mn with the engine operating with full augmentation. Table 4 summarizes cycle and max power performance characteristics for this engine at Sea Level Static, 30,000 ft, 0.9 (combat), Mn, 50,000 ft, 0.9 Mn (subsonic cruise), and 75,000 ft, 2.5 Mn conditions (supersonic cruise).

TABLE 4. - FIGHTER CONVENTIONAL ENGINE CHARACTERISTICS

Altitude	0	30,000	50,000	75,000
Mach Number	0	0.9	0.9	2.5
Fan Inlet Cor. Airflow, lb/sec	197	197	197	120
Fan Pressure Ratio	6.21	6.23	6.30	3.65
Bypass Ratio	0.19	0.19	0.19	0.278
Overall Compression Ratio	25.9	25.9	26.1	11.8
Compressor Exit Temperature, R	1460	1355	1295	1850
Combustor Temperature, R	3800	3550	3450	4060
Inlet Ram Recovery	0.97	0.97	0.97	0.930
Fan Efficiency, %	81	81	81	85
Compressor Efficiency, %	89	89	88	89
High Turbine Efficiency, %	90	90	88	90
Low Turbine Efficiency, %	92	92	91	90
Net Thrust (Dry), lbs	20,400	-	3,331	3,100
TSFC (Dry), lb/hr-lb	0.958	-	1.068	1.56
Net Thrust (Max), lbs	27,800	13,115	5,200	5,310
TSFC (Max), lb/hr-lb	1.64	1.82	1.82	2.26

Supersonic through-flow fan engine. - The STFF engine illustrated in Figure 42 is similar to the STFF engine. It is a two spool engine with a single-stage supersonic fan and a four-stage high-pressure compressor. It incorporates a fixed-geometry inlet upstream of the fan and a fixed-geometry supersonic diffuser after the fan to decelerate the core flow to the the high compressor. It has a single stage high and low pressure turbine, and a core afterburner. The supersonic fan used for this engine is the same as that employed previously for the SST and the aerodynamic performance is presented in Figures 21 through 25. For this application, the fan was operated at a 13% higher wheel speed to provide a total pressure ratio of 4.0 at the Mach 2.5 cruise condition. The overall compression ratio at the Mach 2.5 flight condition was

9.9; it was selected to limit the compressor discharge temperature to 1860R. Table 5 summarizes cycle and maximum performance characteristics at sea level static, 30,000 ft, 0.9 Mn, 50,000 ft, 0.9 Mn, and 75,000 ft, 2.5 Mn.

TABLE 5. – FIGHTER STFF ENGINE CHARACTERISTICS

Altitude	0	30,000	50,000	75,000
Mach Number	0	0.9	0.9	2.5
Fan Inlet Cor. Flow, lb/sec	247	288	288	147
Fan Pressure Ratio	3.33	4.0	4.0	4.0
Bypass Ratio	0.68	0.60	0.61	0.12
Overall Compression Ratio	13.3	17.5	17.5	9.9
Compressor Exit Temperature, - R	1211	1237	1180	1860
Combustor Temperature, - R	3320	3560	3430	4060
Inlet Ram Recovery	1.0	1.0	1.0	.987
Fan Efficiency, %	82	80	80	85
Compressor Efficiency, %	89	89	88	87
High Turbine Efficiency, %	90	90	90	90
Low Turbine Efficiency, %	92	91	90	93
Net Thrust (Dry), lbs	19,420	–	4,240	5,440
TSFC (Dry), lb/hr–lb	0.906	–	1.13	1.50
Net Thrust (Max), lbs	23,550	13,804	–	7,440
TSFC (Max), lb/hr–lb	1.53	1.67	–	1.92

Figure 43 compares the performance of the conventional and supersonic fan engines at the subsonic cruise condition. Although the STFF engine has a higher bypass ratio than the afterburning turbofan (Tables 4 and 5) at this 50,000 ft, 0.9 Mn condition, its lower overall compression ratio results in a 6% higher TSFC at intermediate power and a 5% higher fuel consumption during cruise.

Figure 45 compares performance of the two engines at the Mach 2.5 supersonic cruise condition. The STFF engine provides a 9% improvement in supersonic cruise TSFC. Since the STFF engine is operating at 70% of intermediate power at Mach 2.5, it should provide further improvements over the conventional engine at supersonic cruise Mach numbers above 2.5.

Figures 45 through 49 summarize the variations in fan airflow, fan pressure ratio, bypass ratio, overall compression ratio, and combustor temperature for the STFF and conventional engines. These variations are similar to those described in the previous section for the supersonic transport engines. The main inlet designs and recovery schedules are the same as those used in the SST analysis.

Mission analysis. – The STFF and conventional engines were installed in the Mach 2.5 fighter and flown over the mission profile specified in Figure 50. The results of this study showed the supersonic through flow fan engine powered aircraft to have a 2% lower takeoff gross weight (TOGW) than the conventional afterburning turbofan. The 2% lower TOGW for the STFF engine is due to its improved climb/acceleration, supersonic fuel consumption and lighter inlet, which offset a 32% increase in engine weight resulting from the larger fan which is required for the STFF engine to achieve the combat sustained load factor of 6.5 G's at 30,000 ft, 0.9 M.

Summary of results. – Table 6 summarizes the Mach 2.5 fighter aircraft and propulsion system characteristics for the conventional and supersonic through–flow fan engines. The 2% reduction in TOGW is due to a 7% reduction in fuel weight and a 55% reduction in inlet weight, which offset a 32% increase in engine weight.

The STFF engine does provide a 7% reduction in fuel consumption due to its improved climb/acceleration, combat and supersonic cruise fuel consumption. Since the STFF engine augments only its core stream, its maximum augmented specific fuel consumption at supersonic speeds is 7 to 15% better than that of the conventional engine. The STFF engine also produces 0 to 40% more maximum augmented thrust during the supersonic climb and acceleration. These features reduce the climb/acceleration fuel by 22%, and its combat fuel by 9%. At the Mach 2.5 cruise condition, the STFF engine has a 9% better begin–cruise specific fuel consumption which is due to its improved cycle, higher inlet pressure recovery, and non–augmented operation. This TSFC improvement combined with a 12% higher cruise aircraft L/D result in a 17% lower supersonic cruise fuel usage.

TABLE 6. – FIGHTER SYSTEM SUMMARY

Engine	Conv.	STFF	Δ%
Takeoff Gross Weight, lbs	38,070	37,250	–2
Airflow Size (30K/0.9 Mn), lb/sec	197	288	+46
30000 ft/0.9 Net Thrust (1 Eng),	13,115	13,800	
Aircraft Empty Weight, lbs	16,295	16,120	
Payload, lbs	2,200	2,200	
Fuel, lbs	14,525	13,530	–7
Engines (2), lbs'	3,580	4,730	+32
Inlets (2), lbs	1,470	670	–55
Max A/B Climb/Accel. Fuel, lbs	3,570	2,775	–22
Combat Fuel, lbs	1,620	1,480	–9
Supersonic Cruise, Fuel, lbs	3,580	2,965	–17
Subsonic Climb/Cruise/Loiter Fuel, lbs	5,755	6,310	+10
Supersonic Cruise L/D	4.72	5.28	+12

4.3 Mach 3.5 Cruise Missile

The Mach 3.5 cruise missile is a projected year 2000 single engine supersonic intercontinental cruise missile having a range of 3500 nautical miles with JP–10 type fuel. It has an overall length of 30 ft and a wing span of 15 ft. It is designed for airlaunch at M_0 = 0.6 and 30,000 ft; solid rocket boosters accelerate the missile to the cruise Mach number of 3.5 and 85,000 ft. It has a start–of–cruise gross weight of 8600 lb and carries 3400 lb of fuel.

Conventional engine. – Propulsion system cycle studies were conducted for the Mach 3.5 cruise missile to determine the optimum conventional dry turbojet cycle that satisfied the Mach 3.5 thrust and TSFC requirements. Based on a missile weight of 8600 lbs and a lift/drag ratio of 5.2, a begin cruise thrust of 1650 is required. For a missile range of 3500 n.mi. and 3400 lbs of fuel a TSFC of 1.6 is required to perform the mission.

Cycle studies were conducted to determine the impact of overall compression ratio (OPR) and combustor exit temperature (CET) on inlet corrected airflow and TSFC at Mach 3.5. Figure 51 shows that the engine airflow required for 1650 lb thrust would be increased with higher overall pressure ratios and be reduced with higher combustor temperatures. Figure 52 shows that generally the specific fuel consumption would be decreased with higher pressure ratios and be increased with higher combustor temperatures; however, the results did show a minimum TSFC at a temperature of 3040° R at an OPR = 2.75 for the maximum compressor exit temperature of 1860° R.

Figure 53 illustrates the relationships between CET, OPR, and inlet airflow at Mach 3.5 to achieve a net thrust = 1650 lbs and a TSFC = 1.60. The maximum compressor discharge temperature of 1860 R limits OPR to 2.75. The smallest engine would have an inlet corrected flow of 42.4 lb/sec and a combustor temperature of 3040 R.

Table 7 summarizes the cycle and performance characteristics for this conventional dry turbojet. This engine is comprised of a three–stage compressor and single–stage turbine.

TABLE 7. – CRUISE MISSILE ENGINE CHARACTERISTICS

Engine	Conventional Turbojet	STFF Turbofan
Altitude, ft	85,000	85,000
Mach number	3.5	3.5
Net Thrust, lbs	1650	1650
TSFC, Lb/hr–lb	1.60	1.60
Inlet Pressure Recovery	0.87	0.97
Compressor Inlet Corrected Flow, lb/sec	42.4	38.0
Compressor Inlet Actual Flow, lb/sec	37.3	37.3
Overall Compression Ratio	2.75	2.75
Compressor Discharge Temperature, R	1860	1860
Diffuser Pressure Loss, %	–	10
Combustor Exit Temperature, R	3040	3300

Supersonic Through-Flow Fan Engine. – Propulsion system cycle studies were conducted to determine the optimum non-mixed dry turbofan engine employing a supersonic through-flow fan. This study assumed the same levels of component performance as the SST application. Preliminary results indicated that a fan pressure ratio of 1.6 would produce the lowest levels of TSFC for constant compressor exit temperature of 1860 R.

Fan performance: The supersonic through-flow fan for the cruise missile was designed to provide a pressure ratio of 1.6 at the Mach 3.5 cruise condition. At this flight condition the local Mach number of the fan face is approximately Mach 3.0. A mean rotor Mach number of 1.5 was assumed for the rotor. The blade chord was calculated for a two-shock wave conciliation on the expansion surface. This resulted in the blade shapes shown in Figure 54. This fan was designated STFF-9; the leading and trailing mean chamber angles of the rotor and stator are shown in the figure. The flow passage was contracted to provide a static pressure ratio of 1.0 across the blade rows. The performance for this fixed-geometry fan is shown in Figures 55 and 56. This fan would provide slightly improved total pressure ratio below the design Mach number; and fall off at higher speeds. For this single operating point engine the off-design performance is not needed, but the capability is there, nevertheless. For example, it may be possible to increase the range by accelerating with the STFF turbojet between Mach 2.5 and 3.5, and trade off solid rocket weight for fuel weight.

Engine performance: Two turbofan engine cycle were selected for comparison with the conventional dry turbojet used for this application. The first cycle, a 0.33 bypass ratio and 2340 F CET, provided af TSFC, 5.8% below that of the conventional turbojet. In order to provide the required cruise thrust this engine required 56% higher airflow than the conventional turbojet. The large flow size required for the STFF engine would result in increased missile diameter which will increase missile weight and drag and offset the TSFC advantage.

The second cycle had a bypass rati of 0.33 and the same airflow size as the conventional turbojet. This reduced airflow size is achieved by increasing the CET to 2850 F. This engine should have a similar diameter to that of the conventional turbojet, eliminating concern over increased missile weight and drag. This cycle has a TSFC comparable to the dry turbojet.

The inlet weight for the conventional engine, is only 65 lbs, or 5.6% of the propulsion system weight. Early NASA estimates of the weight reduction of inlets for STFF engines showed a 2/3 reduction compared to the conventional mixed compression inlet. Applying this reduction to the SICM inlet results in a 43 lb weight reduction. This represents and equivalent 1.3% of the fuel weight. However, some of this weight benefit would be lost, because this engine requires a supersonic diffuser after the fan to diffuse the core flow to subsonic velocities. This diffuser would increase the weight of STFF, making the benefit even smaller. The performance characteristics of this STFF engine is summarized in Table 7.

Vehicle Mission Analysis. – The potential benefits of using a STFF engine in a Supersonic Intercontinental Cruise Missile (SICM) were investigated. The SICM is launched from a subsonic aircraft and rocket boosted to 85,00 ft 3.5 Mach number. An airbreathing engine then propels the missile at Mach 3.5 for a range of 3500 n.mi. Studies conducted by Boeing have determined that a single spool non-augmented turbojet provides the best conventinal propulsion system.

Since the SICM airbreathing propulsion system is designed for operation at Mach 3.5 only, there is no performance advantage for the STFF engine. Both the conventional and STFF engines can be designed to provide comparable performance.

Table 8 shows that a 43 lb weight reduction in the inlet will allow the fuel load to be increased by 43 lbs. This 43 lb fuel weight increase provides a 1.3% range improvement for the STFF engine. This benefit

would disappear with less optimistic assumption of component performance or increased engine weight estimates.

TABLE 8. - CRUISE MISSILE SYSTEM SUMMARY

Propulsion system	Conventional Turbojet	STFF Turbofan	Δ %
Range at Mach 3.5, n.mi.	3,500	3,545	1.3
Being Cruise Weight, lbs	8,600	8,600	
Missile Empty Weight, lbs	3,622	3,622	
Payload, lbs	400	400	
Fuel, lbs	3,356	3,399	1.3
Fuel System, lbs	392	392	
Engine, Lbs	765	765	
Inlet, lbs	65	22	
Average Cruise L/D	5.2	5.2	
Engine TSFC @ Mach 3.5	1.60	1.60	

4.4 Mach 5 Cruise Vehicle

The supersonic fan engine evaluated for this application was a hydrogen-fueled air-turbo-rocket (ATR) engine. Preliminary cycle studies were conducted to provide design information and fan performance requirements. Two fans were designed; each was installed in a conceptual engine configuration and engine performance was calculated. The STFF-ATR engine characteristics and performance was compared with an over/under subsonic ATR/ramjet configuration which was evaluated in a P&W study of advanced engines for high Mach number applications (Ref. 17).

Preliminary cycle studies. – Preliminary cycle studies were conducted to provide information needed to make design decisions before conceptualizing this engine design. There were decisions concerning the overall cycle, supersonic versus subsonic combustion, fan pressure-ratio requirements, flow area requirements, and the amount of variable geometry necessary to operate over the speed range from SLS to the Mach 5 cruise condition.

Preliminary engine configuration: The STFF-ATR engine configuration evaluated in these studies is shown in Figure 57. The engine had a fixed conical forebody and a fixed capture area, a hypothetical fan, F, which could achieve any specified total pressure ratio, an $H_2 - 0_2$ gas generator, GG, which drove the turbine, T, which provided the correct amount of work to drive the fan, a combustor, C, and exhaust nozzle. The flow path through this engine was completely "rubber". The upper half of the figure shows the geometry assumed for subsonic combustion and the lower half shown the geometry assumed for supersonic combustion. Performance was calculated for 5 flight conditions including SLS, subsonic loiter (M_0 = 0.9), transonic (M_0 = 1.25), mid supersonic speed (M_0 = 3.0), and the Mach 5 cruise condition.

Method of analysis: The STFF-ATR engine was evaluated using the Ram-Cycle computer program developed at UTRC. This program provides a front-to-back analysis of the flow through the engine. The inlet section includes the oblique shock losses, boundary layer losses, and calculates the flow spilled by the centerbody; the fan section calculates the average supersonic (or subsonic) flow conditions leaving the fan for a specified total pressure ratio and fan efficiency; it also calculates the compressor work done. This work was matched to the turbine work and gas-generator flow for a specified turbine pressure ratio and turbine efficiency. The gas generator was operated at a hydrogen rich condition that had a temperature of 2500 R. The flow in the converging supersonic diffuser after the fan includes shock losses and boundary layer losses. The amount of compression was determined by specifying an average throat Mach number, M_3, which at the Mach 5 cruise condition was a nominal M_3 = 1.8; however this throat Mach number was varied up to M_3 = 2.4. At lower flight speeds, the throat Mach number was reduced.

For the supersonic combustion configuration, the program calculates the combustor exit conditions for a specified heat release distribution and overall combustion efficiency, η_b , which varied between 90 and 100% according to the following relationship.

$$\eta_b = 1 - .1\phi^2 \qquad \text{Eq. 37}$$

where ϕ is the stoichiometry of the hydrogen before combustion. The combustor calculation also included some core losses and boundary layer losses. The nozzle calculation included a 2% core loss plus boundary layer losses.

For the subsonic combustion configuration, the flow was decelerated to subsonic velocities through a "normal shock" in the throat region which included divergence and friction losses in addition to the ideal shock losses; it was decelerated to lower speeds in the subsonic diffuser which had an assumed efficiency of 75%. Fuel was added and burned in the constant-area combustor with friction losses and a combustion

efficiency as specified by Eq. 37. The flow was reaccelerated in the convergent–divergent nozzle which had a 2% core loss plus boundary layer losses. The throat areas of the supersonic diffuser and C–D nozzle were varied as needed to accommodate all the flow which entered the fan. The nozzle exit pressure ranged between 1.0 to 1.75 x the free–stream static pressure as the flight speed ranged from subsonic to Mach 5.

Supersonic vs subsonic combustion: The impact of supersonic combustion was evaluated at the Mach 3 and 5 flight conditions. Since the supersonic through–flow–fan does work on the flow without incurring the losses associated with decelerating the flow to subsonic velocities, a supersonic diffuser, followed directly by a diverging supersonic combustor and nozzle would eliminate most of the large diffusion losses from a supersonic combustion configuration.

The performance of the subsonic and supersonic combustion configurations at the Mach 5 cruise condition is presented in Figures 58 and 59. Calculations were made for fan total pressure ratios, P_{T_R}, of 1.0 and 1.5. The pressure ratio of 1.0 is the equivalent of removing the fan and operating like a ramjet (RJ), or scramjet, (SCRJ), as labeled in the figure. The pressure ratio of 1.5 may not seem like much, but at this Mach 5.0 flight condition, the incoming total pressure of the air is approximately 530 times the free–stream static pressure i.e., at the 70K ft flight altitude; the static pressure is 0.65 psi; the total pressure of the air flowing into the fan would be approximately 345 psi; and the exiting total pressure would be 517 psi. The performance was calculated over a range of stoichiometries, ϕ . For the ramjet or scramjet operation all the H_2 fuel was added into the combustor and the engines could be operated over the full range of stoichiometries; however, when the fan was used, the gas generator flow was set by the compressor work requirements, and the hydrogen rich portion of the gas generator set the minimum stoichiometry for the engine at ϕ gg. Additional hydrogen could be added to the combustor to increase the stoichiometry to 1.0.

The results, presented in Figure 58, show that subsonic combustion would provide greater thrust than supersonic combustion with and without fan compression. The compression done by the fan increases the thrust, but the specific impulse, shown in Figure 59, is reduced significantly. That is because only 40% of the weight of the gases from the gas generator is hydrogen, the remainder is water, Since the impulse is based on the total weight of gas generator propellant, and not just the hydrogen which is availalbe for reacting which the air, the specific impulse of an air–turbo rocket engine is always penalized by the amount of extra oxidizer which is carried on board.

Similar results were obtained at the Mach 3.0 flight condition. Fan pressure ratios of 1.5 and 2.0 were examined. The results are shown in Figures 60 and 61. At this lower flight speed, the difference between supersonic and subsonic combustion is even more pronounced. the supersonic combustion engine had about 1/3 less thrust and lower specific impulse. Increasing the fan total pressure ratio provided greater thrust and slightly lower impulse for the subsonic combustion engine. At this intermediate speed, thrust is probably more important than fuel specific impulse.

It was concluded from the results at these two supersonic flight conditions, that the engine should be operated with subsonic combustion and with no compression work at the Mach 5 cruise condition, since the cruise range is directly related to the engine specific impulse. In fact, the engine may want to be oversized, so it could be throttled at the cruise condition to provide higher impulse than that obtained at the max thrust, stoichiometric condition.

Engine performance at the subsonic and transonic flight speeds was evaluated for the subsonic combustion configuration only. The thrust performance at the transonic condition, (M_0 = 1.25) is presented in Figure 62. Calculations were made at four fan total pressure ratios ranging from 2 to 5. At this flight

speed, the fan was assumed to operate as a supersonic through-flow fan; the fan exit Mach number ranged from 1.6 to 2.2. Increasing the fan pressure ratio provided a substantial increased in thrust, with only a small reduction in impulse (not shown). It should be noted that increasing the pressure ratio, also increases the minimum ϕgg, resulting in a smaller operating range at the higher fan pressure ratios. Fan pressure ratios between 2 and 4 look attractive at this flight speed.

The subsonic performance at 0.9 Mach is presented in Figure 63. In this figure the thrust is normalized by the total pressure rather than the dynamic pressure used in the definition of the thrust coefficient. At this flight condition the conversion factor is approximately 3, ie. $C_T \approx 3xF_N/P_TA_c$. This thrust normalizing parameter was used for the subsonic performance, because when normalized in this manner the performance presented at this subsonic flight condition, can be used to represent the performance at other subsonic flight conditions (within approximately 5%), i.e. the SLS performance (not shown) is similar to this.

At this subsonic flight condition, the fan was operated in the transonic mode with subsonic exit flow. A wide range of fan pressure ratios ranging from 2 to 8 were investigated. Increasing the fan pressure ratio provided a significant increase in the engine thrust; and very little change in the fuel specific impulse. Increasing the compressor work increases the gas generates flow, and the min ϕgg increases; at a pressure ratio of 8, the stoichiometry provided by the hydrogen rich gas generator gasses approaches one. Operation at fan pressure ratios between 3 and 5 looks attractive at the subsonic flight speeds; at higher pressure ratios the thrust improvement is reduced and the operating range is narrowed.

The results of the preliminary cycle studies, indicated a range of desired fan total pressure ratios at each flight speed. These results are summarized in Figure 64. The desired range of fan total pressure ratios varies between 3–5 at subsonic speeds down to zero at the Mach 5 cruise condition. A fan which can operate with in this band would be suitable for an STFF–ATR engine for a Mach 5 cruise vehicle.

Fan performance. – Two variable–pitch, split–rotor, split–stator fan configurations were designed for this application. These split–stage fans are designated by VPRS–1 and VPRS–2. The first fan had a pressure ratio of approximately 2.2 at a fan inlet $M_1 = 2$ design condition. This second fan had a pressure ratio of approximately 2.8 at the M = 2 design condition.The mean blade geometry and performance of fan configuration VPRS–1 is presented in Figures 65 through 69. The mean blade geometry and performance of fan configuration VPRS–2 is presented in Figure 70 through 74. The subsonic fan performance, presented in Figures 66, 67, 71, and 72, is plotted as a function of the corrected airflow, Wc/A, for specified values of the corrected rotor velocity, Vc. The supersonic fan performance is, presented in Figures 68, 69, 73 and 74, is plotted as a function of the inlet Mach number, M_1, for specified values of the mean rotor Mach number, M_R . A second scale shows values of the inlet corrected airflow, Wc/A.

Both fans provide total pressure ratios between 3 and 4 with subsonic (transonic) inflow conditions. With supersonic inflow velocities, configuration VPRS–1 provides a maximum pressure ratio of approximately 3 dropping off to 1.0 at a fan inlet Mach number slightly in excess of 3 (a flight Mach number of about 4). At this condition ($P_{T_R} = 1$) the fan work is low but not yet zero; the windmilling condition (Work = 0) occurs at a slightly higher Mach number with a total pressure ratio less than 1.0. At supersonic velocities, configuration VPRS–2 had a maximum pressure ratio approaching 4, dropping off to 1.0 at a fan inlet Mach number slightly under 4. At the Mach 5 cruise condition the fan inlet Mach number is about 4 and the windmilling rotor Mach number is approximately 1.3. At this windmilling condition the rotor speed would be approximately 1500 ft/sec, which is the design rotor speed.

Engine characteristics. – A supersonic through–flow–fan, air–turbo–rocket (STFF–ATR) engine concept was selected and engine geometries were specified for each of the two fan configurations de-

scribed above. The flow conditions along the entire engine flow path were determined and engine performance was calculated. The STFF–ATR engine characteristics and performance were compared to an over/under ATR/RJ configuration evaluated in a previous P&W study (Ref. 17).

STFF–ATR engine concept design: The preliminary engine cycle results, discussed previously, were a series of design point calculations which required a "rubber" engine to meet the flow area requirements. For example, the throat area of the supersonic diffuser downstream of the fan required a variation from 5 to 33% of the inlet capture area, and the nozzle throat area required a variation from 8 to 110% of the inlet capture area. Certainly, there extreme changes in geometry cannot be accomplished in a practical engine design and some compromises must be made to arrive at a realistic engine concept. Where possible one would like to specify fixed–geometry components, and if variable components are required, to keep the range of variation to a minimum using a hardware concept that is buildable. With this philosophy in mind, the engine concept shown in Figure 75 was selected for this study.

The STFF–ATR engine concept shown in Figure 75 is similar to the engine schematic shown previously in Figure 57; however the internal flow path is fixed except for the cowl door (which by–passes some of the fan flow) and the exhaust nozzle throat. The variation in nozzle throat area is a factor of about 2, which can be accomplished with a state–of–the–art annular nozzle.

The engine consists of a fixed geometry conical inlet which is designed to have the shock–on–lip at Mach 5. The variable–pitch, split–blade fan is located inside the cowl lip. All the fan flow is decelerated in the convergent annular supersonic diffuser. The amount of compression can be adjusted by the cowl doors or flaps which form the outer surface. At the Mach 5 design condition the doors are closed and no flow is spilled. The fixed diffuser throat is sized to accept all the fan flow at this Mach 5 condition. At lower speeds, such as the Mach 2 flight condition depicted in the lower half of the figure, the doors are ajar, by–passing some of the flow and reaccelerating it in the divergent passage between the fixed structure and the movable cowl door. The pressure recovery through the normal shock system in the divergent throat was calculated in a manner which reflects the losses which would be incurred with no boundary layer bleed. There is a small additional pressure rise in the subsonic diffuser which establishes the pressure level for the turbine exit flow mixer and entrance to the constant–area combustor. A variable–throat–area, convergent–divergent exhaust nozzle was used. the nozzle exit area was 1.5 x the inlet capture area.

The fan performance was obtained from the fan maps, the turbine work was set equal to the fan work plus fuel pump work. The gas generator and turbine were sized at the Mach 1.5 condition where the compression work was a maximum. The turbine had a design pressure ratio of 10 which would convert about 40% of the energy in the hydrogen rich gas–generator flow to useful turbine work. Over most of the speed range the gas generator was operated at on O/F ratio of 1.153 which produced a temperature of 2500 R and left 40% of the gas as unreacted hydrogen. At the high Mach number conditions (M_0 = 3 & 4), where less turbine work is required, the O/F was reduced to .833 which reduced the temperature to 2000 R and left 49% of the gas as unreacted hydrogen.

Two engine geometries were specified; one for using the low compression fan VPRS–1 and one using the higher compression fan VPRS–2. The engine flow areas of these two designs are given in Table 9. The flow areas of the two engines are very similar; the fixed throat area, A_3, at entrance to the core flow was slightly (3%) larger for the second engine. This small change plus the higher compression ratio of the second fan resulted in less spillage and a significant reduction in the throat area variation of the by–pass nozzle, A_{BY}. The combustor areas and nozzle exit area were the same, and the required area variations of the primary nozzles, A^*_5, were approximately the same.

TABLE 9. - STFF-ATR ENGINE AREAS

A/A_c		VPRS-1	VPRS-2
Fan	A_1	0.500	0.500
	A_2	0.394	0.365
	A_3	0.121	0.125
	A_{by}	0 to .111	0 to .058
Turbine	A_T^*	0.00405	0.00317
	A_{TX}	0.0345	0.0330
	A_B	0.500	0.500
	A_5^*	0.200 to .412	0.200 to .431
	A_e	1.500	1.500

STFF-ATR engine performance evaluation: Engine performance was calculated at 9 flight conditions, from SLS to the Mach 5 cruise condition. The flight path used for these calculations is one in which the vehicle accelerated from 0 to .6 Mn at SL, climbs to 20,000 ft, .9 Mn, accelerates through the transonic region at constant altitude to Mach 1.5, then climbs while it accelerates to Mach 5 maintaining a 1500 psi dynamic pressure. The actual altitudes and dynamic pressures used in the calculations are shown by the symbols in Figure 76. These conditions approximate the assumed trajectory of the supersonic climb path. In this section of the report, the results were corrected to the 1500 psf dynamic pressure flight path. In the next section, which shows comparisons with the conventional ATR/RJ, the actual conditions were used to be consistent with the previous ATR studies.

The following section describes the main operating characteristics of the engine, starting with the inlet and ending with the nozzle. The inlet has a fixed-geometry forebody consisting of a 9-deg cone plus 4-deg of isentropic compression to a 13 deg conical surface upstream of the fan. The performance characteristics of this inlet are shown in Figures 77 & 78. The total pressure ratio and Mach number entering the fan are shown in Figure 77. The total pressure loss is mainly due to the boundary layer, the shock loss is about 1/4 of that shown. The Mach number at the face of the fan is considerably less than the flight Mach number, close to 4.0 at the Mach 5 cruise condition. Note the discontinuity in the curve just below Mach 1.5. At Mach number of 1.5 and above, the fan was operated as a supersonic device; below Mach 1.5 the fan was operated as a subsonic device with an inlet Mach number of 0.8; for flight speeds between Mach 1 and 1.5 a normal shock would be forced upstream of the inlet to decelerate the flow to subsonic velocity. The inlet relative weight flow and additive drag are shown in Figure 78. The inlet was designed to capture 100% of the flow at Mach 5; at transonic Mach numbers about 50% of the flow is spilled efficiently by the conical forebody. Note, that the flow discontinuity at the transition point is small.

Using the fan face conditions provided by the inlet and the fan performance presented previously in Figures 65 through 74, a fan operating point was selected which had a mean rotor velocity of 1500 ft/sec. This design wheel speed resulted in a rotor Mach number which varied from 1.35 at SLS up to approximately 1.5 at Mach 2, and dropping again at the higher flight speeds down to approximately 1.3 at the Mach 5 windmilling condition. The resulting total pressure ratios for the two fans are shown in Figure 79. Both provided a total pressure ratio near 4 at subsonic conditions and both dropped off to a pressure ratio of approximately 0.55 at the Mach 5 windmilling condition. In between, the second fan configuration

(VPRS–2) provided higher total pressure ratios. The first configuration (VPRS–1) provided about 75% of these values. The fan inlet and exit Mach numbers are given in Figure 80. When operating as a subsonic fan below Mach 1.5, the fan exit Mach numbers are considerably less than the fan inlet Mach number. At low supersonic velocities (where the fan does a lot of work) the supersonic fan accelerates the flow to a higher Mach number, but at the high flight speeds, the exiting Mach number was less than the inlet Mach number, especially at the Mach 5 windmilling condition. At this windmilling condition, there was a total pressure loss across the fan; however associated with this was a significant amount of supersonic diffusion which reduced the supersonic diffusion required by the following compression region.

The supersonic fan exit flow was diffused in the annular region between the centerbody and the variable cowl flaps or door which provided a variable flow contraction ratio. The performance of this aft diffuser is shown in Figure 81. The upper curve of the upper figure (labeled throat) presents the total pressure ratio across this convergent supersonic diffuser. The lower curve shows the additional losses associated with decelerating the flow to subsonic velocities at the burner entrance. The lower figure shows the Mach numbers at the diffuser throat and burner entrance. The symbols shown in these figures indicate the associated free–stream Mach numbers. Note that as the free–stream Mach number varies from 1.5 to 5.0, the fan exit Mach number only varies between 2.3 and 3.2, and the supersonic diffuser exit or throat Mach number varies between 1.3 and 1.8. During subsonic operation of the fan, the subsonic fan exit flow was accelerated to sonic conditions at the diffuser throat.

The throat of this supersonic diffuser is where the flow was split, the core flow–entering the fixed engine duct and the remainder spilled overboard through the cowl door as shown in the engine schematic (Fig. 75). Figure 82 shows the airflow characteristics of these two engines. The upper curve shows the flow which enters the inlet and is compressed by the fan, it is the same as the inlet flow presented earlier in Figure 78. The lower two curves show the core flow which enters the main engine, the difference is the by–pass flow. The second fan configuration VPRS–2 provided greater compression of the flow, and thus more flow could pass through the fixed–throat area and enter the engine. There is a significant discontinuity in the core flow schedule at the transition Mach number. When operating in the subsonic mode, the cowl doors would be positioned at an area which chokes the flow at the second throat; when transiting to the supersonic mode of operation the doors would be opened (quickly) spilling more flow, dropping the pressure and letting supersonic conditions to be established through the fan.

The bypass flow is reaccelerated through the divergent oblique exhaust nozzle formed between the fixed engine structure and the variable cowl doors (see engine schematic, Fig. 75). Because of the compression work which has been alone on this flow, this flow can be accelerated to a higher velocity than the free–stream velocity, thereby providing thrust. The velocity of this by–pass flow and the exhaust velocity of the main engine (core) flow is shown in Figure 83. At subsonic flight conditions the velocity of this by–pass flow is approximately 2000 ft/sec., providing a significant amount of thrust; at higher flight speeds the thrust from the by–pass flow decreases, becoming zero at a flight speed of approximately 3.6. Thus spilling flow at flight speeds at Mach 4 and above would result in a spillage drag. Note that the airflow schedule (Fig. 82) for the second fan configuration VPRS–2, does not spill at Mach 4 and above.

The main engine (core) flow which is heated in the combustor to high temperatures has a much higher exhaust velocity, thereby providing significantly more thrust–per–lb. of airflow. Thus the engine total thrust is maximized by maximizing the flow through the main (core) engine; however this does not necessarily maximize the fuel specific impulse.

The combustor pressure is shown in Figure 84. The second configuration with the VPRS–2 fan has higher combustor pressures. The pressures are quite reasonable, below 75 psia up to Mach 3, then climbing to about 110 psia at Mach 5, 1500 psf flight condition. At a higher cruise altitude where the dynamic pressure is only 1000 psf, the combustor pressure would be reduced to 75 psia. If the supersonic accelera-

tion climb path above Mach 3 were changed to reduce the dynamic pressure from 1500 to 1000 psf at Mach 5, the combustor pressures would not exceed 75 psia.

The work required by the fan and the gas-generator flow rate required to drive this compressor is shown in Figure 85. The maximum compressor work required for a 25 ft^2 capture area engine is approximately 65,000 BTU/sec or about 90,000 HP. The original engine was configured with a reduction gear box between the turbine and the fan; however, this large power requirement led to the elmination of the gear box and the use of a multi-stage turbine to extract the energy from the gas generator flow.

The engine and bypass nozzle throat areas are shown in Figure 86. The main (core) engine throat area requires an area variation from approximately 20 to 43% of the capture area. This amount of variations can be attained with a state-of-the-art annular nozzle. The by-pass throat area varied from zero at the cruise condition to a maximum of 11% for the VPRS-1 fan and 6% for the VPRS-2 fan. Either of these requirements could be met with only a small amount of movement of the cowl doors.

The thrust of these two engine configurations is presented in Figure 87. an STFF-ATR engine having a capture area of 25 ft^2 would provide approximately 70,000 lb. of take-off thrust, 50,000-70,000 lb. of thrust through the transonic region, and a thrust in excess of 50,000 lb. over the entire supersonic acceleration-climb-path. The second engine using the VPRS-2 fan would provide approximately 25% greater thrust than the first engine along this supersonic acceleration path.

The fuel specific impulses of these engines are presented in Figure 88. The impulses are comparable with the second engine being slightly better over the low end of the speed range. The level of specific impulse (2000 - 2500 sec) which is obtained by these STFF-ATR engines at low speeds is considerably less than would be obtained from a conventional turbofan because only 40% of the propellant is combustable H_2 fuel, the remaining 60% is H_20. However, at Mach 5, where the engine is operating like a ramjet, all the fuel is hydrogen and the impulse obtained is 3500 sec. Furthermore, the impulse is increased when the engine is throttled to lower power (lower ϕ) settings as shown in Figure 89. Operation at half the max thrust, at ϕ = .4, would increase the fuel specific impulse to about 4400 sec.

The results presented in these last three figures show that the engine designed with higher pressure ratio fan, VPRS-2, would provide greater thrust and impulse, over the lower spreed portion of the flight trajectory, and comparable performance at the Mach 5 cruise condition. Therefore, this engine configuration was selected as the baseline STFF-AIR to be compared with the conventional ATR engine.

Performance comparison: The performance of the supersonic through-flow air-turbo-rocket (STFF-ATR) engine is compared with that of a conventional air turbo rocket ramjet engine (ATR-RJ) herein. The conventional ATR-RJ concept is illustrated in Figure 90. This concept consists of an air turborocket (ATR) engine and a ramjet in an over/under configuration. The ATR has a 2 stage conventional fan powered by a seven stage turbine. An oxygen/hydrogen burner provides fuel rich flow to the turbine. This fuel rich flow is then mixed with the fan discharge flow and burned in the afterburner. This ATR is operating from Mach 0 to approximately Mach 3.5. The ramjet burner is turned on at Mach 1.2. At flight Mach Numbers above 3.5, all the inlet airflow passes through the ramjet.

Tables 10 and 11 provide a summary of the STFF-ATR and conventional ATR-RJ maximum power engine performance at several points along the climb path, shown previously in Figure 76. The airflow levels shown are based on sizing both engines to produce 72,000 lbs installed thrust at the 50,000 ft., 3.0 Mn condition. This results in an ATR-RJ that has an ATR with a maximum fan inlet corrected airflow of 260 lb/sec at sea level static, and a ramjet with a ramburner area of 8.5 ft^2. The thrust levels shown in these tables are the net thrust which includes the inlet drag.

TABLE 10. - STFF-ATR PERFORMANCE (MAX POWER)

Altitude, ft.	0	20000	50000	70000
Mach Number	0.1	1.5	3.0	5.0
Inlet Capture Area, ft^2	25.3	25.3	25.3	25.3
Inlet Recovery	0.999	0.990	0.968	0.913
Total Inlet Airflow, lb/sec	603	872	587	550
Total Inlet Cor. Flow, lb/sec	602	584	208	49.1
Fan Pressure Ratio	3.84	3.50	1.8	0.55
Bypass Airflow, lb/sec	139	296	74	0
Turbine Temperature, R	2500	2500	2020	-
Main Burner 0_2 + H_2, lb/sec	26.3	38.2	27.4	-
Shaft horsepower, HP	65,400	96,900	43,000	-
Turbine Expansion Ratio	9.6	10	6.64	-
Afterburner H_2, lb/sec	3.4	0.7	1.1	16.1
Total (H_2 + 0_2), lb/hr	107,000	140,200	102,700	57,900
Nozzle temperature, R	4360	4420	4630	5050
Nozze Pressure Ratio	3.1	10.9	44.8	183
Nozzle Cv	.985	.985	.985	.985
Net Thrust	69,600	85,000	72,000	56,300
TSFC lb/hr-lb	1.54	1.65	1.44	1.03
Nozzle Throat Area, ft^2	10.8	9.6	7.4	5.1
Nozzle Exit Area, ft^2	13.7	26.5	38.0	38.0

TABLE 11. - CONVENTIONAL ATR-RJ PERFORMANCE (MAX POWER)

Altitude, ft.	0	20000	50000	70000
Mach Number	0	1.5	3.0	5.0
Inlet Capture Area, ft^2	28.35	28.35	28.35	28.35
Inlet Recovery	.90	.969	.76	.51
Total Inlet Airflow, lb/sec	234	529	605	517
Fan Inlet Airflow, lb/sec	234	358	298	-
Ramjet Inlet Airflow, lb/sec	-	171	307	517
Total Inlet Cor. Flow, lb/sec	260	362	272	82.7
Ramjet Inlet Cor. Flow lb/sec	-	117	138	82.7
Fan Inlet Cor. Flow, lb/sec	260	245	134	-
Fan Pressure Ratio	3.20	2.90	1.70	-
Turbine Temperature, R	2320	2460	2460	-
Main Burner O_2, lb/sec	10.9	17.1	15.5	-
Main Burner H_2, lb/sec	8.8	12.8	11.6	-
Turbine Horsepower, HP	20,500	32,400	22,200	-
Turbine Expansion Ratio	2.38	2.42	1.94	-
Ram Burner H_2, lb/sec	0.0	4.7	9.1	15.0
Total O_2 + H_2, lb/hr	71,050	124,140	130,100	53,860
Nozzle Temperature, R	4425	4330	4430	4780
Nozzle Pressure Ratio	2.98	7.74	42.2	333
Nozzle Cv	.958	.965	.976	.975
Net Thrust, lbf	30635	43750	72000	45940
TSFC, lb/hr-lb	2.13	2.87	1.81	1.12
Nozzle Throat Area, ft^2	6.2	13.5	10.7	2.65
Nozzle exit area, ft^2	38.9	38.9	38.9	38.9

Figure 91 compares the inlet total pressure recovery for the fixed conical STFF-ATR inlet and for the variable-ramp two-dimensional inlet of the ATR-RJ concept. The short inlet for the STFF-ATR engine provides much higher recoveries because it is only diffusing the flow a small amount to a lower supersonic velocity wherever the conventional inlet is diffusing the flow to subsonic conditions.

Figure 92 compares the inlet airflow schedules for the STFF-ATR and conventional engines. For the STFF-ATR system, all of the inlet flow passes through the fan. The conventional ATR-RJ begins operating at Mach 1.2, and above Mach 3.5 all the inlet flow passes through the ramjet. Figure 92 shows

that the supersonic fan engine passes much more flow than the conventional fan ATR at Mach numbers below 2.

Figures 93 and 94 show the fan inlet corrected airflow and pressure ratio variations with Mach number for both engines. The conventional fan ATR, is not operated above Mach 3.5. The fan in the STFF-ATR operates at all flight conditions. Above Mach 4, the STFF fan total pressure ratio is less than 1.0, as described previously. Figure 95 illustrates the fan operating lines during supersonic flight for both engines. Figure 96 compares the conventional ATR-RJ engine's inlet corrected flow schedule with that provided by the inlet. The inlet corrected flow reflects the mass flow ratio shown in Figure 97 and inlet pressure recovery schedule shown previously in Figure 91. The total engine flow below Mach 3.0 is less than the inlet flow capacity, requiring that a large amount of air bled or spilled. The resulting total inlet drag is presented in Figure 98. The additive drag of the STFF-ATR engine is also shown in this figure. This inlet requires no boundary layer bleed, the fan passes all the air captured by the inlet, and the bypass flow produces thrust. Thus the inlet drag of the STFF-ATR engine is an order of magnitude less than that of the conventional ATR-RJ.

Figure 99 presents the maximum augmented net thrust along the climb path shown for the STFF-ATR and ATR-RJ engines. The STFF-ATR engine was sized to provide the same thrust as the conventional ATR-RJ at Mach 3. For this size engine the STFF-ATR has twice as much thrust as the conventional ATR-RJ at Mach Numbers below 1.25 because it flows about twice as much airflow, (see Fig. 92). Above Mach 4.0 both engines are basically operating as ramjets and the STFF-ATR provides more thrust at Mach 5 because it passes slightly more airflow through the burner and has no inlet drag.

Figure 100 compares the maximum augmented specific fuel consumption (TSFC) rates for both engines. This TSFC is the ratio of the total propellant (hydrogen plus oxygen) flow rate divided by the total net thrust. The STFF-ATR has a lower TSFC at the low Mach Numbers because of its lower inlet drag and because the bypass air provides thrust. The overall propellant/fan flow for the STFF-ATR is much lower than that of the ATR-RJ as shown in Tables 10 and 11. The higher fan pressure ratio also increases the STFF-ATR specific thrust, which reduces fuel consumption.

At the Mach 5 cruise condition, both the STFF-ATR and ATR-RJ engines operate as ramjets. In the STFF-ATR engine, all the flow passes through the fan, which is windmilling, and is then burned in the augmentor. In the conventional ATR-RJ all the inlet flow passes through the ramburner. Since the total airflow for both engines is burned stoichiometrically the overall efficiencies which is reflected by the TSFC's are similar. Figure 101 presents the part-power performance for both engines at 70,000 ft., Mach 5.0 as the ramburner fuel flow is varied. The difference is primarily due to inlet drag.

Conceptual design analysis. - As part of this supersonic through-flow-fan air-turbo-rocket (STFF-ATR) study a conceptual design of the engine was performed in sufficient detail to determine the major issues associated with the mechanical execution of the concept.

The STFF-ATR and conventional ATR-RJ performance presented previously in Tables 10 and 11 shows that the 20,000 ft. 1.5 Mn flight condition produces the largest shaft horsepower requirement for both engines. Therefore, this operating point is used to design their turbines. Since both engines burn pure oxygen and hydrogen in the main combustor, it is desirable to maintiain the burner flow at a low level to minimize the fuel consumption. The turbine temperature for both engines is kept below 2500 F to use uncooled turbines.

Table 12 summarizes the fan, burner, and turbine operating characteristics for the STFF-ATR and ATR-RJ concepts. The conventional ATR-RJ engine, shown in Figure 102, incorporates a two stage 2.9 pressure ratio fan designed with a tip speed of 1590 ft/sec. The total oxygen/hydrogen flow of 29.8 lb/sec

in the main burner is one-twelfth of the fan inlet flow of 355 lb/sec. This produces a turbine work requirement of 768 Btu/lb. The turbine is a direct drive design which requires seven stages to produce the 768 Btu/lb specific work with an efficiency of 93%.

TABLE 12. - STFF-ATR AND ATR-RJ DESIGN SUMMARY

Operating conditions at 20,000 ft, 1.5 Mn

	ATR-RJ	STFF-ATR
Inlet Capture Area	28.35	25.3
Number of Fan Stages	2	1
Fan Corrected Airflow, lb/sec	245	584
Fan Inlet Hub/Tip Ratio	.40	0.708
Fan Inlet Specific Flow, lb/sec	40.0	45.7
Fan Tip Diameter, in.	36.6	68.1
Fan Inlet Rim diameter, in.	14.6	48.2
Fan Tip Speed, ft/sec	1600	1732
Fan Rotor Speed, RPM	10015	5829
Fan Airflow, lb/sec	358	872
Fan Pressure Ratio	2.9	3.5
Fan Efficiency, %	85.7	84.3
Fan Specific Work, btu/lb	64.5	79
Shaft Horsepower, HP	32,400	96,900
Burner O_2 + H_2 Flow, lb/sec	29.8	38.2
Turbine Inlet Temperature, R	2460	2500
Turbine Specific Work, btu/lb	768	1794
Turbine Rim Diameter, in.	22.1	39.4
Turbine Rim Speed, ft/sec	'965	1000
Number of Stages	7	15
Rim Velocity Ratio	.41	.41
Turbine Efficiency, %	93.2	90.0
Turbine Pressure Ratio	2.42	10

The STFF-ATR engine is illustrated in Figure 103. It's fan design, shown in Figure 104, is based on a tip speed of 1732 FPS and a 0.708 hub to tip diameter ratio which results in a rotor speed of 5829 RPM. The fan blade is designed in two sections. The front section (40 percent of the total chord) has variable pitch; the rear section has fixed geometry. This variable pitch capability allows the proper incidence angles

of the blade to be maintained for stable operation and the highest possible efficiencies. The supersonic flow is best handled with long-chord, high-solidity blading. This results in a design with a solidity of 3.0. This is considerably greater than a conventional design with a solidity of 1.0 to 2.0. This high solidity reduces the static pressure mismatch between the suction and pressure surfaces of the blade and therefore eliminates the strong shock losses which result in the process to reach equilibrium. The fan stator is also split, with the front section (50% chord) variable.

It was initially intended to employ a geared connection between the STFF fan and the turbine in order to maintain high turbine speeds and minimize the number of turbine stages. However, the extremely large airflow and high pressure ratio demands 97,000 horsepower from the turbine. The total mass flow in the turbine of 38.2 lb/sec is one twenty third of the fan flow resulting in a turbine specific work level of 1794 Btu/lb. This small turbine mass flow results in turbine inlet and exit areas of 44 in.^{2} and 120 in.^{2} respectively to achieve the proper turbine Mach numbers. This results in a small diameter, high speed turbine to be matched with a large diameter, low speed fan. Table 13 summarizes the geared turbine configurations examined for gear ratios of 2 and 3. These geared configurations result in a gearbox with an unacceptable weight.

TABLE 13. - STFF-ATR TURBINE OPTIONS

Operating conditions at 20,000 ft/1.5 Mn

Turbine Configuration	Geared		Direct Drive		
Gear Ratio/Stages	2	3	11	15	20
Turbine Speed,rpm	11,660	17,490	5,829	5,829	5,829
Rim Speed, fps	1600	1600	1170	1000	740
Rim Radius, in.	15.72	10.48	23.0	19.7	17.0
Inlet Area, in.^{2}	44	44	44	44	44
Inlet Tip Radius, in.	16.16	11.12	23.3	20.05	17.4
Insert blade Height, in.	.44	.64	.30	.35	.40
Exit Tip Radius, in.	16.9	12.2	23.8	20.65	18.1
Exit Blade Height, in.	1.2	1.70.		8	.951.1
Specific Work, btu/lb	1794	1794	1794	1794	1794
Work/Stage, btu/lb	299	299	163	120	90
Rim Velocity Ratio	..42	.42	.42	.42	.42

Three ungeared turbine designs with 11, 15, and 20 stages were then examined, as shown in Table 13 to determine which design would be best. The turbine design with 15 stages results in a root radius of 19.7 inches. This provides a minimum acceptable blade height at the inlet to the turbine of 0.35 inches and 0.95 inches at the turbine exit. This turbine provides a rim velocity ratio of 0.42 and an efficiency of 90%. This 15 stage ungeared design was selected for the mechanical design study.

STFF-ATR mechanical design analysis. - The STFF-ATR configuration, shown in Figure 103, evolved into an arrangement with a single-stage variable-pitch fan cantilevered from a structural case

which houses the engine thrust bearing and blade actuation hydraulic cylinder. A long (108 inch) conical compression surface is mounted ahead of the fan, and held concentric by inlet vanes. The turbine is driven by a case-mounted, annular Lox-hydrogen burner and is straddle-mounted between the engine bearings.

The fan discharge flow is ducted around the turbine and mixed with the turbine discharge flow ahead of the integrated Lox spraybar/flameholders. The nozzle is regeneratively cooled and, has variable convergent - divergent geometry.

Fan design: Figure 104 illustrates the mechanical arrangement of the variable-pitchs split-blade fan installation. In this application the fan and inlet must operate at temperatures up to 1800 F, while the disks must be kept below 1250 F to avoid oxidation. The need to build in thermal compliance among the various assemblies dictates slip-fits, and strain-relief features where parts mate. In addition, provisions must be made for precise fits in critical areas such as the blade tips. Perhaps the most significant design challenge will be the variable-pitch fan mechanism. The reasons for this are as follows:

- Centrifugal loadings due to airfoil weight will cause the bearing surface to be heavily loaded.
- High temperatures in the area of the rim are detrimental to bearings.
- Absence of conventional lubricants.
- Tolerance, stack-ups associated with having a large number of parts.

Unlike the fan/pitch mechanism the actual disk design is expected to be relatively straight forward. The reasons for this are that turbine disk design experience is readily applicable.

Bearing compartments: The design of the bearing compartment (bearings, seals, scavenge system, lube system) will be influenced by the designs of the J-58 and 304 engines. The engine features two main bearings, with the turbine rotor straddle-mounted between them. The cross-section has the thrust bearing in the front position, but a tolerance study will be necessary to determine the optimum location with respect to the first stage turbine blades and vanes. Attention to the buffer/purge systems will be a necessity to ensure that a combustible hydrogen/air mixture is not trapped in any compartment.

Blade actuator: The hydraulic actuator for the variable-pitch fan blades is built into the inside of the rotor. Engine oil is used as the actuation medium, with all control valves located in the nacelle.

Combustor/turbine: Figure 105 illustrates the main combustion chamber and turbine designs. The Lox-hydrogen combustion chamber is an annular configuration, mounted to the turbine case between the turbine rotor and the thrust bearing housing. The turbine case is split axially, for assembly reasons, and the turbine which has 15 stages, is integrally bladed. A significant concern will be thermal shock to the parts during the start transient. The turbine is a drum-type rotor with four disks, equally space supporting the blades. This configuration is made possibly by the low RPM. The turbine flow exhausts into the main fan stream via a lobed or "Daisy" mixer. Spraybars and flameholder are integrated into one component and located in the cooler of the two streams to be mixed.

By-pass nozzle: The bypass nozzle, shown in Figure 105 consists of a series of cowl flaps which close on the fixed engine structure. At the Mach 5 design condition they are fully closed, at lower speeds they are varied to control the aerodynamic contraction of the airflow from the fan; upon opening, the cowl flaps form a divergent passage ducting the excess flow overboard. The bypass flow is reaccelerated in this divergent passage.

Main nozzle: The main nozzle is a variable area, convergent-divergent axisymmetric "balance beam" plug nozzle (see Fig. 103). The maximum nozzle exit area of 38.0 square feet was sized for 70K/5.0 Mn max power operation. The maximum nozzle throat area of 10.8 square feet occurs at the sea

level 0.1 Mn condition, Table 10. The maximum nozzle exit area results in a maximum exit diameter of 83.5 inches. The nozzle divergent flap length of 75 inches was chosen to achieve a flap length to maximum exit diameter ratio of 0.90. The plug throat diameter was set by choosing a plug diameter to maximum exit diameter of 0.445, and a plug truncation was based on a plug tip diameter to maximum exit diameter of 0.165; these criteria result in a plug diameter of 37.1 inches and a plug truncation diameter of 13.8 inches. The entire nozzle is regeneratively cooled .

Weights/dimensions: The weights and dimensions of the conventional ATR-RJ and STFF-ATR propulsion systems are summarized in Table 14 for the engines sized for the airflows shown in Tables 10 and 11. The materials used in these engines reflect a technology availability date (TAD) of 2000. Figure 106 shows the external dimensions of these systems. The inlet/nacelle weight of 8580 lbs for the two dimensional ATR-RJ configuration includes the inlet and the entire fixed external nacelle structure. The nacelle has a width of 5.5 ft. The height varies from 5.16 at the inlet to 7.08 ft at the nozzle exit. The exit nozzle area of 38.9 ft^2 was selected based on previous studies of Mach 5.0 systems. The inlet weight of the STFF-ATR includes the nose cone and structural support struts.

TABLE 14. - WEIGHTS AND DIMENSIONS

Propulsion System	ATR-RJ	STFF-ATR
Inlet/Nacelle Weight, lbs	8580	420
ATR Weight, lbs	2350	9580
Ramjet Weight, lbs	3000	-
Total Weight, lbs	13,930	10,000
Inlet Capture Area, ft^2	28.35	25.3
Inlet Length (to fan face), ft.	-	10.0
Inlet Height/Diameter, ft.	5.16	5.68
Inlet Width, ft.	5.49	-
Fan Face Tip Diameter, ft.	3.05	5.68
Total Nacelle Length, ft.	81	28.6
Max Nozzle Exit Area, ft^2	38.9	38.0
Nozzle Exit Height/Diameter, ft.	7.08	8.96
Ram Burner Area, ft^2	8.5	12.6
SLS Thrust, lbs	30,635	69,500
Thrust/Weight	2.20	6.95

The ATR weight for the conventional ATR-RJ includes the fan, main burner, turbine and augmentor weights. The ramjet weight includes the ramburner, nozzle, actuators, pump, plumbing and control system weights.

The ATR weight for the STFF-ATR includes the fan, outer case, burner, turbine, augmentor, nozzle, actuators, pump, plumbing and control system weights.

Table 14 also lists the SLS thrust of the two engines; these results show that the STFF-ATR has a SLS thrust/weight ratio of 6.95, which is 3 times that of the conventional ATR-RJ value of 2.2.

Mission analysis. - Studies were conducted to determine the Takeoff Gross Weight (TOGW) of a Mach 5 strategic penetrator system having a total range of 4000 n. mi. The conventional over/under ATR-RJ powered aircraft is configured with four engines in two two-dimensional pods. The STFF-ATR aircraft has two engines in separate axisymmetric pods.

The mission evaluated is comprised of a takeoff and a climb/acceleration to the Mach 5.0 at 83,000 ft. cruise condition. A 5000 lb payload is carried throughout the 4000 n. mi. range.

Previous studies of this strategic penetrator have shown that a system designed with a takeoff thrust loading, i.e., total takeoff thrust/takeoff gross weight (TOGW), of 0.45 provided sufficient excess thrust during the climb and acceleration to the 83,000 ft, Mach 5.0 cruise condition to produce the lightest weight vehicle. Therefore in the current study, the propulsion systems are sized to produce a takeoff thrust loading of 0.45. Since the STFF-ATR engine has a takeoff thrust/engine weight which is three times that of the conventional ATR-RJ, it will have a much smaller propulsion system weight fraction than the conventional ATR-RJ. This weight advantage will result in a significantly lower aircraft system weight.

Table 15 compares the aircraft weights for the STFF-ATR and conventional ATR-RJ powered systems. The STFF-ATR produces a TOGW of 68,726 lbs, which is 62% lighter than the 182, 234 lb ATR-RJ powered aircraft. This TOGW advantage is mainly due to the STFF-ATR's lighter propulsion system, which produces a propulsion system (inlet, nacelle, engine, fuel system) weight fraction of 0.14, while the conventional ATR-RJ has a 0.28 propulsion system weight fraction. The STFF-ATR also has better fuel consumption rates during the climb/acceleration, and at the Mach 5.0 cruise condition.

TABLE 15. - MISSION SUMMARY

Engine	ATR-RJ	STFF-ATR
TOGW, Lbs	182,234	68,726
Number of Engines	4	2
Takeoff Thrust/TOGW	0.45	0.45
Engine Scale Factor	0.659	0.222
Takeoff Thrust/Engine, Lbs	20,500	15,500
Scaled Capture Area, Ft^2	18.7	5.6
Aircraft Empty Weight, Lbs	54,520	27,392
Payload Weight, Lbs	5,000	5,000
Fuel Weight, Lbs	69,949	26,569
Fuel Weight/TOGW	384.	.387
Propulsion Group Weight, Lbs	52,765	9,765
Propulsion Weight/TOGW	.289	.142
Supercruise Power Setting, % Max.	49	92
Supercruise TSFC, Lb/hr-lb	1.08	99

Since there is a significant difference in propulsion system weight fraction between the two systems, a weight sensitivity study was conducted. Figure 107 shows that if the STFF-ATR weight were increased to

produce the same propulsion weight fraction as that of the conventional ATR-RJ, its TOGW would be 29% lower than that of the ATR-RJ. This lower TOGW is due to the STFF-ATR's lower climb and cruise TSFC.

Figure 108 illustrates the excess power that the STFF-ATR and conventional ATR-RJ propulsion systems would provide when sized for a takeoff thrust loading of 0.45. This excess thrust is measured in how fast the airplane can climb in feet per second at any flight condition. As Figure 108 shows, both aircraft have similar climb rates at low Mach Numbers since their takeoff thrust loadings are the same. At the higher Mach numbers, the conventional ATR-RJ has a much higher acceleration rate which allows that aircraft to reach its cruise condition faster. However, the STFF-ATR has sufficient excess power at all flight conditions and cruises at Mach 5.0 at 92% of maximum power.

REFERENCES

1. Ferri, Antonio, *Problems Related to Matching Turbojet Engine Requirements to Inlet Performance as a Function of Flight Mach Number and Angle of Attack*, presented at 11th AGARD Combustion and Propulsion Panel Meeting, Paris, December 1956, AGARDograph no. 27.

2. O'Brien, R. L., S. F. Gadboin, B. Dunn, *Investigation of the Supersonic Through-Flow Compression Concept*, Volume I Performance Potential and Mechanical Design Study, Volume II Analytical and Experimental Investigation of Supersonic Cascades and Diffuser A. F. Report AFAPL-TR-67-60, June 1967.

3. Boxer, Emanuel, *The Variable-Pitch Supersonic Inflow Compressor*, NASA SP-148, Conference on Hypersonic Aircraft Technology, May 16-18, 1967.

4. Sabatella, J. A., ed.: *Advanced Supersonic Propulsion Study*, (P&W TM-4871, Pratt & Whitney Aircraft, NAS3-16948), NASA CR-134633, 1974.

5. Szeliga, R. and Allan, R. D.: *Advanced Supersonic Technology Propulsion Study*, (R74AEG330, General Electric Co., NAS3-16950), NASA CR-134904, 1975.

6. Howlett, R. A., et al: *Advanced Supersonic Propulsion Study Phase II, Final Report*, (PWA-5312, Pratt & Whitney Aircraft, NAS3-16948), NASA CR-134904, 1975.

7. Allan, R. D.: *Advanced Supersonic Propulsion System Technology Study, Phase II, Final Report*, (B75AEG508, General Electric Co., NAS3-16950), NASA CR-134913, 1976.

8. Howlett, R. A., et al: *Advanced Supersonic Propulsion Study, Phase III, Final Report* (PWA-5461, Pratt & Whitney Aircraft, NAS3-19540), NASA, CR-135148, 1976.

9. Howlett, R. A. and Streicher F. D.: *Advanced Supersonic Propulsion Study, Phase IV, Final Report*, (PWA-5547-4, Pratt & Whitney Aircraft, NAS3-19540), NASA CR-13523, 1977.

10. Allan, R. O. and Joy, W.: *Advanced Supersonic Propulsion System Study, Phase III and IV, Final Report*, (R77AE635, General Electric Co., NAS3-19544 Modification 4), NASA CR-135236, 1977.

11. Trucco, H: *Study of Variable Cycle Engines Equipped With Supersonic Fans, Final Report*, (ATL TR 201 Advanced Technology Laboratories Inc., NAS3-17559), NASA CR-134777, 1975.

12. Franciscus, L. C.: *Supersonic Through-Flow Fan Engines for Supersonic Cruise Aircraft*, NASA TM-78889, 1978.

13. Tavares, T. S., *A Supersonic Fan Equipped Variable Cycle Engine for a Mach 2.7 Supersonic Transport*, Final Report for NASA Grant NAG3-697, 1986.

14. Franciscus, L. C. *The Supersonic Through-flow Turbofan for High Mach Propulsion* AIAA-87-2050 at AIAA/SAE/ASME Joint Propulsion Conference June 1987.

15. Hobbs, D. E., J. Norton, & W. Harvey, Section on Aerodynamic Design, Test & Performance from *Energy Efficient Engine Shroudless Hollow Fan Blade Technology* Program Status Review May 19, 1984. Pratt & Whitney, CEB.

16. Lynch, et al. *Advanced Supersonic Technology Concept Study Reference Characteristics*, (LTV Aerospace Corp., Hampton, VA), NASA-CR-132374, December 21, 1973.

17. Powell, T. , *High Speed Propulsion Assessment*, Task II, Interim Technical Report FR 19753, Pratt & Whitney, GEB, February 27, 1987.

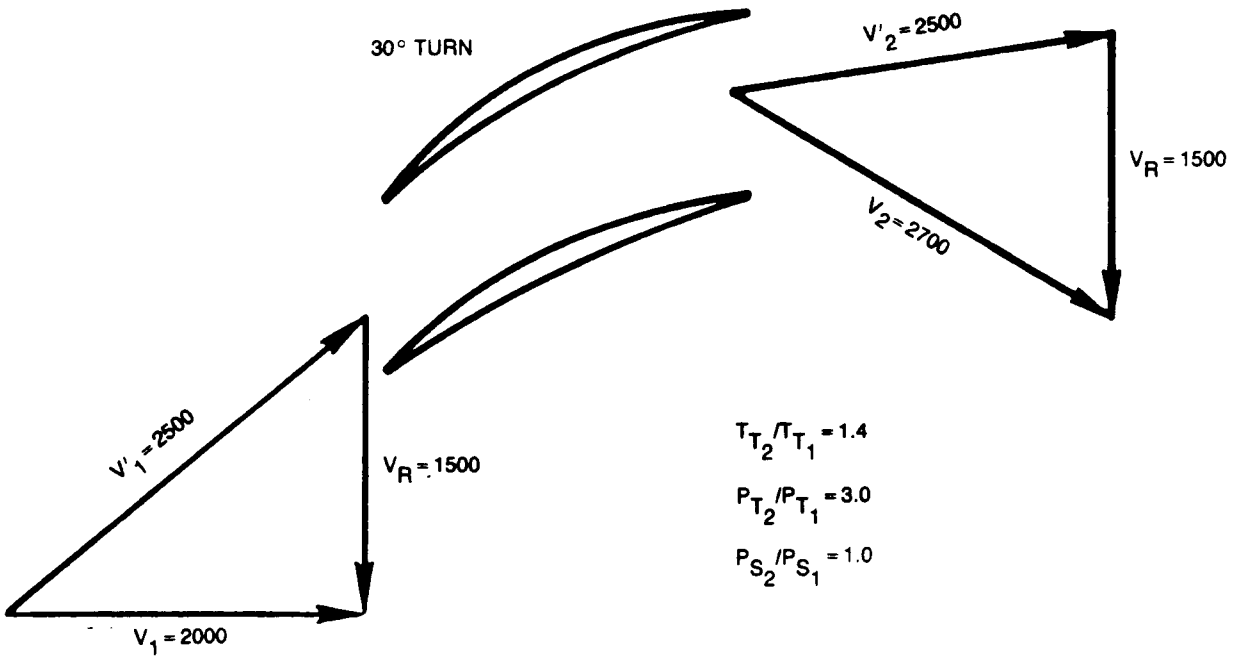

Figure 1. STFF velocity diagram.

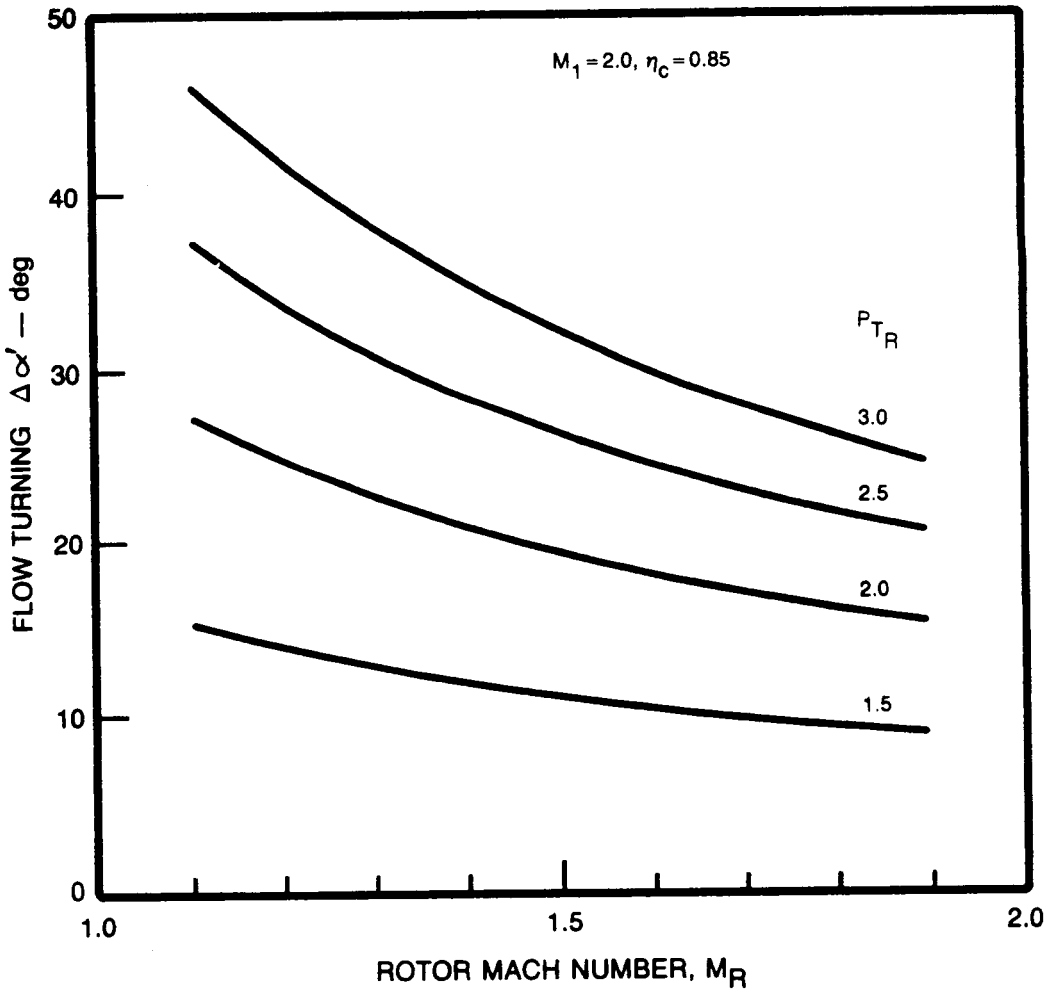

Figure 2. Design point flow turning.

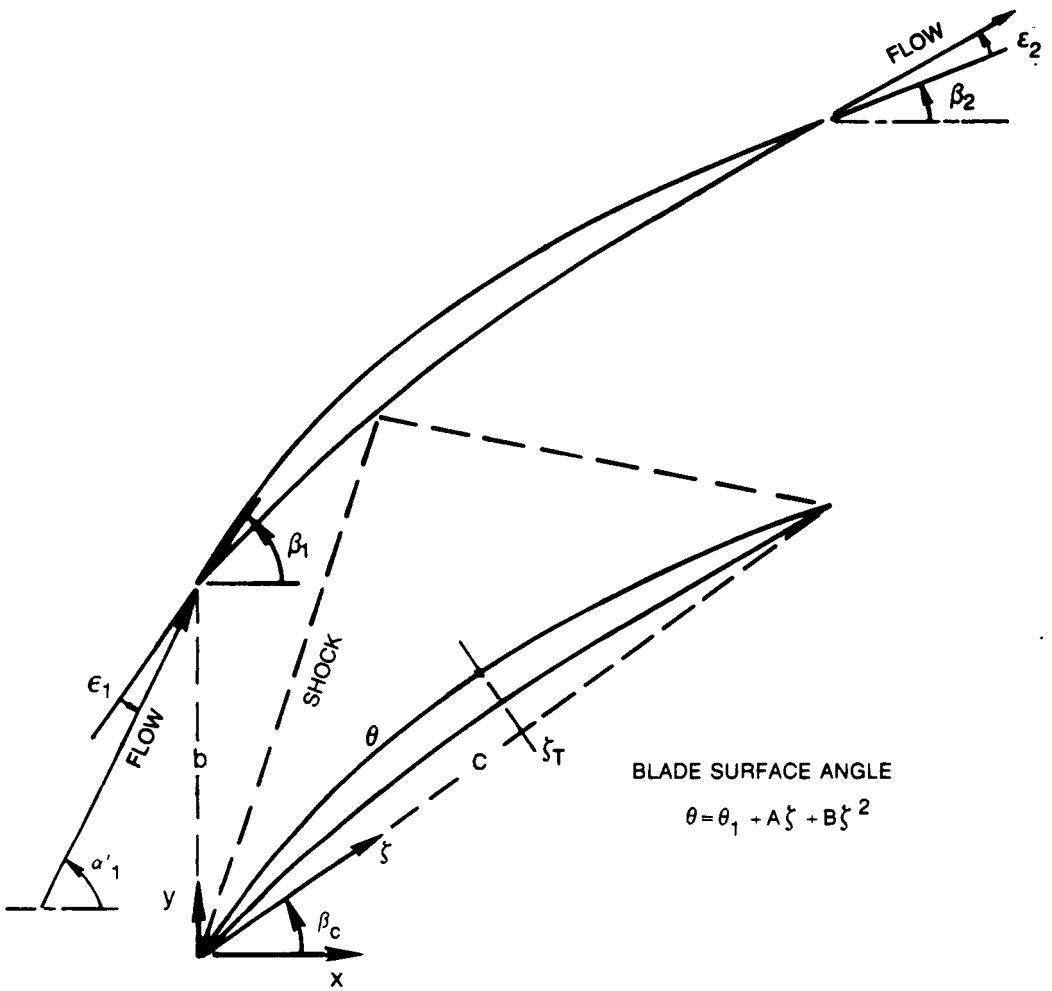

Figure 3. Blade geometry.

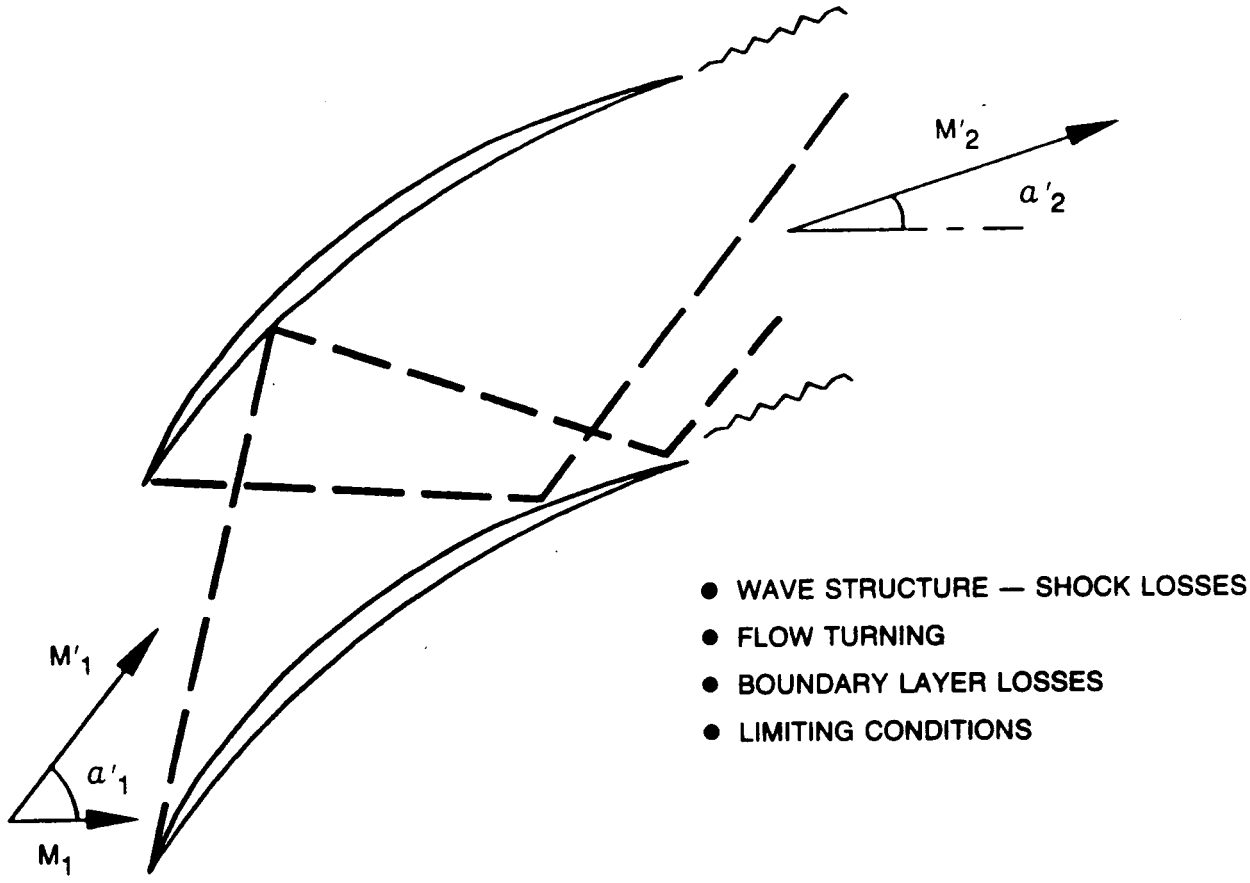

Figure 4. Flow modeling in performance deck.

STFF 3, $M_1 = 2.0$, $M_R = 1.5$, $P_{T_2}/P_{T_1} = 2.5$

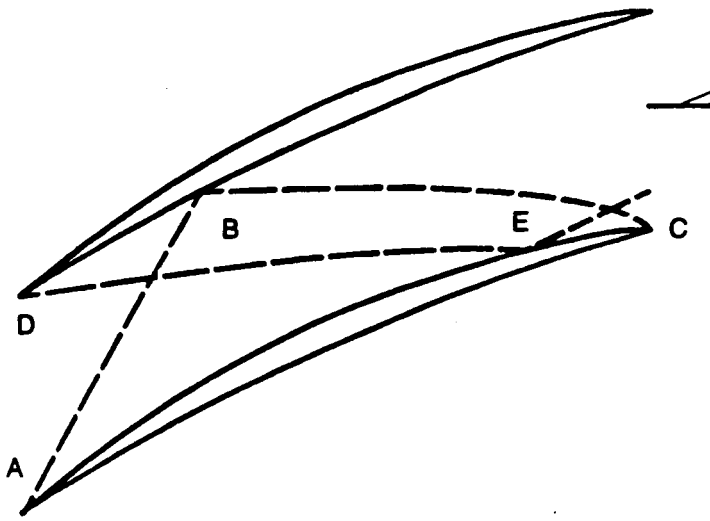

		STFF	CHARACTERISTICS
A	δ	= 4.00	4.00
B	δ	= 3.48	3.81
C	δ	= 5.04	4.48
D	δ	= 4.00	4.00
E	δ	= 4.64	4.93
F	α	= 10.28	11.30

Figure 5. Comparison of shock strength.

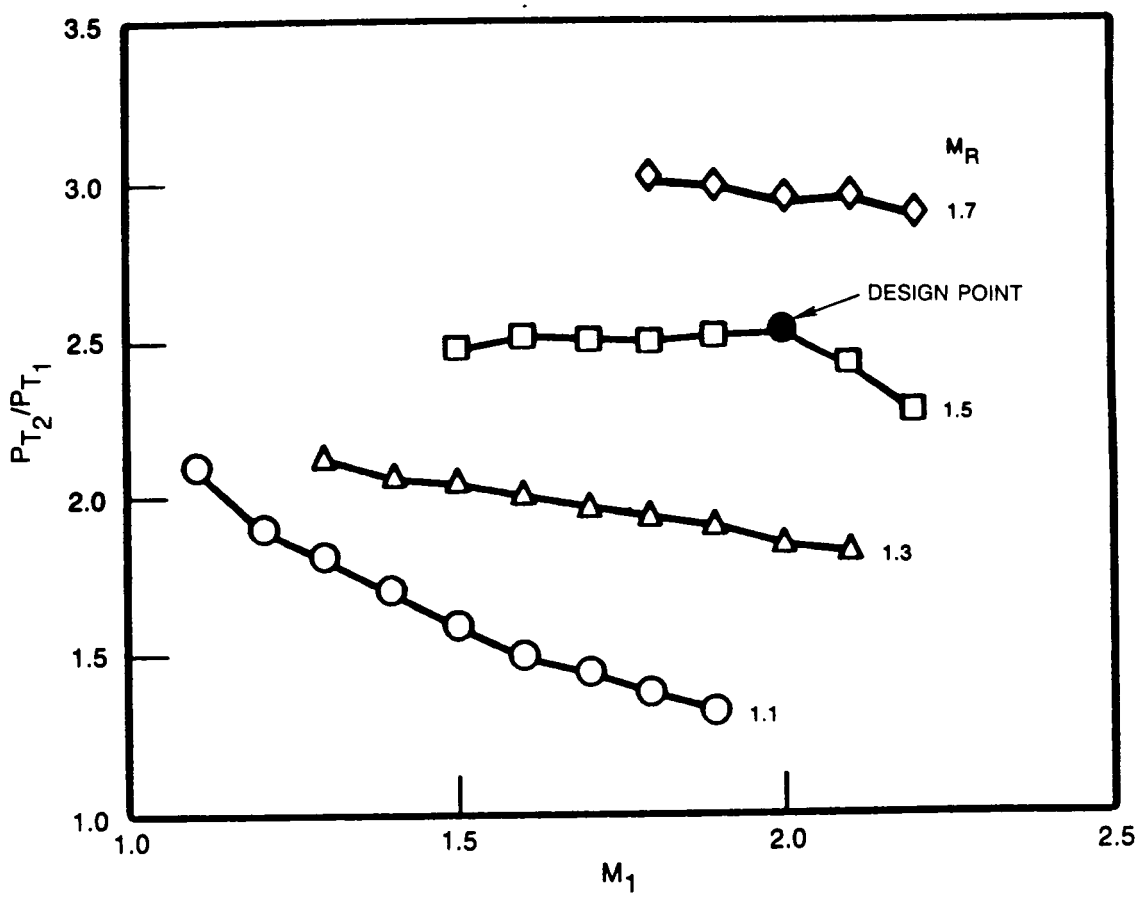

Figure 6. Total pressure ratio — STFF-3.

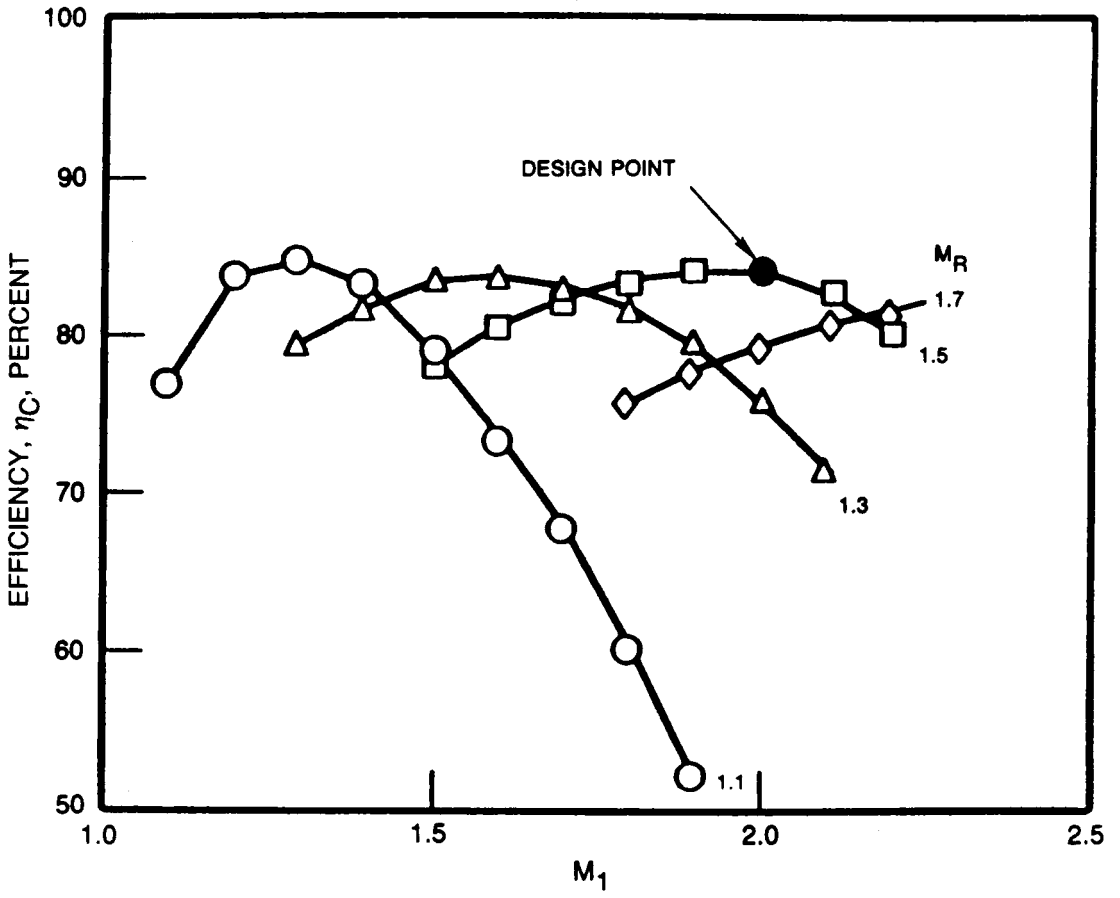

Figure 7. Fan efficiency — STFF-3.

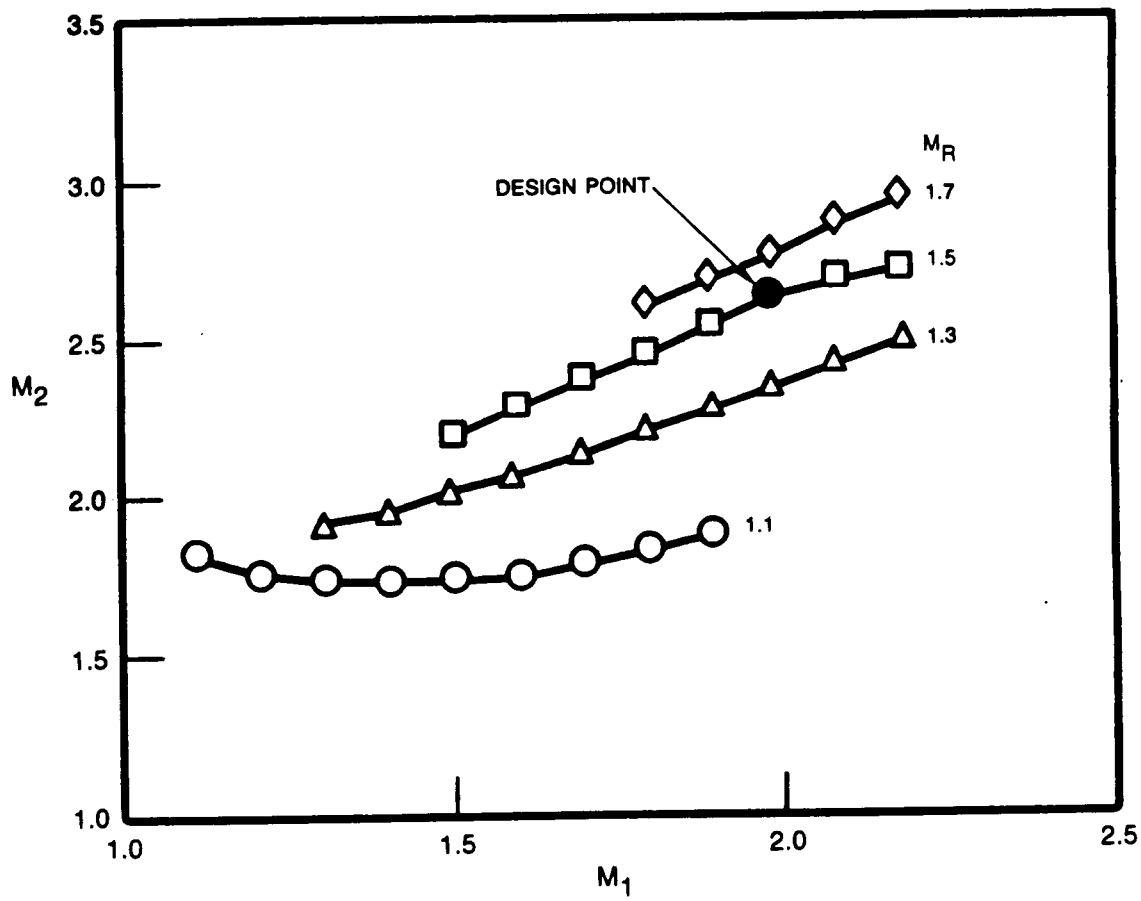

Figure 8. Fan exit Mach no. — STFF-3.

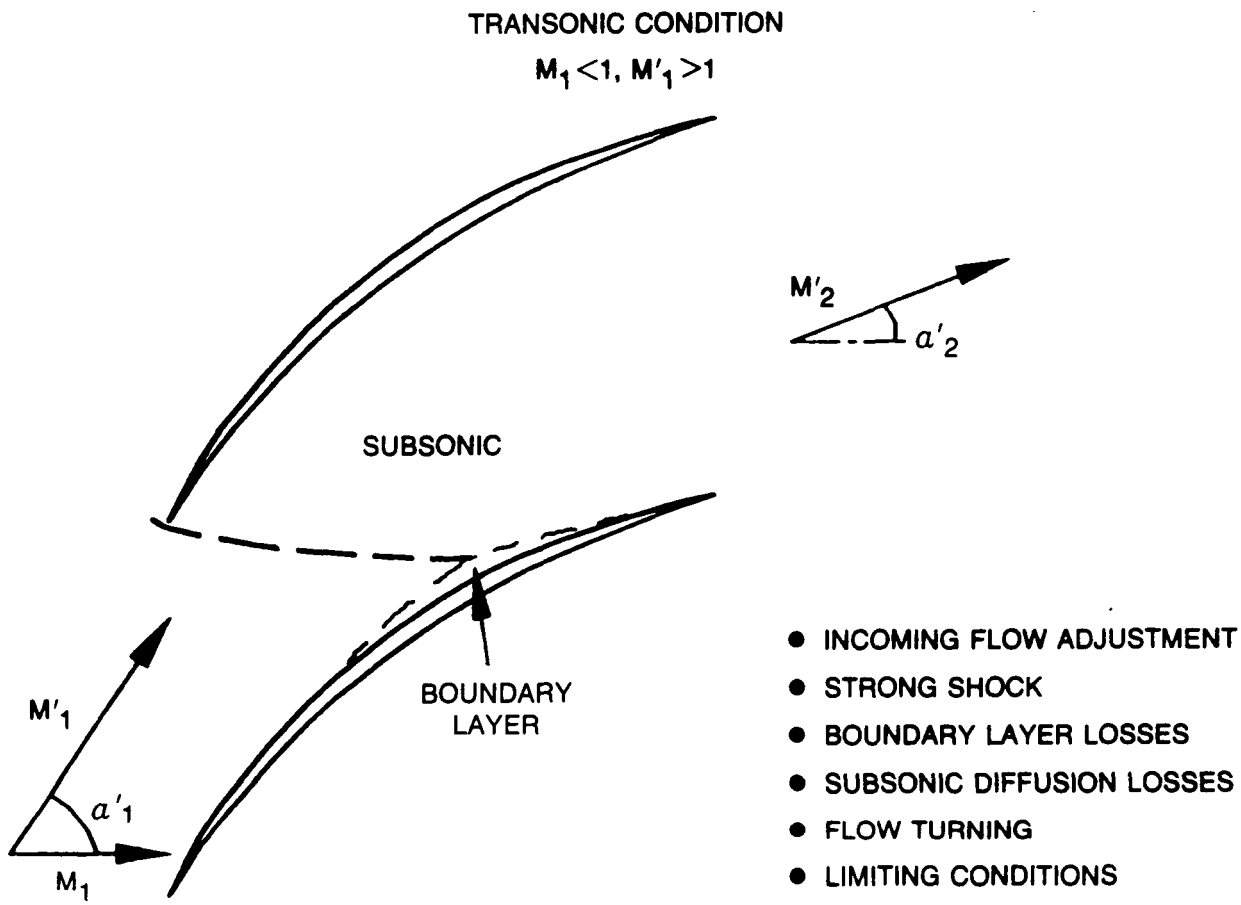

Figure 9. Flow modeling in transonic region.

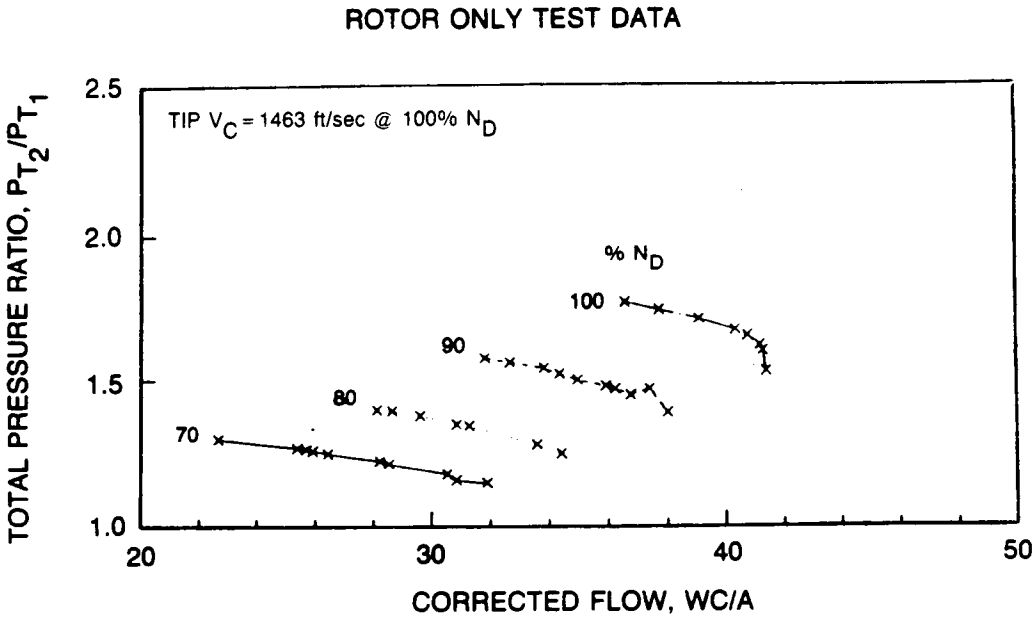

Figure 10. Measured fan performance — TS27.

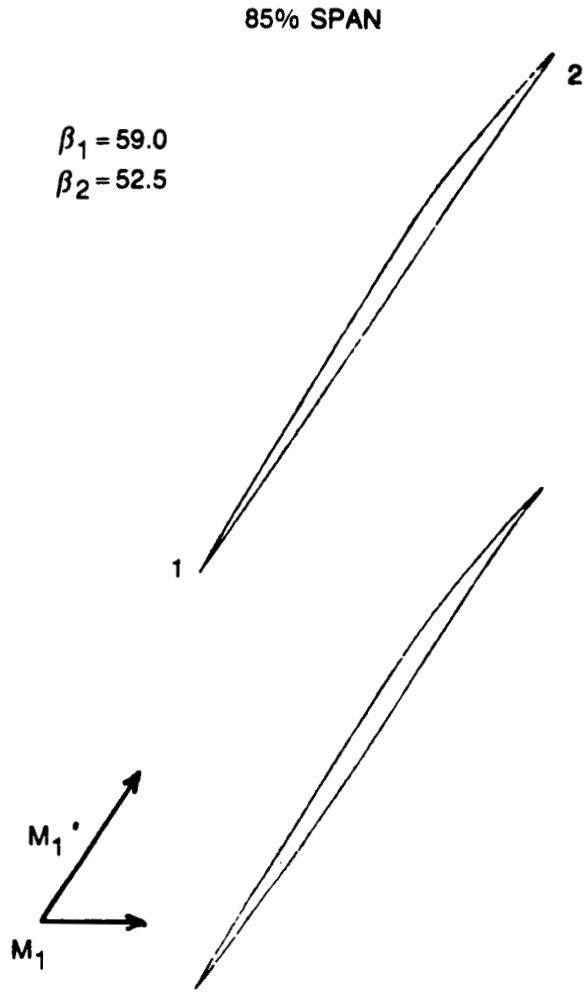

Figure 11. Blade shape — TS27

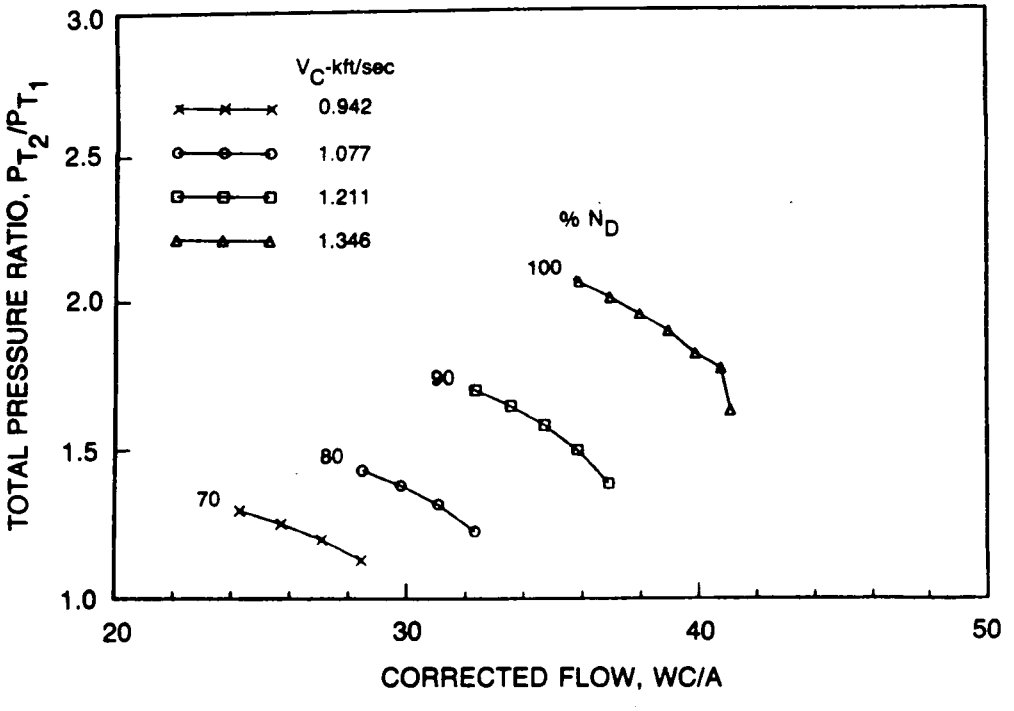

Figure 12. Calculated fan performance — TS27.

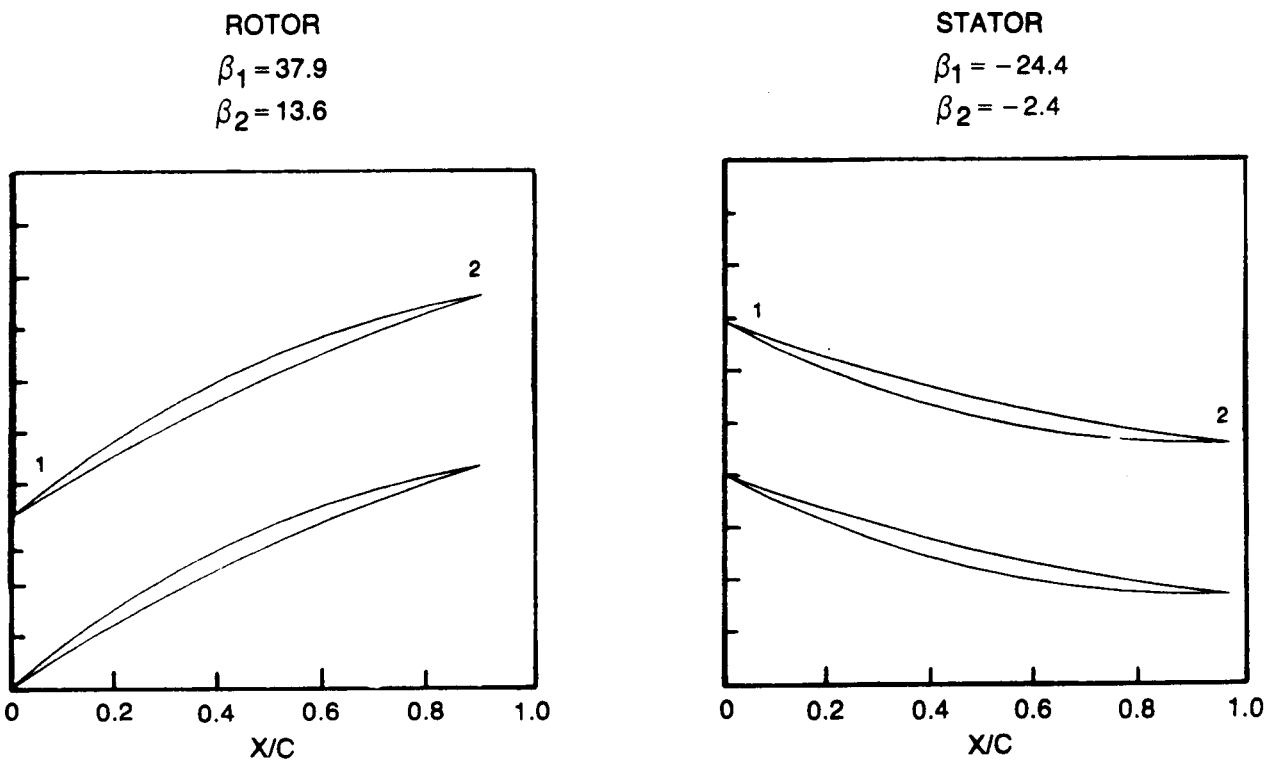

Figure 13. Blade shapes — STFF 4.

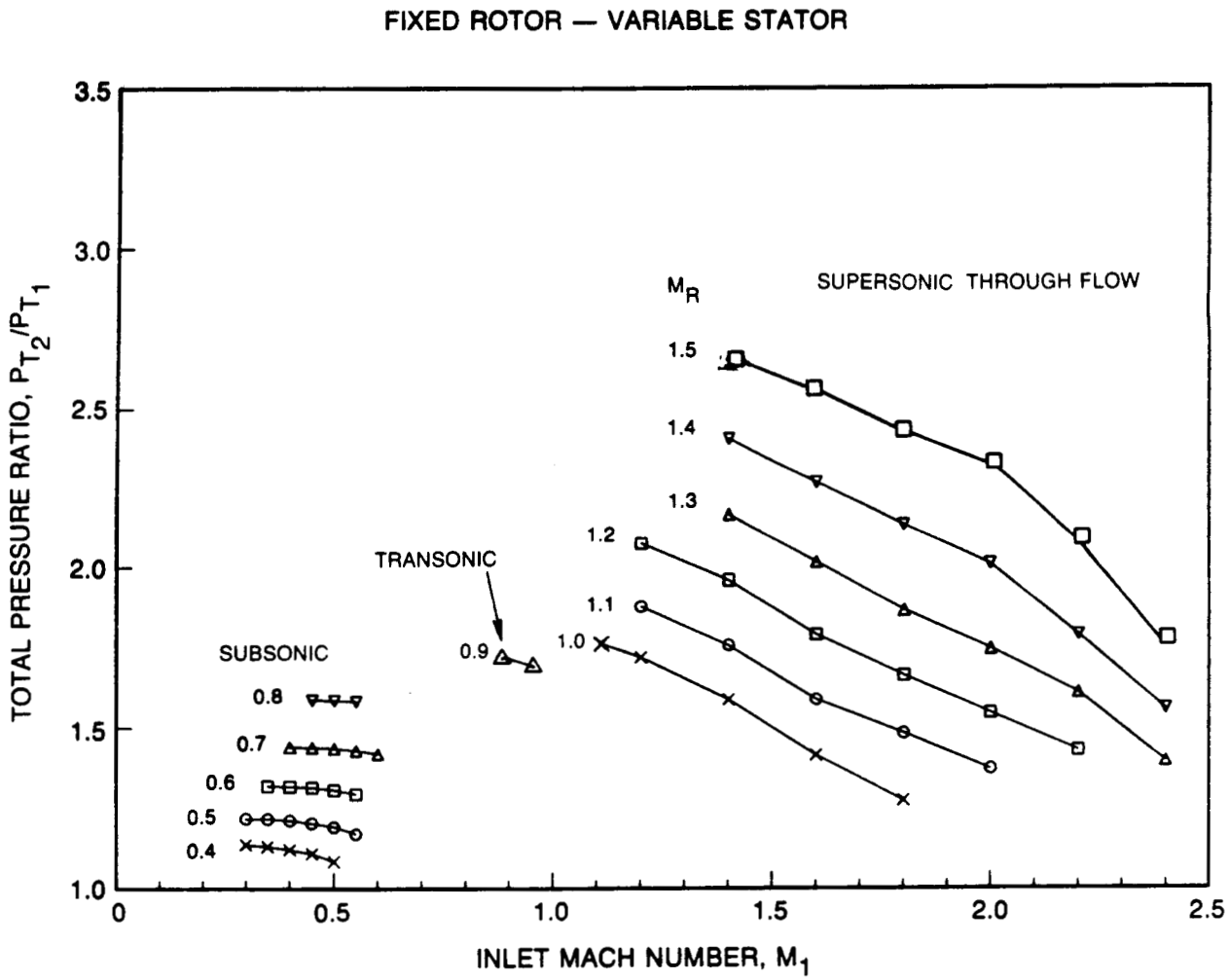

Figure 14. Fixed-rotor total pressure ratio — STFF 4.

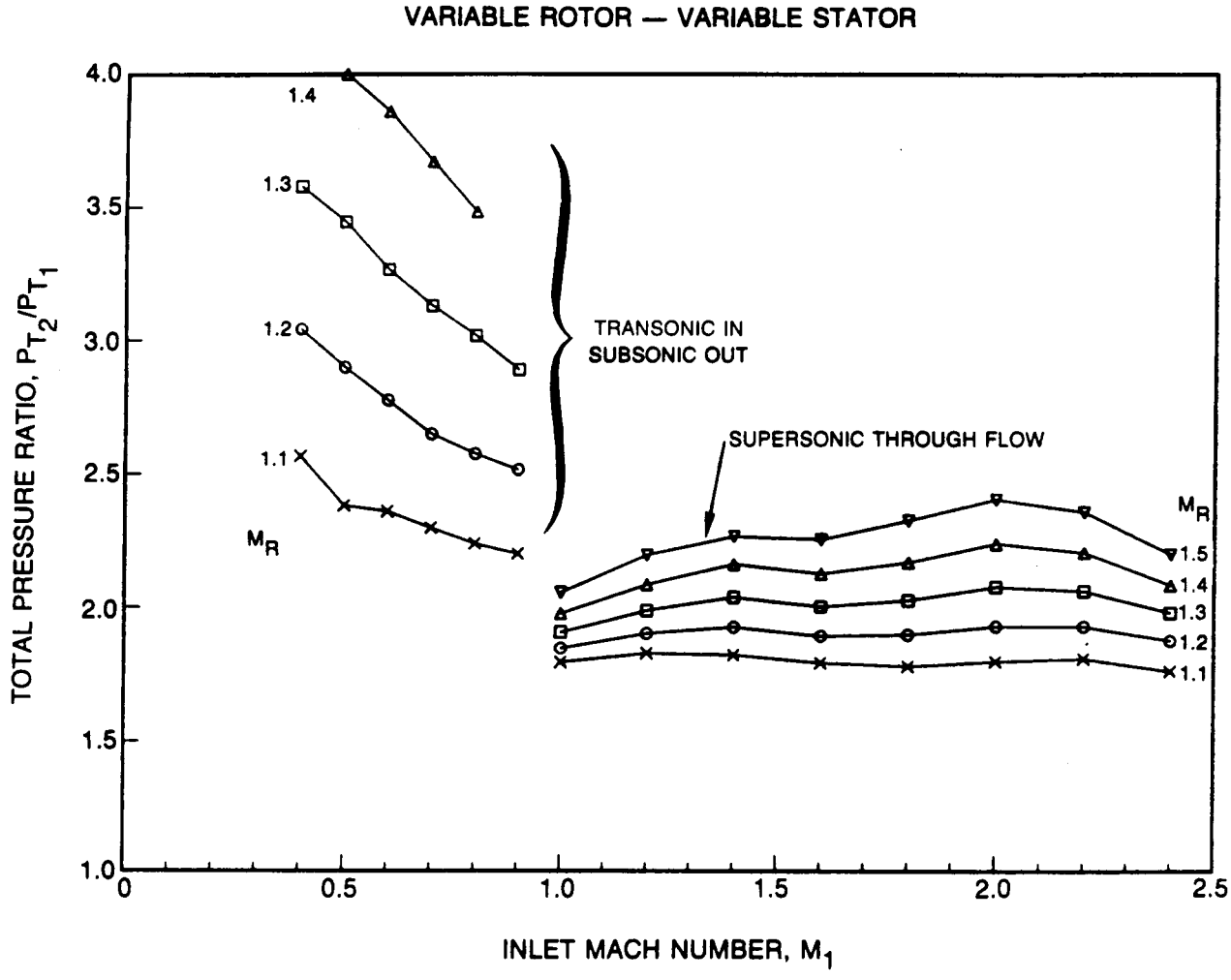

Figure 15. Variable rotor total pressure ratio — STFF 4.

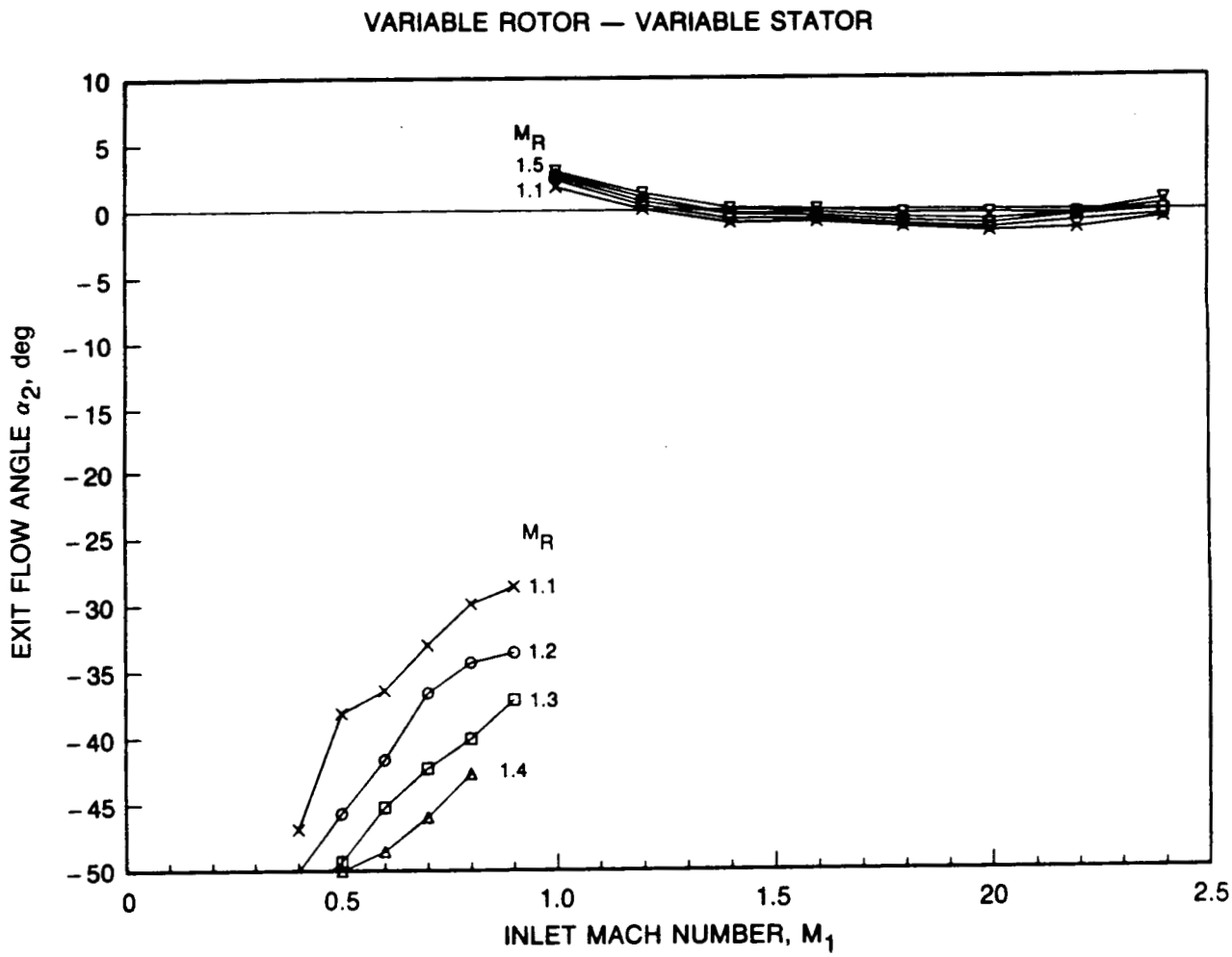

Figure 16. Fan exit flow angle — STFF 4.

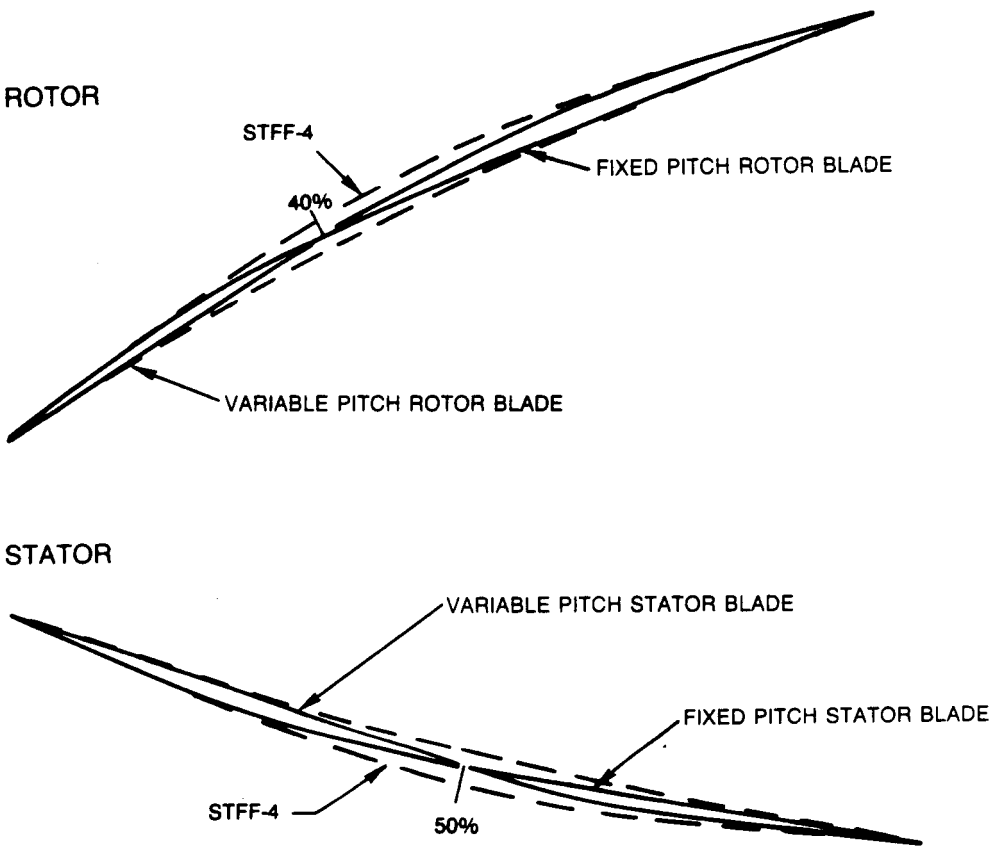

Figure 17. Blade shapes — VPRS-1.

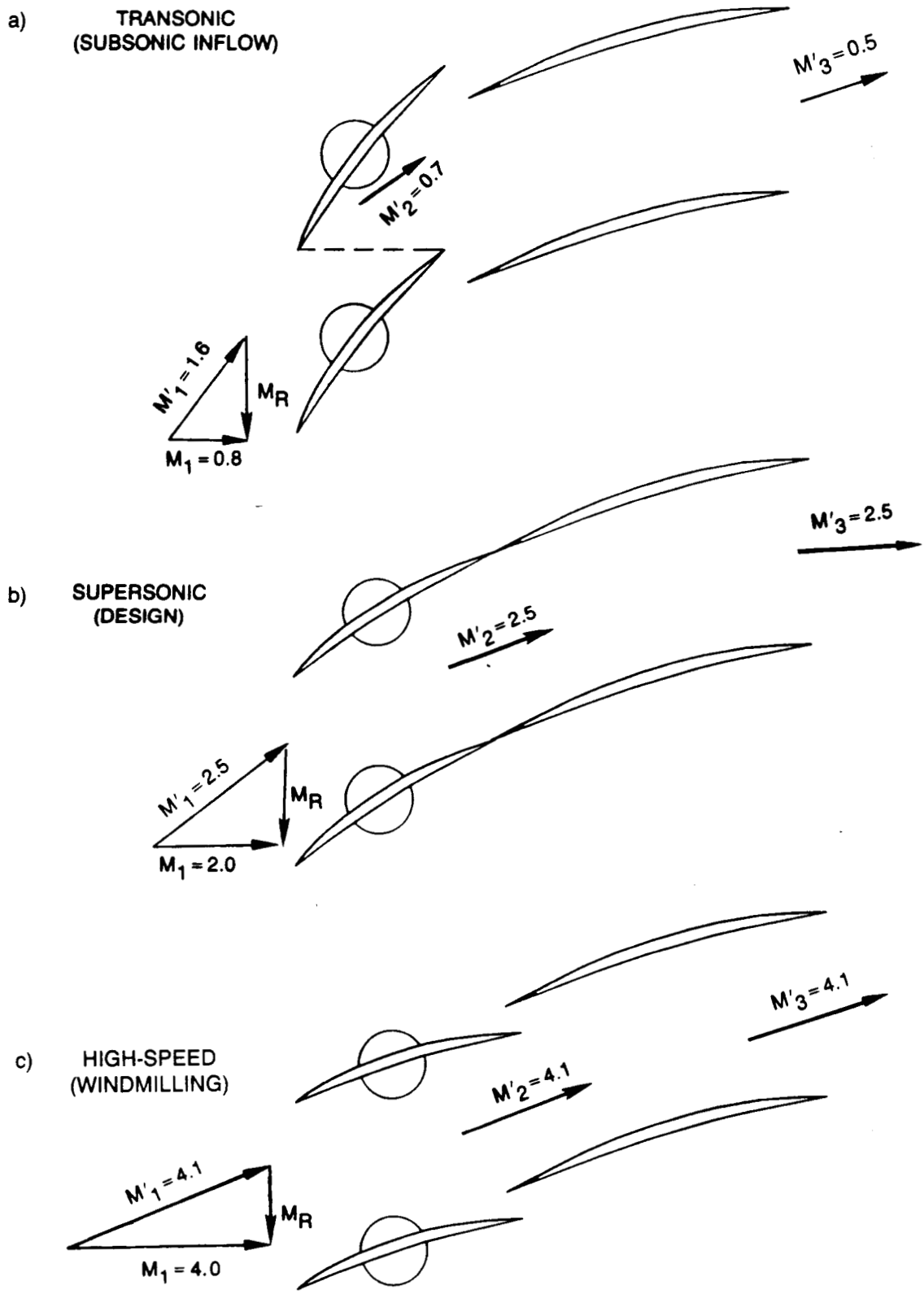

Figure 18. Variable-pitch split-rotor geometries.

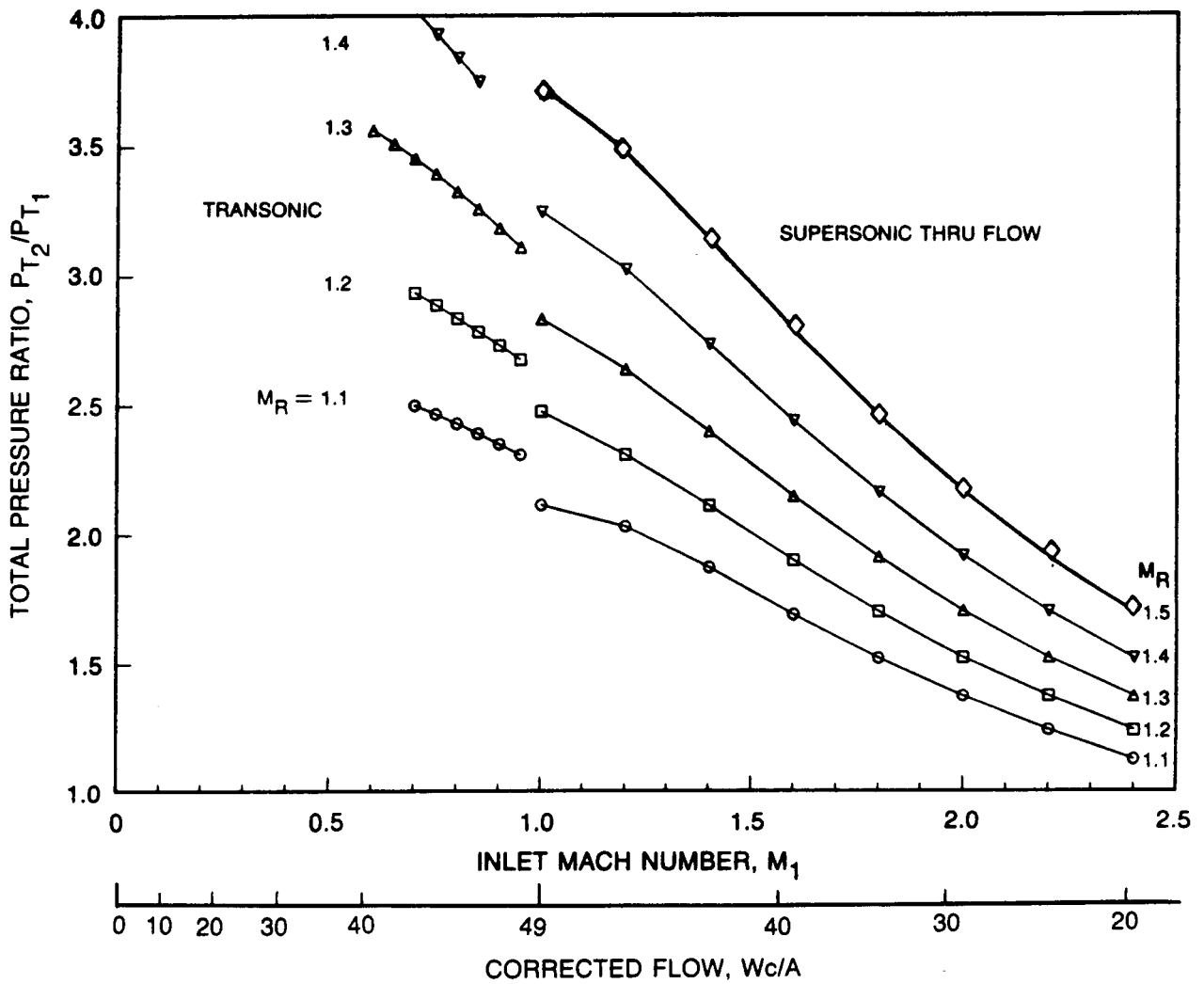

Figure 19. Fan performance VPRS-1.

MACH 2.32 SUPERSONIC TRANSPORT

SUPERSONIC FAN ENGINE (AFTERBURNER)

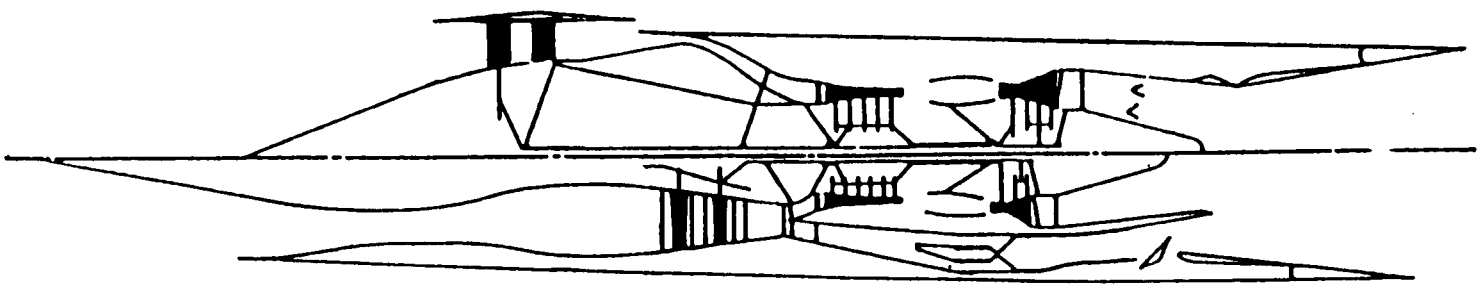

CONVENTIONAL FAN ENGINE (DUCT BURNER)

Figure 20. Supersonic fan engine/conventional flowpath comparison.

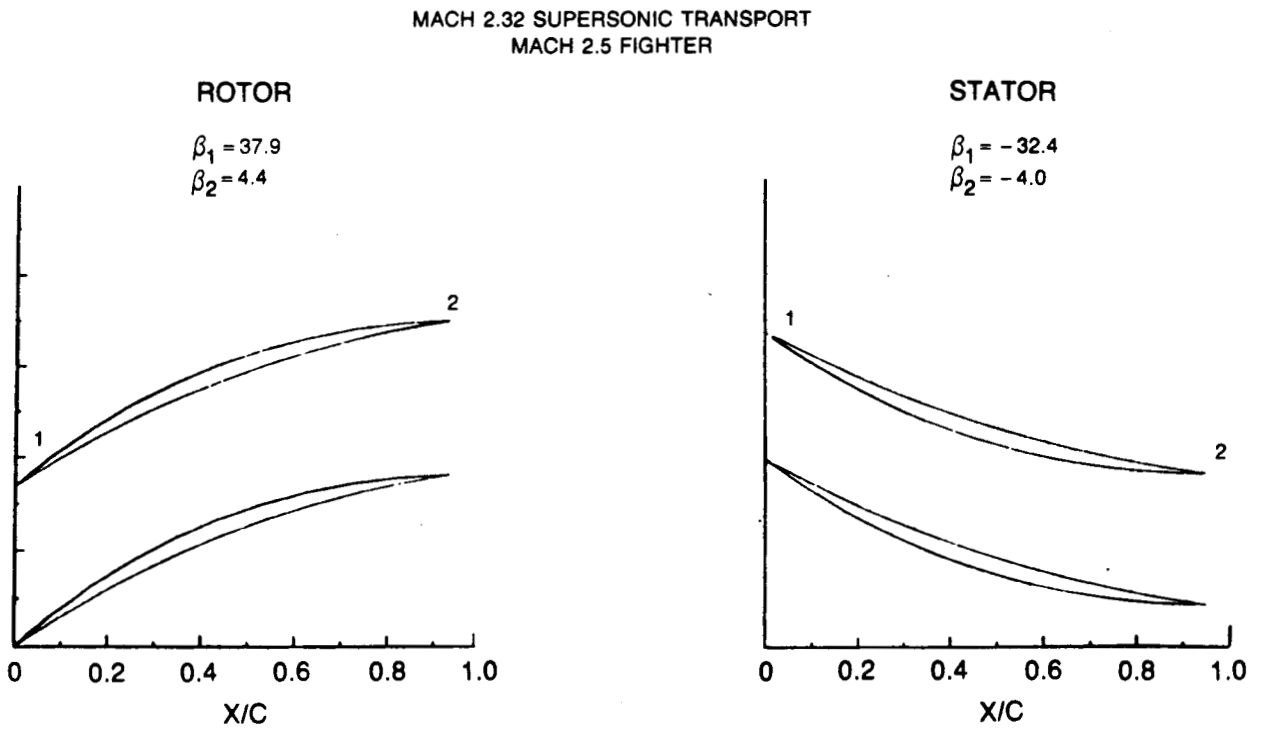

Figure 21. Blade shapes STFF-8.

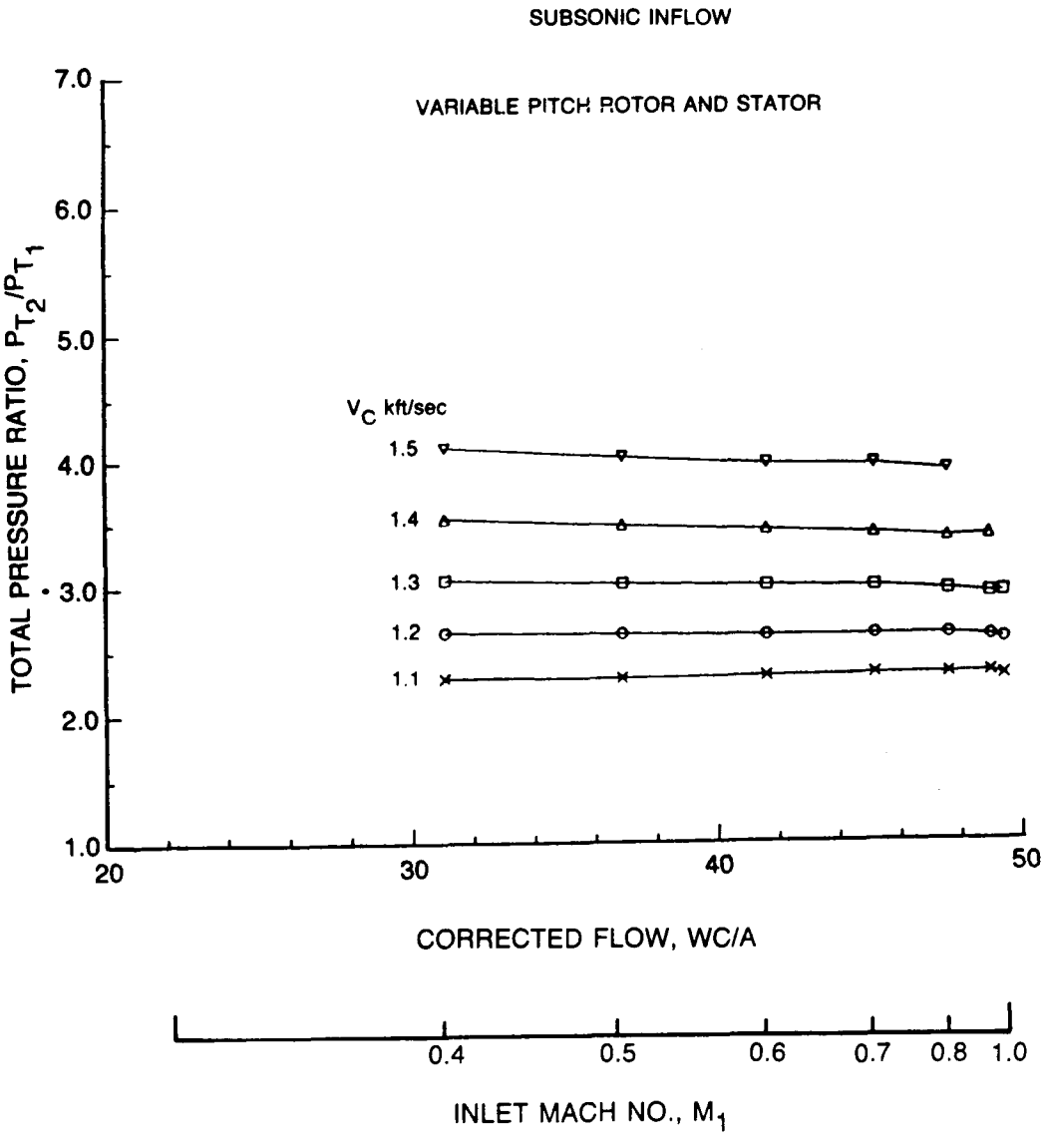

Figure 22. Subsonic total pressure ratio — STFF-8.

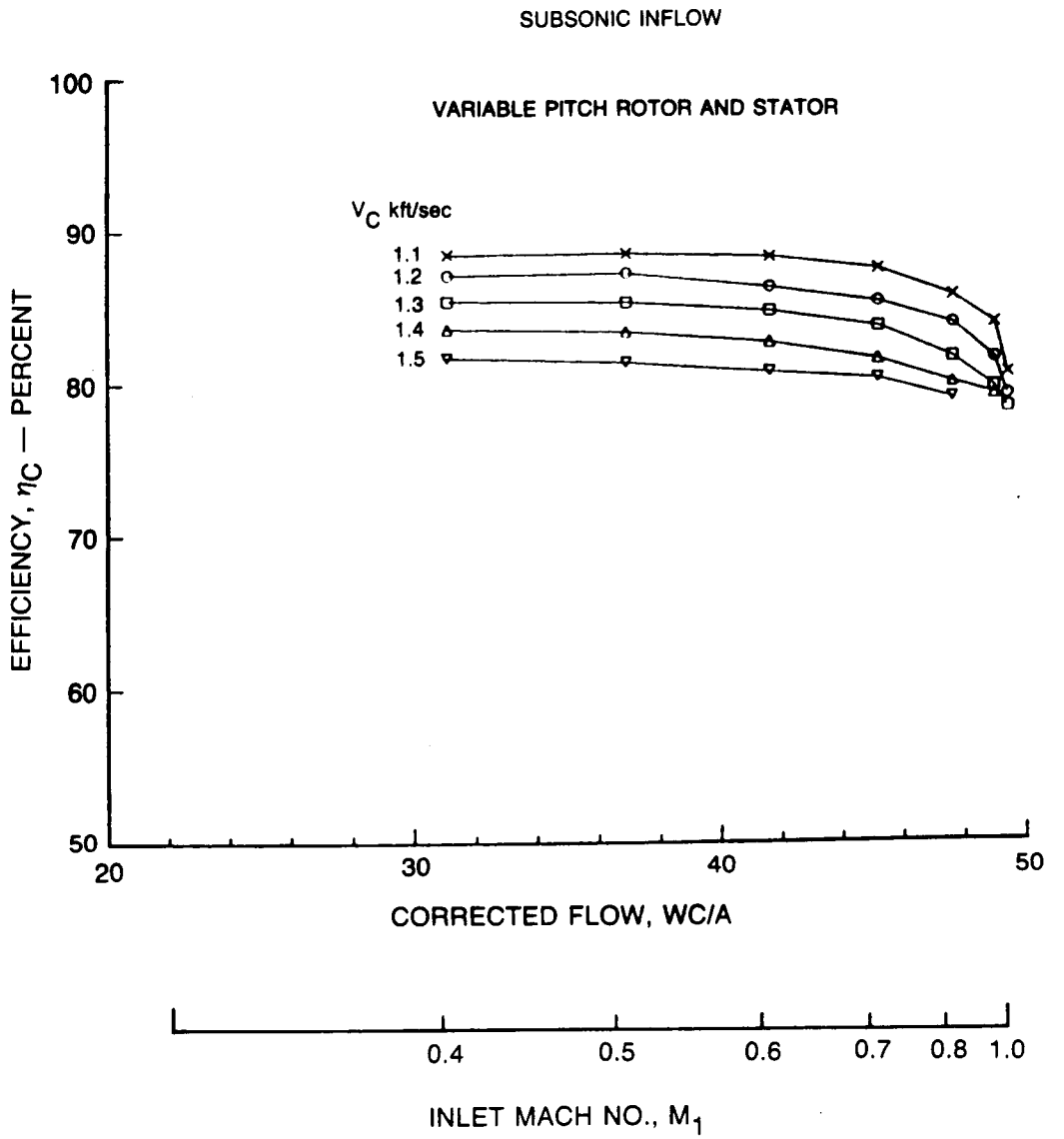

Figure 23. Subsonic fan efficiency — STFF-8.

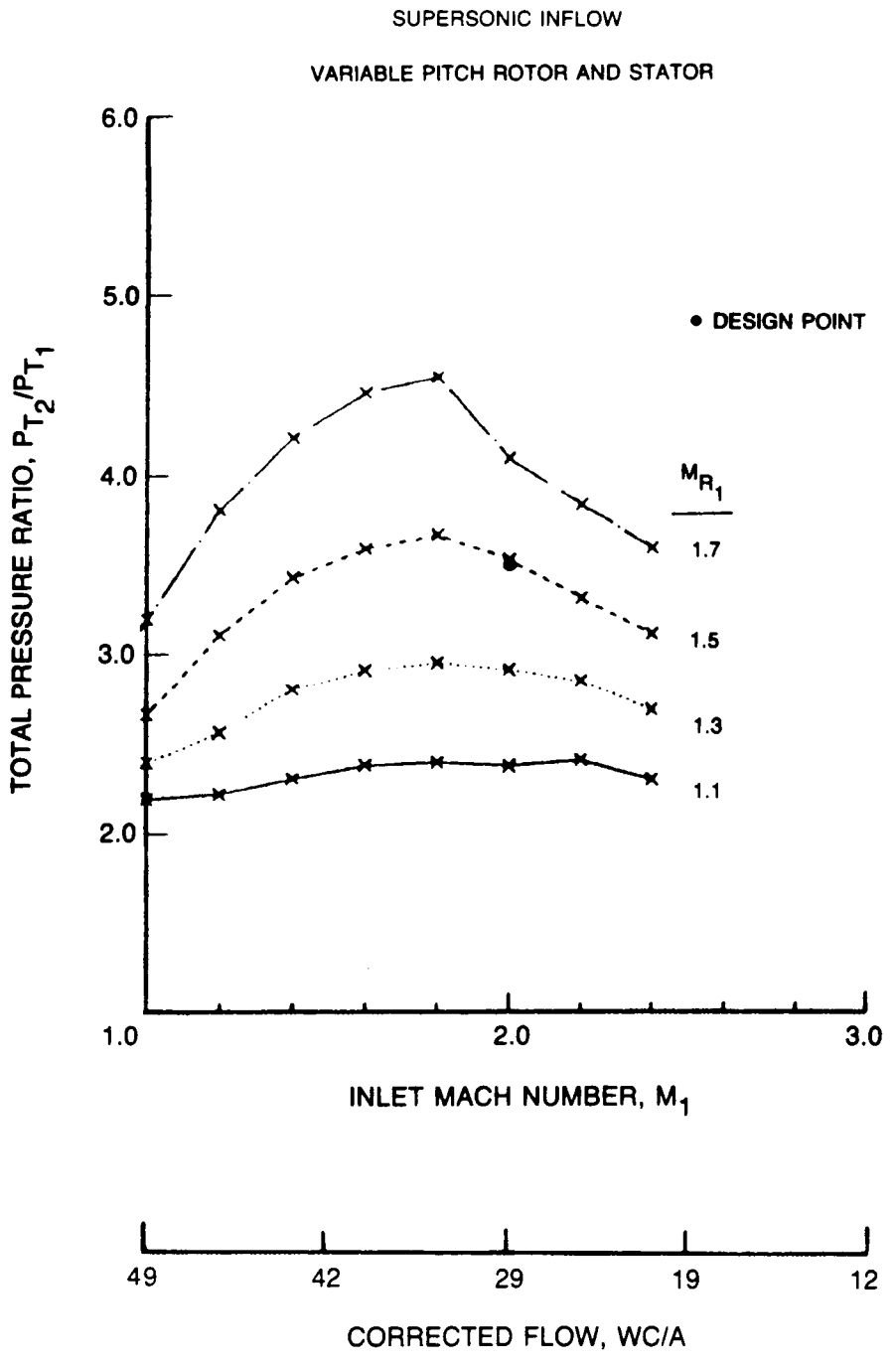

Figure 24. Supersonic total pressure ratio — STFF-8.

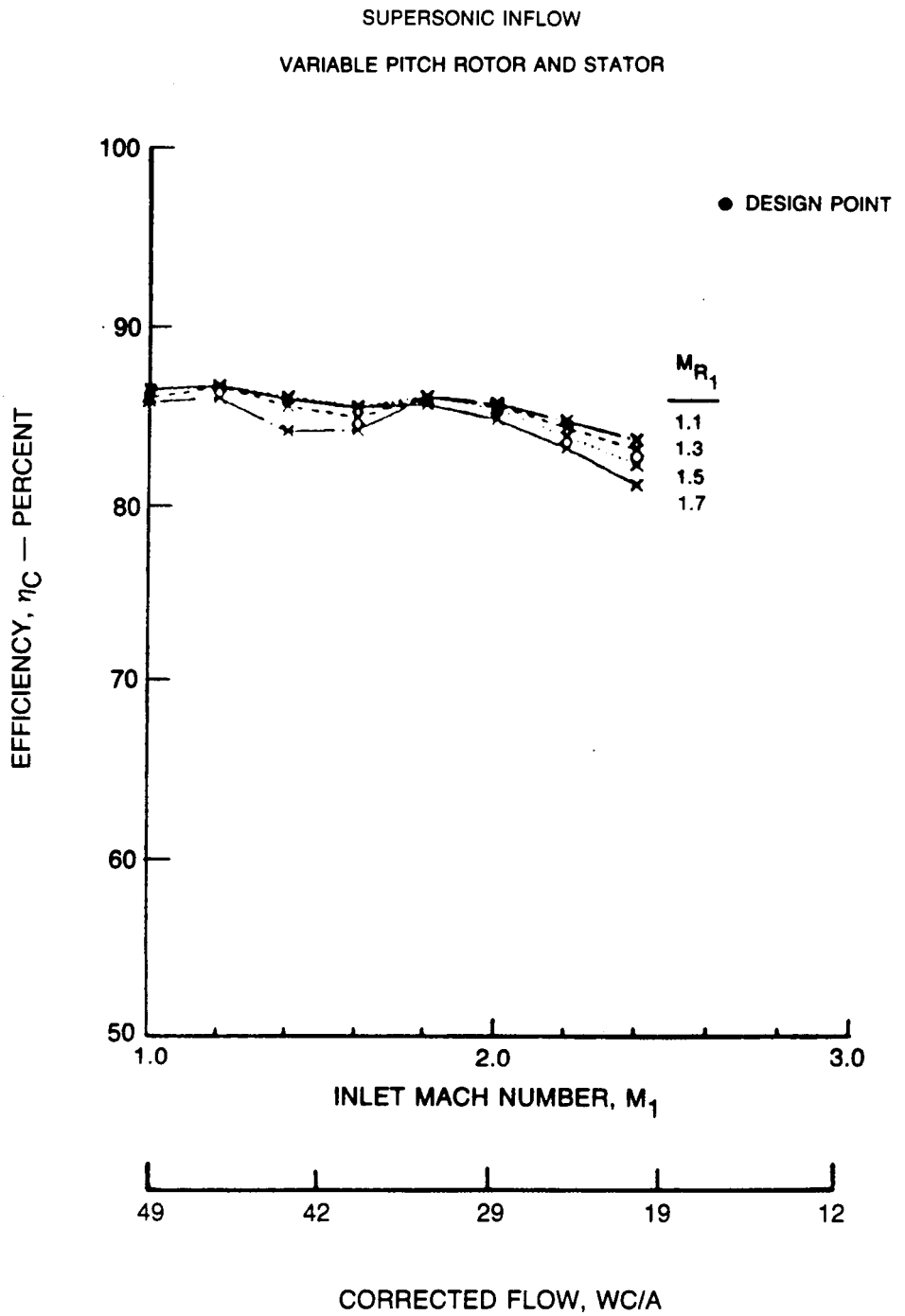

Figure 25. Supersonic fan efficiency — STFF-8.

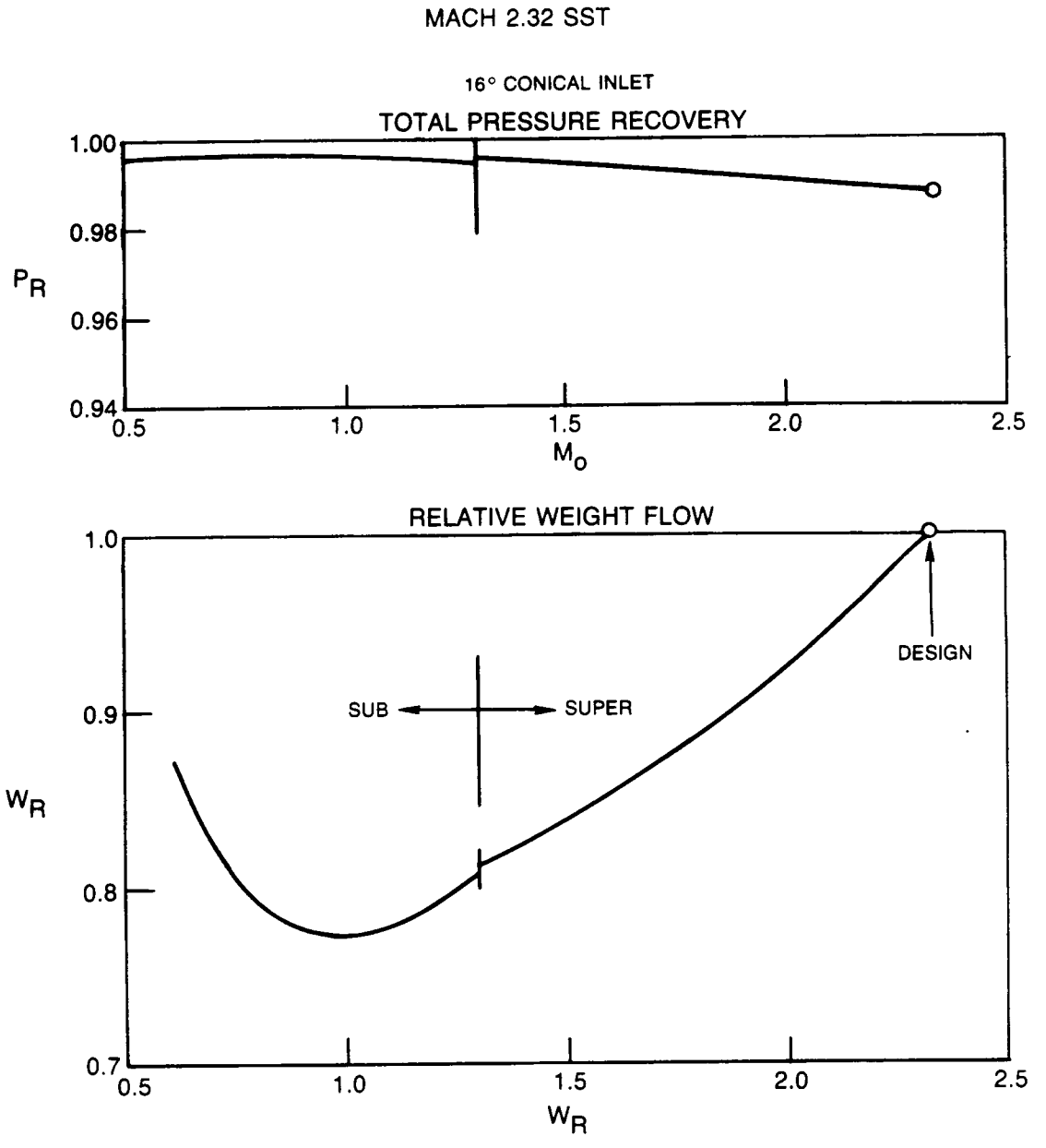

Figure 26. STFF inlet flow characteristics.

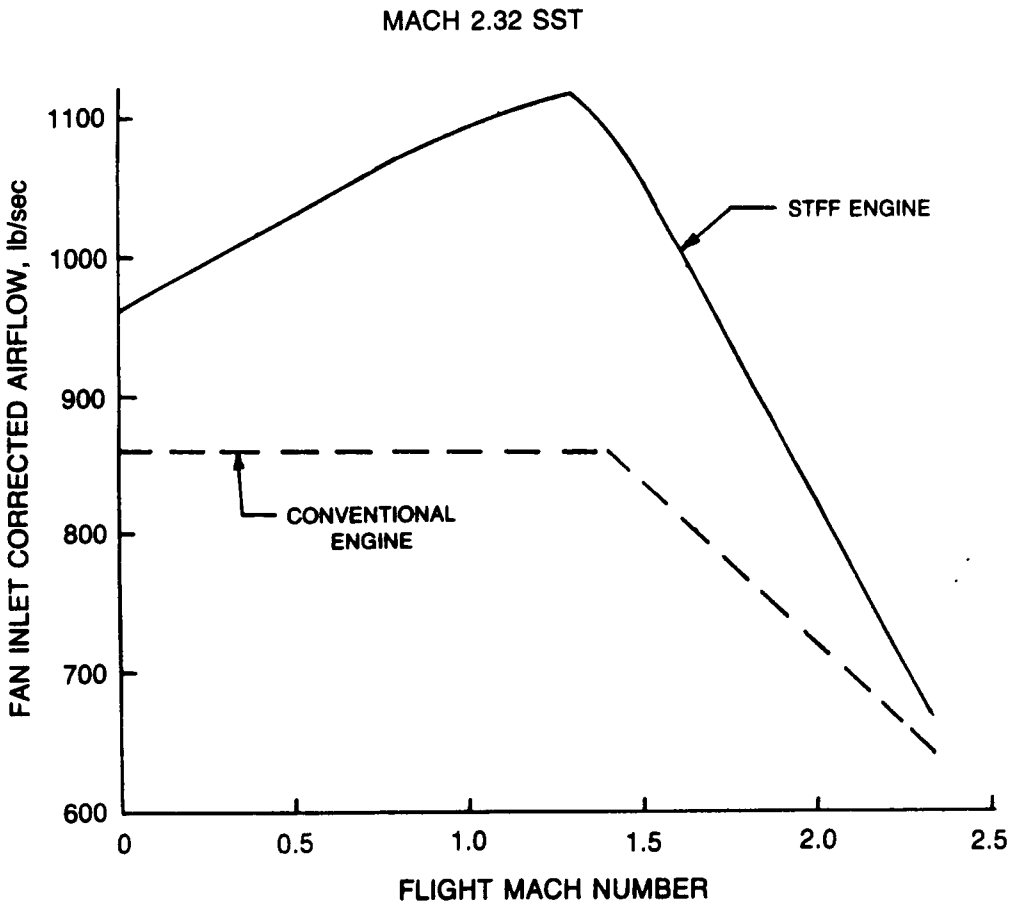

Figure 27. Fan inlet correct airflow schedules.

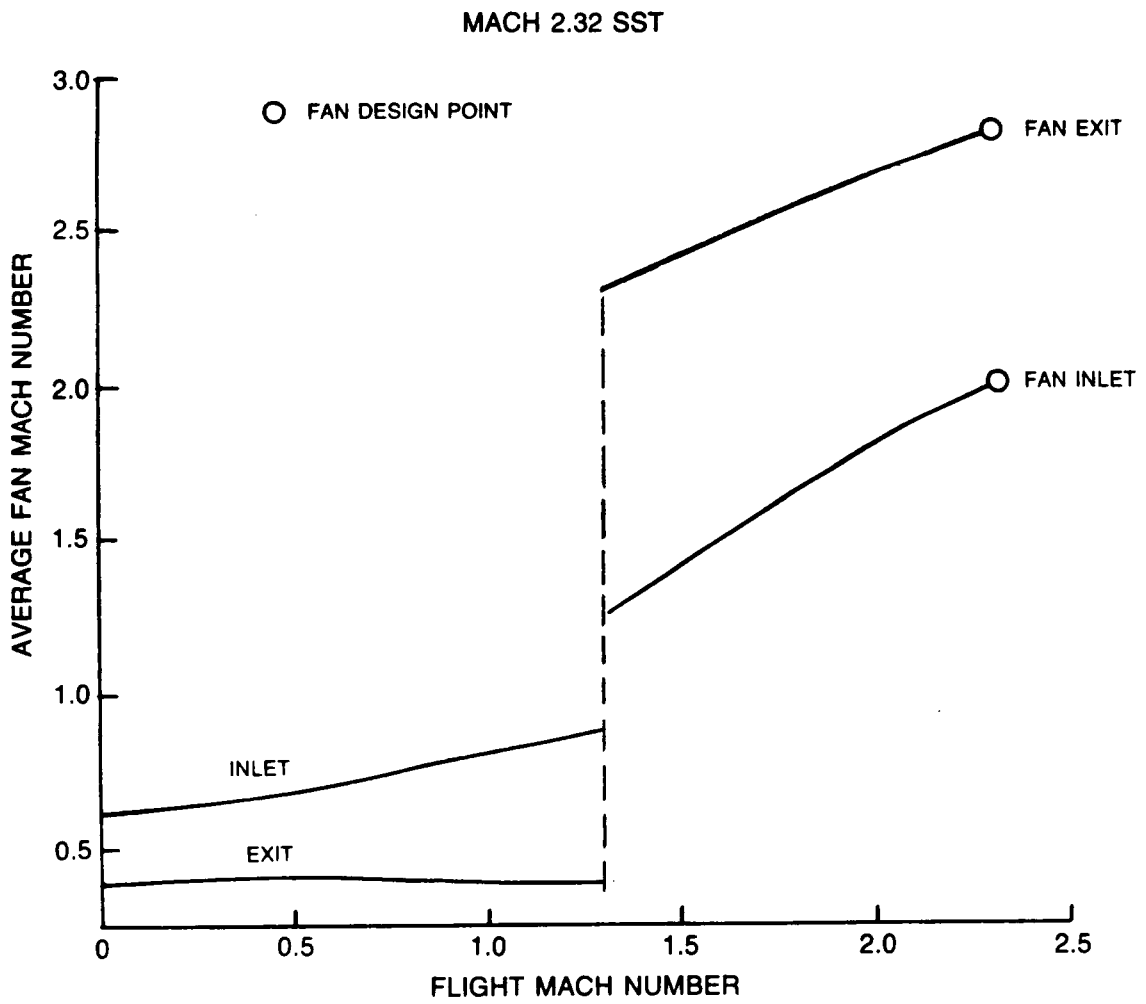

Figure 28. STFF fan inlet and exit Mach numbers.

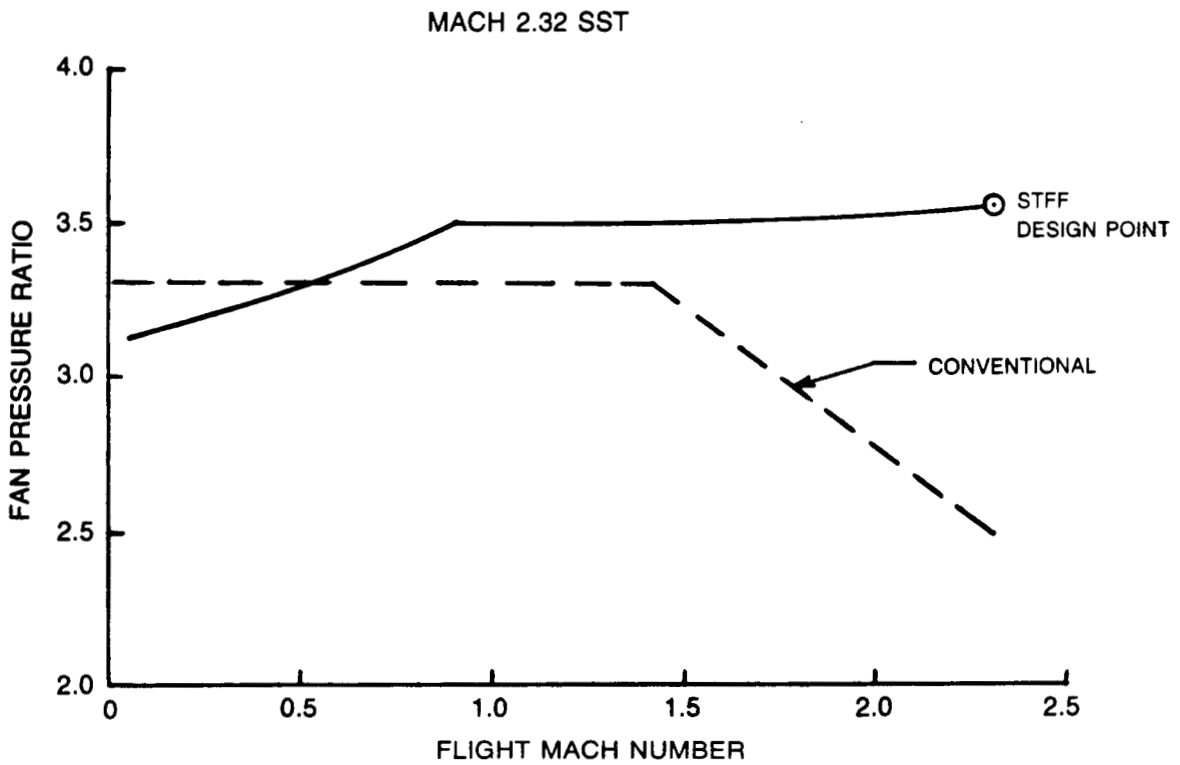

Figure 29. Fan pressure ratio variation with flight Mach number.

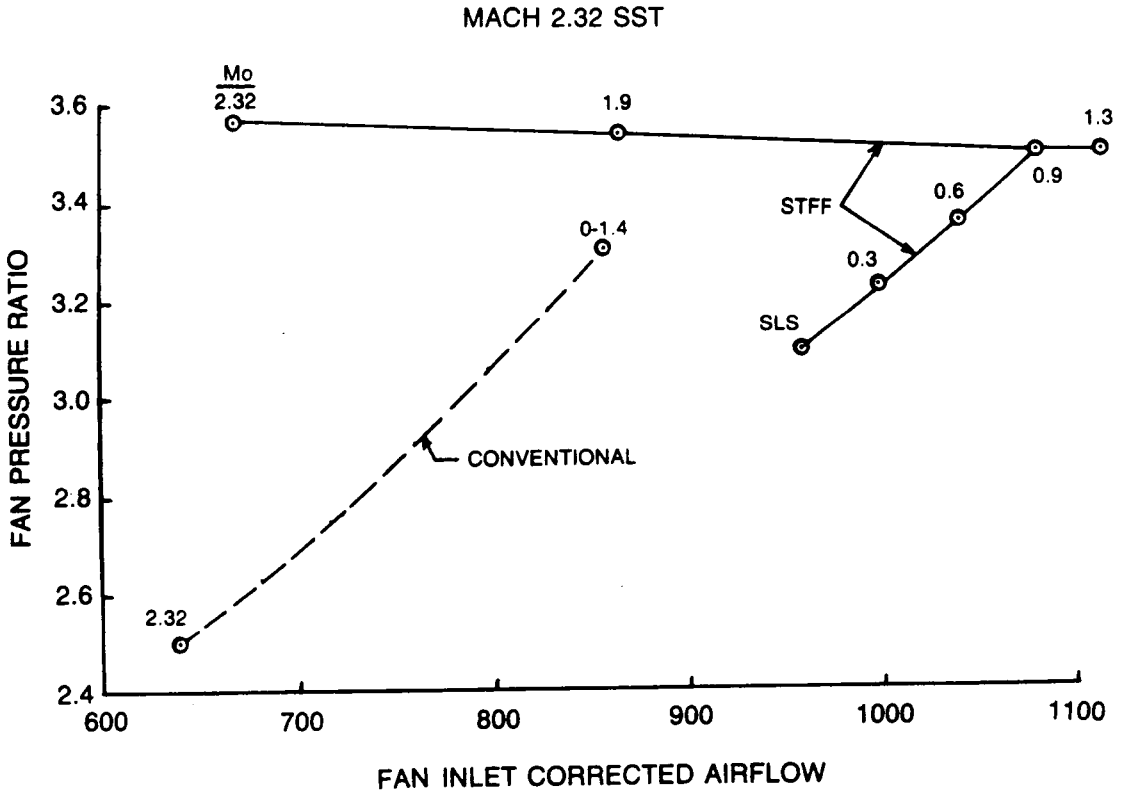

Figure 30. Fan operating line characteristics.

MACH 2.32 SST

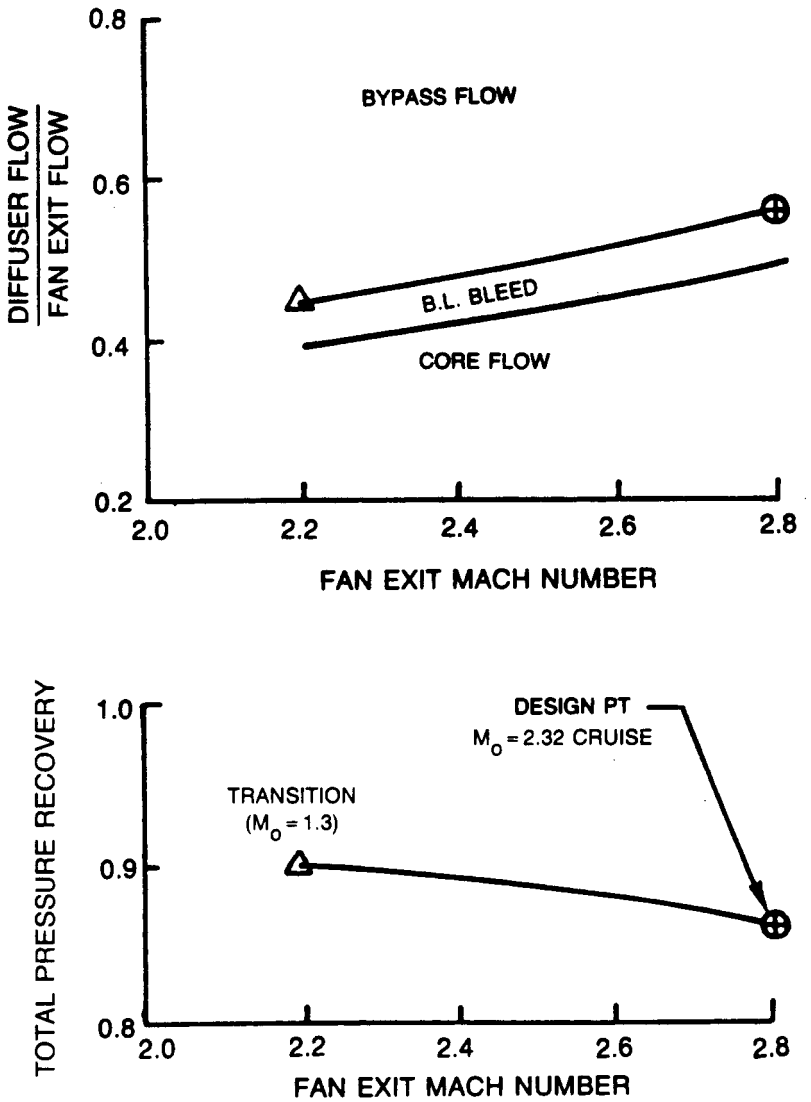

Figure 31. Supersonic diffuser characteristics.

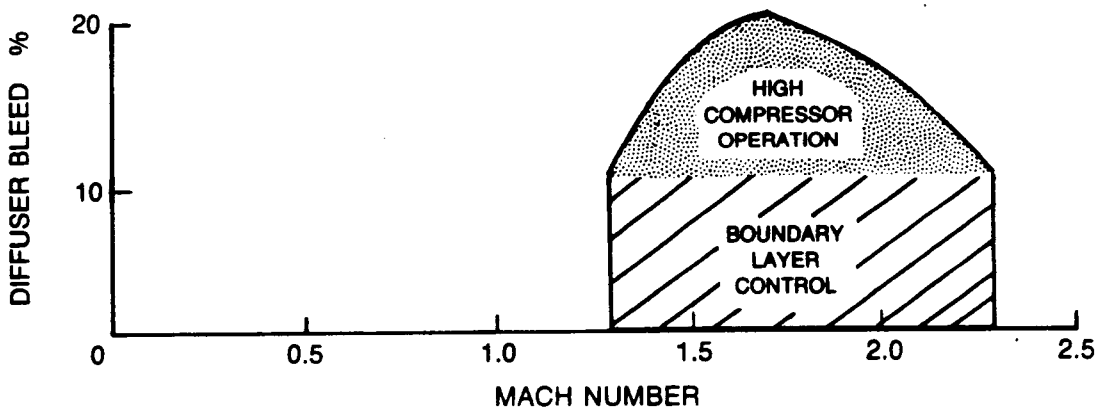

Figure 32. Supersonic diffuser bleed requirements.

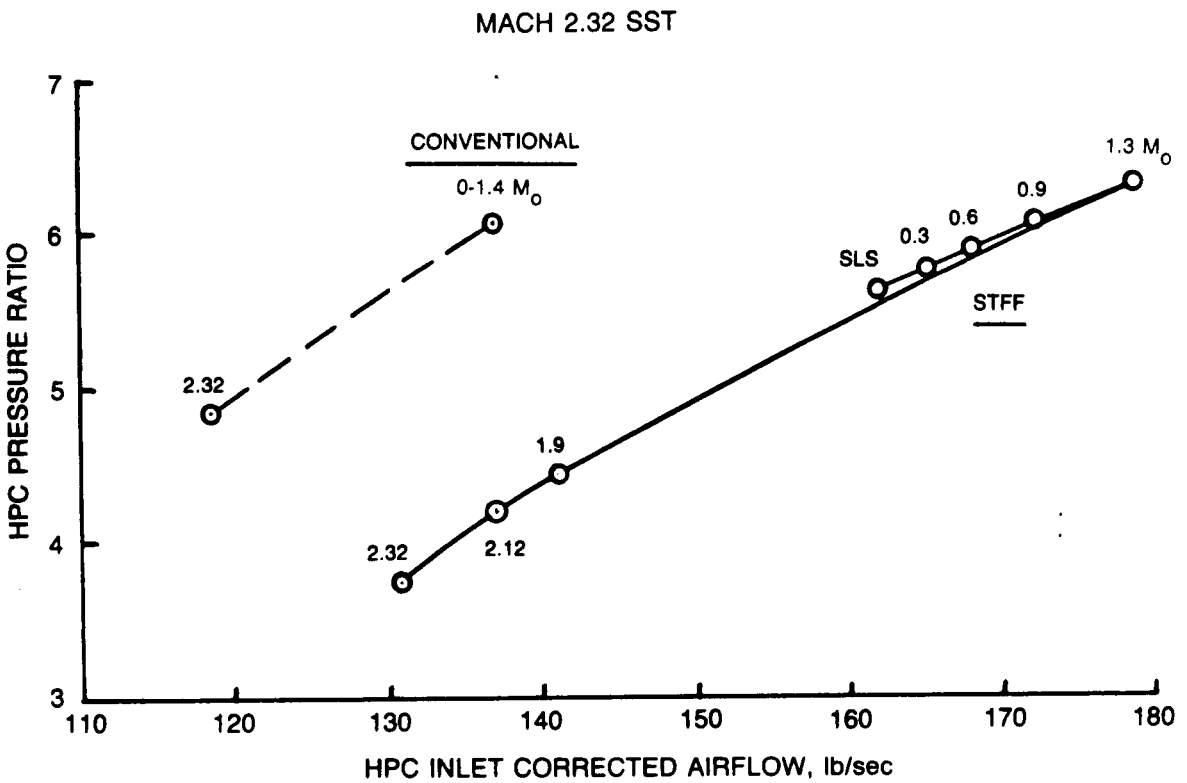

Figure 33. High compressor operation for conventional and STFF engines.

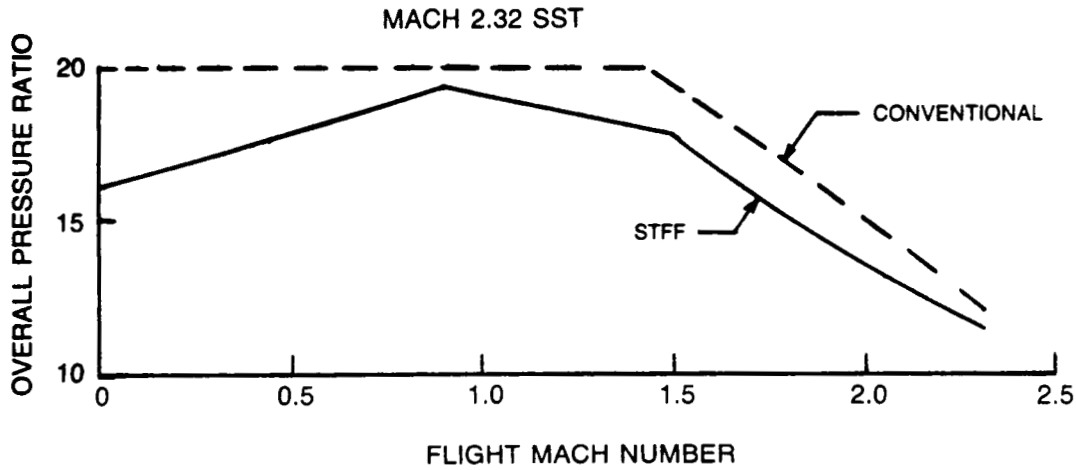

Figure 34. Overall compression ratio variation with Mach number.

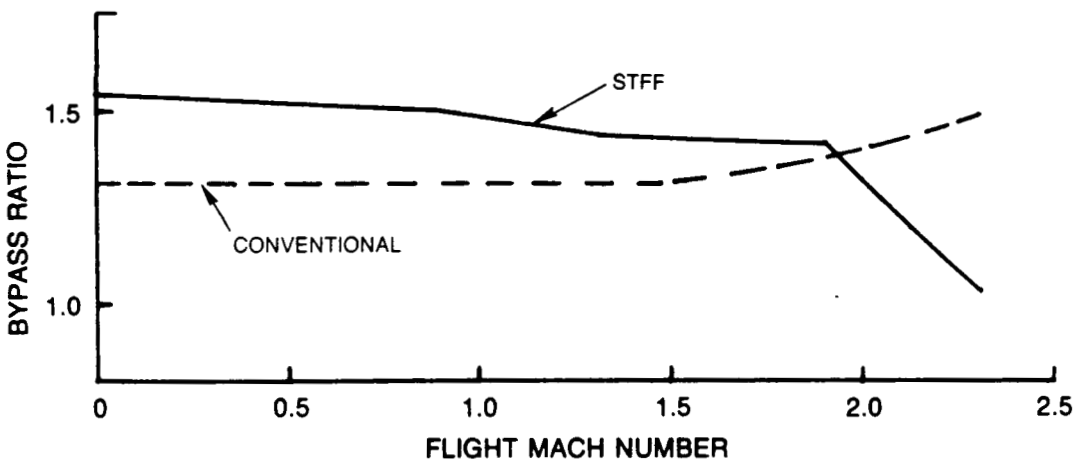

Figure 35. Bypass ratio variation with Mach number.

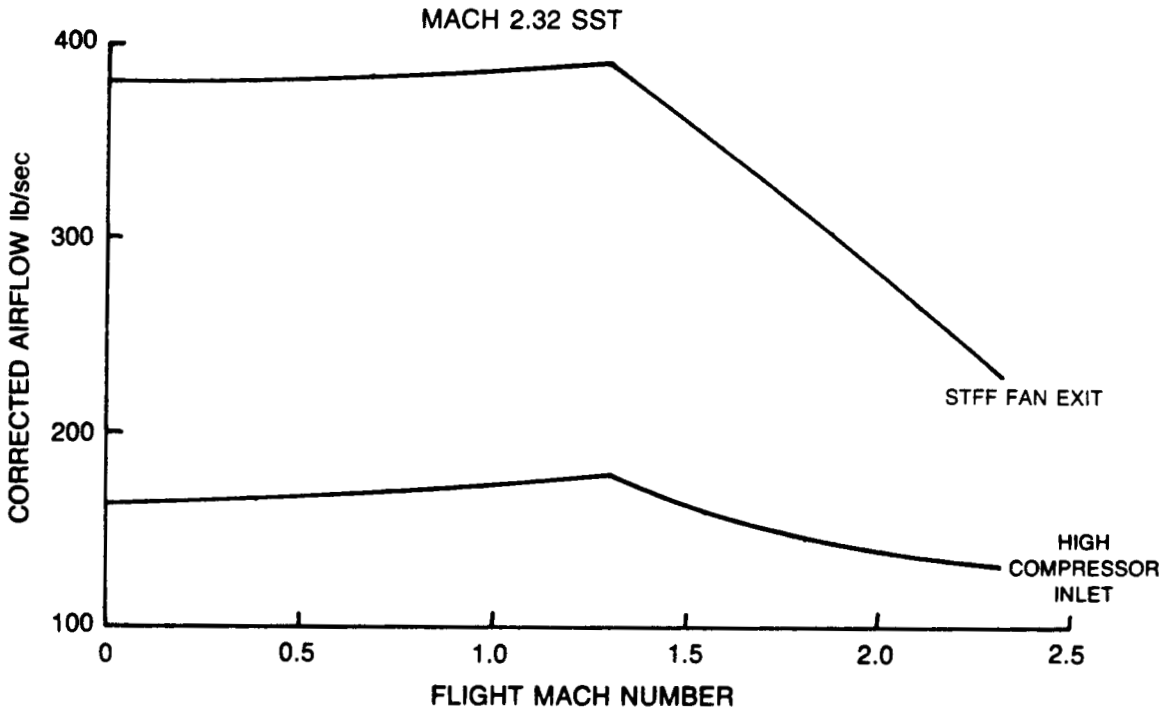

Figure 36. STFF fan exit and HPC corrected flow variations.

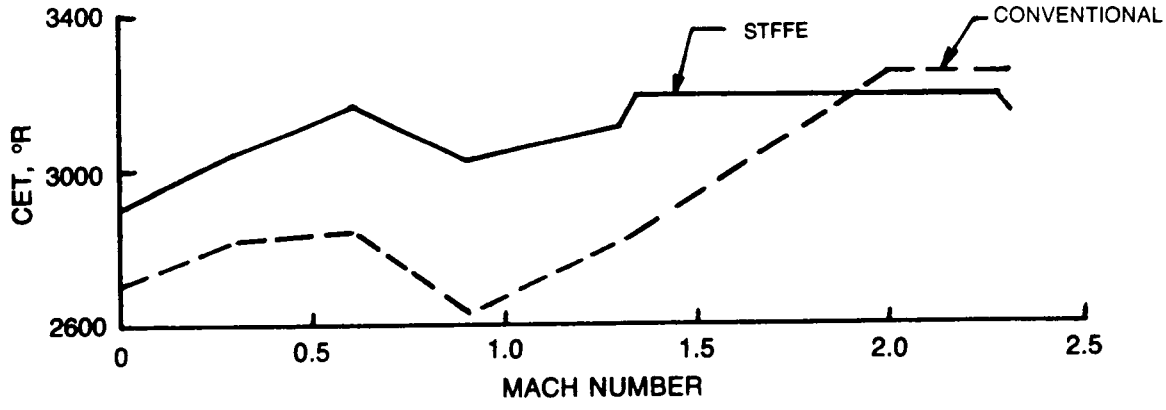

Figure 37. Combustor temperature schedules.

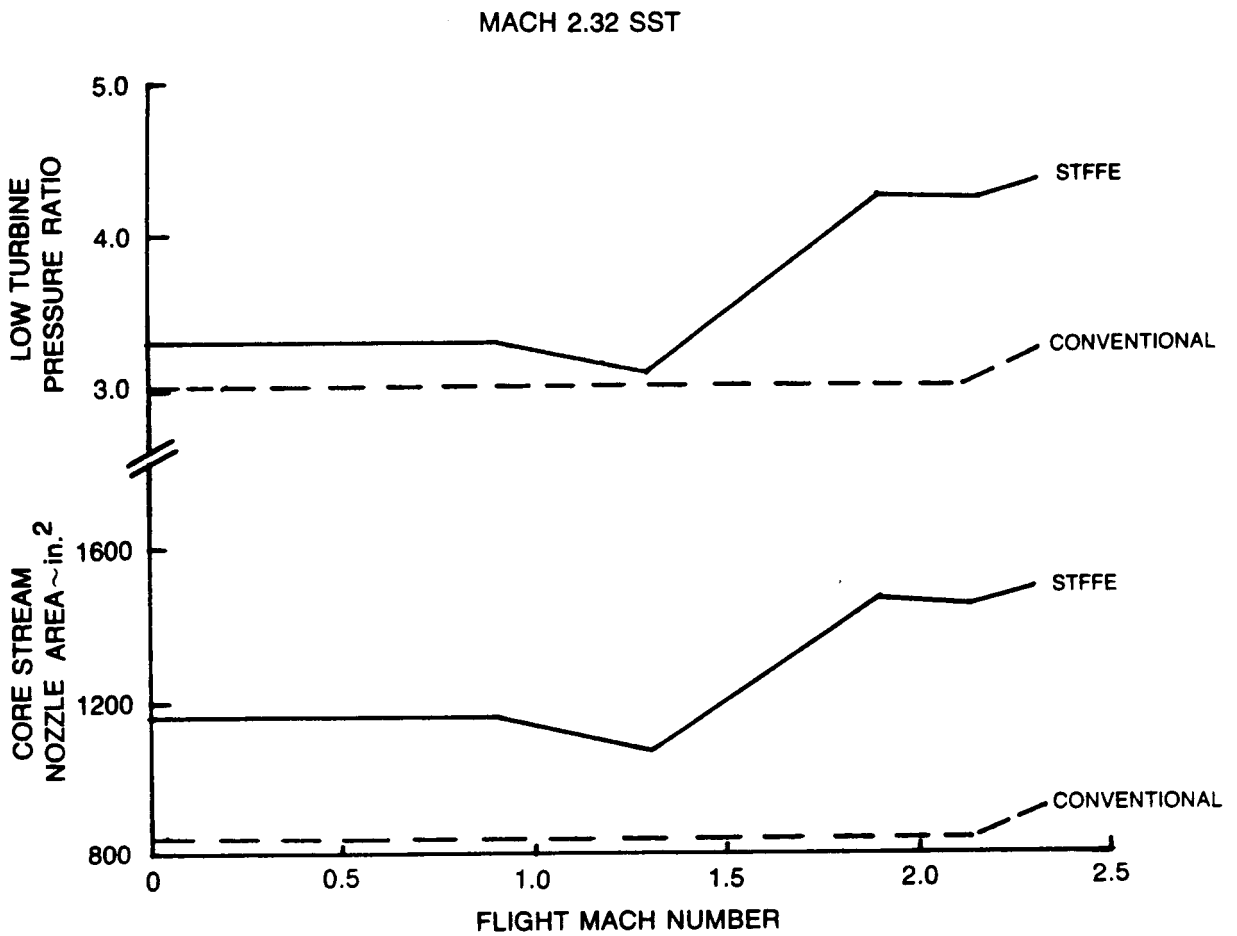

Figure 38. Low turbine pressure ratio and core stream nozzle area.

C-2

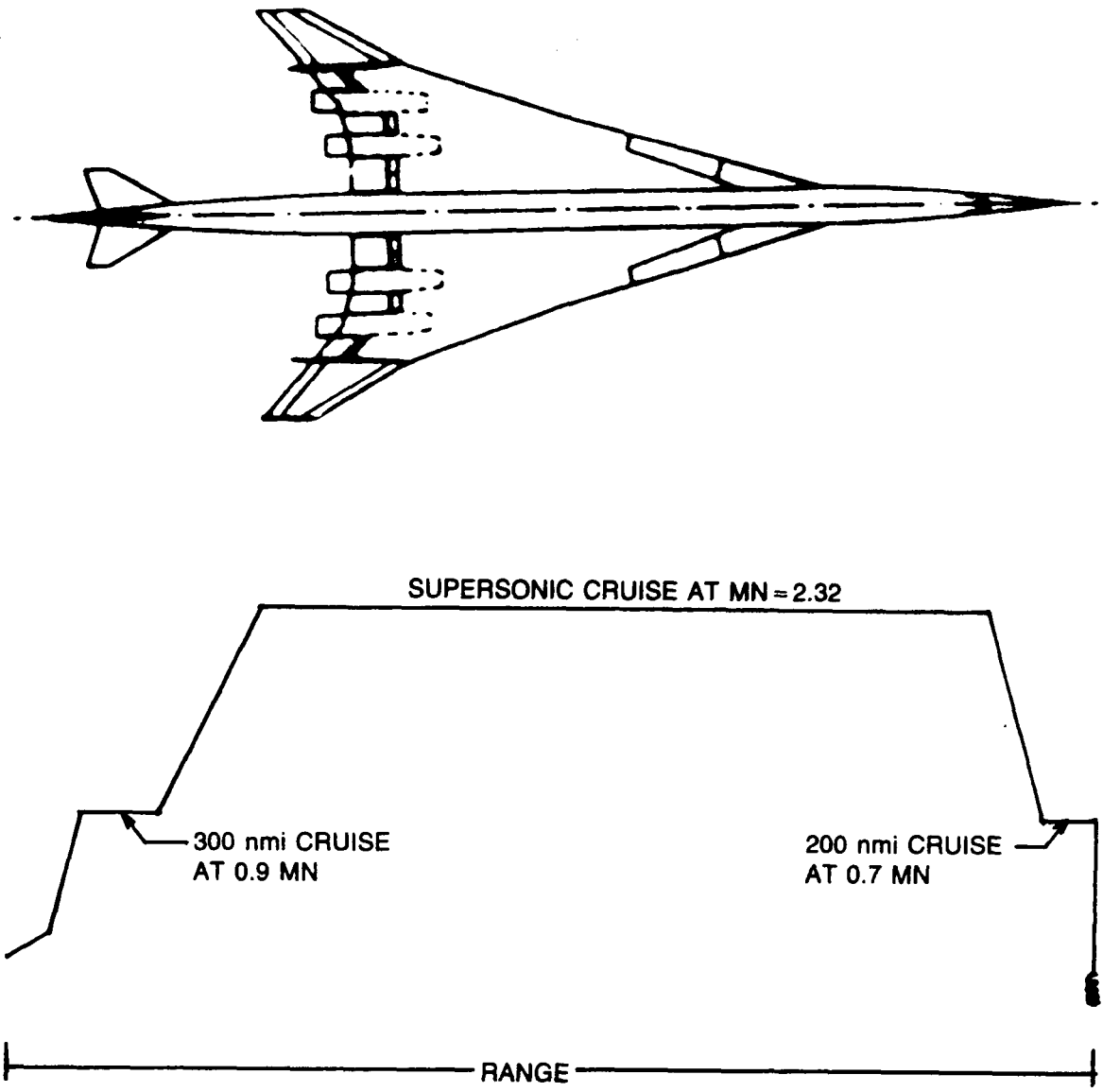

Figure 39. Supersonic transport mission profile.

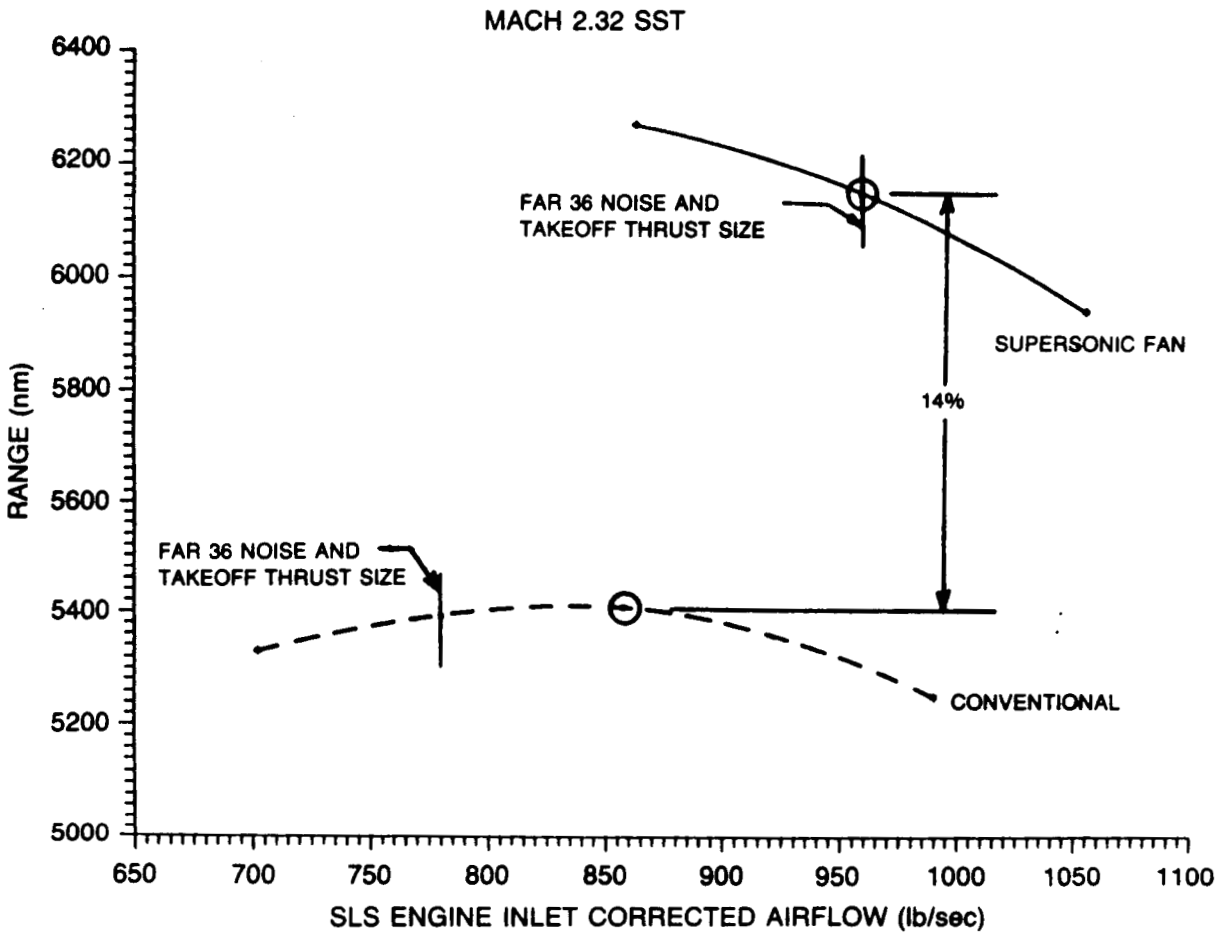

Figure 40. Supersonic fan engine/conventional engine range comparison.

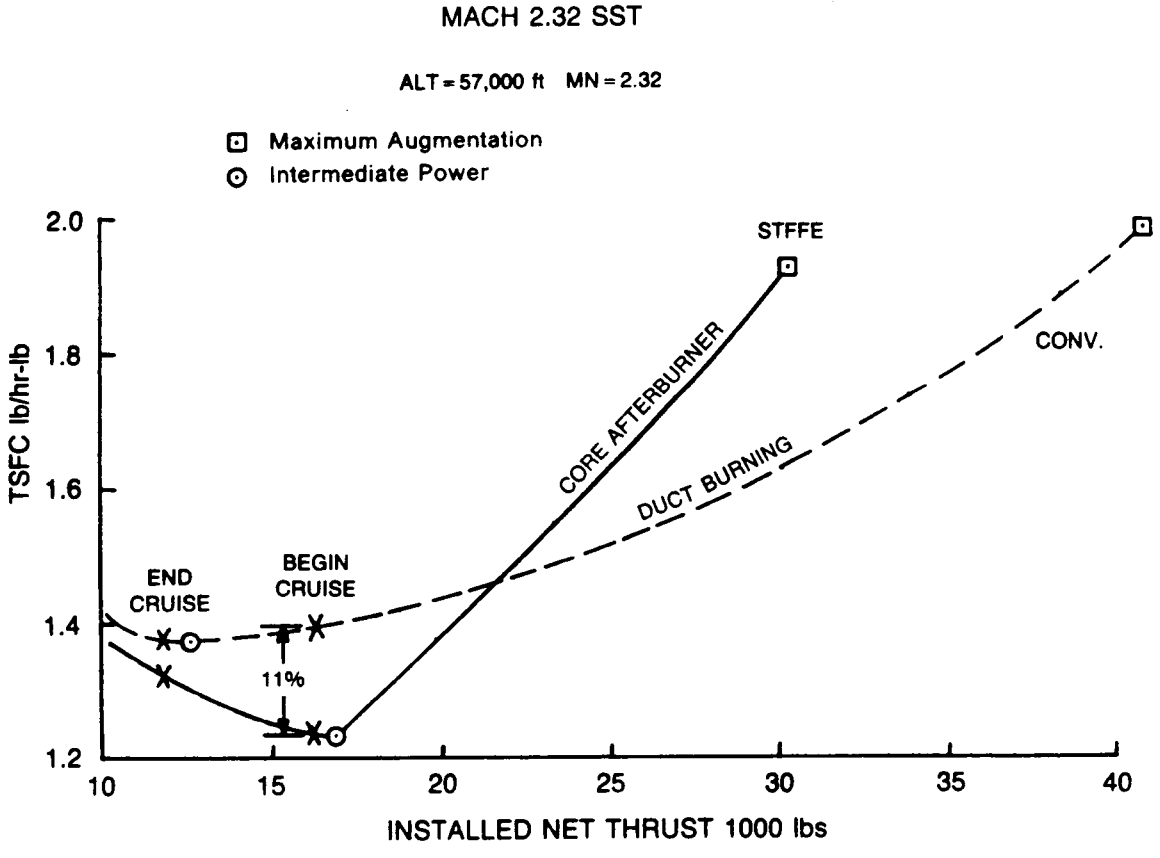

Figure 41. Thrust specific fuel consumption comparison.

MACH 2.5 FIGHTER

SUPERSONIC FAN ENGINE (AFTERBURNER)

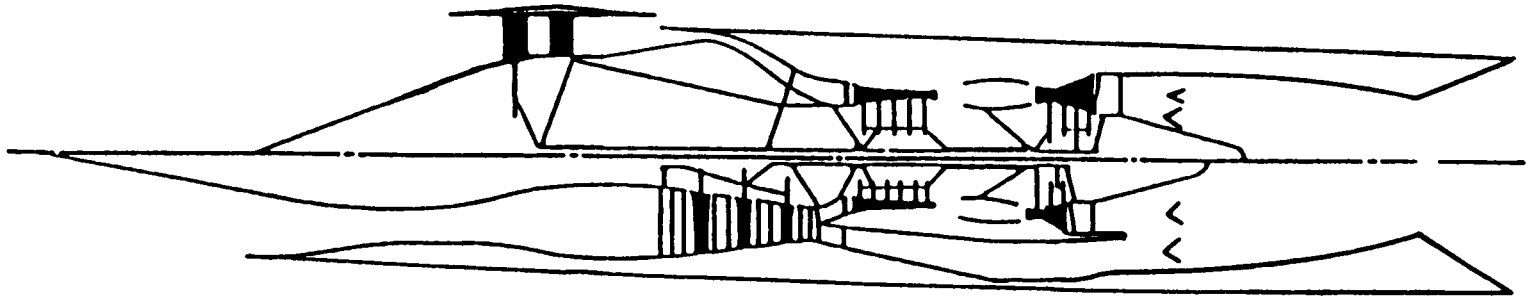

CONVENTIONAL FAN ENGINE (AFTERBURNER)

Figure 42. STFF and afterburning turbofan comparison.

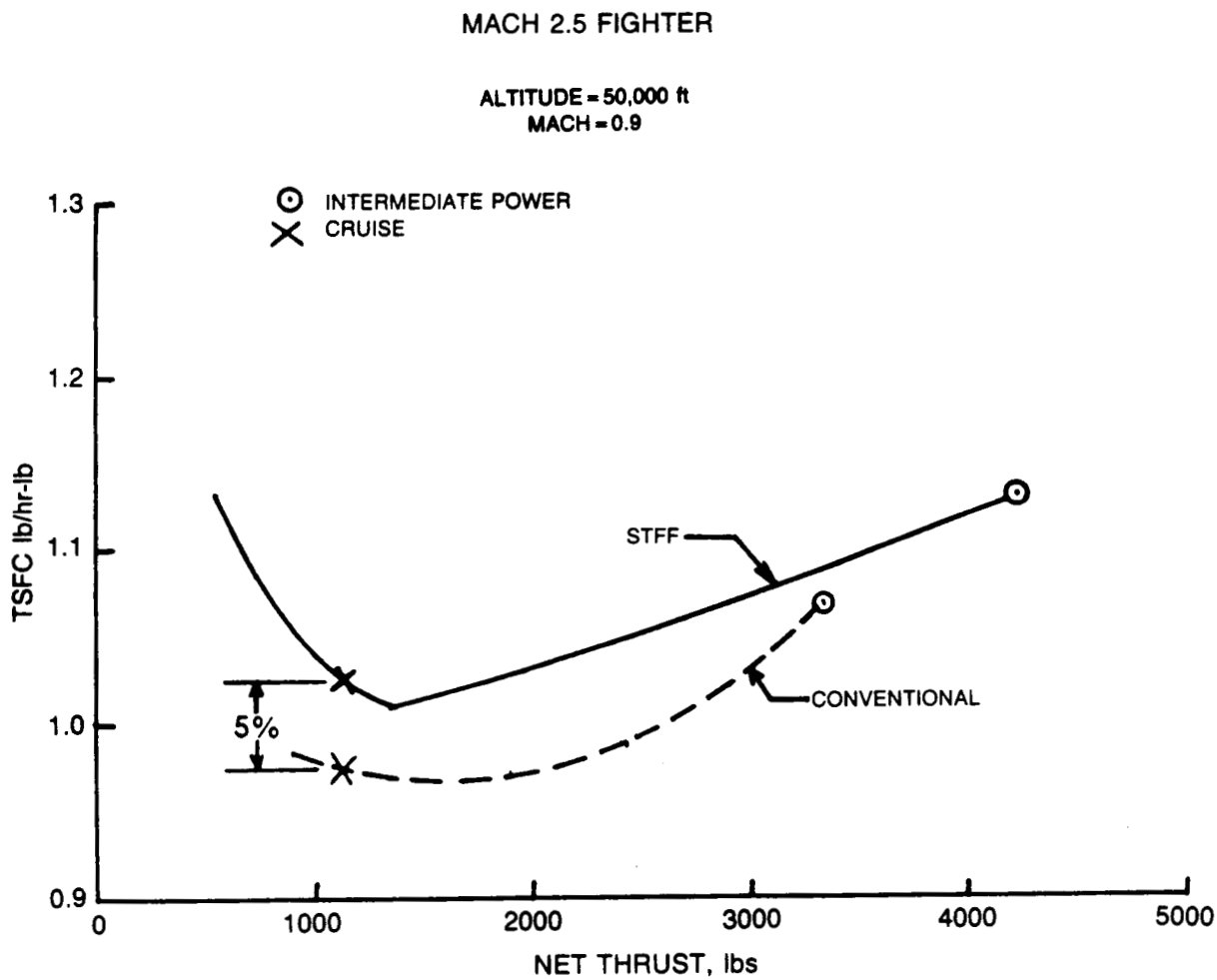

Figure 43. Thrust specific fuel consumption at subsonic cruise.

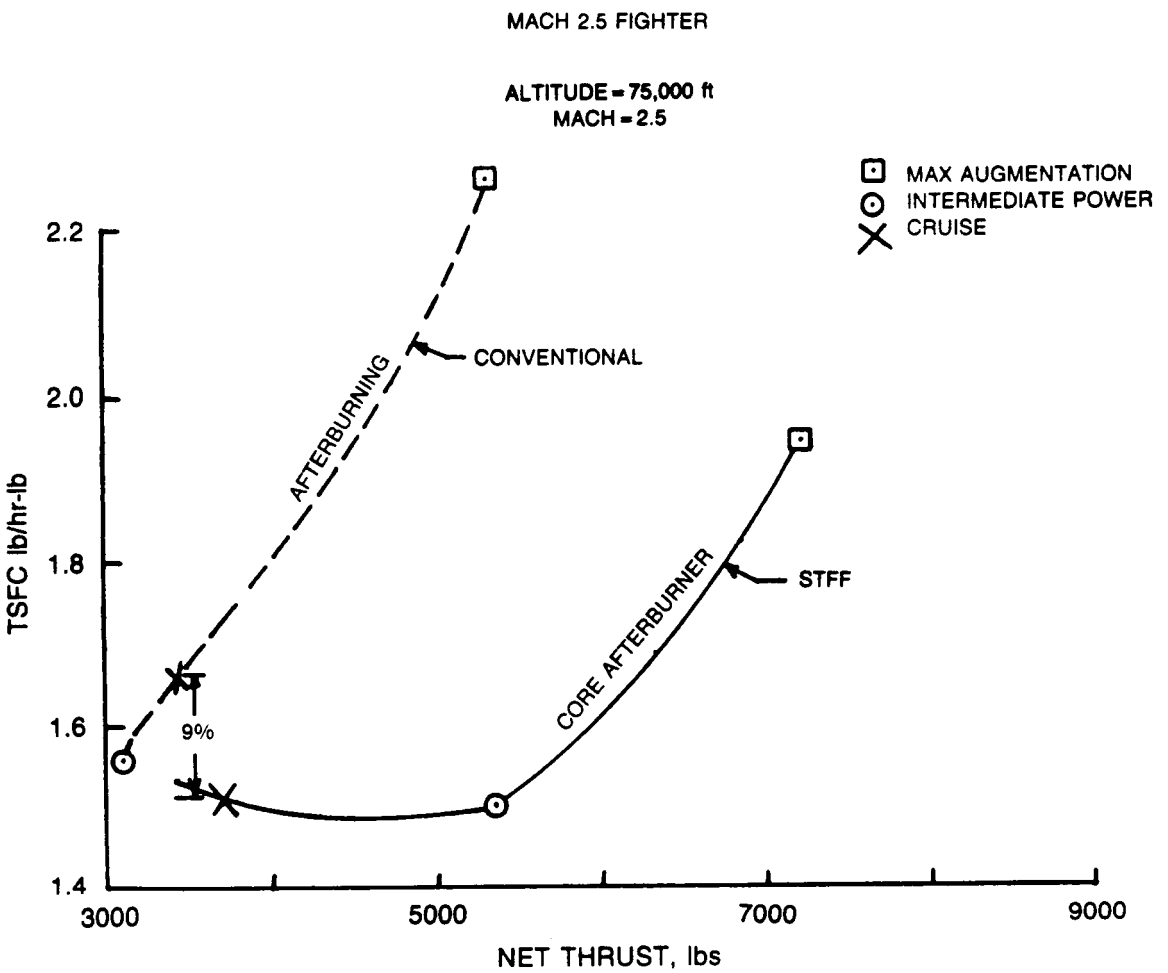

Figure 44. Thrust specific fuel consumption at supersonic cruise.

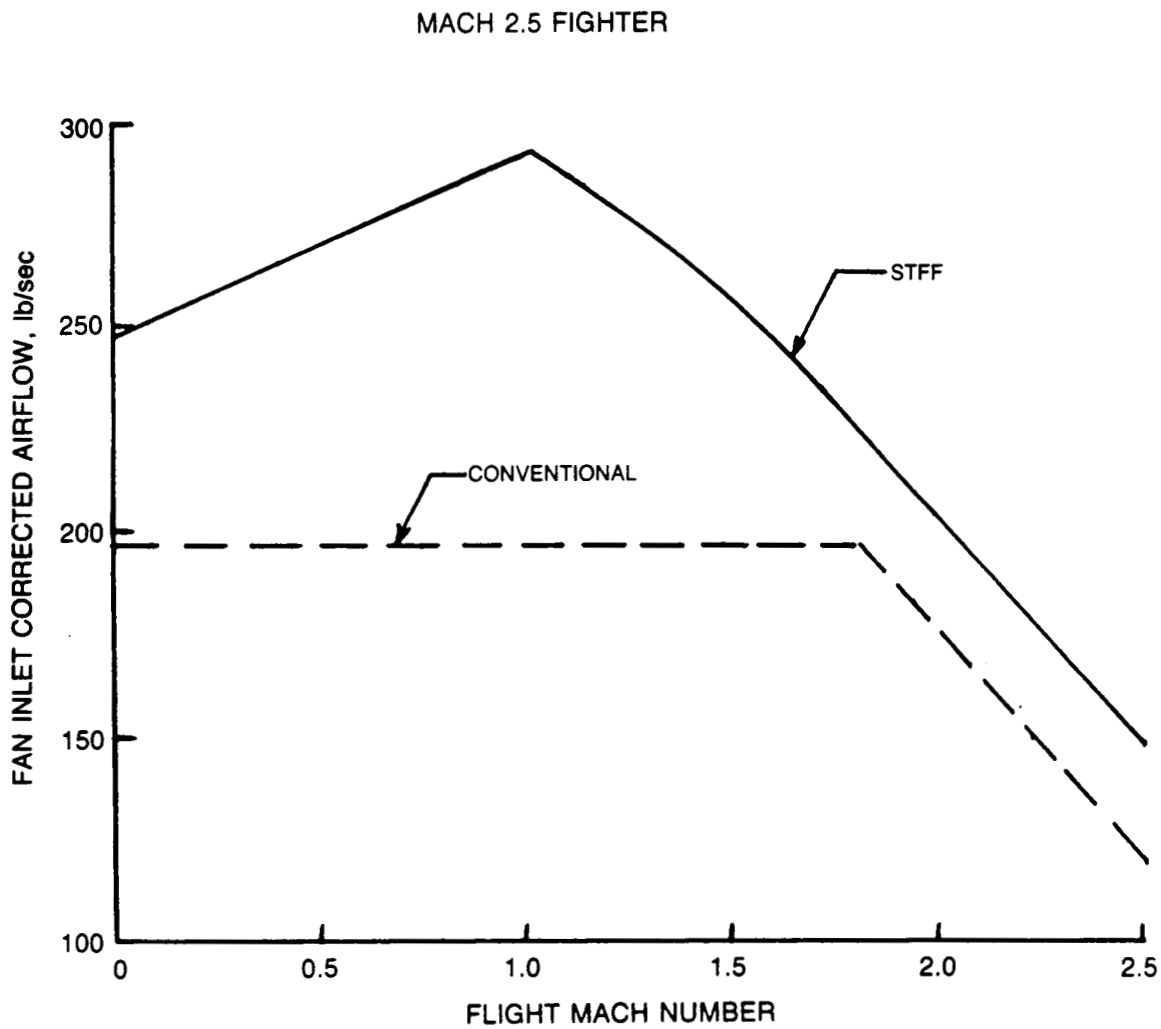

Figure 45. Fan inlet corrected flow schedules.

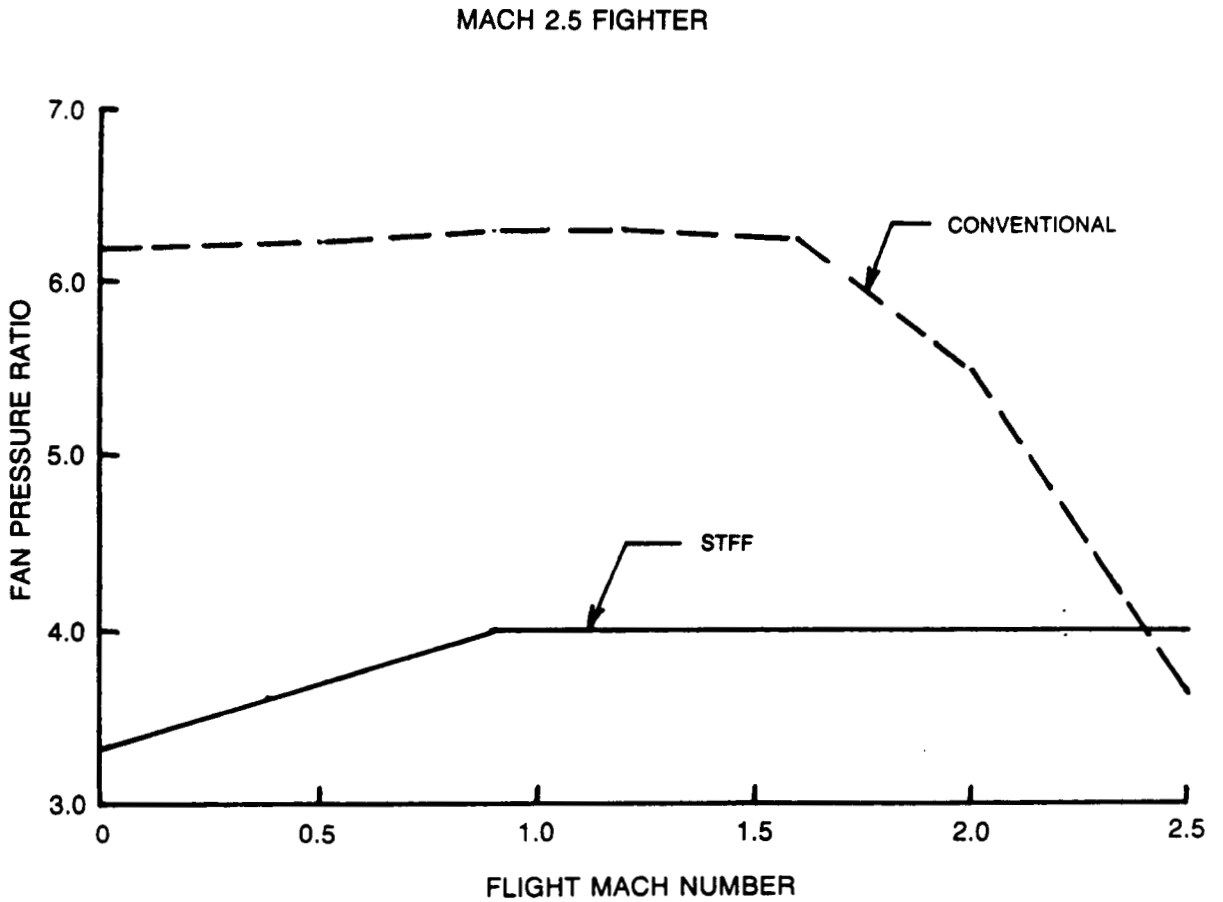

Figure 46. STFF and conventional fan pressure ratio comparison.

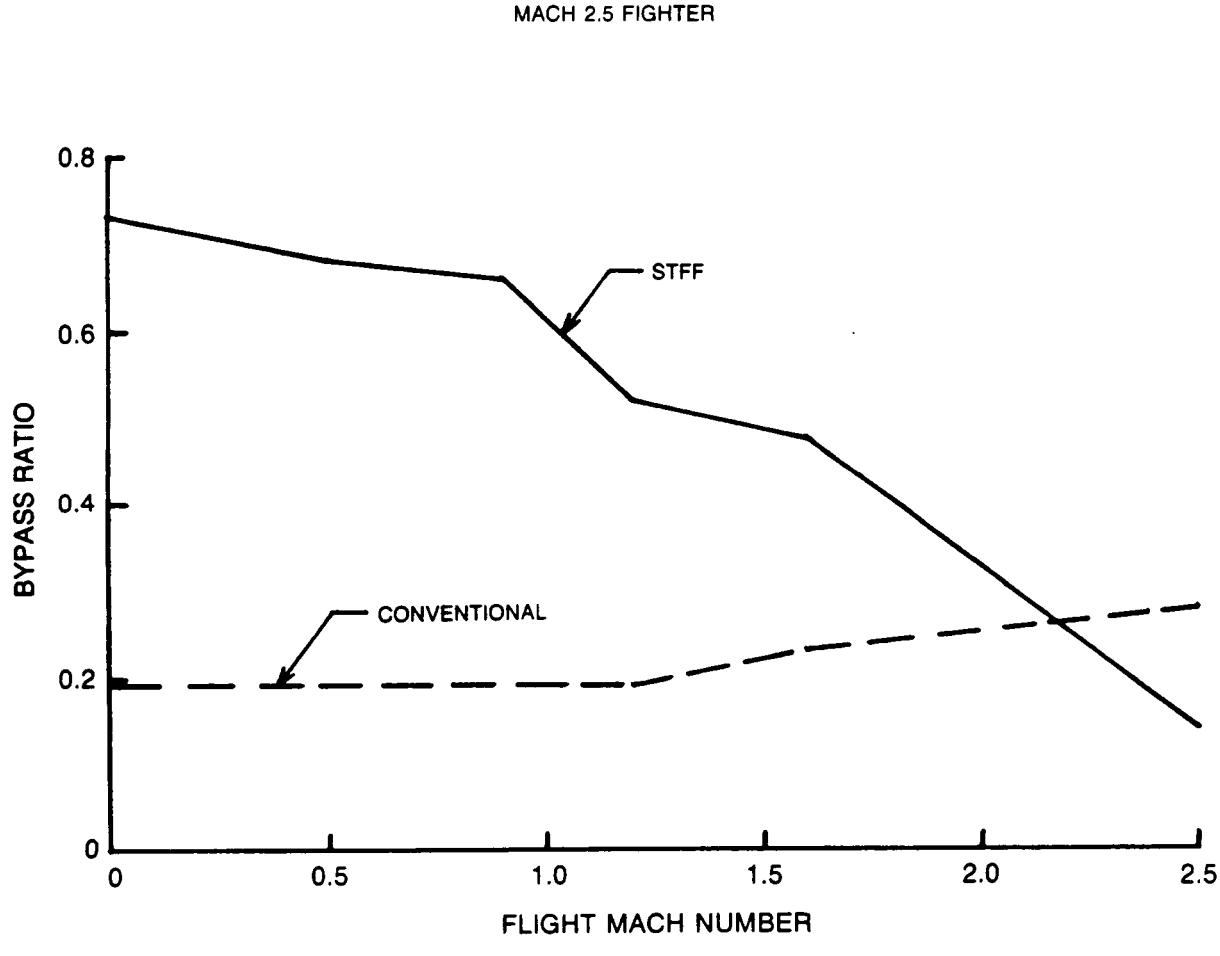

Figure 47. STFF and conventional bypass ratio comparison.

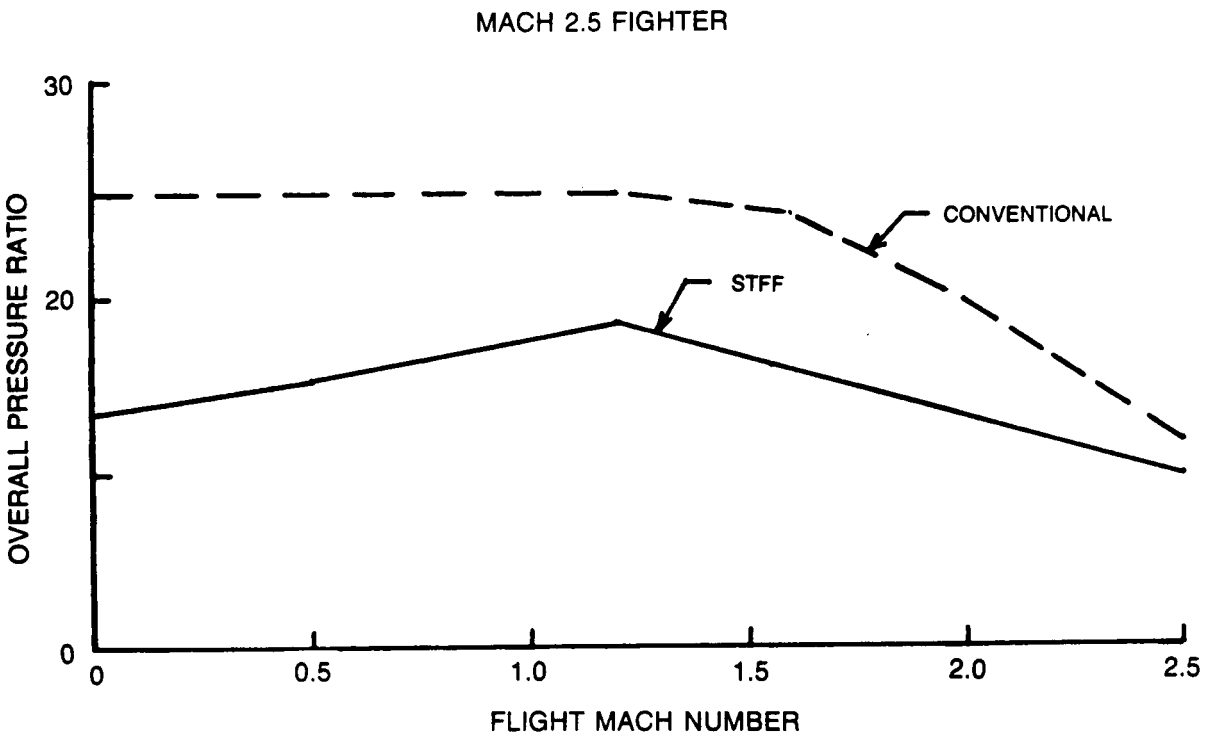

Figure 48. STFF and conventional overall pressure ratio comparison.

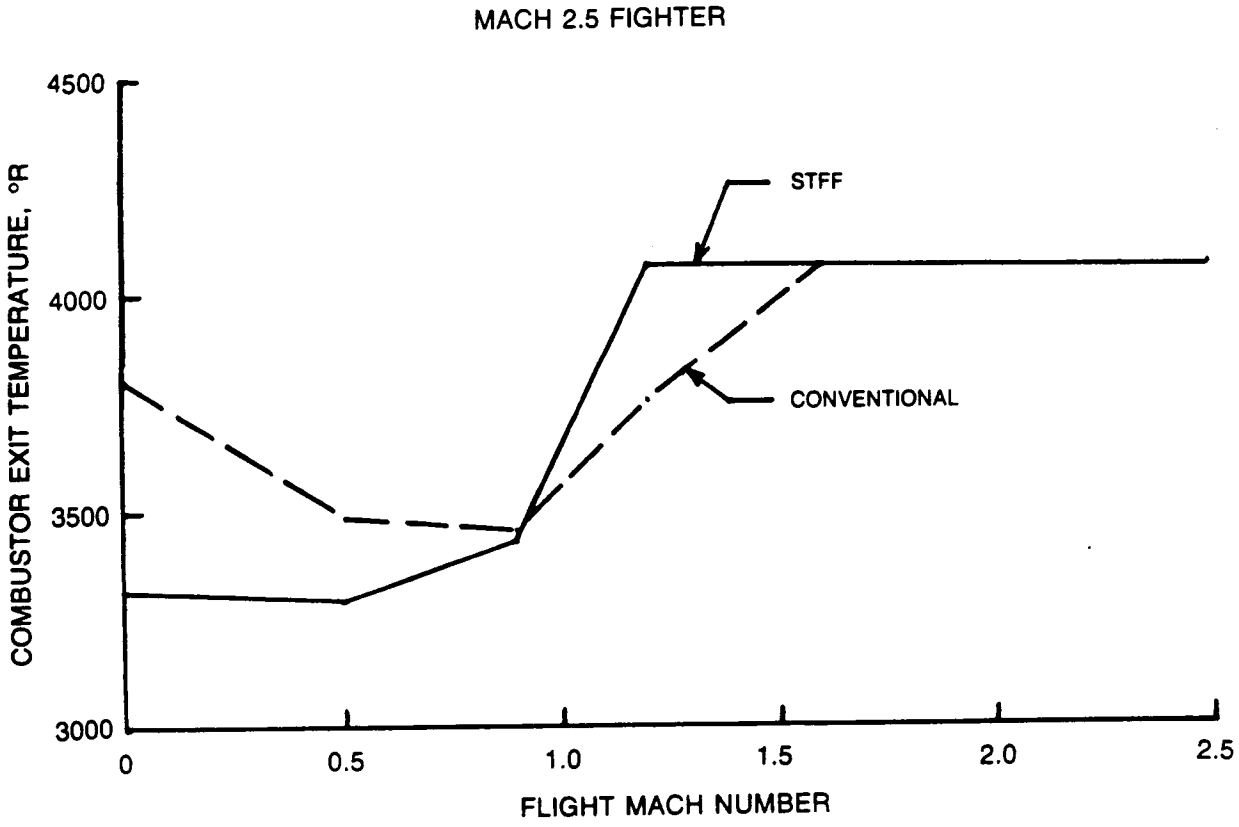

Figure 49. STFF and conventional combustor temperature comparison.

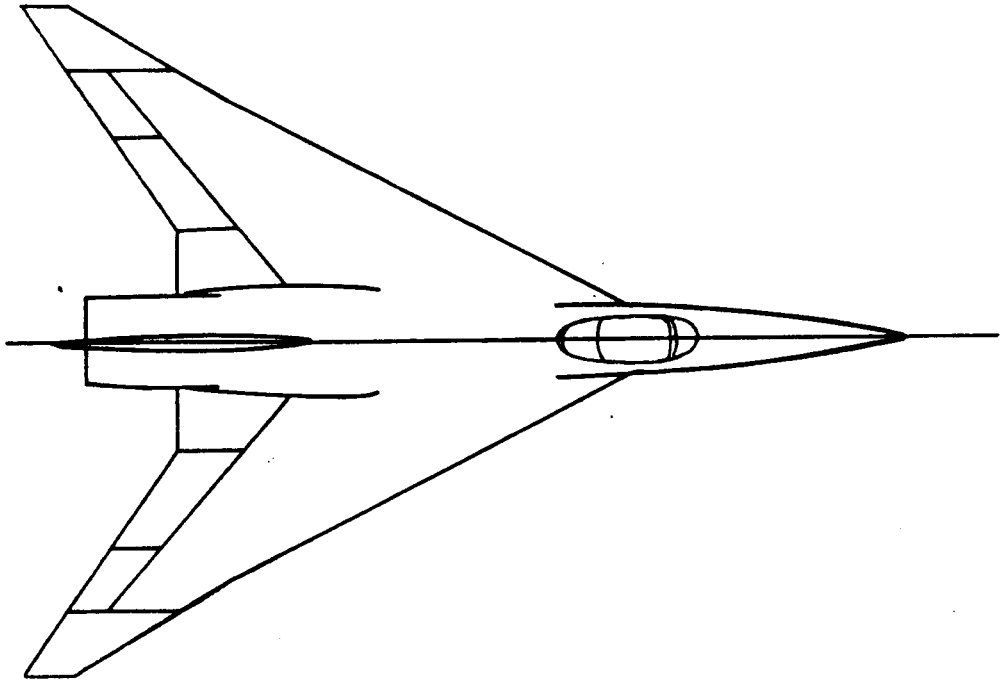

PAYLOAD	2100#
ACCELERATION	35 sec (0.8-1.6/30 K)
MANEUVERABILITY	6.5G'S AT 0.9/30 K
MANEUVERABILITY	7.0G'S AT 2.0/40 K

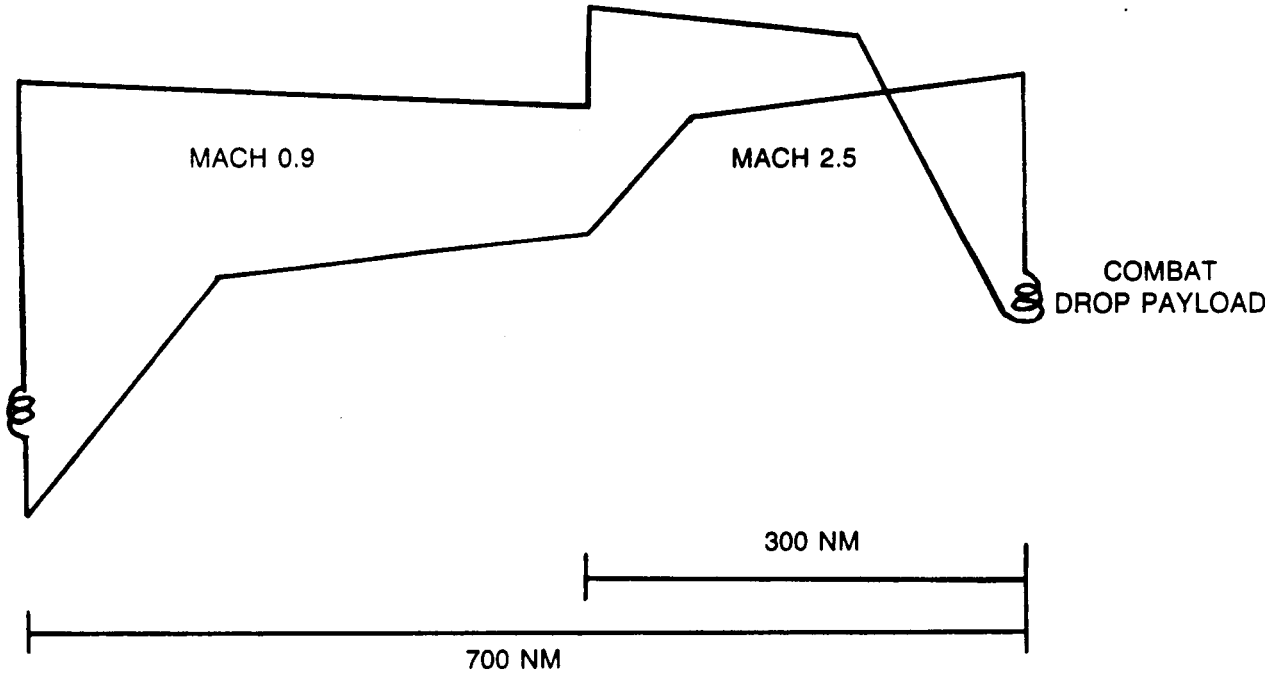

Figure 50. Mach 2.5 fighter mission profile.

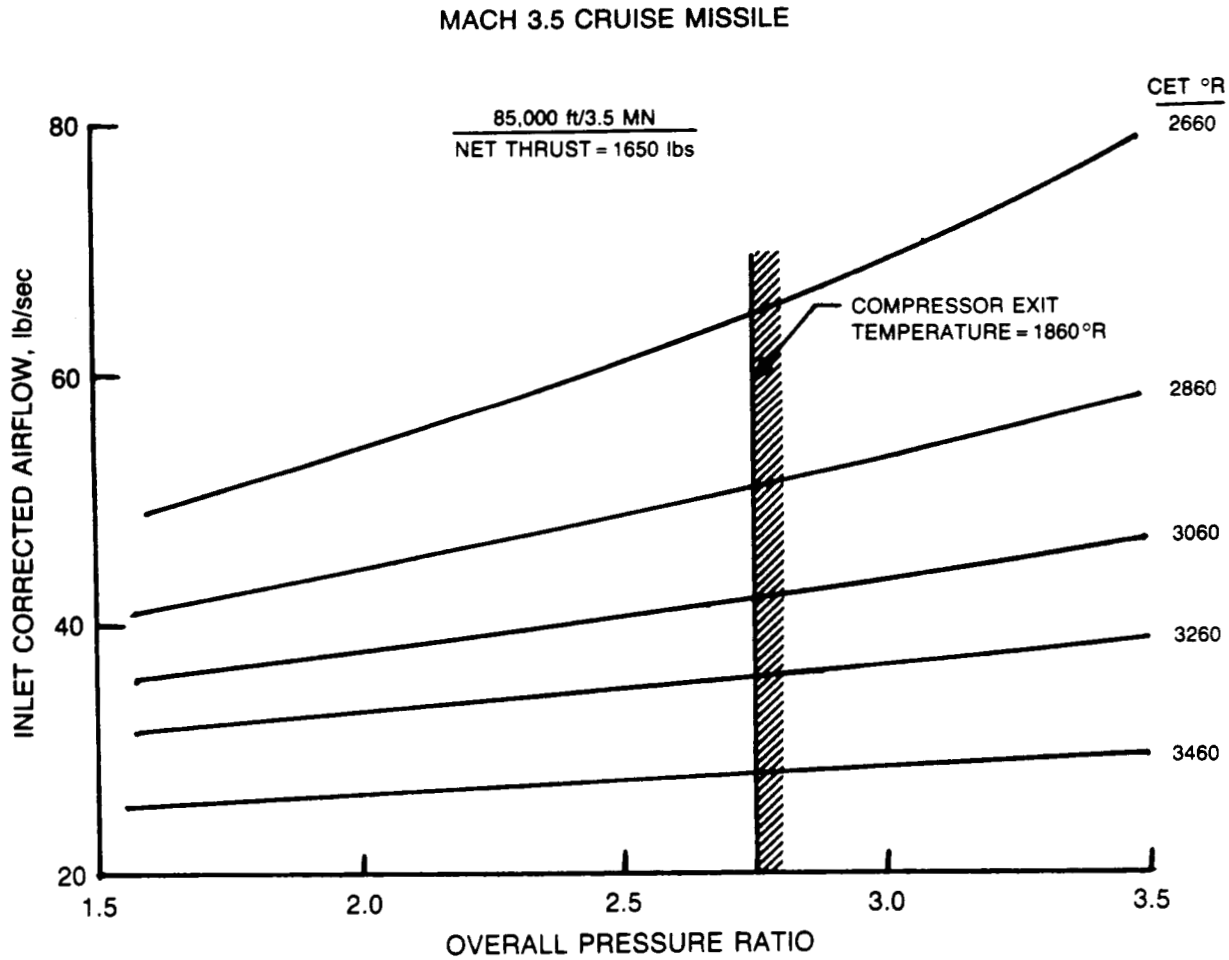

Figure 51. Variation of inlet corrected airflow with OPR and CET.

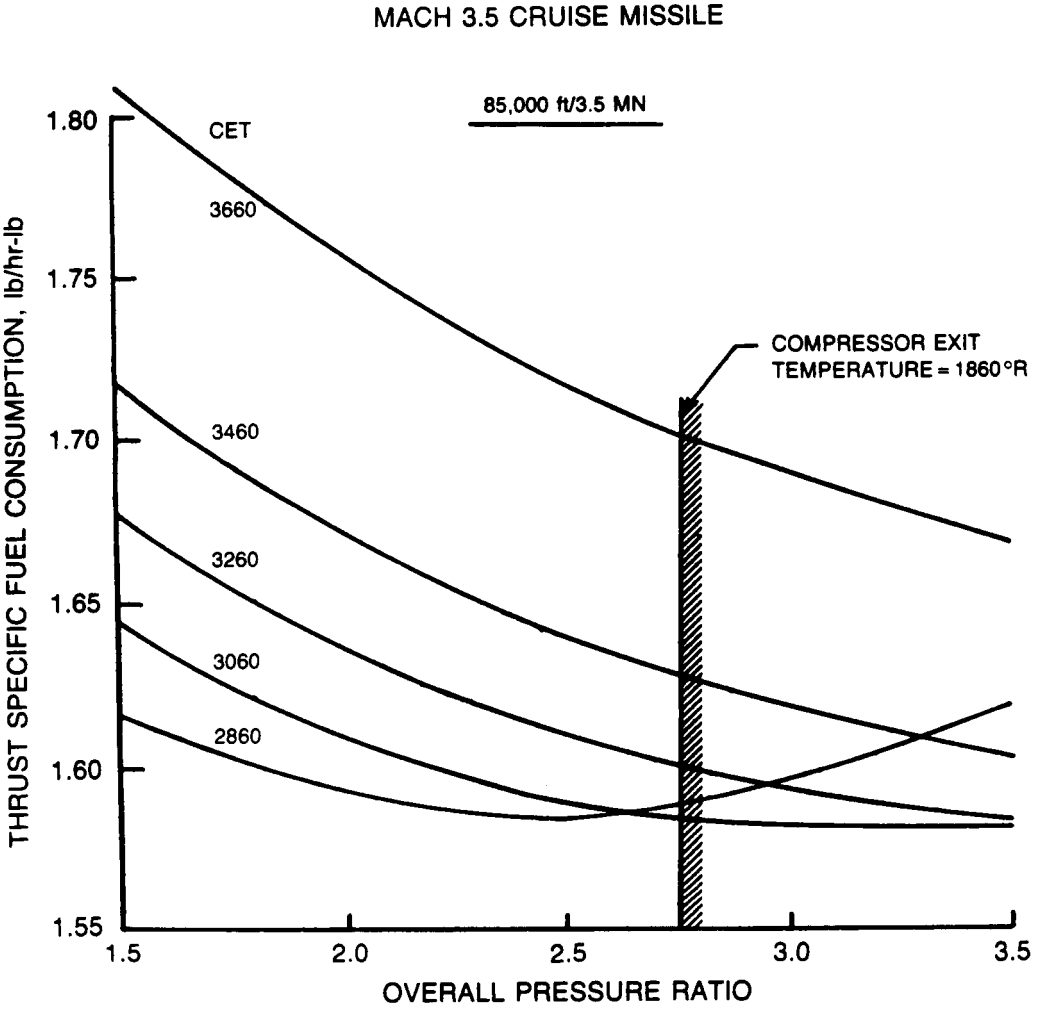

Figure 52. Variation of thrust specific fuel consumption with OPR & CET.

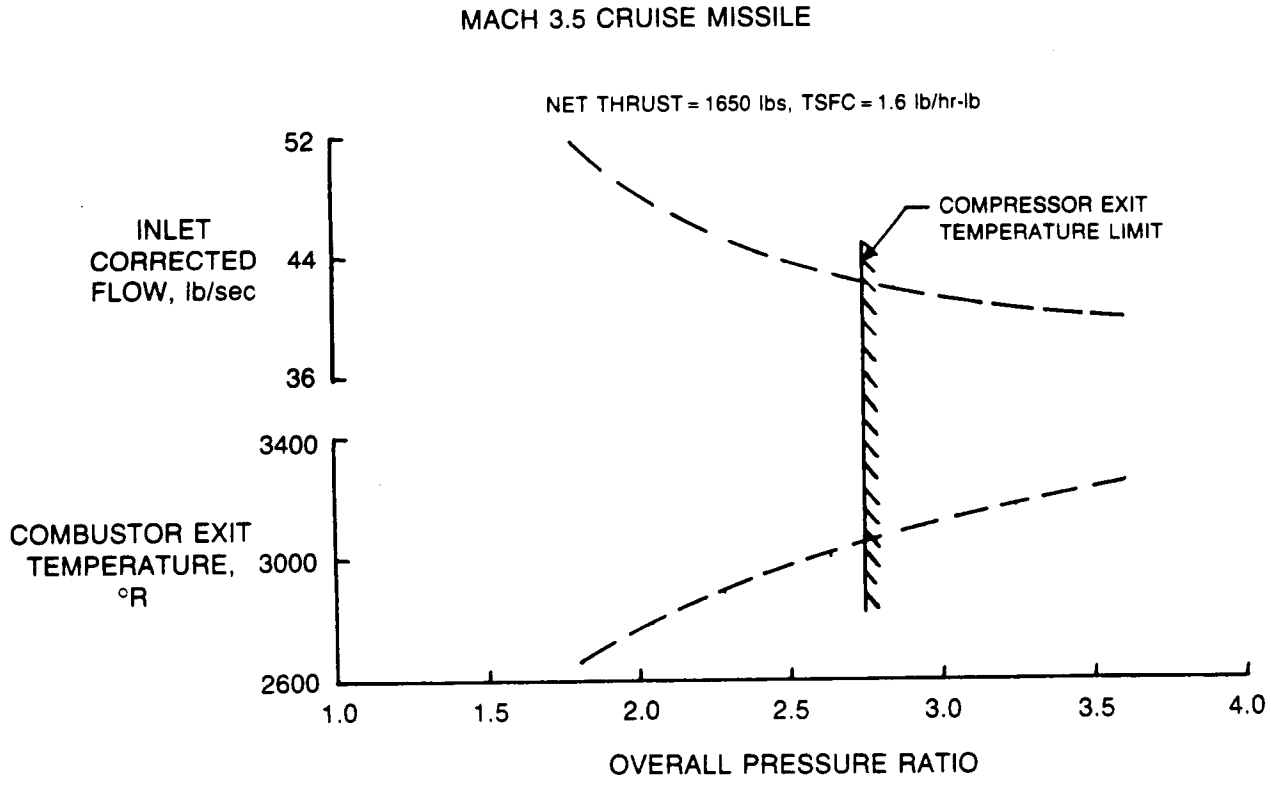

Figure 53. Variation of inlet corrected flow and combustor exit temperature with overall pressure ratio.

MACH 3.5 CRUISE MISSILE

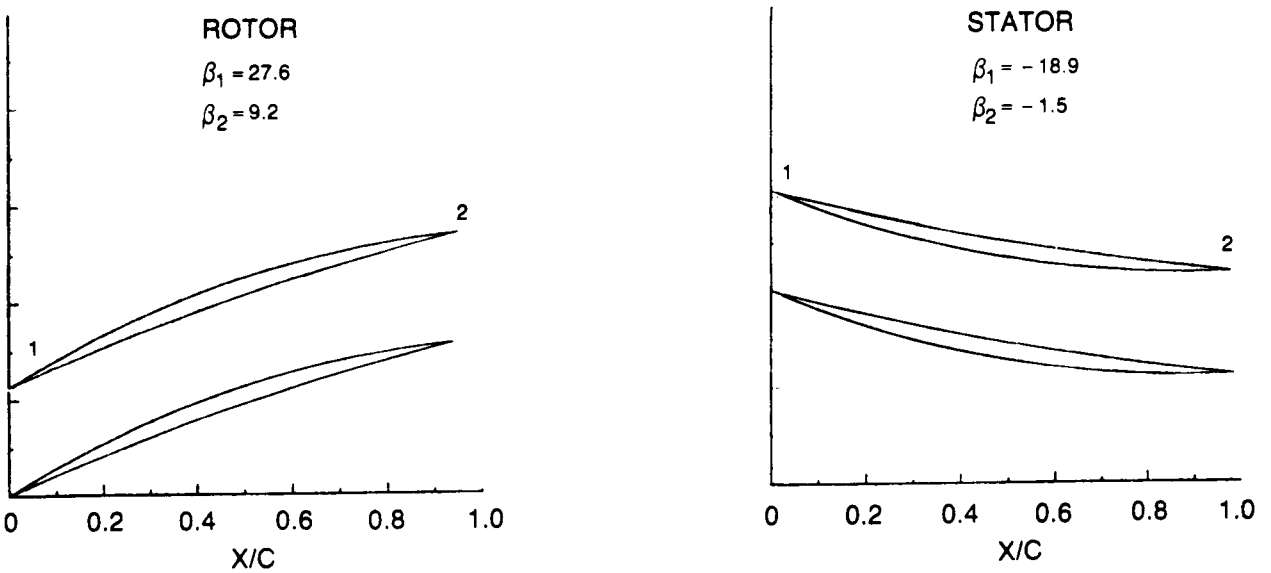

Figure 54. Blade shapes STFF-9.

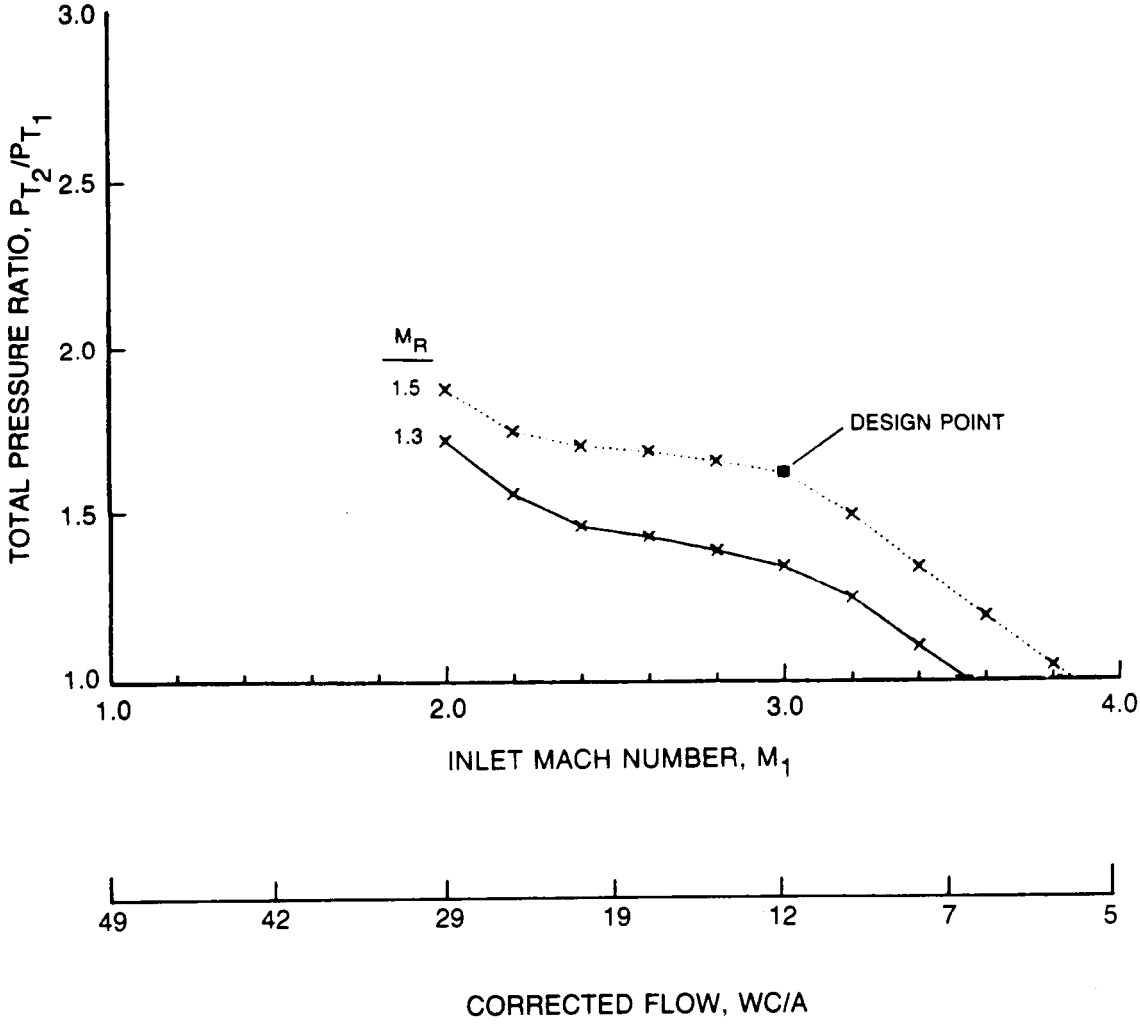

Figure 55. Total pressure ratio STFF-9.

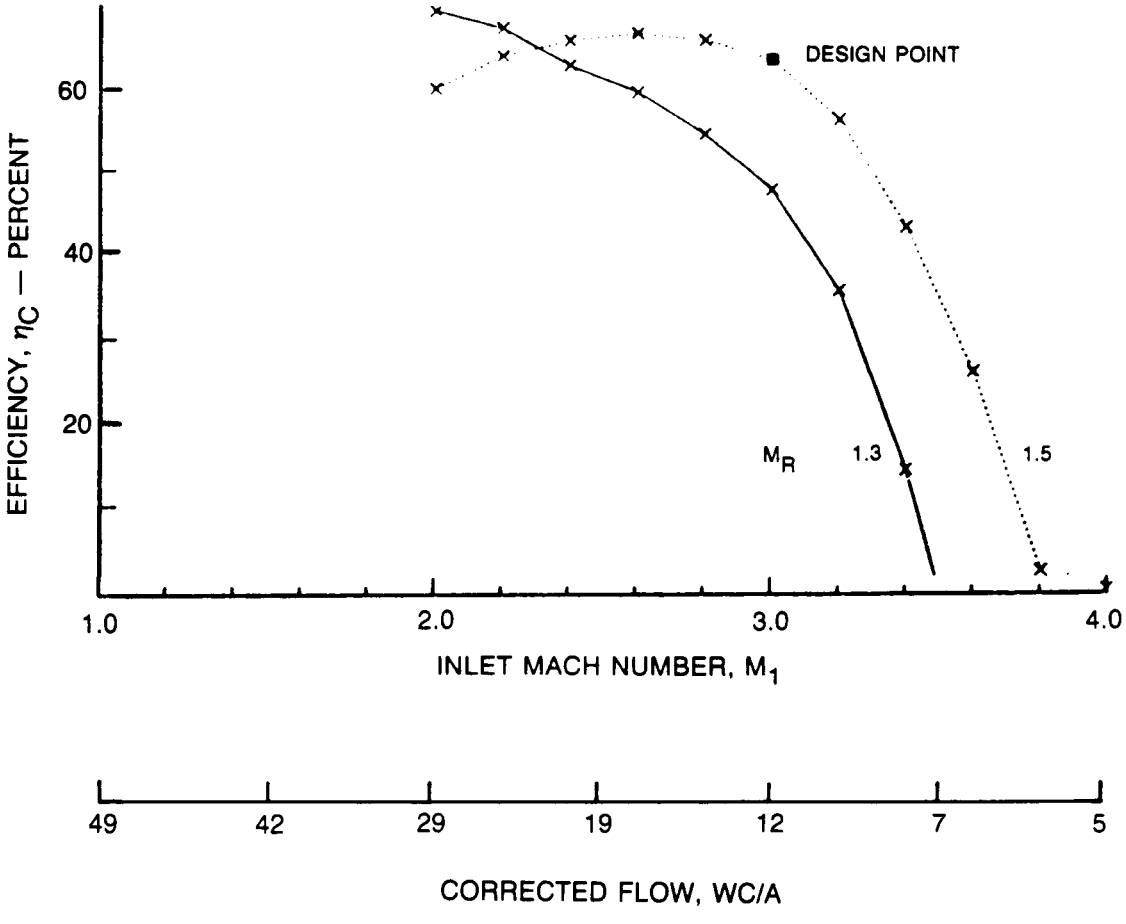

Figure 56. Fan efficiency STFF-9.

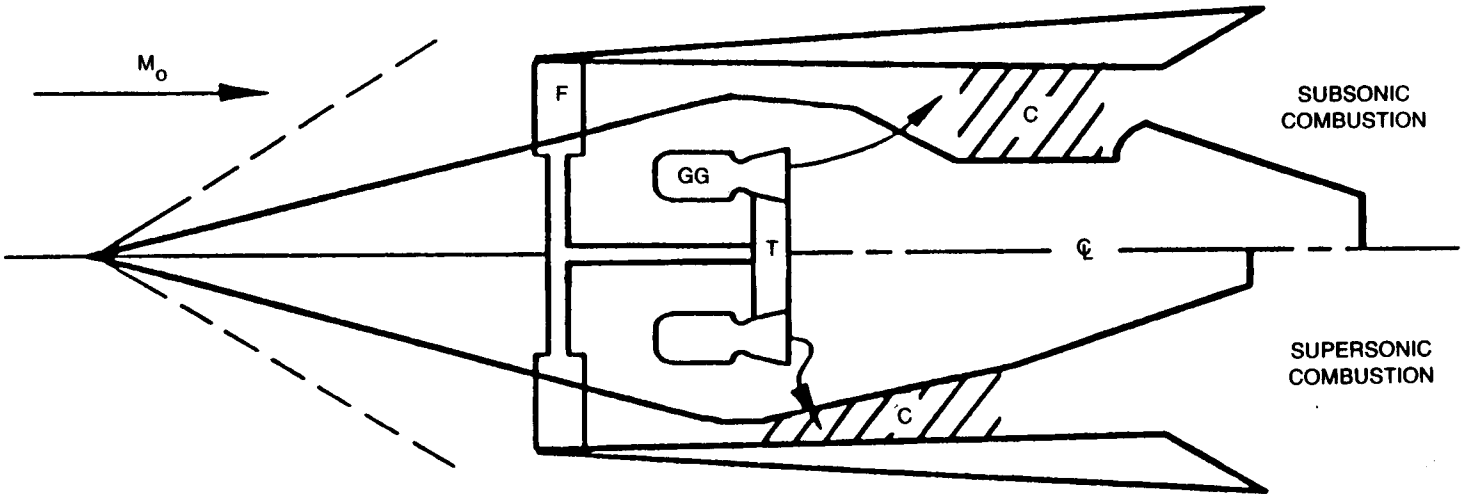

Figure 57. STFF-ATR engine schematic.

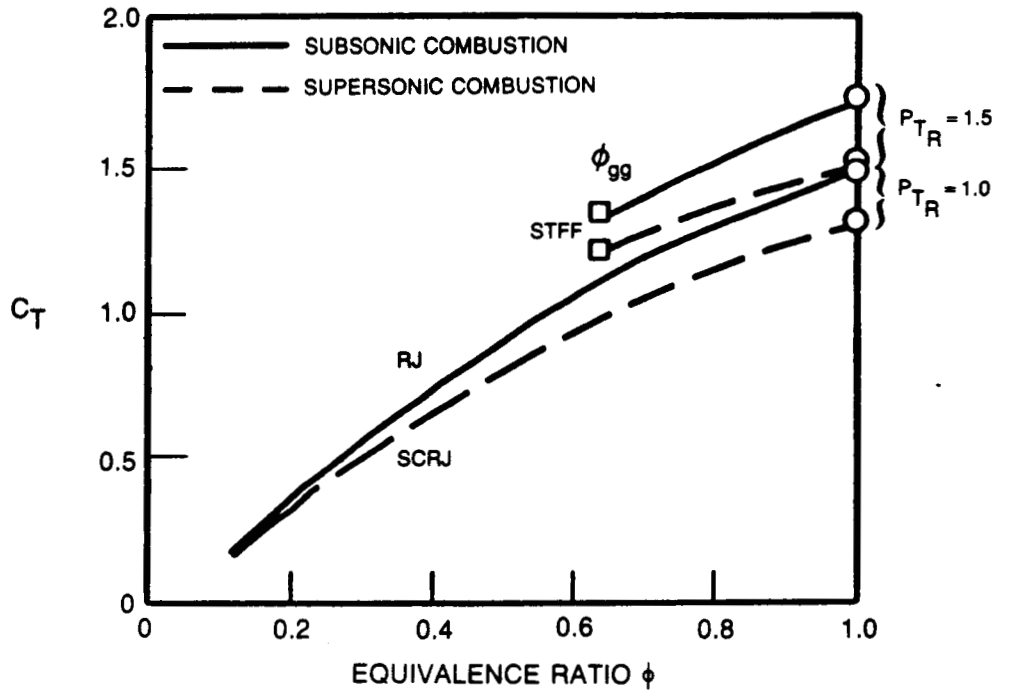

Figure 58. Engine thrust coefficient at Mach 5.

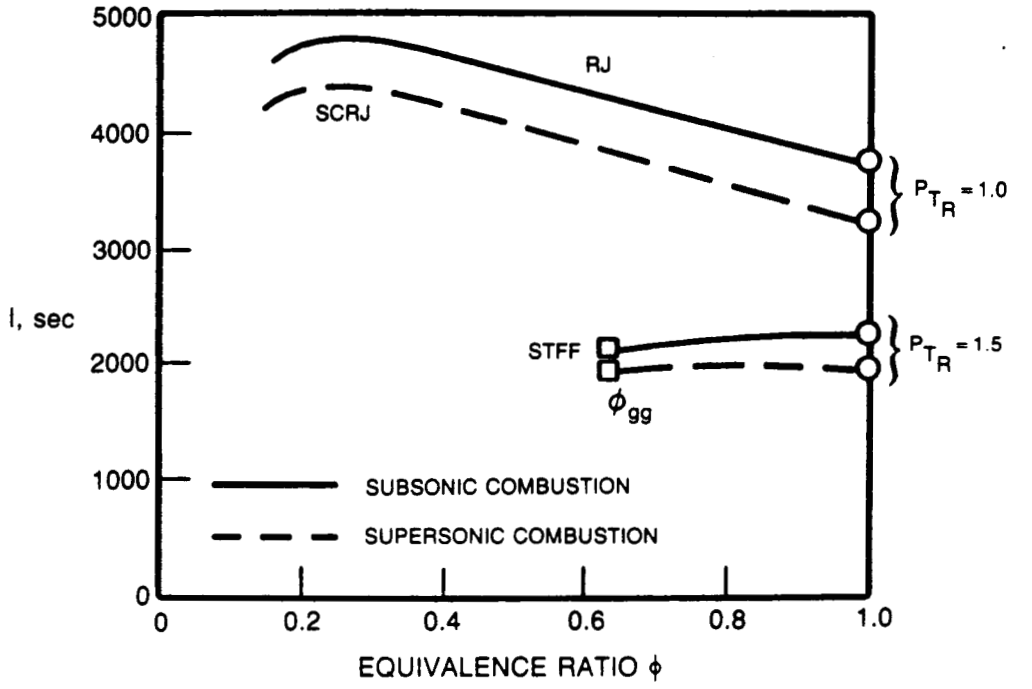

Figure 59. Engine fuel specific impulse at Mach 5.

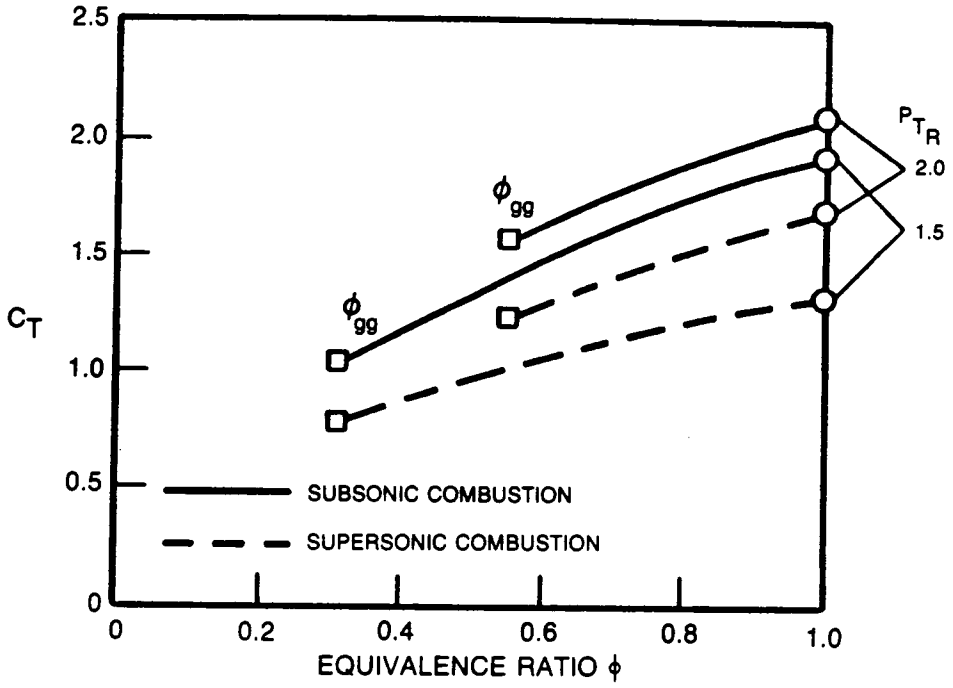

Figure 60. Engine thrust coefficient at Mach 3.

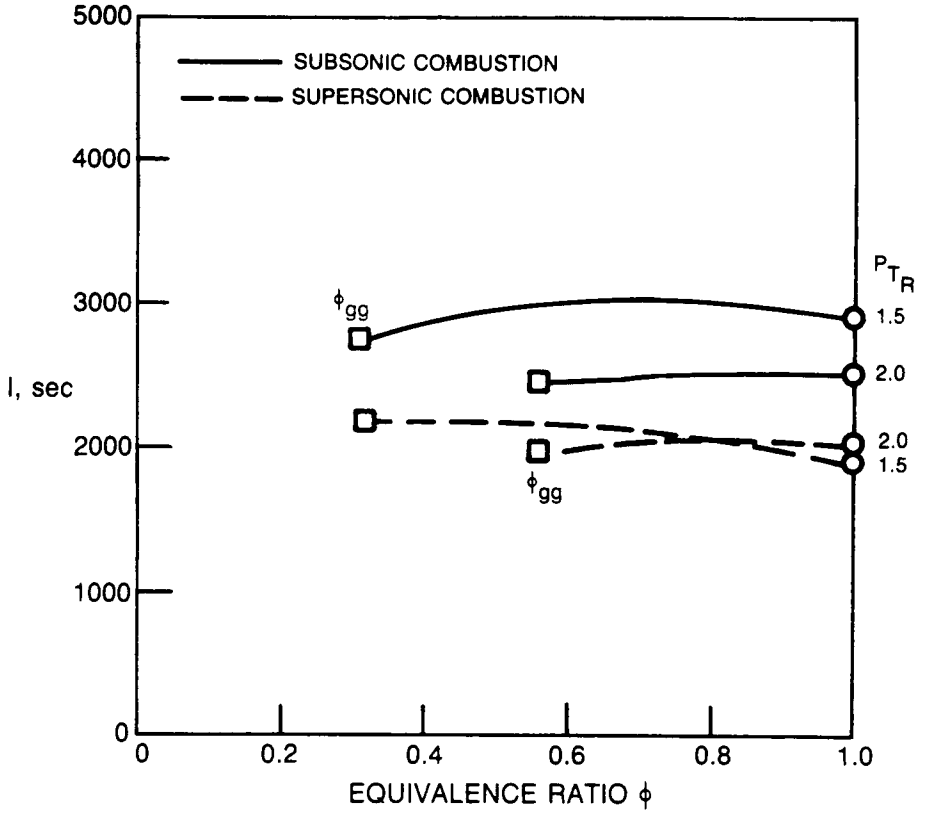

Figure 61. Engine fuel specific impulse at Mach 3.

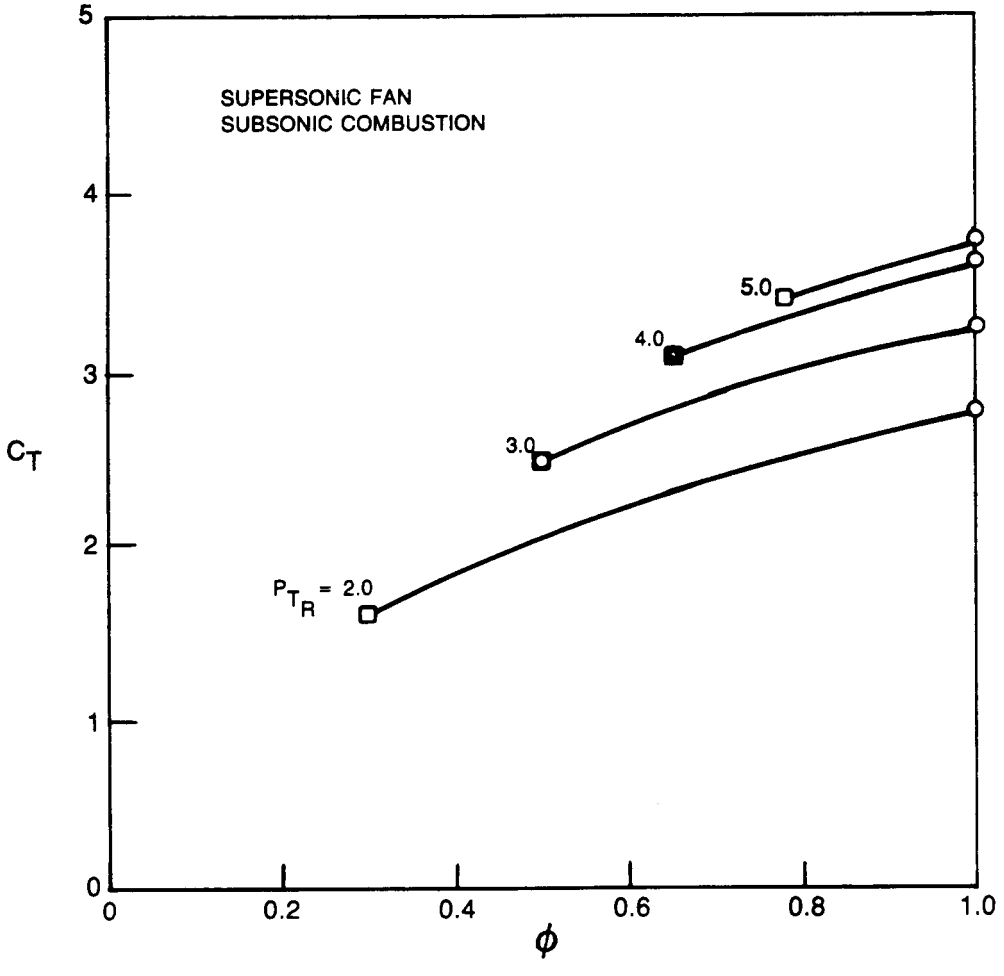

Figure 62. Engine thrust coefficient at Mach 1.25.

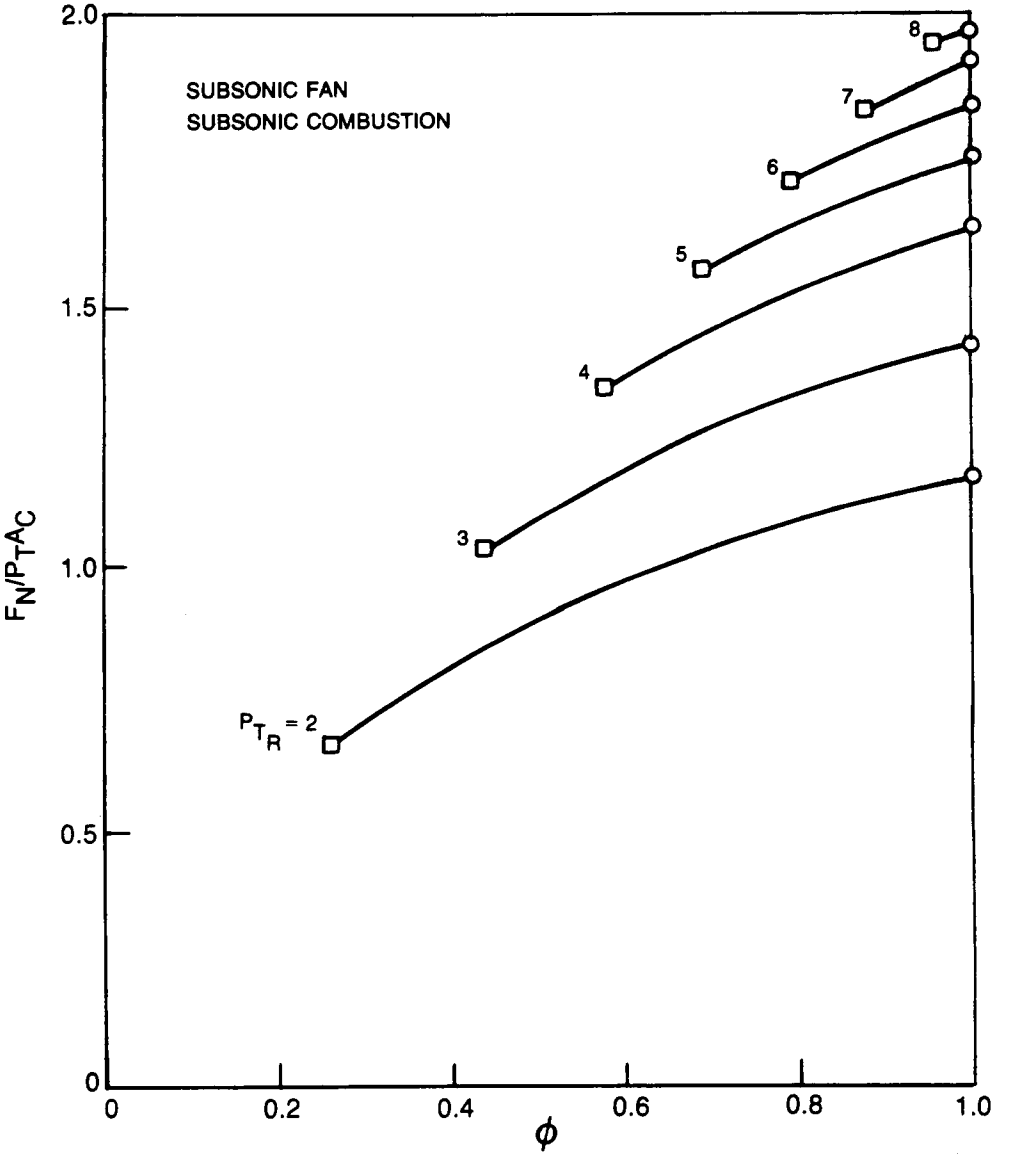

Figure 63. Normalized Engine Thrust at Mach 0.9.

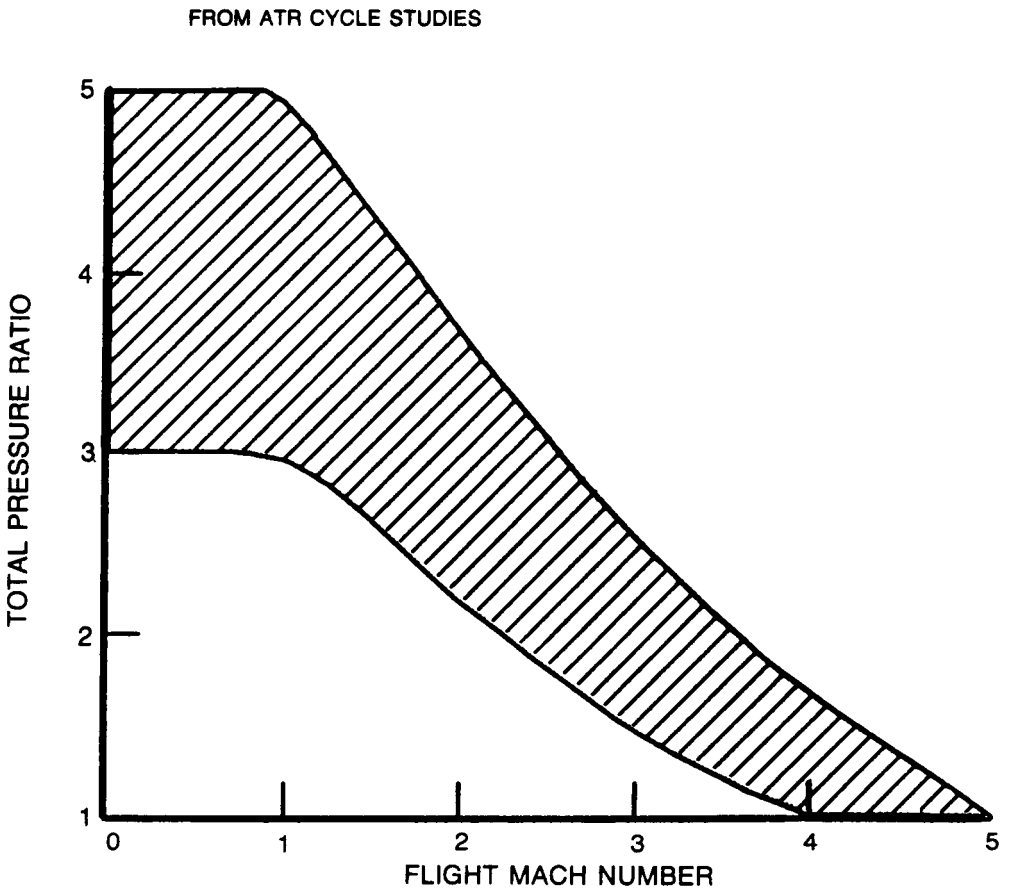

Figure 64. Desired fan pressure ratio.

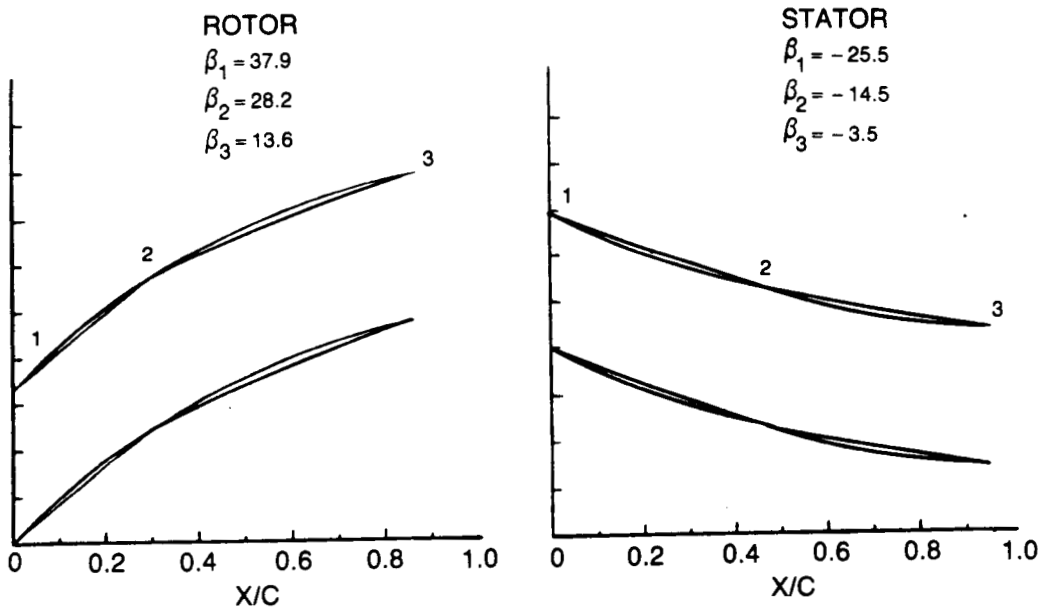

Figure 65. Blade shapes VPRS-1.

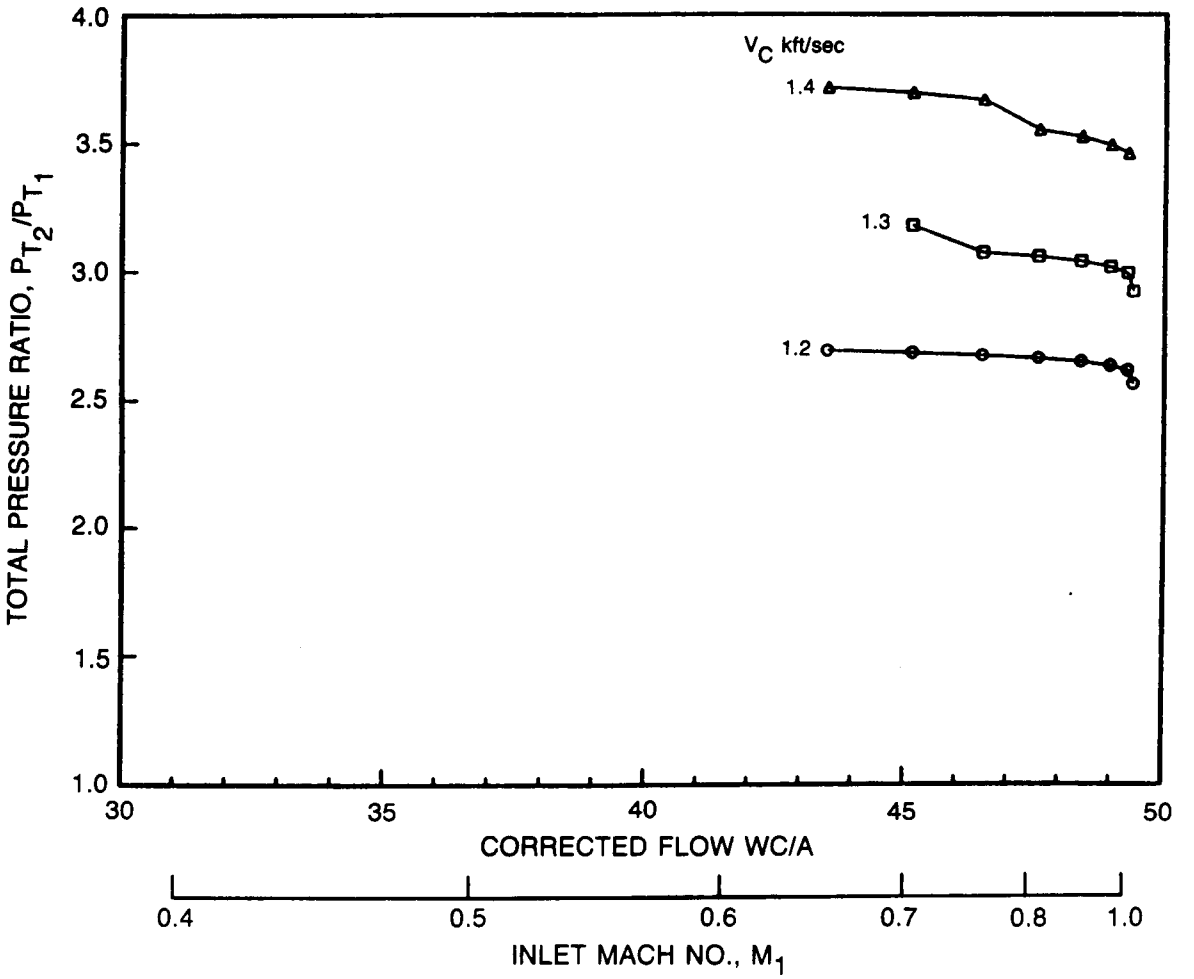

Figure 66. Total pressure ratio VPRS-1 subsonic inflow.

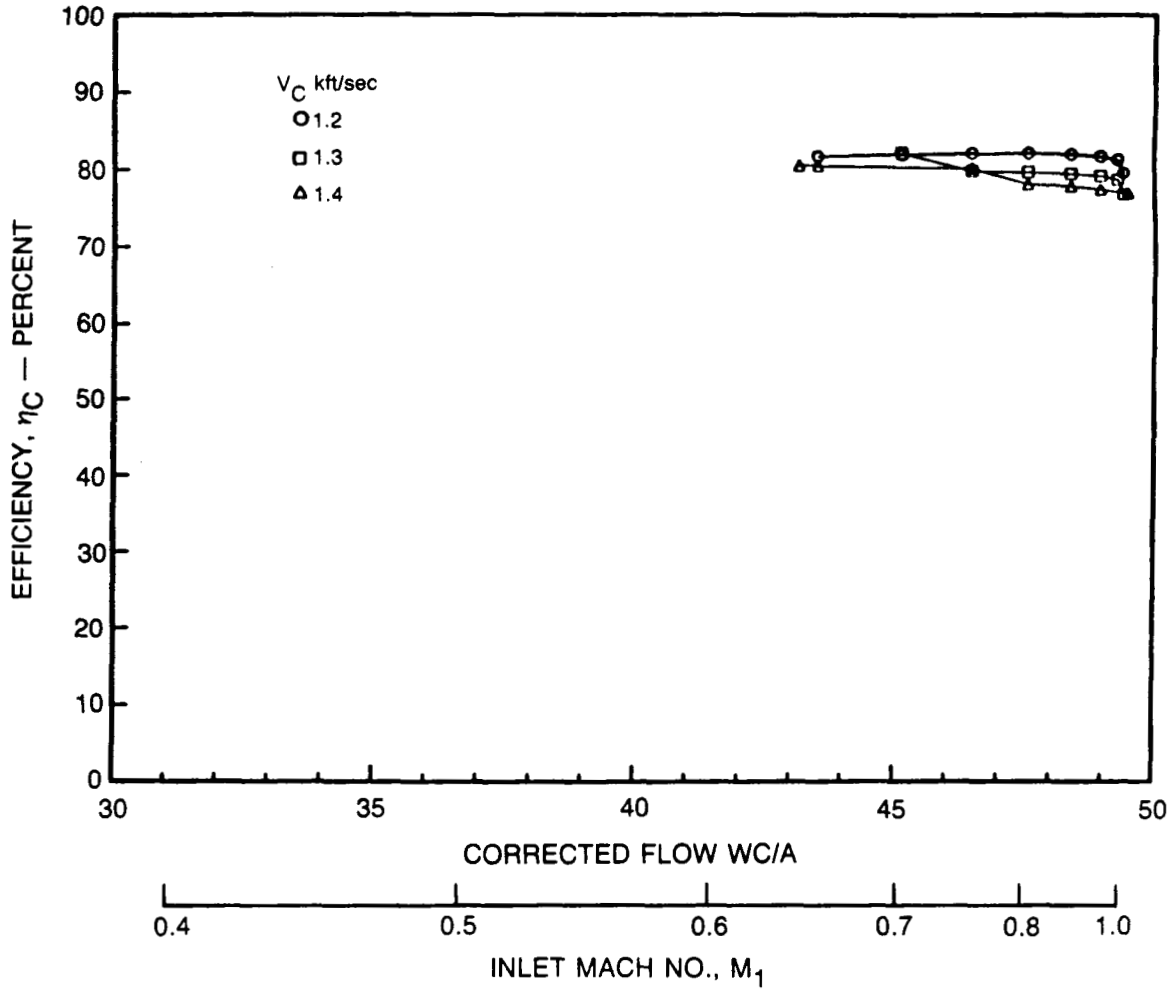

Figure 67. Fan efficiency VPRS-1 subsonic inflow.

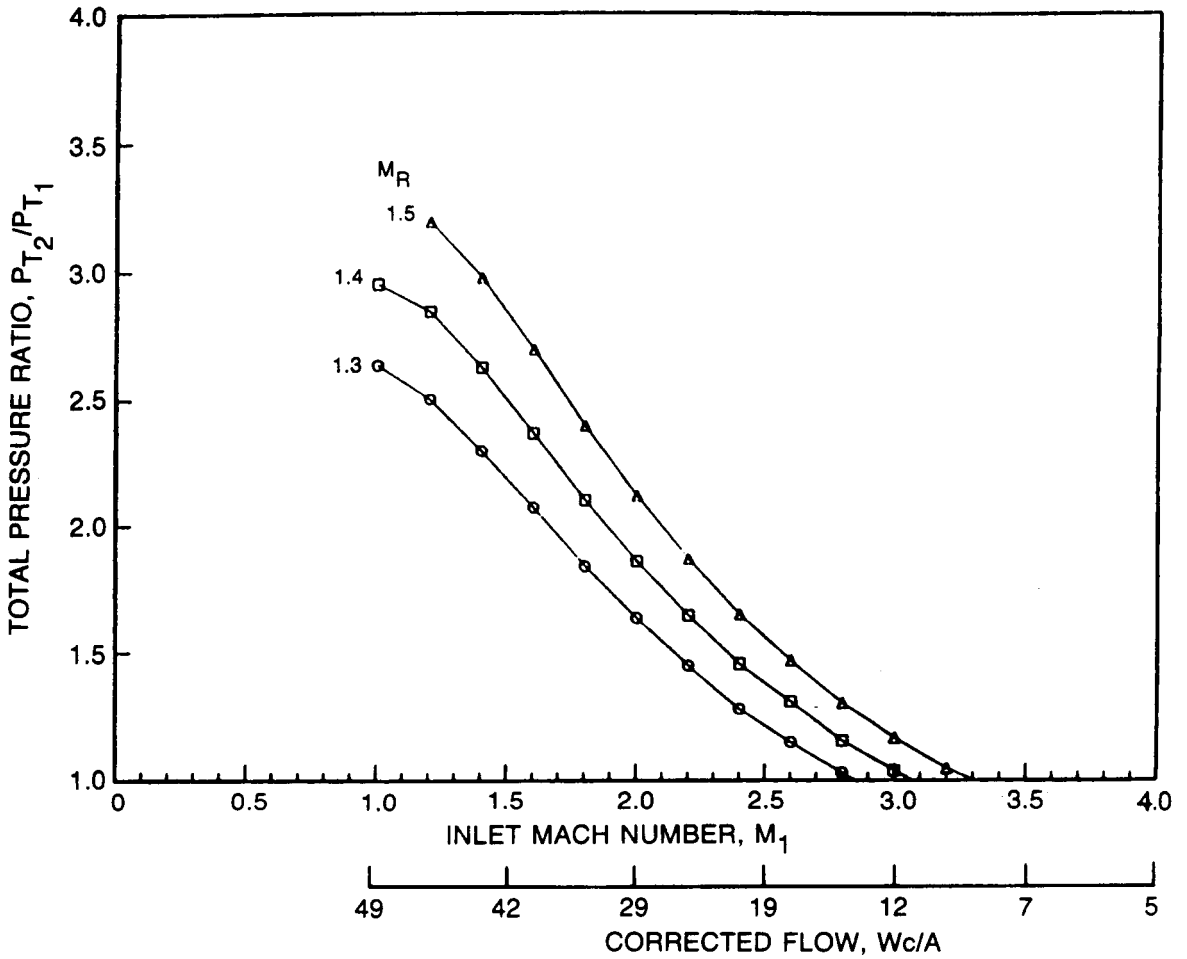

Figure 68. Total pressure ratio VPRS-1 supersonic inflow.

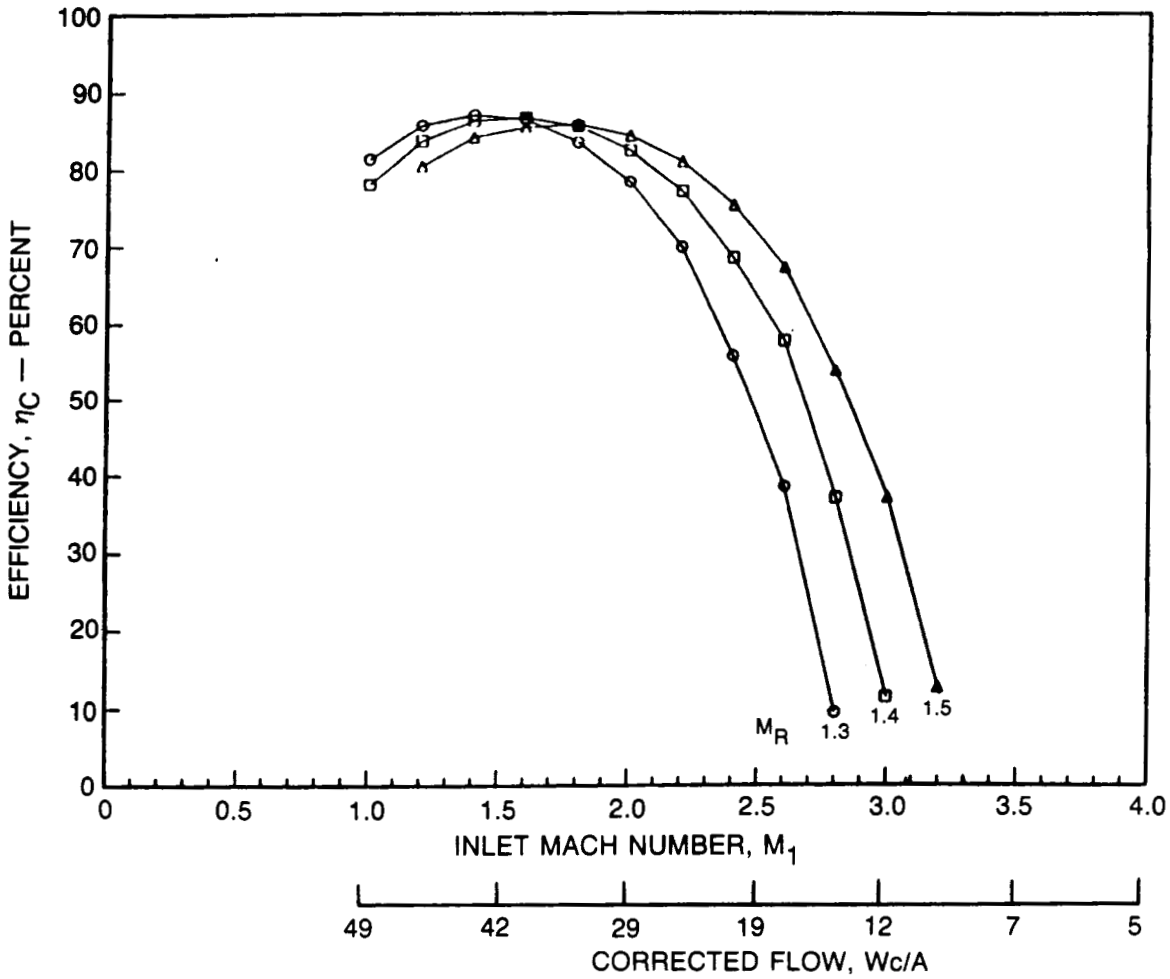

Figure 69. Fan efficiency VPRS-1 supersonic inflow.

MACH 5 CRUISE VEHICLE

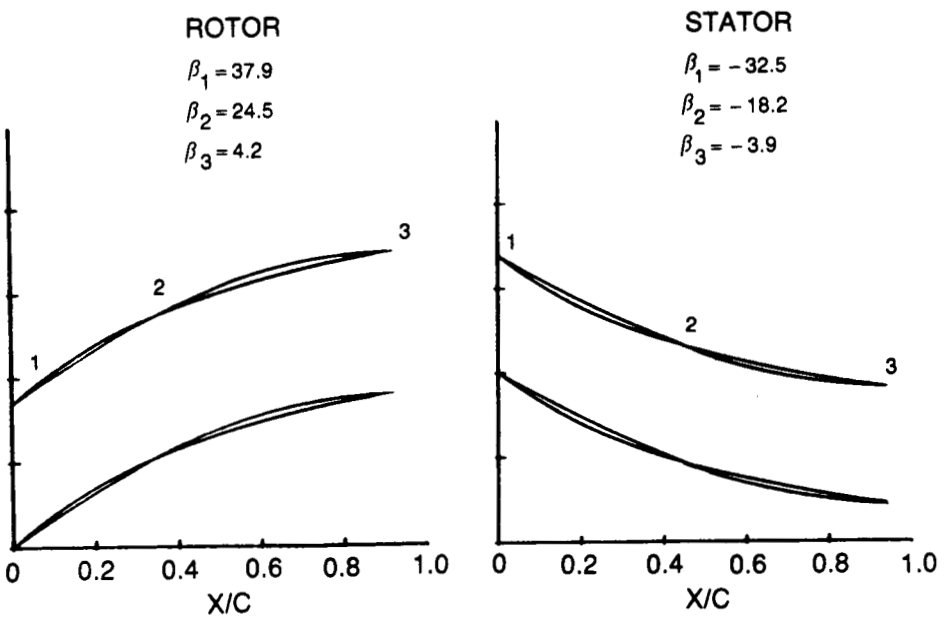

Figure 70. Blade shapes VPRS-2.

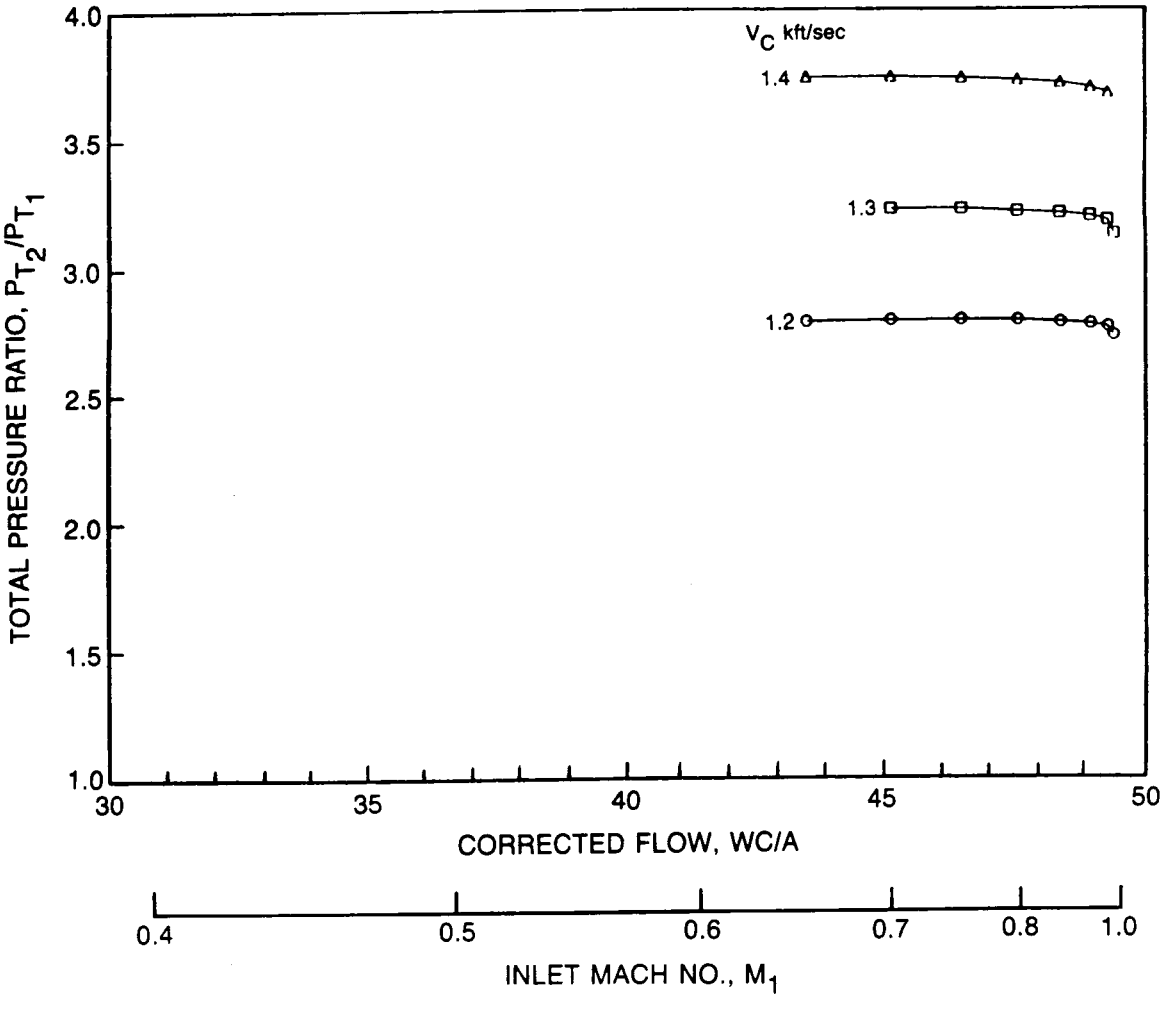

Figure 71. Total pressure ratio VPRS-2 subsonic inflow.

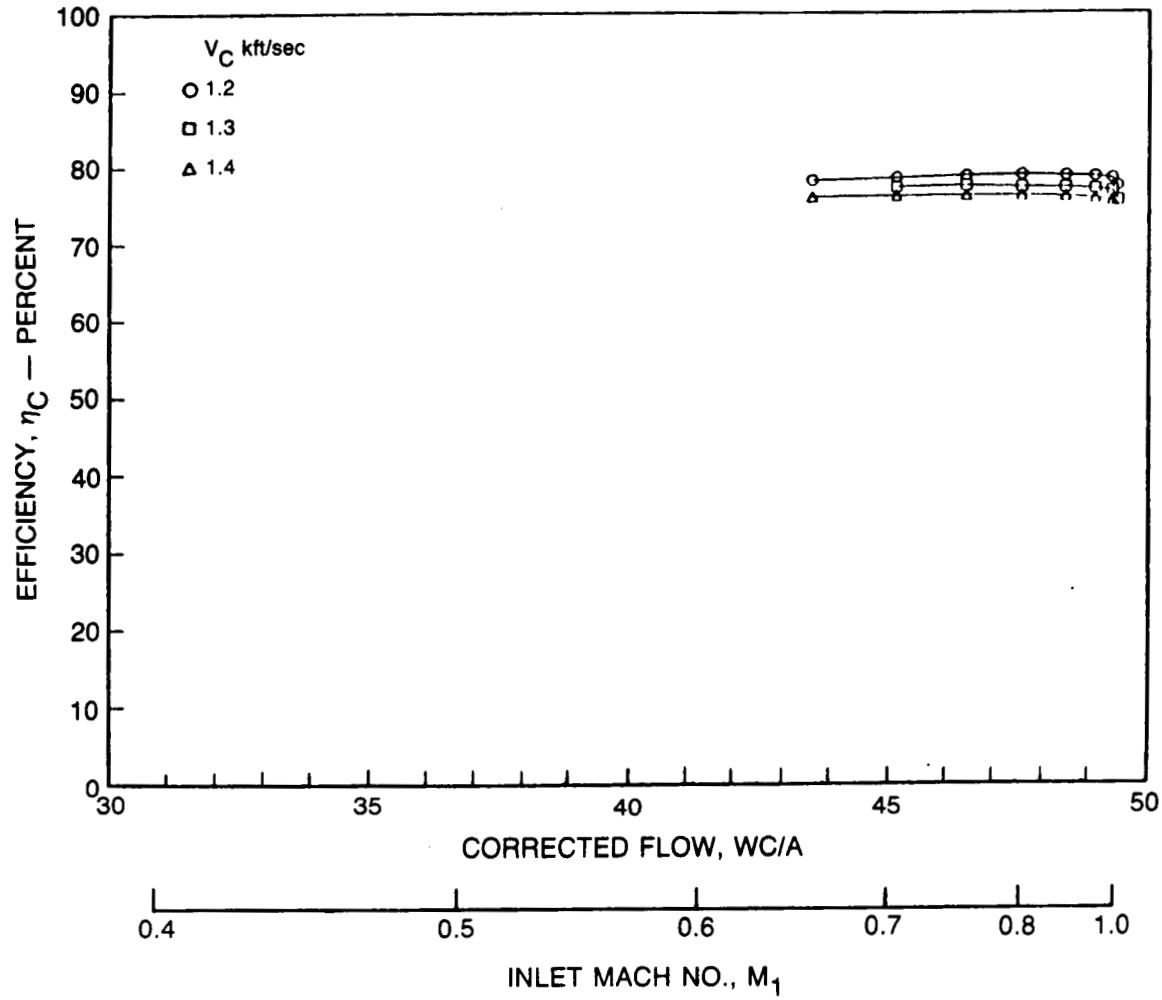

Figure 72. Fan efficiency VPRS-2 subsonic inflow.

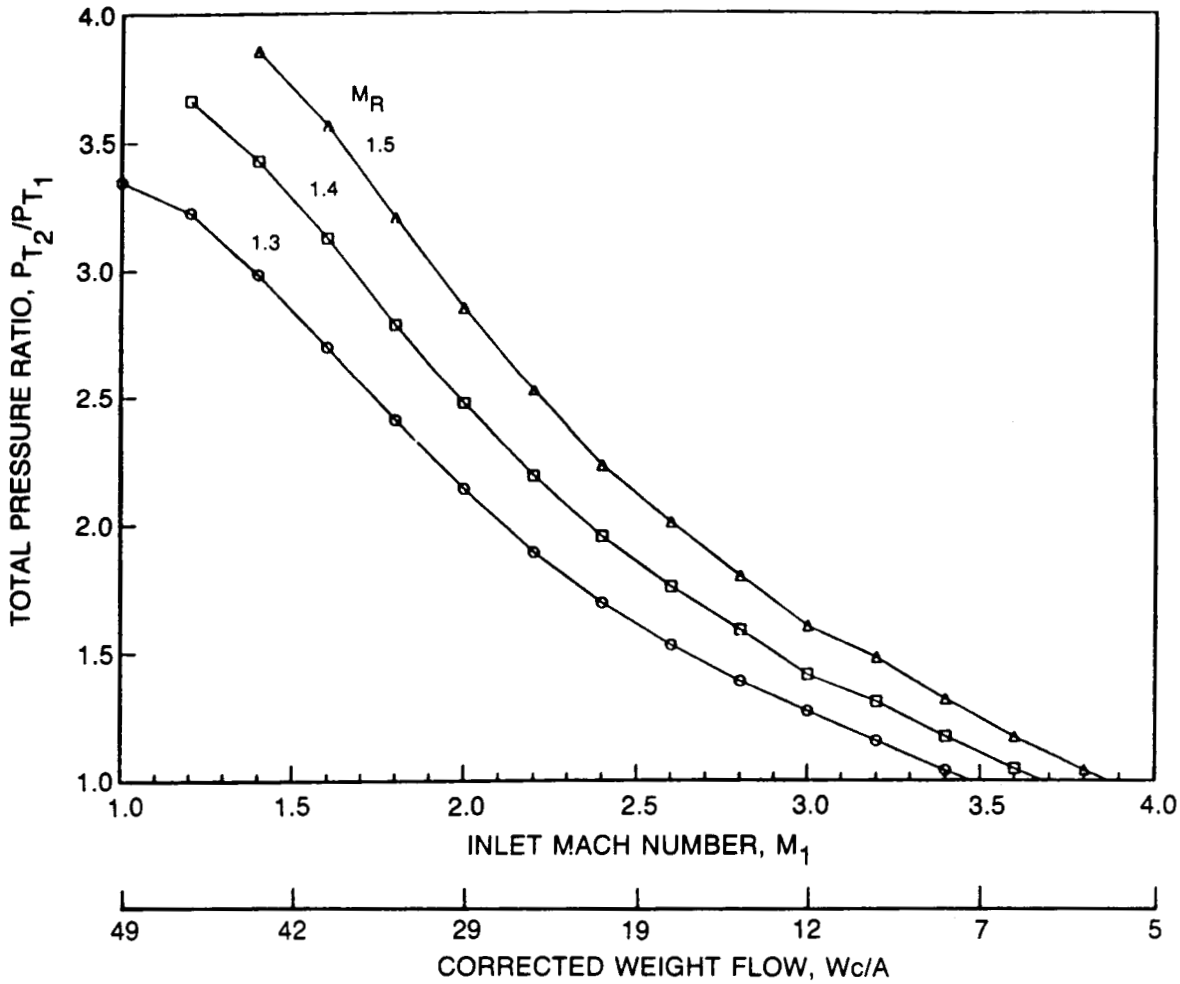

Figure 73. Total pressure ratio VPRS-2 supersonic inflow.

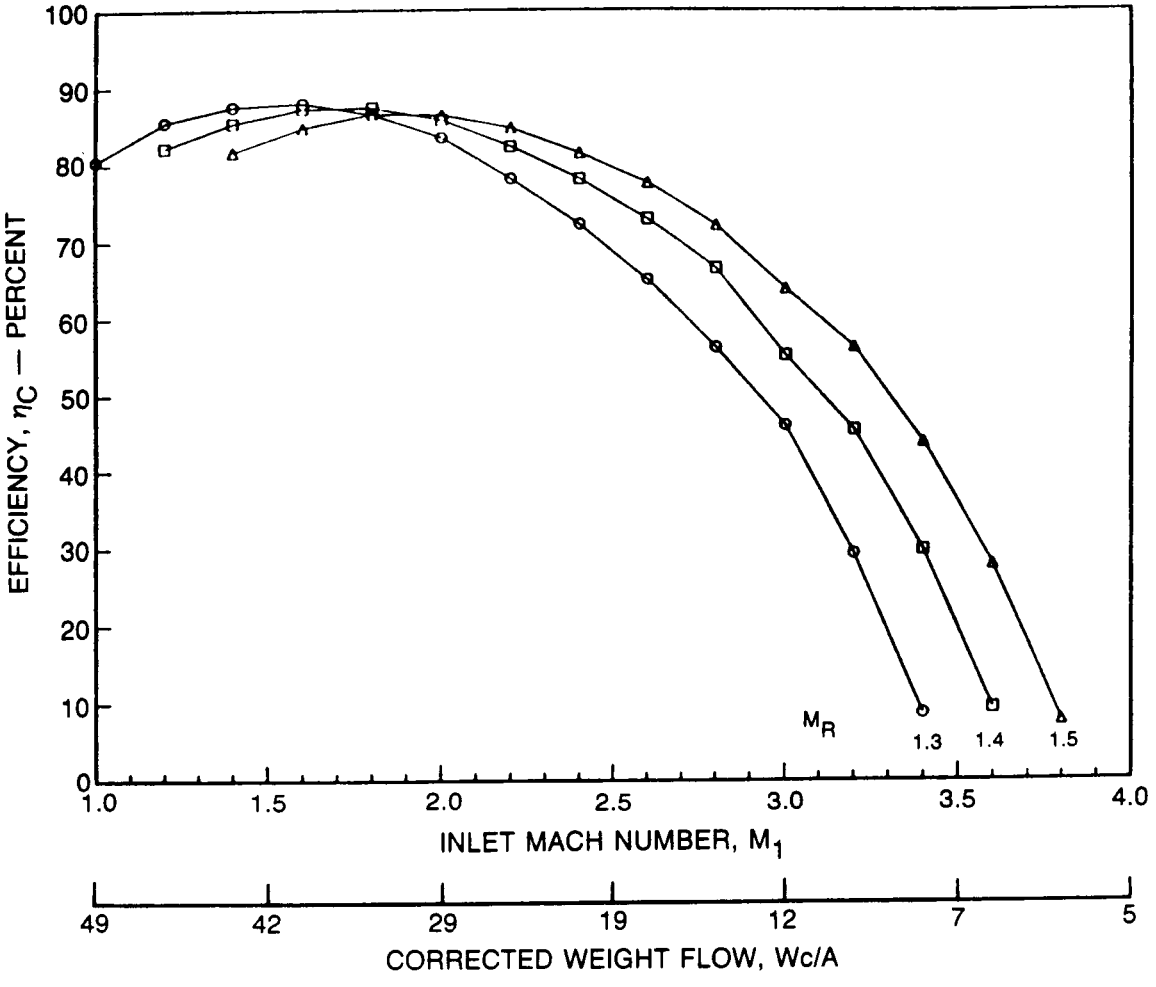

Figure 74. Fan efficiency VPRS-2 supersonic inflow.

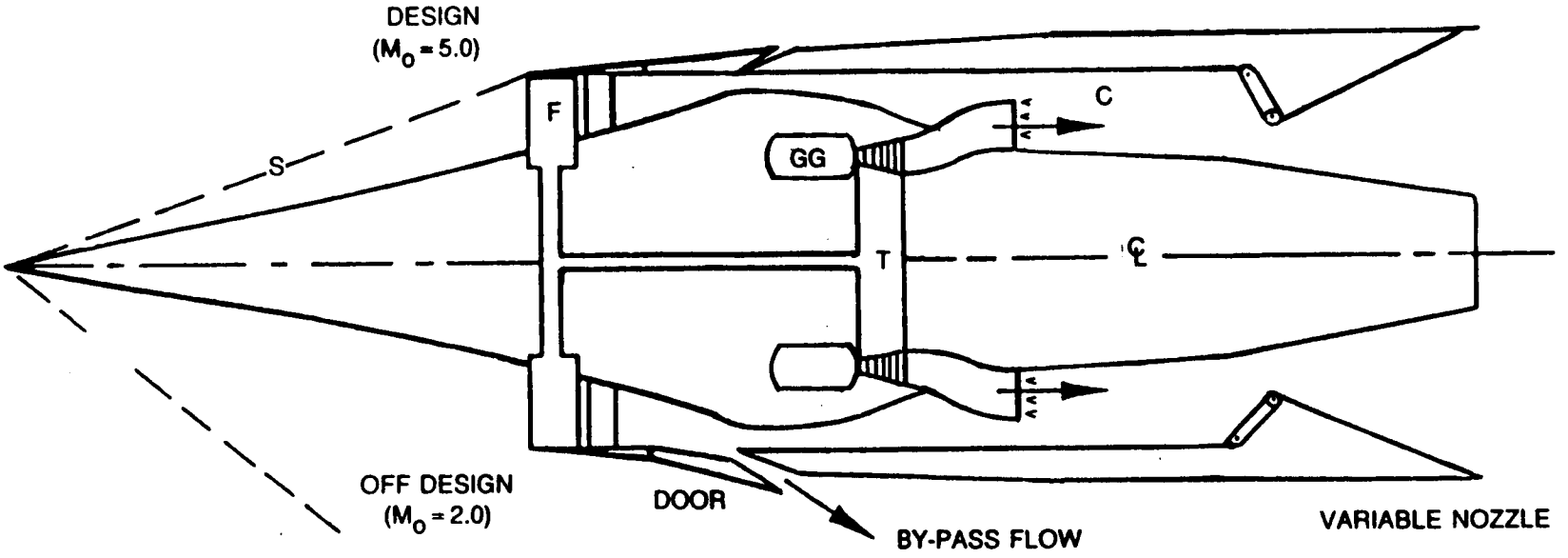

Figure 75. STFF-ATR engine configuration.

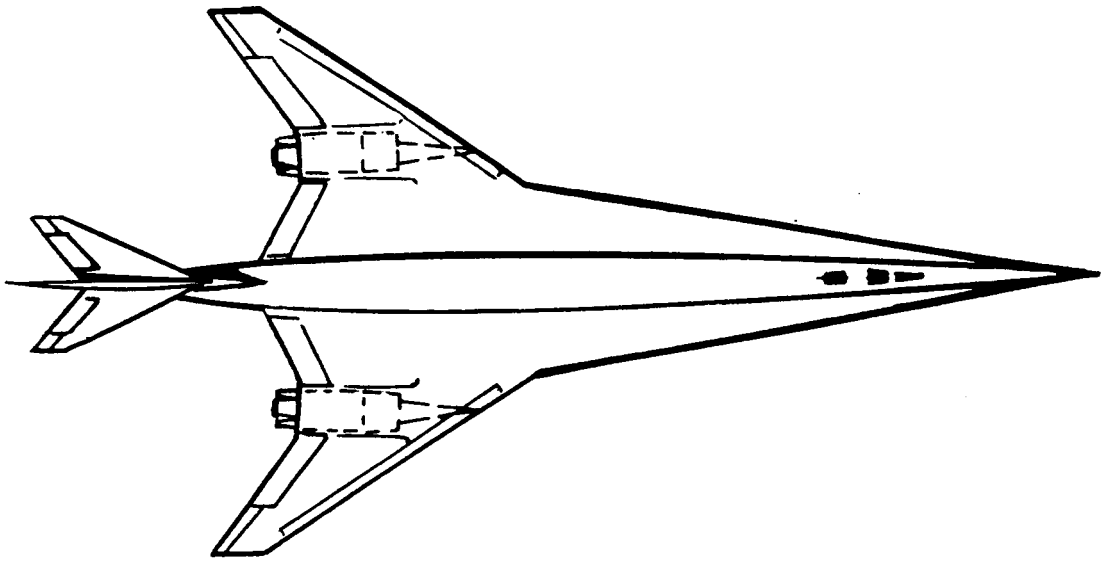

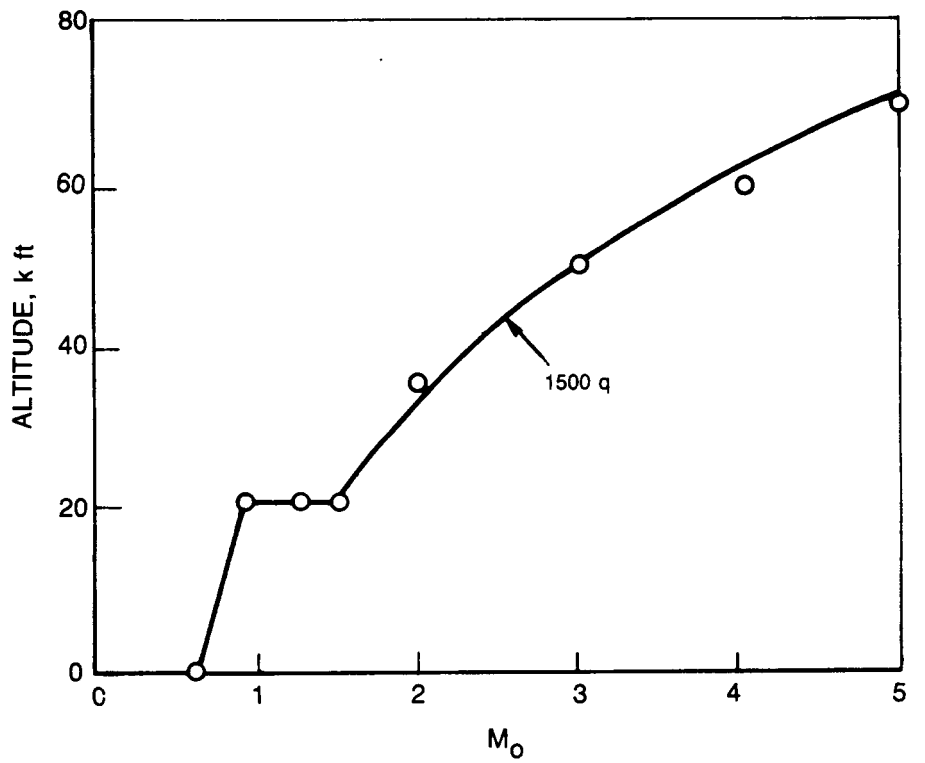

Figure 76. Flight path.

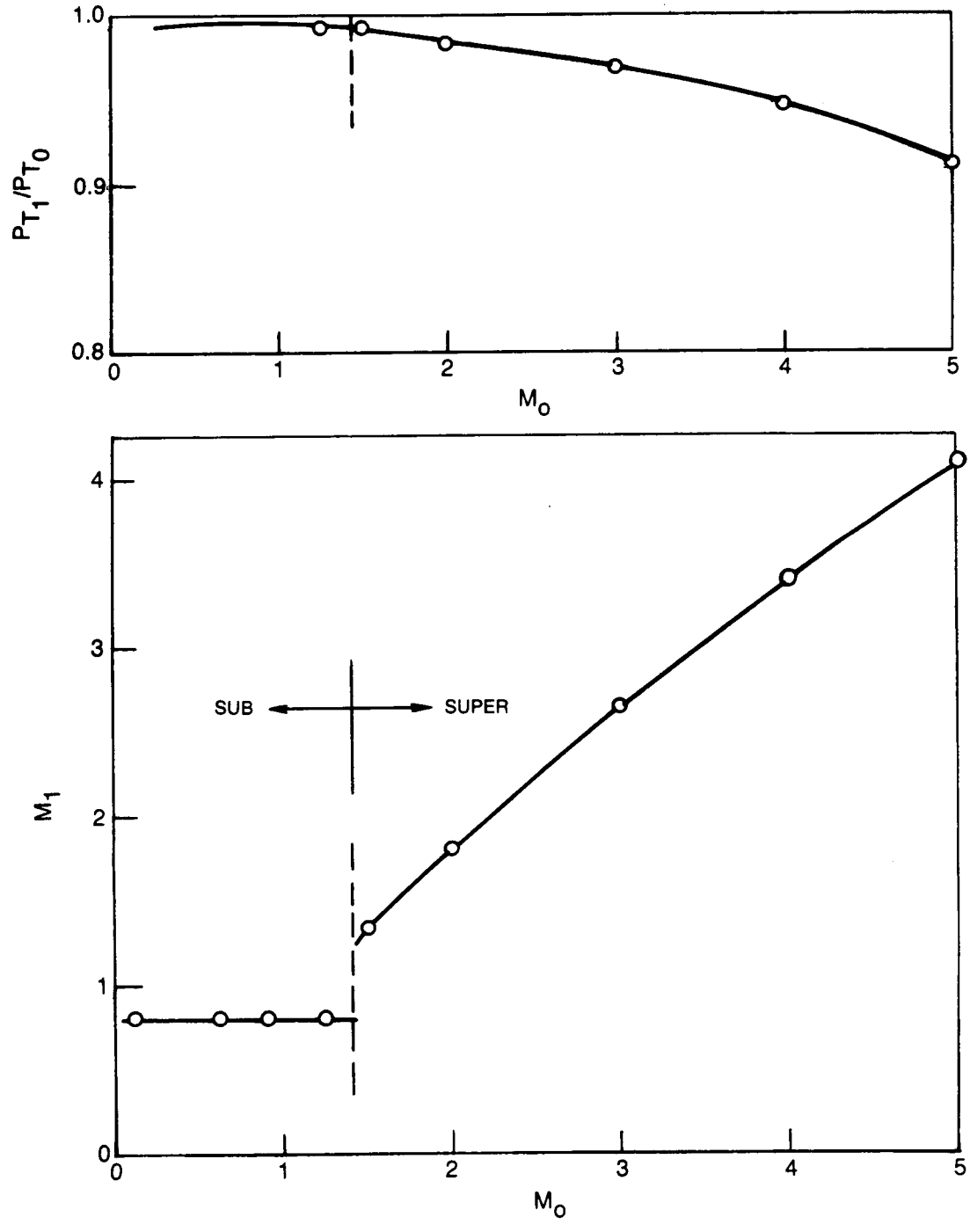

Figure 77. STFF inlet total pressure recovery and fan Mach no.

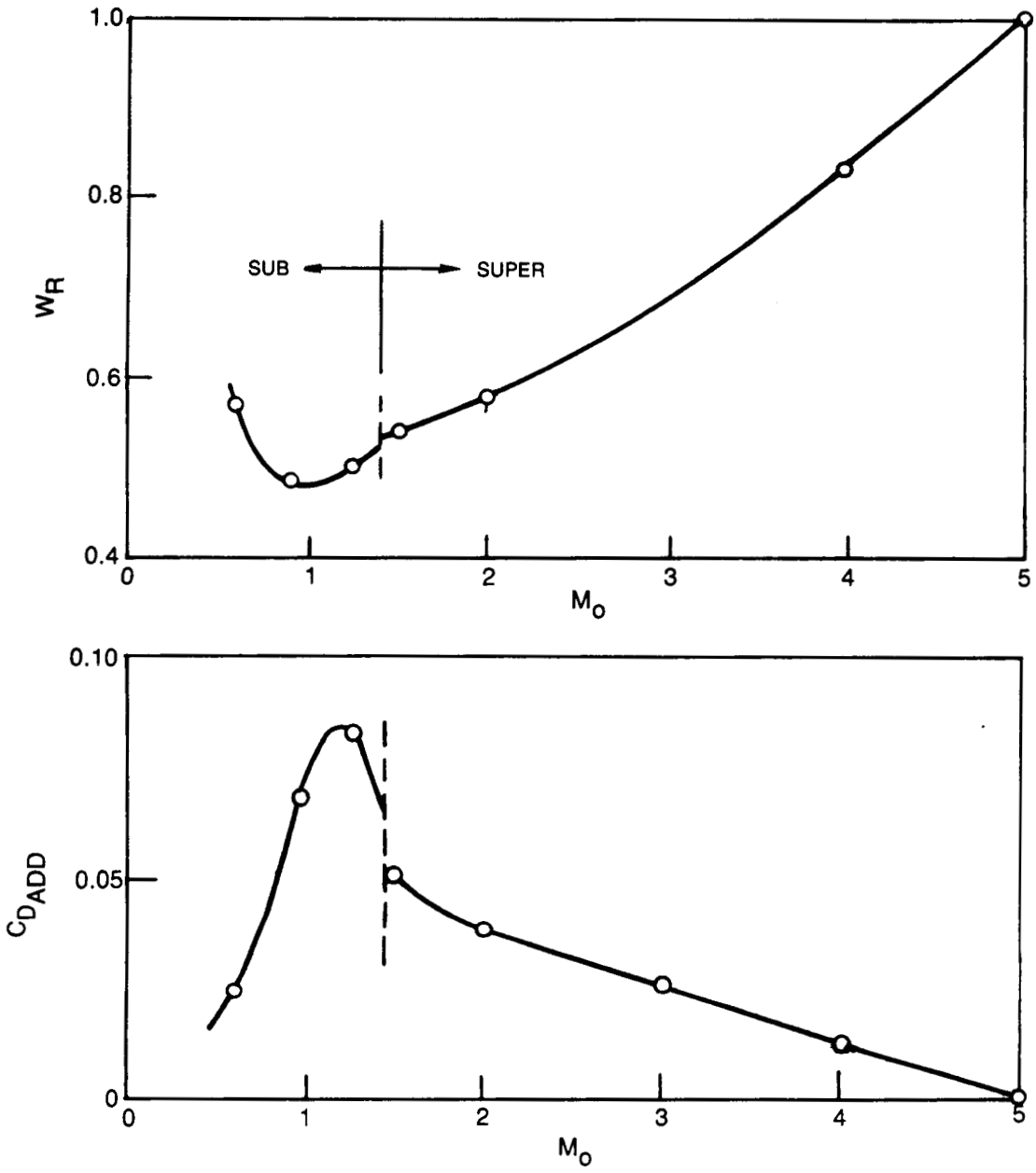

Figure 78. STFF inlet relative weight flow and additive drag.

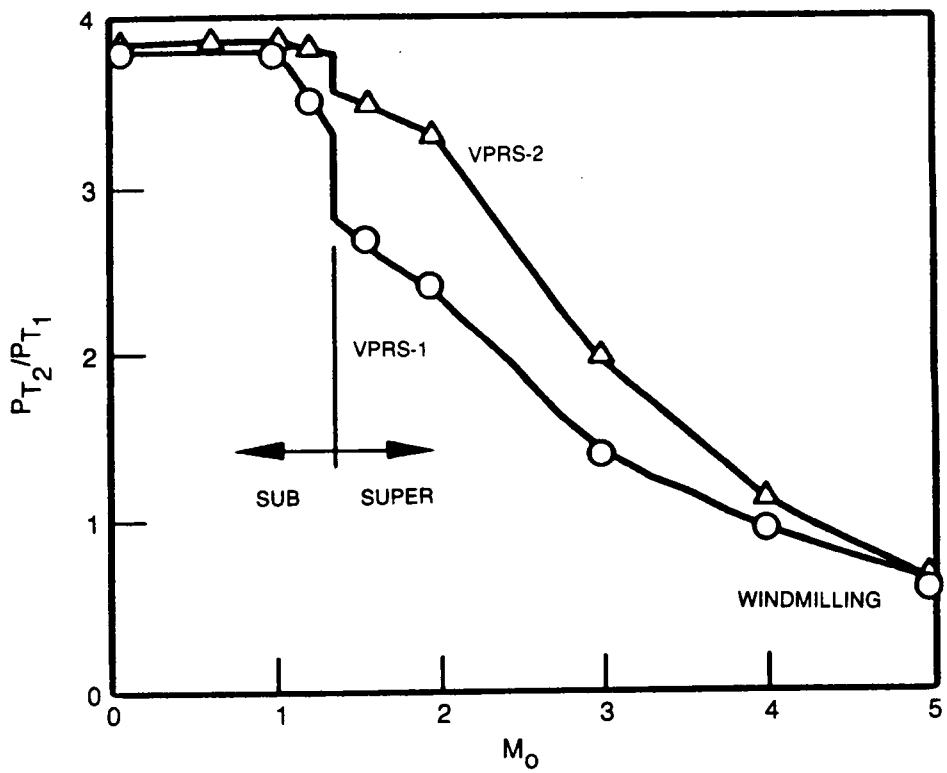

Figure 79. Fan total pressure ratio.

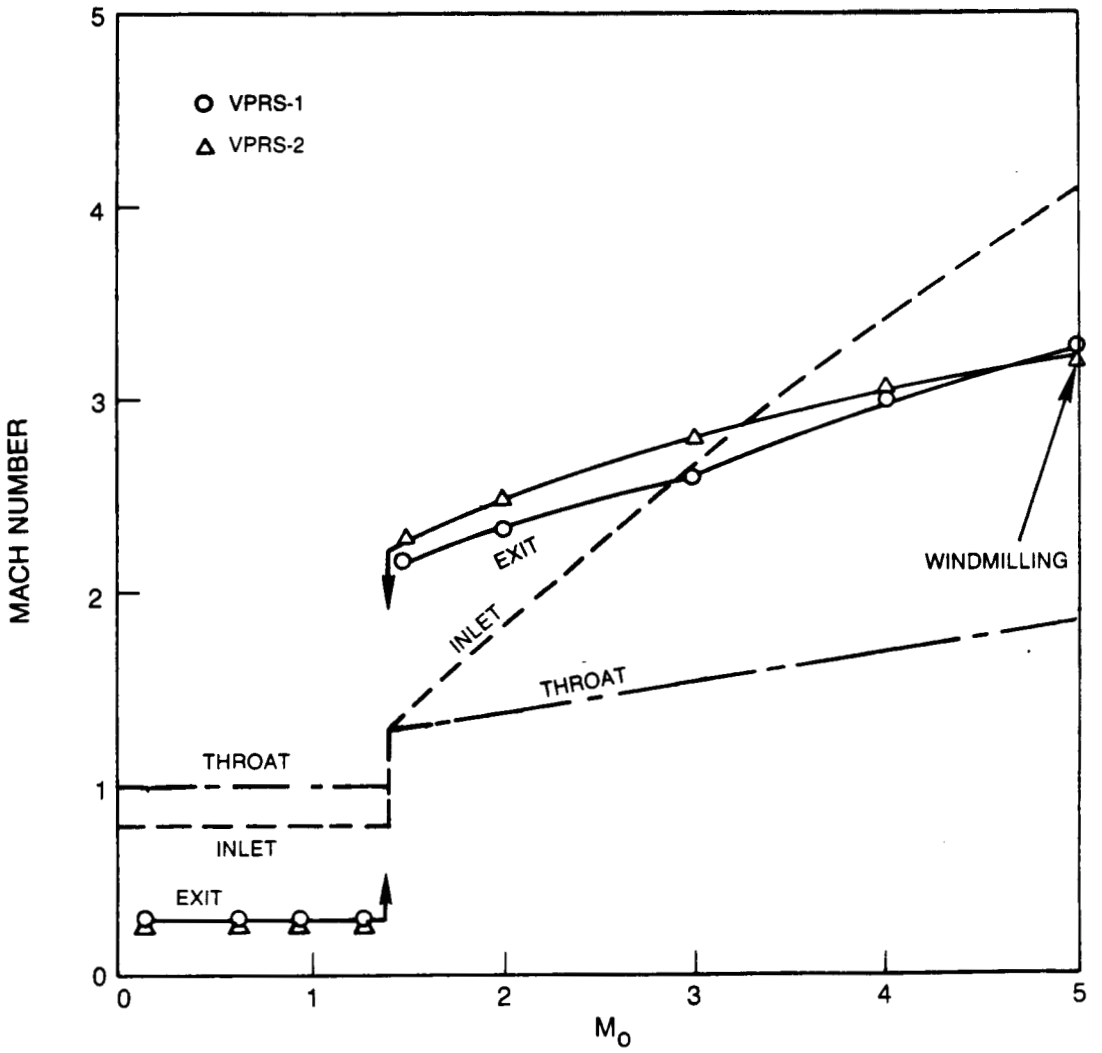

Figure 80. Fan inlet & exit Mach No.

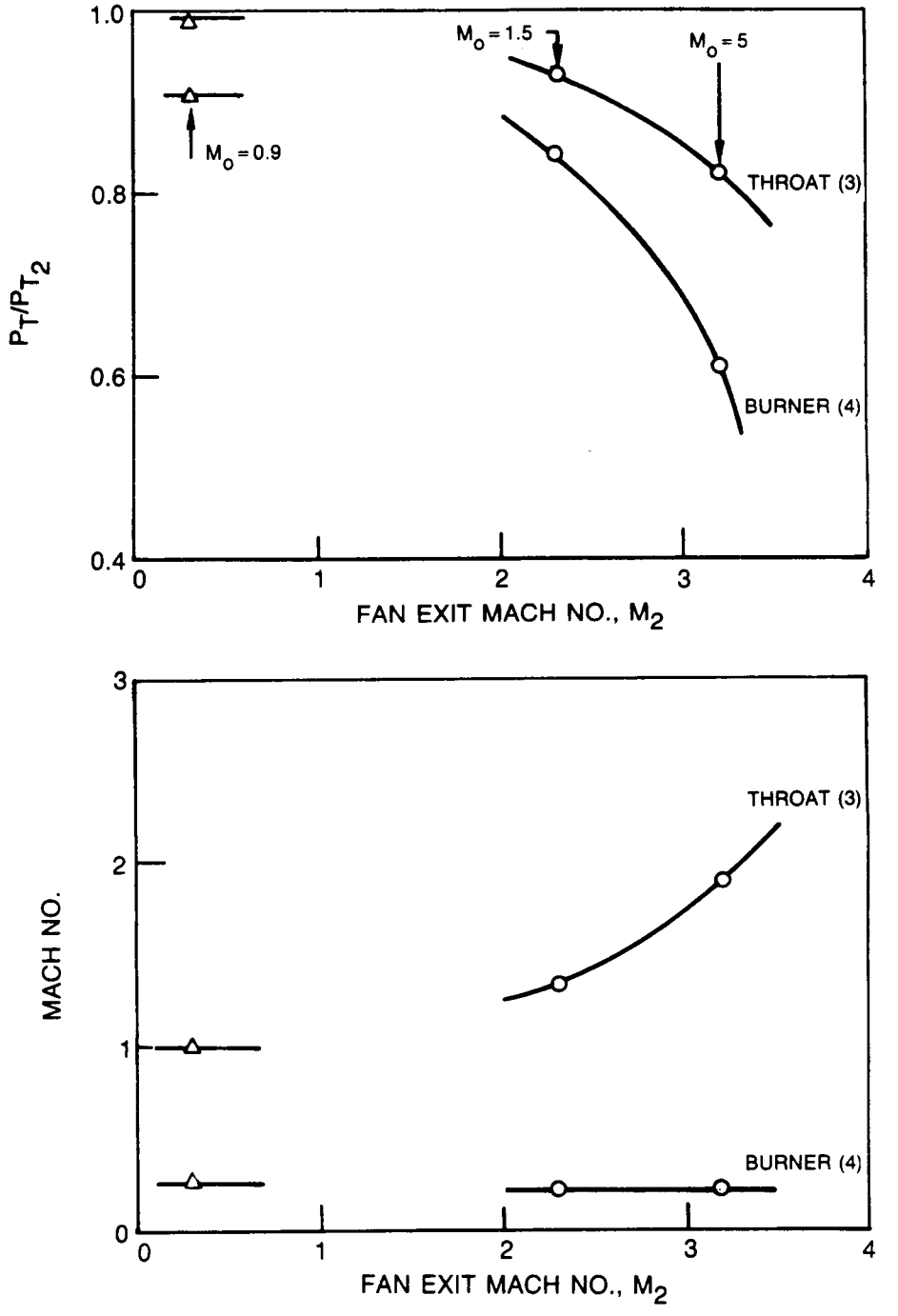

Figure 81. STFF aft diffuser characteristics.

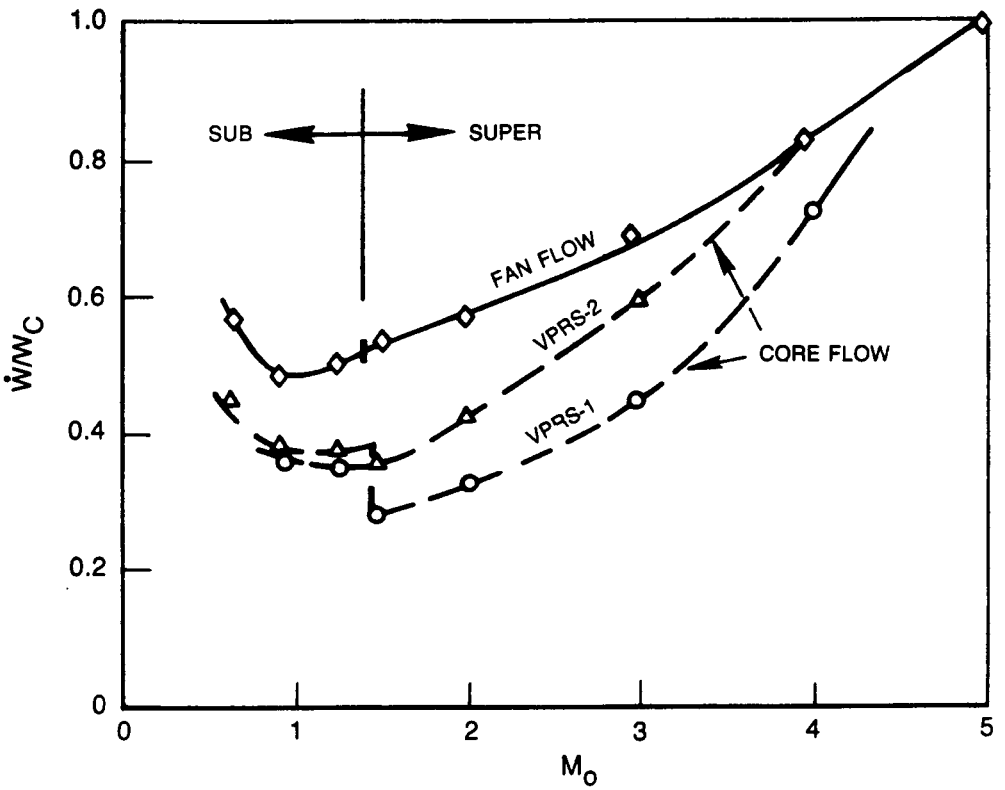

Figure 82. Engine airflow.

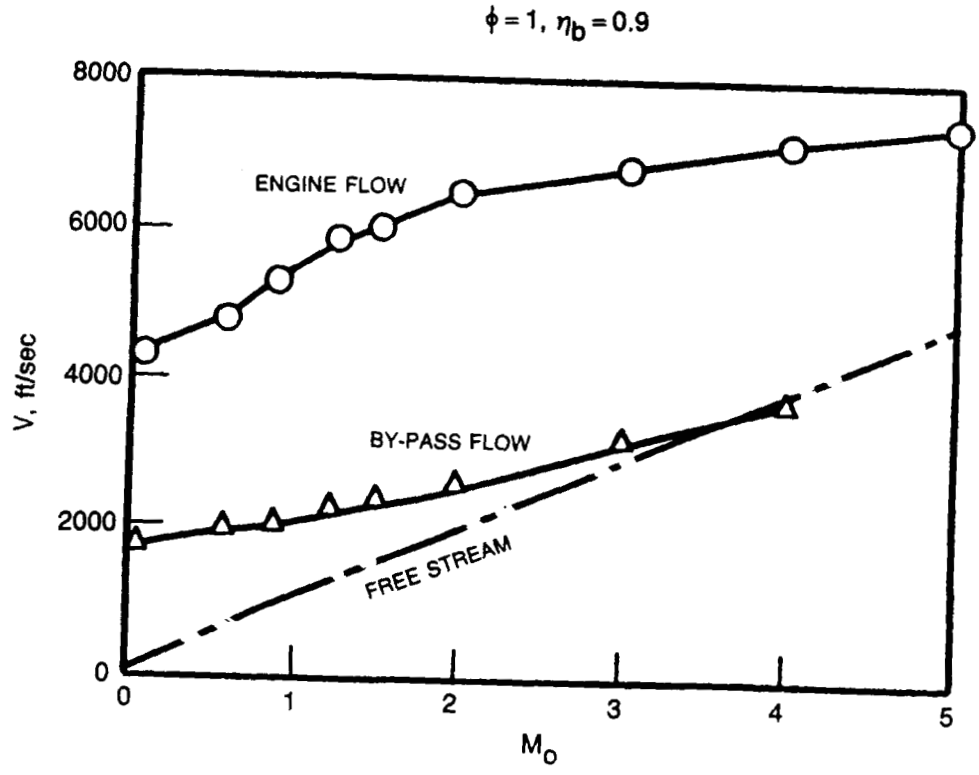

Figure 83. Exhaust flow velocities.

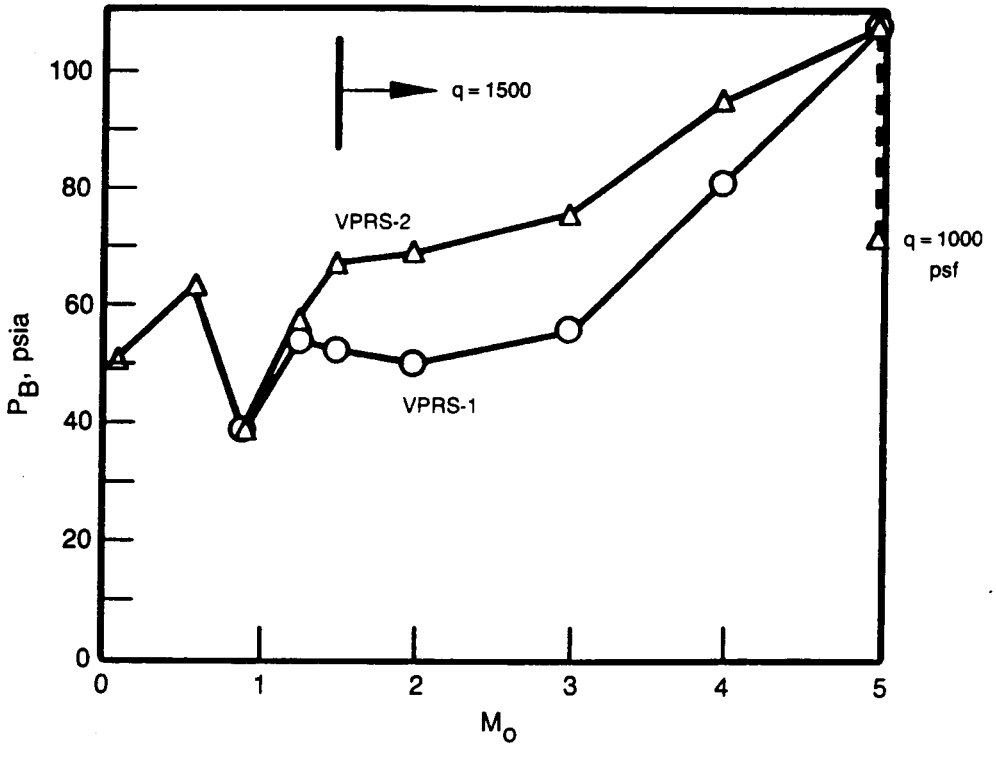

Figure 84. Burner pressure.

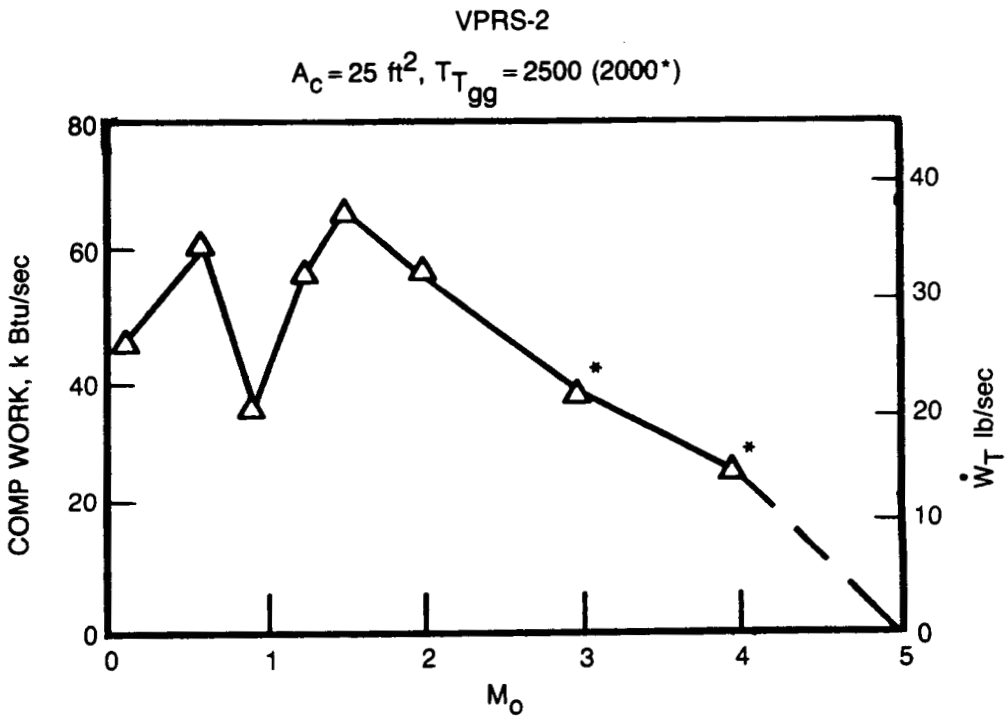

Figure 85. Compressor work and turbine flow.

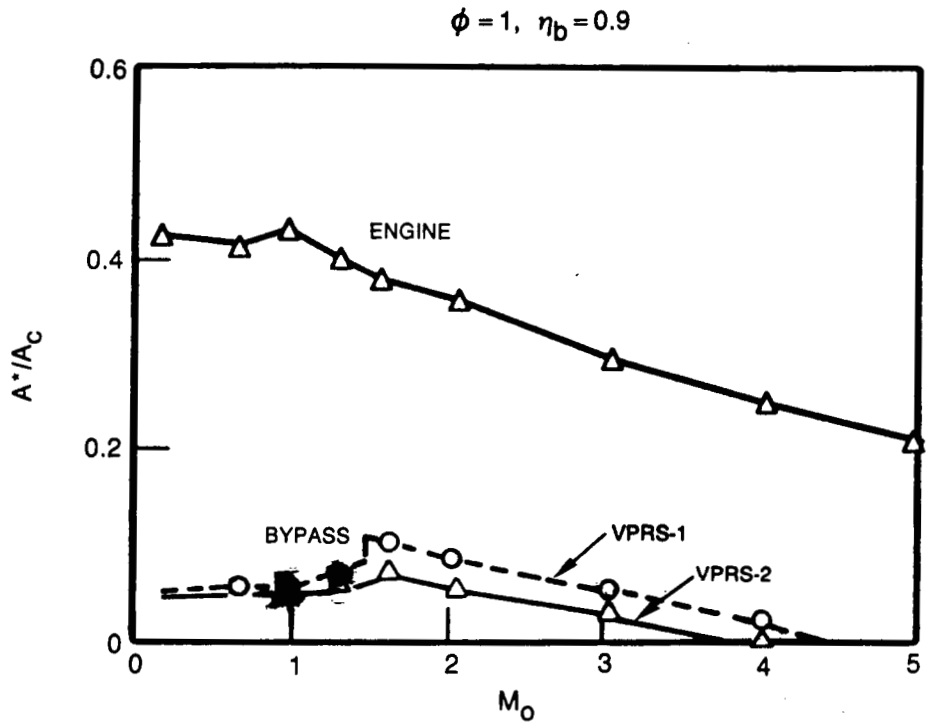

Figure 86. Nozzle areas.

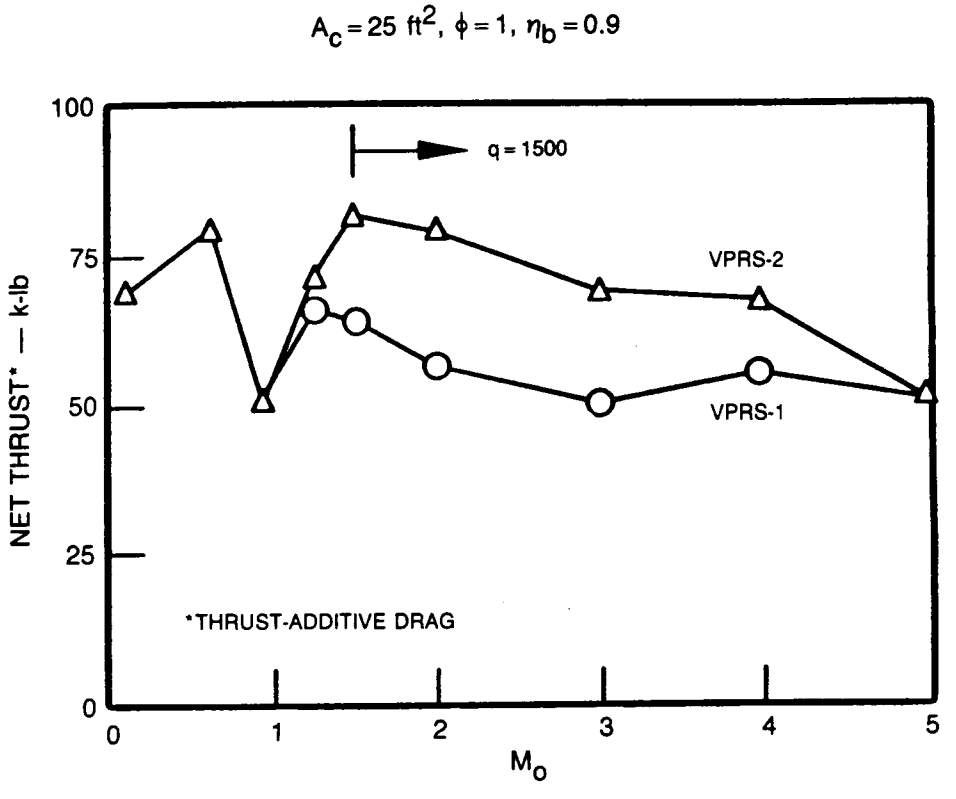

Figure 87. Net thrust.

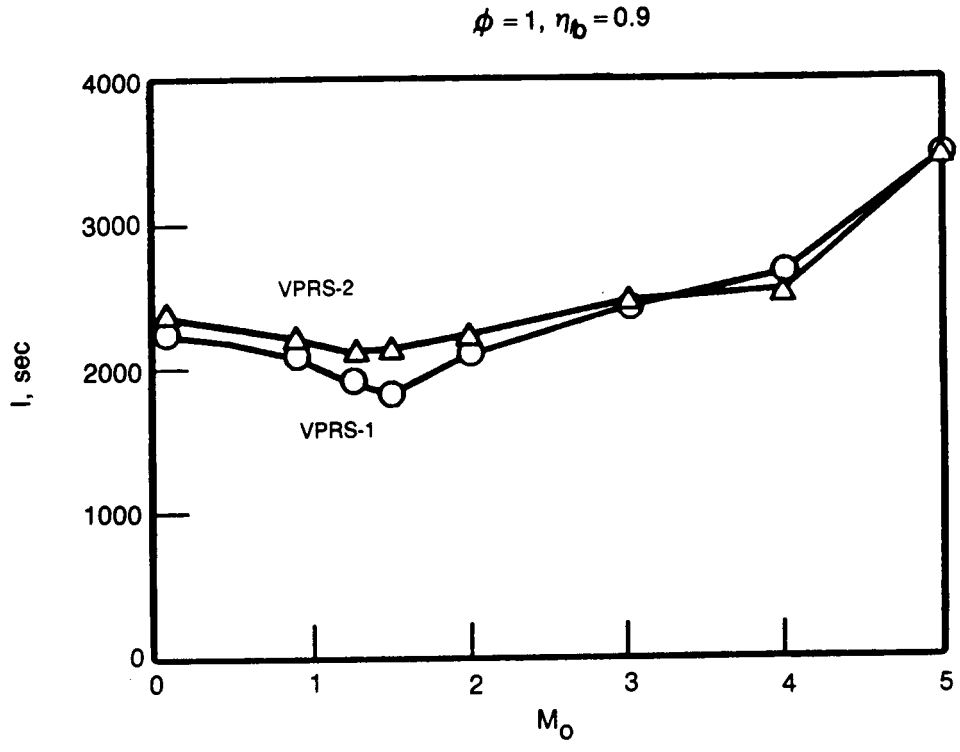

Figure 88. Fuel specific impulse.

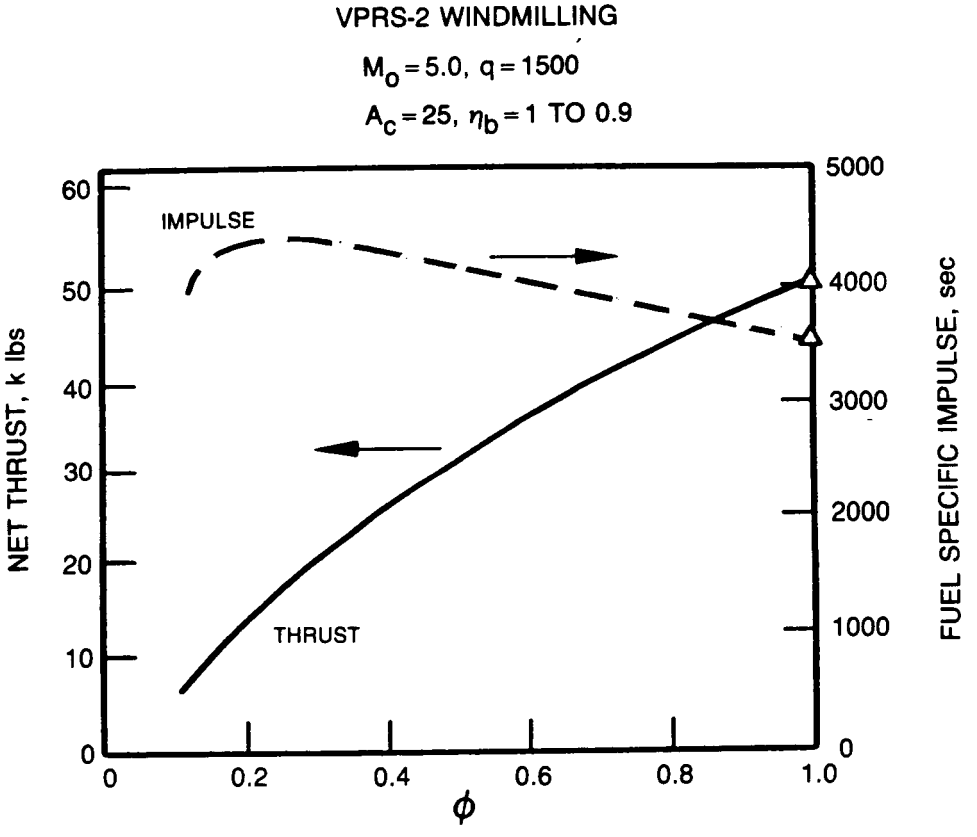

Figure 89. Part power performance.

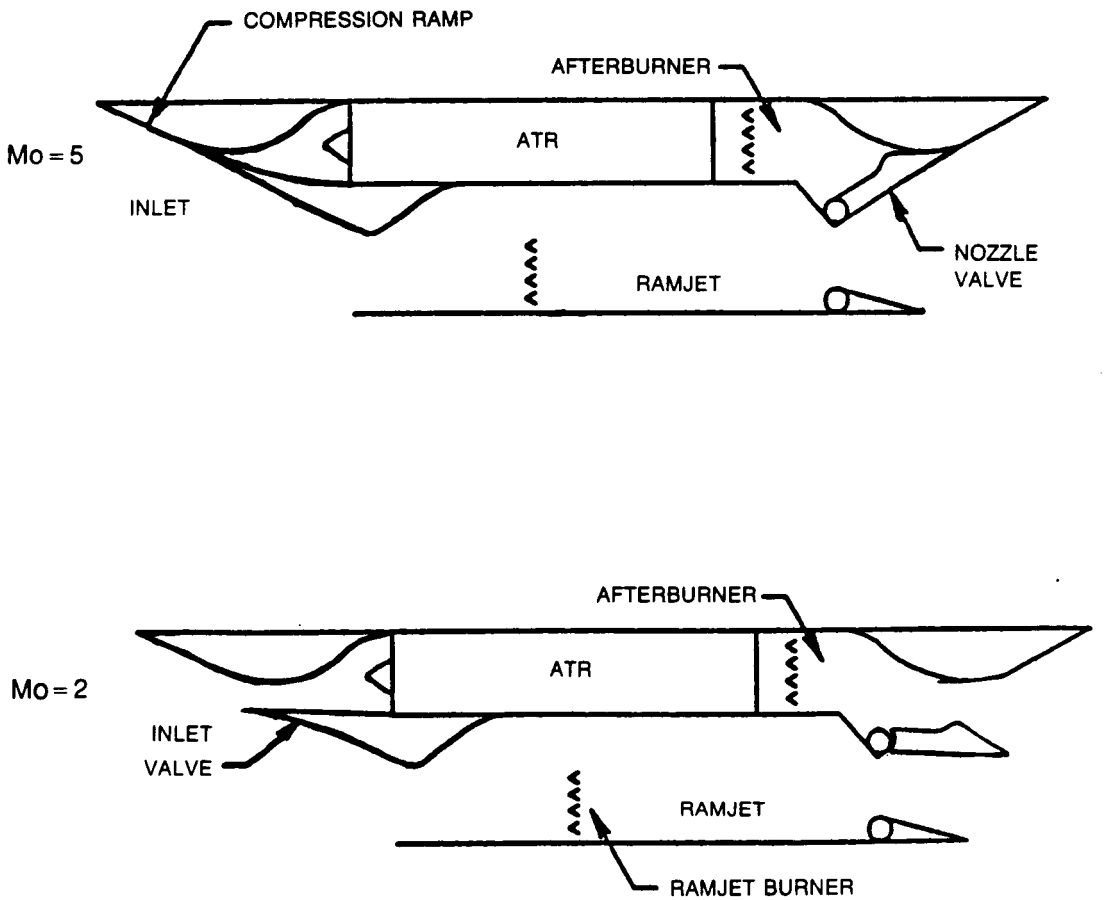

Figure 90. Conventional over/under air turbo rocket/ramjet.

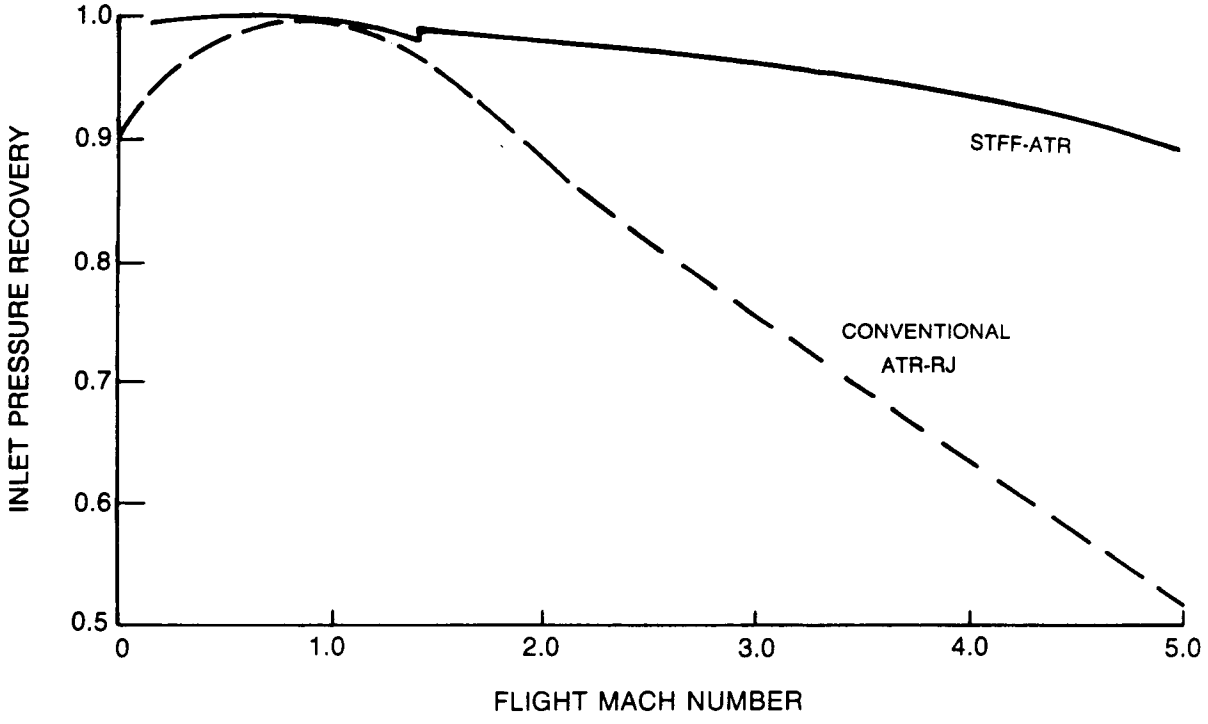

Figure 91. Inlet pressure recovery for STFF and conventional inlets.

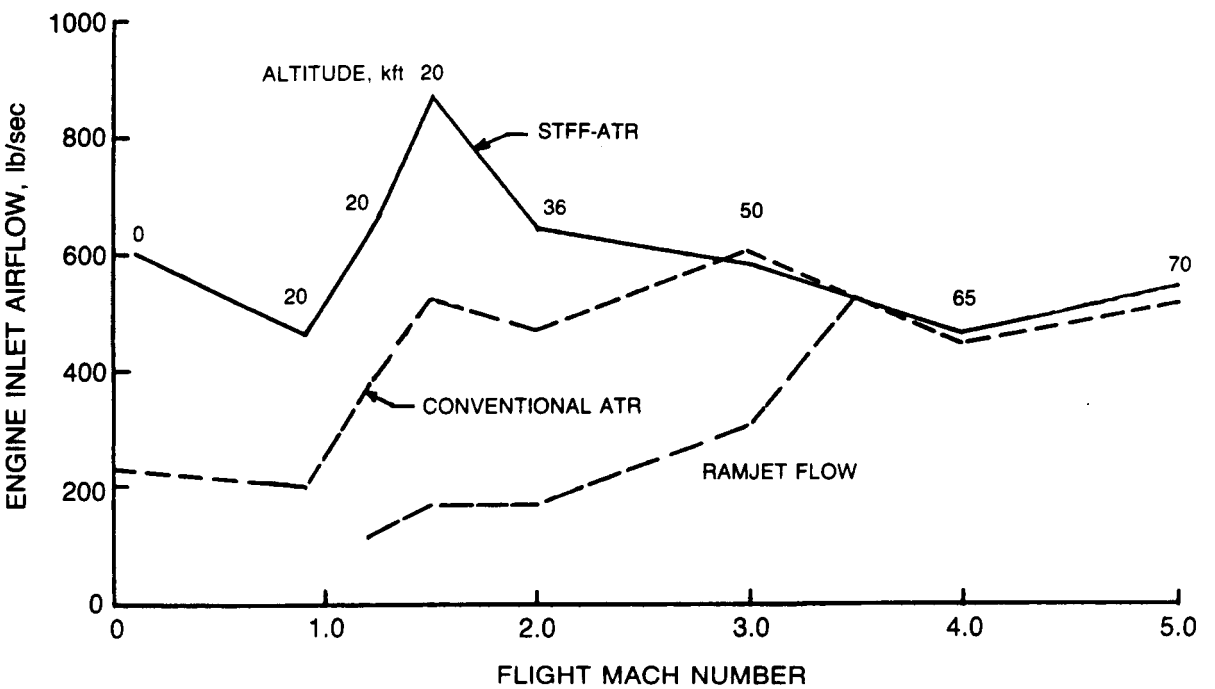

Figure 92. STFF-ATR and ATR-RJ flow schedules.

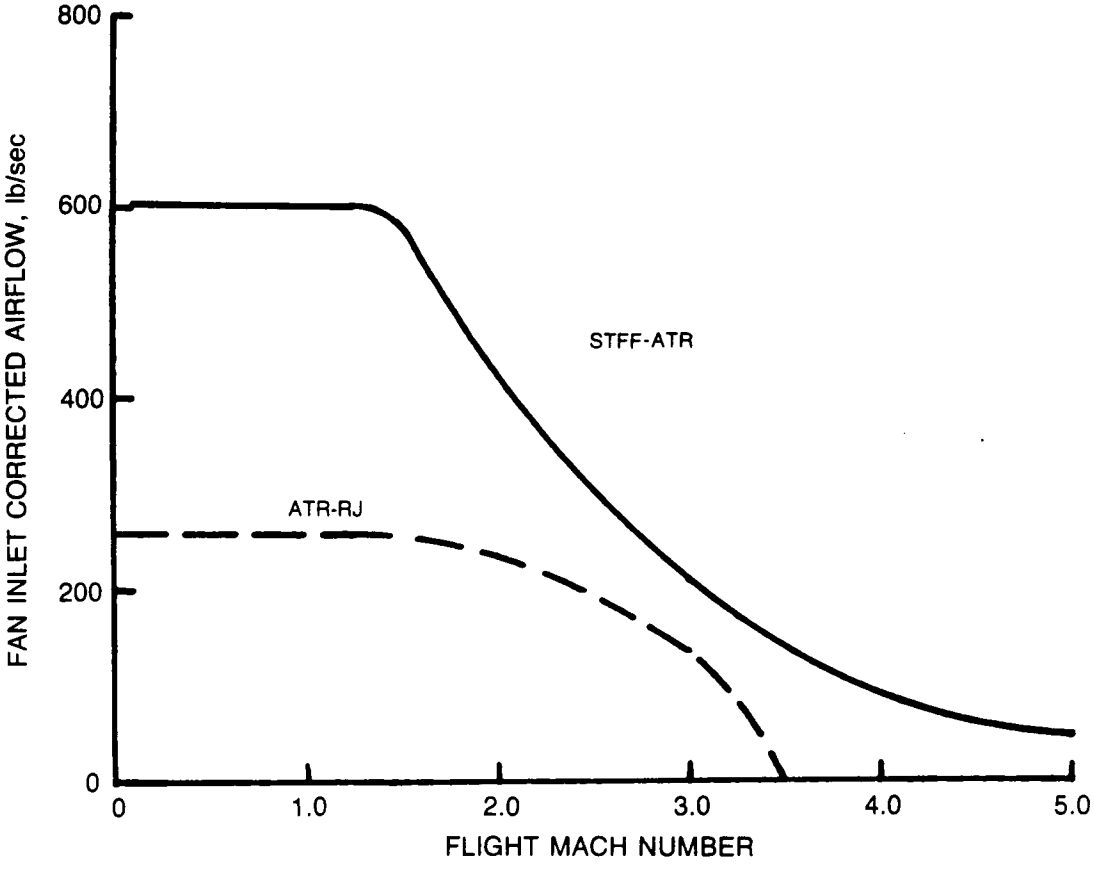

Figure 93. STFF-ATR and ATR-RJ fan inlet corrected airflow schedules.

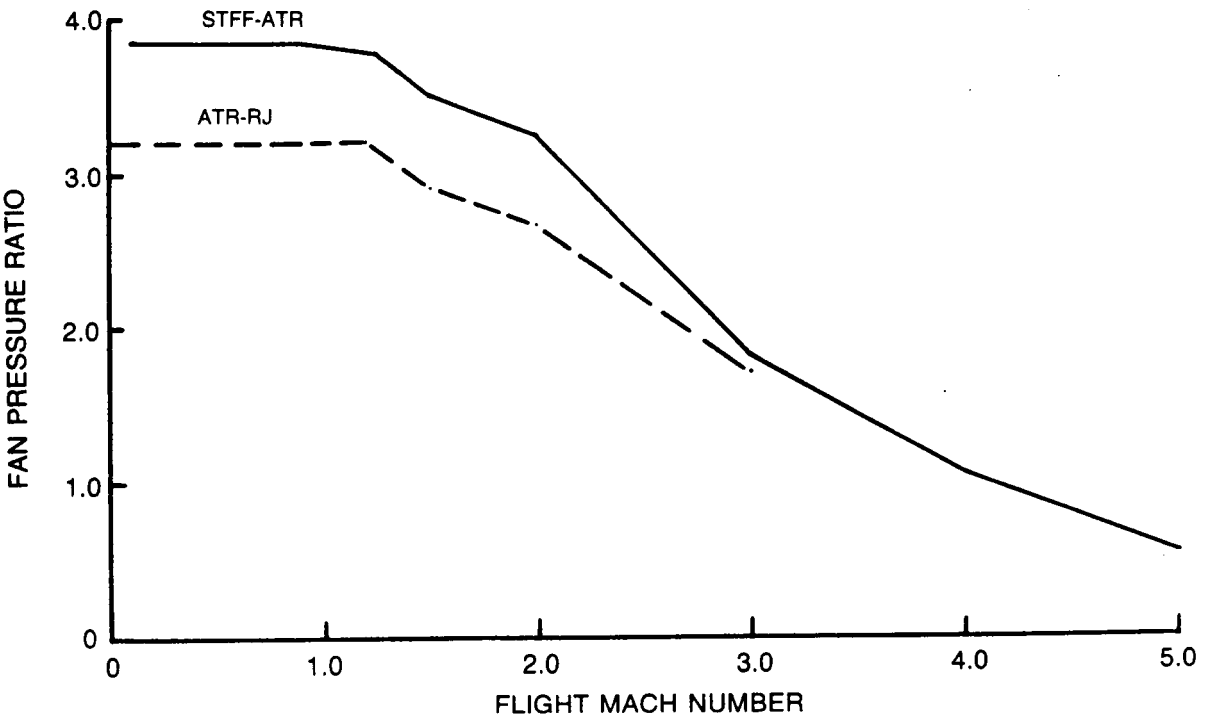

Figure 94. STFF-ATR and ATR-RJ fan pressure ratio.

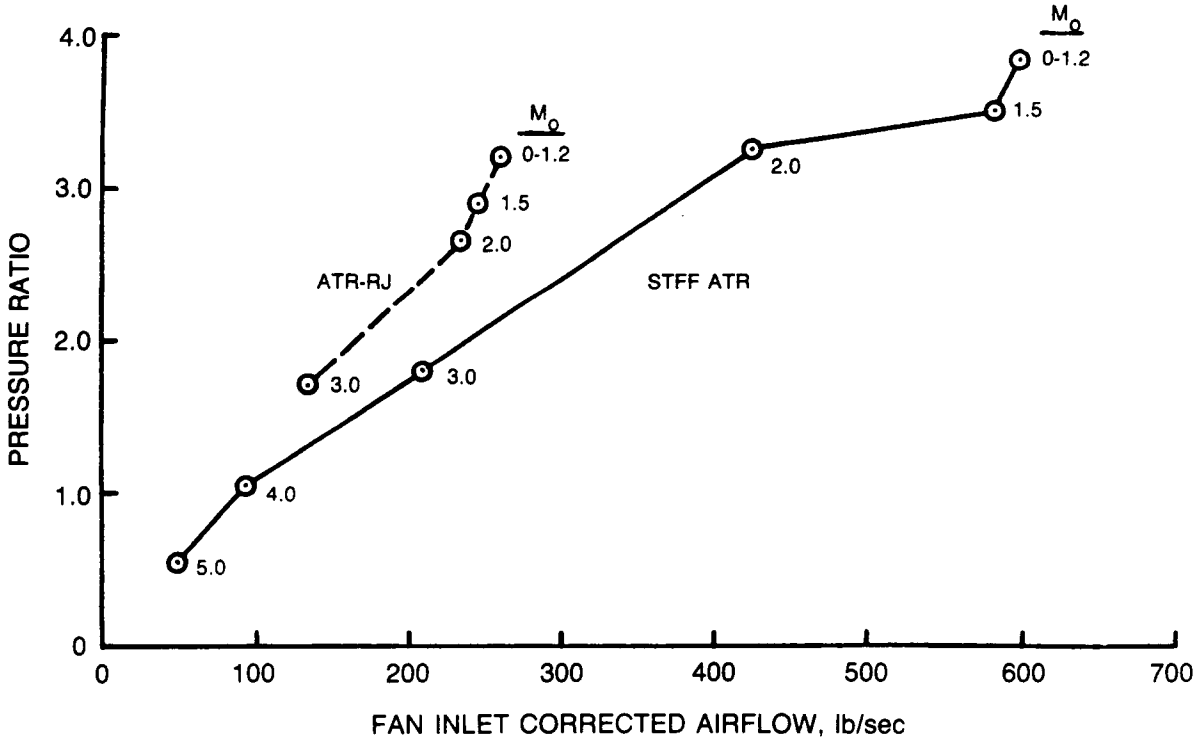

Figure 95. STFF-ATR and ATR-RJ fan operating lines.

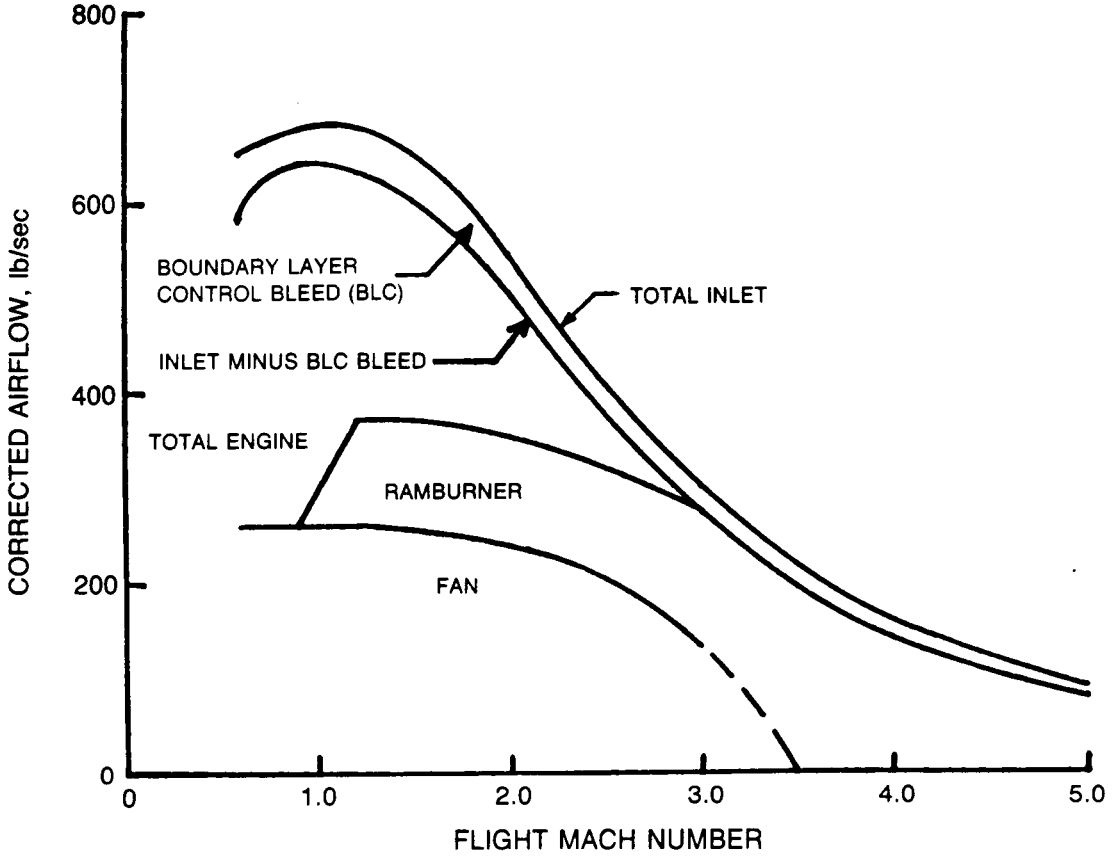

Figure 96. Conventional ATR-RJ inlet/engine corrected flows.

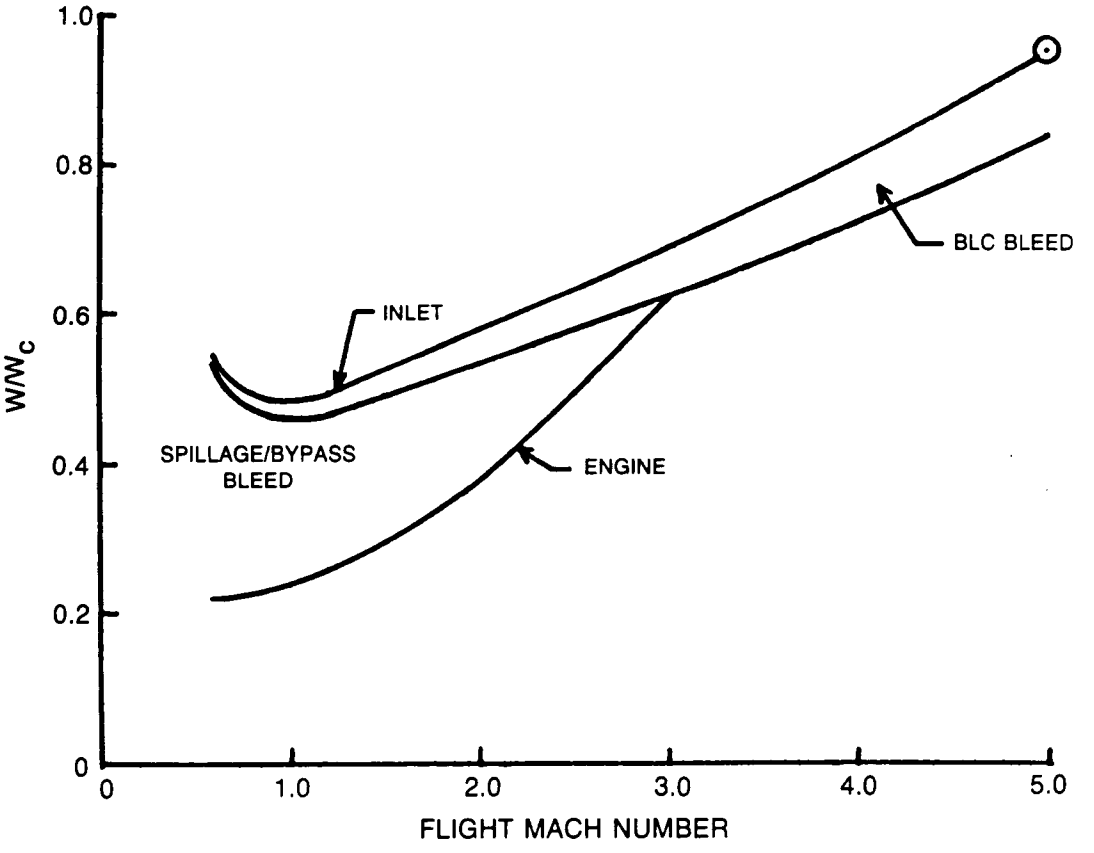

Figure 97. Conventional ATR-RJ inlet mass flow schedule.

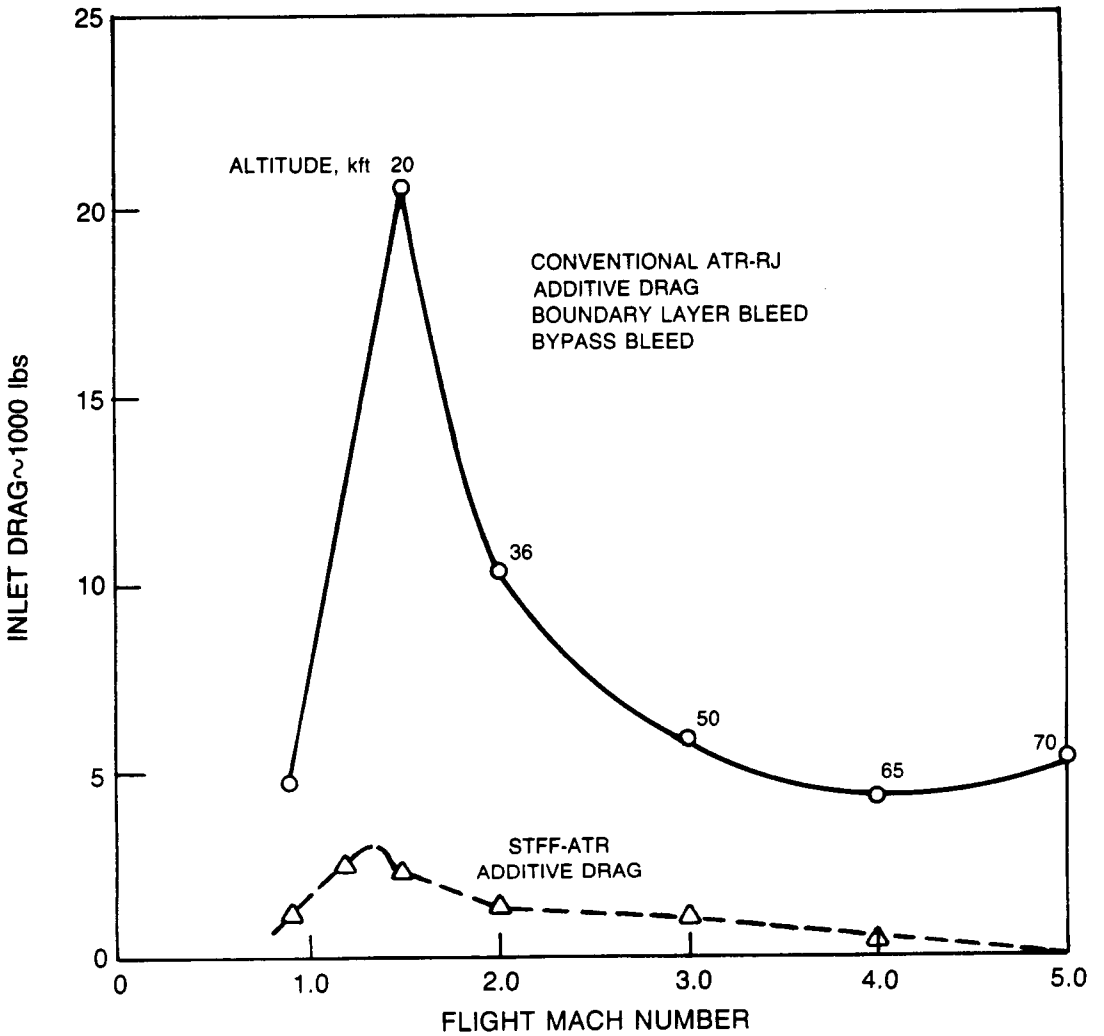

Figure 98. Inlet drag for STFF-ATR and ATR-RJ engines.

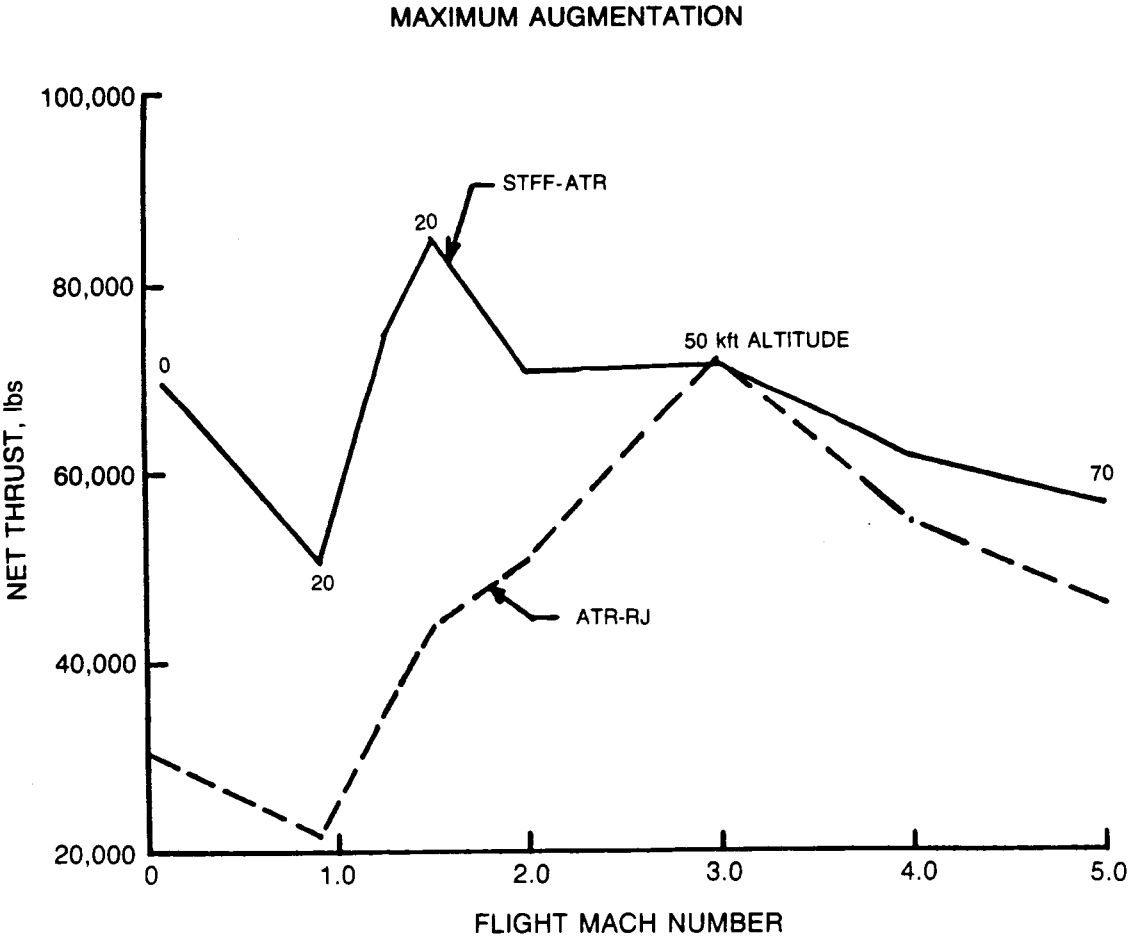

Figure 99. STFF-ATR and ATR-RJ climb thrust.

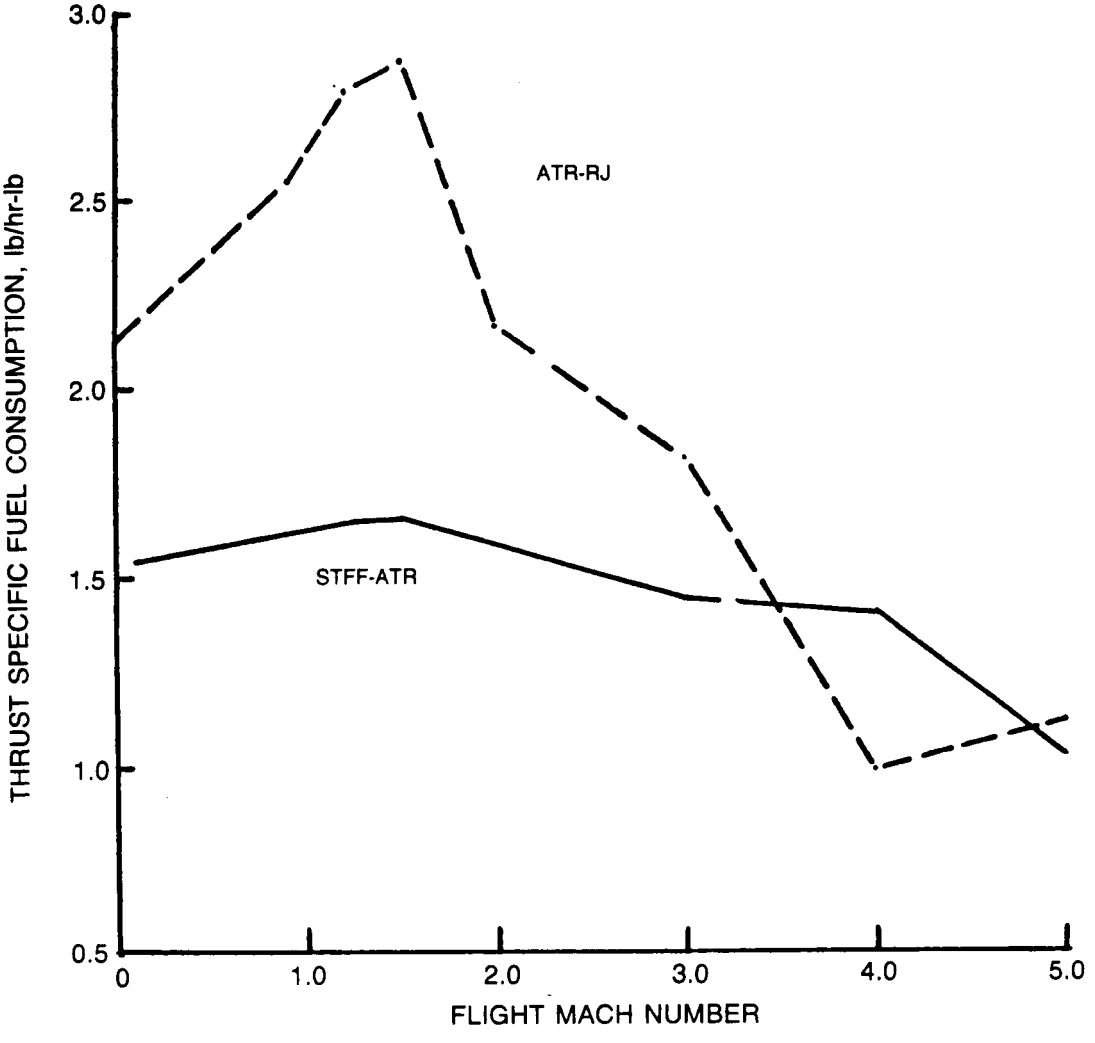

Figure 100. STFF-ATR and ATR-RJ climb TSFC.

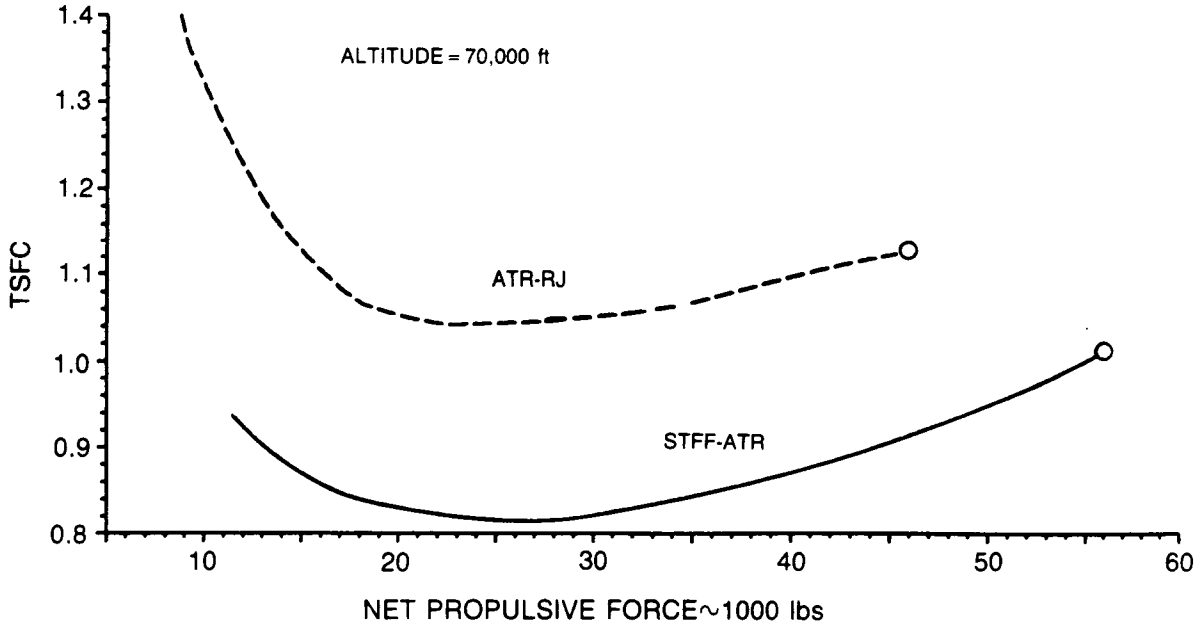

Figure 101. STFF-ATR and ATR-RJ part power performance.

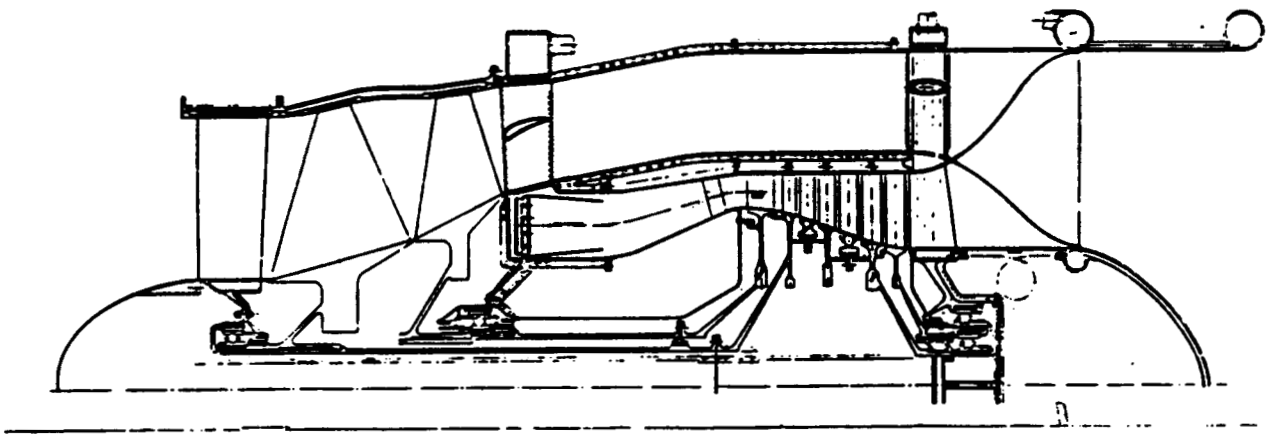

Figure 102. Air turbo rocket with conventional fan.

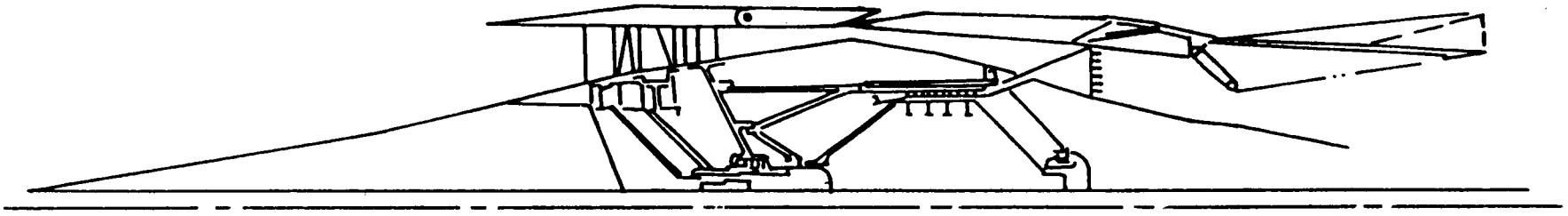

Figure 103. Supersonic through flow fan air turborocket engine.

88—6—80—107

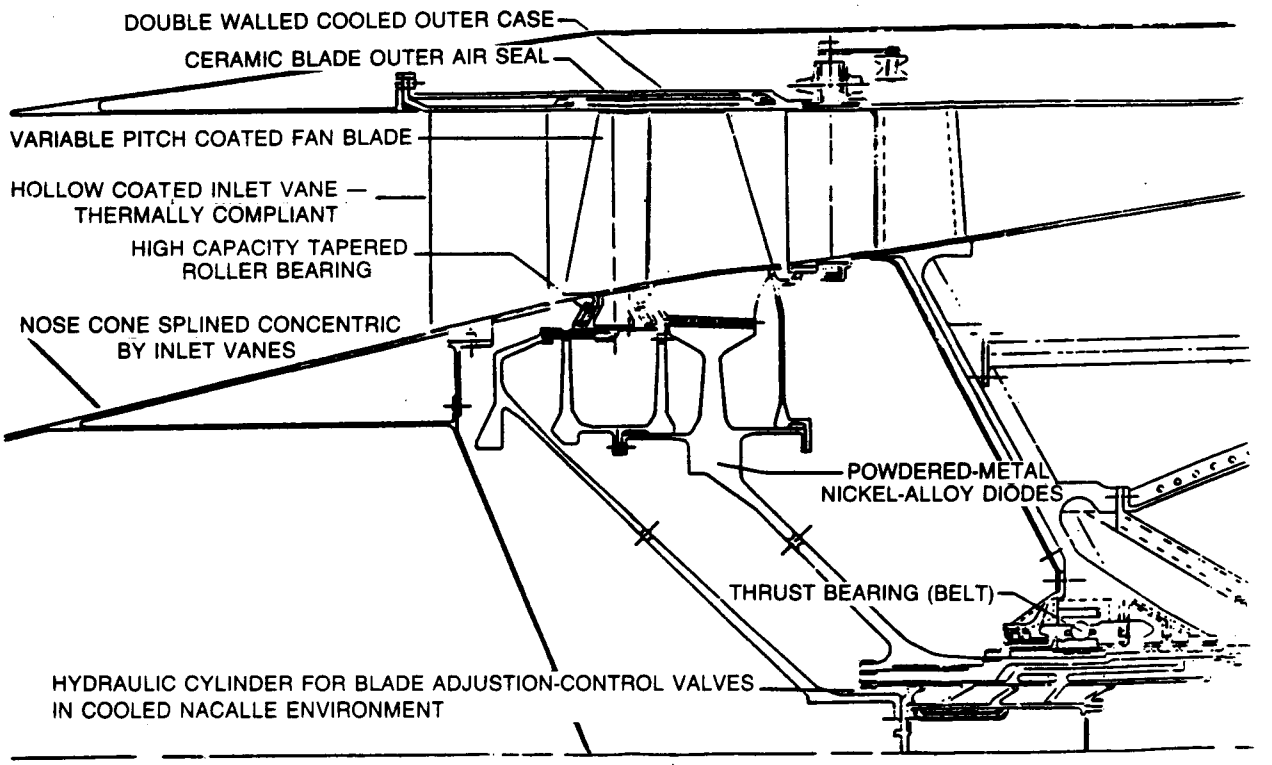

Figure 104. STFF ATR fan design.

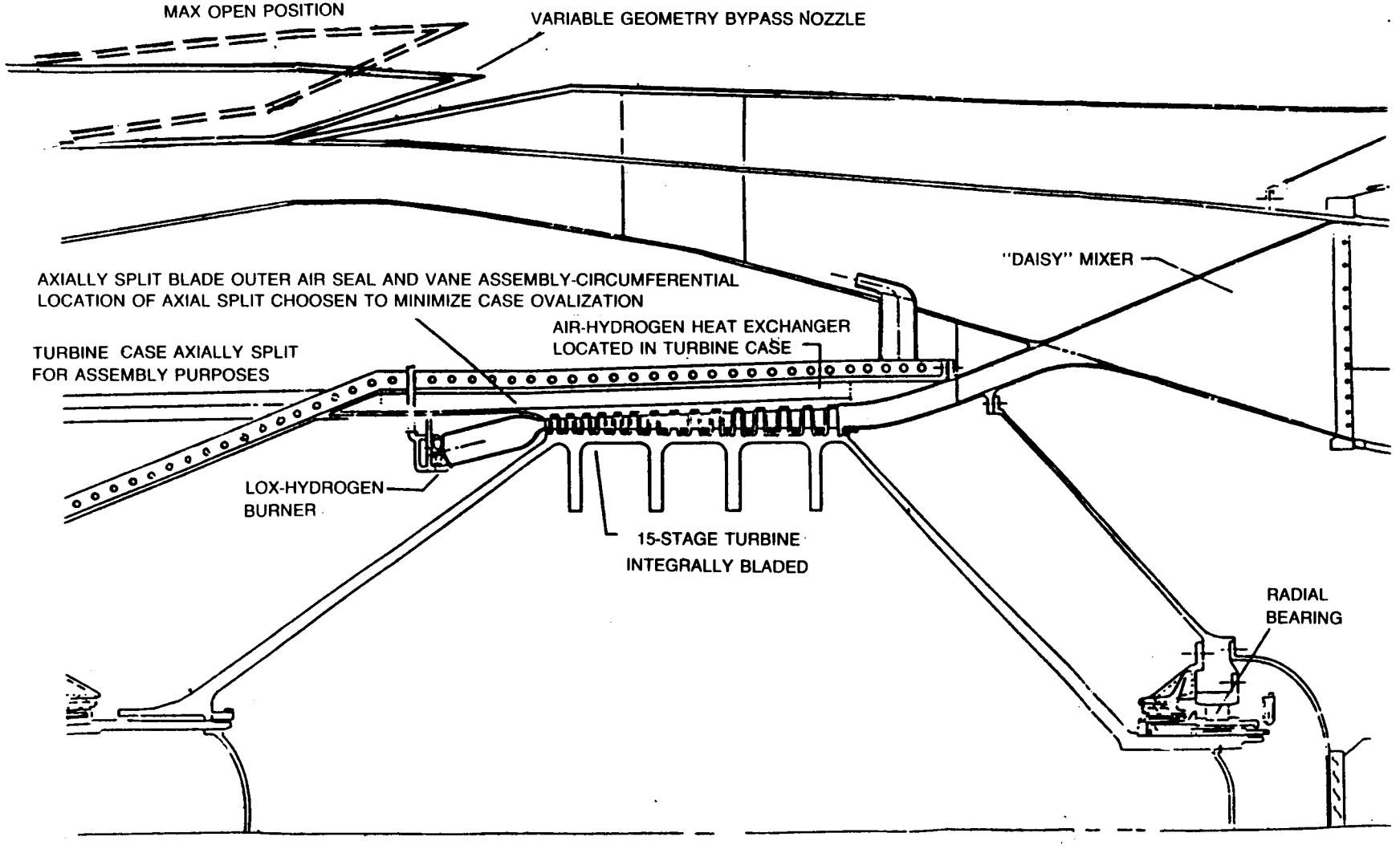

Figure 105. STFF ATR burner turbine bypass nozzle design.

W = 13,900 lbs

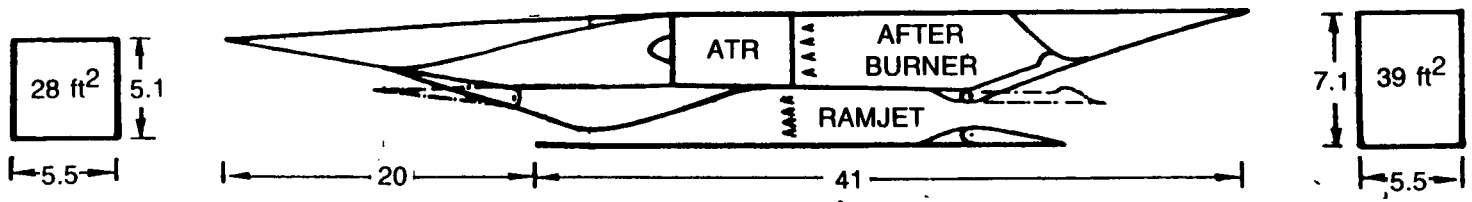

a) CONVENTIONAL OVER/UNDER ATR

W = 10,000 lbs

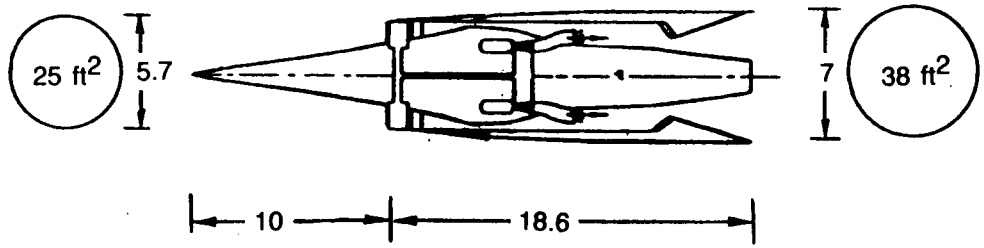

b) SUPERSONIC THROUGH-FLOW FAN ATR

Figure 106. Engine Comparison

88—6—80—115

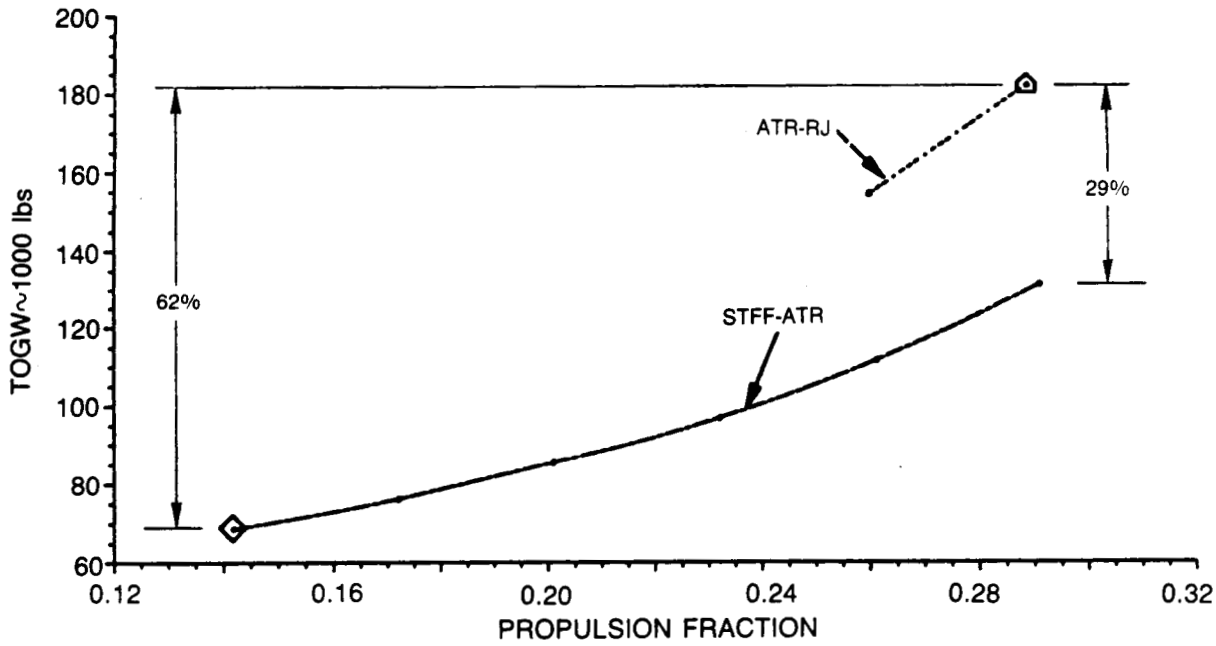

Figure 107. TOGW sensitivity to engine weight and TSFC.

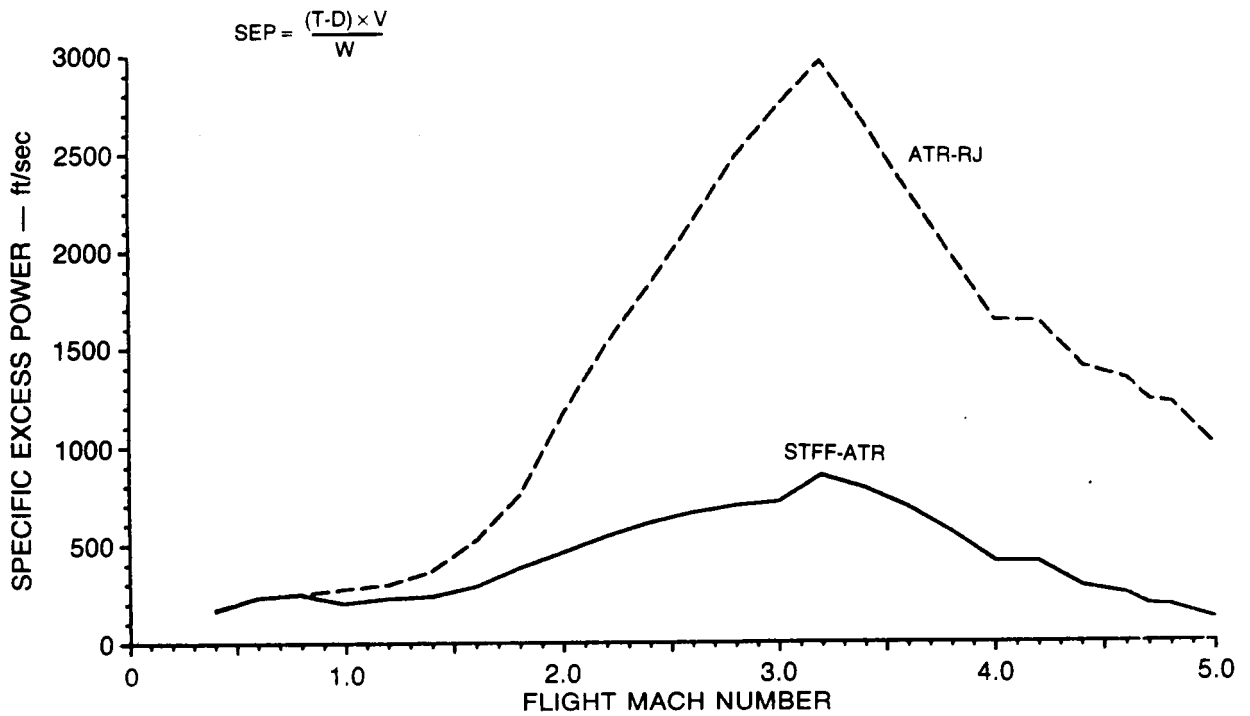

Figure 108. Comparison of specific excess power on climb path.

SUPERSONIC THROUGH-FLOW FAN FINAL REPORT
DISTRIBUTION LIST

NASA Lewis Research Center
21000 Brookpark Road
Cleveland, OH 44135
Attn: 0300/J. Acurio
0173/L. Shaw
0173/R. Graham
1950/Library (10 copies)
2000/N. Saunders
2400/D. Mikkelson
2400/W. Strack
2430/A. Glassman
2420/L. Franciscus (10 copies)
2710/K. Sievers
5100/S. Grisaffe
5110/H. Gray
5110/R. Dreshfield
5120/D. McDaniels
5120/J. Stephens
5130/J. DiCarlo
5170/R. Davies
5200/L. Nichols
5210/C. Ginty
5210/R. Johns
2700/J. Ziemianski
2700/R. Shaw
2700/C. Ball
2750/P. Batterton
2750/B. Blaha
2630/L. Reid
2760/R. Niedzwiecki
2780/R. Coltrin
2780/B. Sanders
2630/R. Gaugler
2420/L. Fishbach

Naval Air Propulsion Center
PO Box 7176
Trenton, NJ 08628-0176
Attn: PE 34/Mr. R. Valori
PE 34/Mr. S. L. Fowler

Naval Air Development Center
Attn: 6052/Mr. John Cyrus
Warminster, PA 18974-5000

Wright Patterson AFB
Attn: AFWAL/POT/Tom Sims
Wright Patterson AFB, OH 45433

McDonnell Douglas Corporation
Douglas Aircraft Company
Advanced Engineering
3855 Lakewood Blvd.
Long Beach, CA 90846
Attn: Mr. D. A. Graf
Mr. Louis Harrington
Mr. Gordon Hamilton

Lockheed Georgia Company
Dept 72-47, Zone 418
86 South Cobb Drive
Marietta, GA 30637
Attn: Mr. W. Arndt
Mr. R. H. Lange

Northwest Airlines, Inc.
Attn: Mr. B. H. Lightfoot
Minneapolis/St. Paul Int'l
St. Paul, MN 55111

TRW Aircraft Components Group
Attn: Dr. C. S. Kortovich
Mail Stop 37
23555 Euclid Avenue
Cleveland, OH 44117

Allison Gas Turbine Division
Attn: Mr. W. L. McIntire
General Motors Corp.
PO Box 420
Indianapolis, IN 46206-0420

General Electric Company
PO Box 156301
Cincinnati, OH 45215
Attn: Mr. Thomas Donohue
Mr. James Johnson MS A326
Mr. James Hartzel MS A326

Boeing Commercial Airplane Company
PO Box 3707
Seattle, WA 98124-2207
Attn: Mr. Malcom McKinnon
Mr. Mark E. Kirchner
Mr. Albertus D. Welliver
Mr. F. H. Brame
Mr. Gary Klees

Rockwell International Corp.
Attn: Leslie M. Lackman
Bethany, OK 73008

American Airlines, Inc.
Tulsa Maintenance and Engineering Center
Attn: Mr. K. Grayson
3800 N. Mingo Road
Tulsa, OK 74151

Delta Airlines, Inc.
Hartsfield Atlanta Int'l Airport
Atlanta, GA 30320
Attn: Mr. C. Daves
Mr. W. J. Overend

United Airlines, Inc.
San Francisco Int'l Airport
San Francisco, CA 94128
Attn: Mr. R. E. Coykendal
Mr. R. D. Tabery

NASA Scientific and Technical (20 copies)
Information Facility
Attn: Accessioning Dept.
PO Box 8757
Baltimore/Washington Int'l Airport, MD 21240

NASA Headquarters
Washington, DC 20546
Attn: RP/J. Facey
RJ/J. McCarthy
RJ/L. Williams
RP/R. Anderson

NASA Langley Research Center
Hampton, VA 23665-5225
Attn: 406/C. Morris
412/J. Morris
410/C. Jackson
412/S. Dollyhigh

NASA Ames Research Center
Moffett Field, CA 94035
Attn: 237-11/T. Galloway